Design and Development of miRNA and stem cell based micro/nano systems as lung disease therapy

A thesis submitted in fulfilment of the requirements for the degree of Doctor of Philosophy (PhD)

Layla Alhasan

M.Sc. in Biological Sciences

School of Applied Sciences

College of Science Engineering and Health

RMIT University

February 2016

DECLARATION

I certify that except where due acknowledgement has been made, the work is that of the author alone; the work has not been submitted previously, in whole or in part, to qualify for any other academic award; the content of the thesis/project is the result of work which has been carried out since the official commencement date of the approved research program; any editorial work, paid or unpaid, carried out by a third party is acknowledged; and, ethics procedures and guidelines have been followed.

Layla Alhasan

12/2/2016

DEDICATION

In the name of Allah, the most gracious, the most merciful

To

My Mother always supports me to reach my full potential

I am eternally grateful to you for your immense love and care

In loving memory of my father

My brothers and sisters who provide me emotional support

This work is a sign of my love to you

ACKNOWLEDGEMENTS

The work described in this thesis was not possible without support and assistance of my primary supervisor **Dr**. **Peggy Chan**. I admire and value her willingness to simultaneously to pursue different projects, which give me opportunity to learn more knowledge about the research. I would like to thank her for patience, encouragement, and long hours without which I could have never accomplished my PhD study. I am eternally grateful to you for your support and care.

My sincere gratitude goes out to my second supervisor **Prof. Leslie Y. Yeo** to always being positive, inspire and great motivational factors during the whole process.

Special thanks for **Prof. Andrew Smith** for being so supportive to me for partial scholarship. Grateful thanks for **Prof**. **Ann Lawrie** for her constructive suggestions, scientific editing and proofreading of my thesis. Thanks for **Dr.Emma Goethals**; I really appreciate your guidance, and the time you spent with me to make my PhD study go well.

Thanks to **Dr. Dodie Pouniotis** who shared her expert knowledge about flow cytometer experience. Special thanks for **Dr. Martin Stebbing** for his assistance with confocal microscopy. I thank our collaborator, **Prof. Wei Shen** for his inputs on my results in liquid marble study. Grateful thanks to **Dr. Muth Pannirselvam** for his help with Rheology experiments and **Mr. Sunly Prum** for his assistance with NMR analysis. Thanks to **Associate Prof. Robert Shanks** for his help with Dynamic mechanical analyser/ RMIT University.

Many thanks to my colleagues especially **Eltaher Elshagmani, Khalid Al Lemailem, Susan Marqus, Hala Almshawit, Kai Wei Cheng, Nooshin Sadeghi, Dr.Amgad Rezk, Nahla Almansour, Mohsina Huq, Mohammed Said, Mohammed Taha, Vishal Mistry, Parsu Budathoki** for their help and support and sincere friendship and I wish all the PhD's good luck with

finishing their thesis. My sincere appreciation geos out to the general/support staff at RMIT especially **Lisa Dias, Leeanne Bickford, David Heathcote, Shannon Fernandes, Yeshvir Singh, Nadia, Dianne Mileo and Ruth** for their help and support.

I am grateful to **Higher Education and Scientific Research/ Iraqi Government** for provided me a scholarship to enabling me to accomplish my PhD studies.

I would like to thank my beloved family members for continuous support through these years. In particular **my mother, brothers** and **sisters** for emotional support always kept my sights firmly set on my goal.

I have a desire to thank my friends here in Melbourne who has been just as loving as my family. **Siham Sayoud, Yuana Nurulita, Basma Khallaf, Alaa Karkashan, Manal, Anood Alenezy, Eman Koshlaf, Sahar Shar**. You listened to me complain, and you made me laugh when I needed.

Lastly, I owe everything to the Almighty **Allah** without whose grace and guidance, none of this would be possible.

Table Contents

List of Figures

List of Tables

Publications

Journal Publications

- **L Alhasan**, W Shen, LY Yeo, PPY Chan, Liquid Marble Miniature Bioreactor - overcoming miRNA transfection limit, under review in **Angewandte Chemie** (submitted).
- **L Alhasan**, A Qi, A Al-Abboodi, A Rezk, PPY Chan, C Iliescu, LY Yeo, Rapid Enhancement of Multicellular Spheroid Assembly by Acoustically-Driven Microcentrifugation, under review in **ACS biomaterials Science & Engineering** (submitted).

- **L Alhasan**, A Qi, A Rezk, LY Yeo, PPY Chan, Assessment of the Potential of a High Frequency Acousto-microfluidic Nebulisation Platform for Inhaled Stem Cell Therapy, **Integr. Biol.**, 2016, DOI: 10.1039/C5IB00206K. Featured in RSC Chemistry World.

- c5ib00206k Chemistry World story now online. A sound idea for treating lung disease. <**http://www.rsc.org/chemistryworld/2015/12/stem-cell-mist-treating-lung-disease**>

- **L Alhasan**, KW Cheng, LY Yeo, PPY Chan, Stem cells differentiation in hydrogel for lung tissue regeneration (in preparation).

Conference Publications

- **L Alhasan**, A Qi, A Al-Abboodi, A Rezk, RR Shilton, PPY Chan, J Friend, L Yeo, Surface acoustic streaming in microfluidic system for rapid multicellular tumor spheroids generation, Proceeding SPIE. 8923 Micro/Nano Materials, Devices and Systems, 89235C. DOI: 10.1117/12.2034050,2013.
- Fatemeh Sarvi; Kanika Jain; **Layla Alhasan**; Tina Arbatan; Wei Shen; Peggy P. Y. Liquid marble as microbioreactor for bioengineering applications. Proc. SPIE 9668, Micro+Nano Materials, Devices, and Systems, 966852 (22 December 2015); doi: 10.1117/12.2201110.

ABSTRACT

Patients suffering from lung diseases are often treated with lung transplantation, which is considered a definitive therapy offered for patients with end-stage lung failure. Because of this, it improves survival rates besides boosting the quality of life for lung transplant recipients. However, lung transplantation suffers from a number of flaws, mainly a scarcity of organs and tissue donors. In this thesis, three approaches were attempted to address these issues. These were gene therapy, microfluidic -device -assisted stem cell delivery and tissue engineering.

MicroRNA (miRNA) is emerging as a new class of gene therapeutics with the promise of healing many diseases. The applications of miRNA often require miRNA to be transfected efficiently inside cells. **Chapter 3** of this work is particularly devoted to investigating the ability of a liquid marble (LM) miniature bioreactor to enhance miRNA transfection. To achieve this, suspended A549 lung cancer spheroids were first generated using liquid marble (LM) by taking advantage of the LM non-adhesive shell, thus promoting the cell-to-cell attachment that is essential for spheroid formation. Next, a tumour suppressor (miR-126) was transfected to spheroids inside LM. It was observed that the resulting miR-126 expression and the subsequent down-regulation in VEGF-A expression reached a level that cannot be reached using conventional methods, such as transfecting miR-126 to monolayer cells or transfecting miR-126 to spheroids generated using liquid suspension methods. There are multiple possible reasons for the greater miRNA expression observed in the LM bioreactor. First of all, miRNA is much smaller than many chemotherapeutic drugs and thus penetrated well into spheroids. Secondly, the PTFE shell possesses ultra-low surface free energy and so does not absorb and waste any miRNA through non-specific adsorption. Lastly, the hydrophobic interface present on the LM shell may play a role in promoting the movement of hydrophilic miRNA towards the centre of the LM where spheroids resided. Overall, this study demonstrates that LM can serve not only as a platform that produces tumour-like spheroids, but also as an efficient microbioreactor vessel that enhances miRNA transfection and outperforms conventional transfection vessels.

As part of this approach, a novel micro-centrifugation device was also developed to generate multicellular spheroids, as shown in **Chapter 4**, these spheroids are useful for lung cancer behaviour and drug screening studies. Intense acoustically driven micro-centrifugation flows were employed to enhance the assembly of multicellular spheroids in the microwells of a tissue culture plate. This ability to interface microfluidics with commonly used tissue culture plasticware is a significant advantage, mainly because it can be multiplied for high-throughput operation and allows the retention of existing analytical equipment designed to fit current laboratory formats. The micro-centrifugation flow induced in microwells coated with a low adhesive hydrogel rapidly enhanced the concentration of BT-474 cells, resulting in tight aggregates within a minute. This was considerably faster than the conventional hanging drop and liquid overlay methods, which typically require a day to maintain their viability. The proposed method affords control of the spheroid dimension simply by modulating the input power, and is a significant improvement over other microfluidic methods that require the fabrication of different geometries and microstructures to generate spheroids of different sizes. The spheroids produced exhibited the concentric heterogeneous cell populations and tight cell-cell interfaces typical of *in-vivo* tumours. Therefore, they demonstrated the applicability of the technique for enhancing a broad spectrum of cancer biology and drug screening studies.

Despite the promise of stem cell therapy for lung therapeutics and repair, there are very few viable means for directly delivering stem cells to locally target the respiratory airways via inhalation. This is not surprising given the significant challenges in aerosolising stem cells, particularly given their susceptibility to damage under the sizable stresses involved in the nebulisation process. The current study presents promising results using a microfluidic acoustic nebulisation platform in **Chapter 5**. This platform is not only low-cost and portable, but its high MHz order frequencies were effective in preserving the structural and functional integrity of mesenchymal stem cells (MSCs) during the nebulisation process. This was verified through an assessment of the viability, structure, metabolic activity, proliferation ability and genetic constitution of the nebulised MSCs using a variety of assays that included: cell viability staining, flow cytometry, reverse transcription, quantitative polymerase

chain reaction and immuno-phenotyping. Given the novelty of inhaled stem cell therapy, comparisons with other delivery methods are difficult at present due to lack of comparable studies. More data for benchmarking are likely to become available in the near future due to the increasing interest in stem cell therapy, given the absence of viable alternative treatment régimes for respiratory ailments to date. Nonetheless, the results in this work provide compelling evidence that the SAW nebulisation platform, with its inherent benefits of low cost and portability, constitutes an attractive tool for the delivery of stem cells via inhalation for the treatment and repair of lung function.

For lung regeneration to be successful, a 3D biodegradable and biocompatible scaffold needs to be synthesised. Various 3D scaffolds have been synthesised previously, ranging from natural to synthetic polymers. However, 3D biodegradable scaffolds for regenerated lung have not been exploited with the aim of regenerating new tissue in damaged lung using stem cell responses that function in a clinical setting. Transplantation of alveolar epithelial cells derived from murine embryonic stem cells (mESCs) that are encapsulated within scaffolds may provide a novel strategy to regenerate lung cells damaged by lung disease.

In **Chapter 6**, a novel tissue scaffold composed of enzymatically cross-linked gelatin was developed. Essentially, mESCs were encapsulated in this scaffold simultaneously with the scaffold being cross-linked. A novel injectable hydrogel system composed of gelatin-3,4-dihydroxyhydrocinnamic acid (Gtn-DHHA) conjugates were cross-linked rapidly by laccase-mediated oxidation to form a hydrogel tissue scaffold which could simultaneously immobilise mESCs. This scaffold system supported the proliferation and differentiation of mESCs into lung epithelial cells in both the presence and absence of growth factors. The stiffness of the hydrogels was readily modulated by altering polymer precursor concentration.

Gtn-DHHA hydrogel was maintained in air-liquid interface (ALI) conditions to mimic the lung micro-environment and mESC differentiation was evaluated by measuring the expression of E-cadherin and

Foxa2, both of which are considered to be definitive endoderm markers. Furthermore, the expression of Pept2, Sema4F, Unc5b, and Ttf1 in hydrogel-encapsulated cells was assessed using the quantitative polymerase reaction (qPCR) and immunofluorescence assays. The expression of these markers was up-regulated in the presence and absence of growth factors, in particular under air-liquid interface by comparison with submerged and control cultures. This scaffold facilitated mESC differentiation into alveolar epithelial cells, even without growth factors, and is therefore a promising approach for lung repair.

In summary, this thesis first presents a novel, effective method—namely liquid marble— for better generation of multicellular spheroids to enhance miR-126 PEI nanoparticles transfection. It then introduces a novel method called a SAW device, which is also used to produce multicellular spheroids, and to generate MSC-laden aerosols to cure small lung damage. Finally, it presents a novel three-dimensional (3D) biodegradable scaffold as an alternative material for an extracellular matrix (ECM) for improved stem cell survival, proliferation, and differentiation. This is considered to be a critical step for *in-vitro* differentiation of ESCs into lung epithelial cells for lung repair and regeneration.

CHAPTER ONE- INTRODUCTION

1.1 Overview

Lung diseases are the leading cause of morbidity and mortality worldwide. Although there is no curative treatment for some lung diseases, lung transplantation gives the only hope since it is the only current therapy available for patients with end-stage lung failure. Besides being able to improve survival rates, it has the capacity to improve the quality of life in lung transplant patients. However, lung transplantation suffers from a critical shortage of donors [1]. This has led to the development of regenerative medicine and tissue engineering, which target repairing and restoration of any type of damaged tissue due to any cause. For this reason, a combination of different approaches such as gene therapy, cell therapy and tissue engineering offers the best alternative to replacement therapies and traditional transplants [2, 3].

Gene therapy is the delivery of genetic-based material (e.g. DNA or RNA) to targeted cells to alter their expression patterns. Cellular gene expression can be manipulated to treat different diseases such as lung cancer. MiRNAs are collectively a class of noncoding RNA and consists of 20–25 nucleotides that function as gene regulators by cleaving and/or inhibiting the translation of target messenger RNA (mRNA) [4] as well as simultaneously regulating a broad set of genes of interest [5]. Due to their ability to trigger synergistic therapeutic effect in cancer, miRNAs have recently emerged as a new class of cancer therapeutics. MiRNAs also play a significant role in various cellular and physiological processes such as organ development [6], apoptosis [7] and differentiation [8].

However, miRNA is negatively charged and may thus be interfered with while interacting with the cell membrane, thereby triggering poor cell uptake. Many approaches have been developed to improve the transfection efficiency of miRNA and prevent miRNA degradation. For example,

nanoparticle vesicles are often used to deliver miRNAs [5]. Gene therapy can be used to treat multicellular spheroids, which comprise three-dimensional (3D) spherical cell aggregates displaying cell-cell and cell-matrix interactions, more closely mimicking *in-vivo* avascular tumour structure and functionality than conventional monolayer cultures, in which intercellular contact is often lost [9, 10]. They are, therefore, of fundamental importance to studies in cancer biology, metastasis and invasion, in addition to therapeutic screening [11, 12]. Several methods have been used to produce these spheroids, all of which first involve the formation of loose cell aggregates, followed by their compaction into tight spheroidal clusters [10].

There is increasing evidence demonstrating the efficacy of stem-cell-based therapies for treatment of an array of lung diseases, including: chronic obstructive pulmonary disease (COPD); pulmonary and cystic fibrosis; and pulmonary hypertension [13, 14]. Direct lung delivery via aerosol inhalation, by contrast, not only facilitates local targeting of the disease or injury-specific regions, but also allows easy and painless administration, has fewer side effects and avoids the need for anaesthesia. Nevertheless, there remain considerable challenges associated with stem cell aerosolisation in particular. The likelihood that the stem cells will survive and retain their function during the nebulisation process is low.

Tissue engineering (TE) is an interdisciplinary field that applies the principles of biology, medicine and engineering to manipulating various biological functions of tissues that restore and replace the injured tissues or organs and produce entirely functional replacements [15, 16]. For repair and regeneration of lung tissue to be successful, 3D scaffolds should be elastic, stretchable and compressible through inhalation, biocompatible, non-toxic, degradable and disappear from the lung post-implantation [17]. The 3D scaffolds are used as platforms for the culture of embryonic stem cells (ESCs) to differentiate them into lung epithelial cells that can replace the dying cells. ESCs are pluripotent cells that are directly derived from the inner cell mass

of embryos and have a unique capability of long-term self-renewal and the ability to differentiate into a variety of specific cell lineages. In addition, stem cells are of paramount importance in regenerative tissue studies and cell-based therapies [18, 19].

1.2 Gene Therapy and Lung Cancer

Gene therapy is broadly defined as the replacement of defective or absent genes within the cell—or the use of gene approaches to affect function or modulate responses—for the treatment of pulmonary diseases, including lung cancer. It can be classified into three categories: (a) gene addition or gene replacement), (b) gene reprogramming and (c) gene repair. Gene addition or replacement is the only approach used in clinical applications that involve adding corrected genes in order to overcome a genetic mutation. This method seeks to treat less complex disorders. Gene reprogramming is a second approach that is used for more complex disorders, in which the gene product may require controlled cell-specific expression or disorders with a dominant phenotype. It can be used to correct defective portions of endogenously encoded mutant RNA transcripts for a given gene [20]. The third approach is gene repair, which seeks to correct mutant sequences in the genomic DNA. However, the efficacy of gene repair is low, with no currently realistic clinical applications [21].

The term “gene therapy” involves a wide range of cure types that all use genetic material to modify cells to aid and effect a treatment [22]. Several preclinical studies have shown their efficiency by testing a range of gene therapy agents. Gene therapy strategies have been tested on gliomas [23] and cancers of the pancreas [24], liver [25] and other organs. Since the safety of gene therapy agents was demonstrated, many cancer patients have participated in gene therapy trials, with few or reduced side-effects [26, 27]. Fever and colds are the most frequent side-effects compared with the more serious side-effects of chemotherapy. In addition, if an agent is injected into the target area, there can be localised swelling and inflammation at the injection site [26, 28, 29]. In lung cancer models, genes

have been introduced into lung cancer cells, repairing normal cellular phenotypes or causing death of the cancer cells [30].

Lung cancer is the leading cause of morbidity and mortality in Australia [31]. It is defined as the uncontrolled growth of abnormal cells in one or both of the lungs. The abnormal cells replicate more rapidly and do not grow into normal lung tissue. Cancer cells can spread from the tumour site into other organs via the bloodstream or lymphatic system. It is expected that approximately 1.6 million new cases will be diagnosed globally each year, leading to about 1.38 million deaths and accounting for 18.2% of all cancer-related deaths worldwide [32]. In 2014, 11,550 Australians were diagnosed with lung cancer (6,720 men and 4,830 women) and an estimated 13,640 people are expected to be diagnosed with lung cancer in 2020 [33].

There are two main histological types of lung cancer that have been classified by pathologists in recent decades: small cell lung cancer and non-small cell lung cancer (NSCLC). NSCLC is the most common and accounts for 85% of all lung cancer cases. It is further subdivided into adenocarcinoma, squamous cell carcinoma and large cell carcinoma (AC, SCC, and LCC, respectively) [34].

NSCLC commonly spreads to different parts of the body more slowly than does small cell lung cancer. Small cell lung cancer accounts for 14% of all lung cancers. It develops more quickly and is more likely to spread to other organs in the body than non-small cell lung cancer. Many techniques have limited effectiveness in lung cancer (LC) treatment [35]. The common treatment for LC is surgery for localised disease. However, most LC cases are diagnosed in advanced stages. As a result, chemo- and/or radiotherapy (CT and RT, respectively) are the major therapeutic options, which make the prognosis of lung cancer very poor, with a median overall survival of only about one year. The selection of treatment and the prognosis depend upon the specific type of tumour [36].

1.3 MiRNA-based gene therapy

1.3.1 MiRNA as a potential biomarker in cancer

MiRNA was discovered in 1993, and was found to control the developmental timing of the nematode *Caenorhabditis elegans* [37]. MiRNAs are small, non-coding, single-stranded RNA molecules, 21–24 nucleotides in length, that target the regulation of gene expression through either degrading the target mRNA or inhibiting translation of the mRNA into protein [38, 39]. The targeted genes can control different processes, such as stem cell division [40, 41], developmental timing [42], organ development, apoptosis, differentiation [43-48], disease [49, 50] and cancer [51, 52] in animals.

The expression of specific miRNA has been proposed as being relevant to certain tumour types. As a result, miRNA signatures have been suggested as being important for the prognosis and prediction of cancer patient survival [53-57]. For example, miRNA was detected in the peripheral blood, making it an innovative biomarker for early cancer detection [58]. In addition, control of angiogenesis is the one mechanism by which miRNA can support tumour growth, by producing new vessels from the pre-existing vessels. Lewis lung carcinoma cells were injected into mice lacking the endothelial Dicer protein, which is important for the generation of miRNA. A deficiency of Dicer in the endothelial cells reduces tumour neo-angiogenesis [59].

1.3.2 MiRNA in lung cancer

Down- or up-regulation of miRNAs is an excellent strategy to study the function of miRNAs in cancer pathogenesis. Cancer is a complex disease characterised by abnormal cell growth and loss of apoptosis function. Recent studies have shown that miRNAs can regulate cell growth and apoptosis [45, 47]. Thus, modifications in the miRNAs' expression levels or modification of the interaction between miRNAs and their mRNA targets could be the main effect of miRNAs on tumour development or progression. miRNA genes were overexpressed in several cancers, such as miRNAs 17–92 in lung and lymphoma [60].

By contrast, other miRNAs (called suppressor) are decreased in some cancers. For example, miRNA let-7 plays a significant role in the pathogenesis of lung cancer and can control lung cancer development. Down-regulated let-7 levels were observed in both *in vitro* and *in vivo* lung cancer studies, resulting in shortened postoperative survival [61]. By contrast, the up-regulation of miRNA let-7 levels in A549 lung adenocarcinoma cell lines led to the inhibition of cancer cell growth [61]. In another example, the miRNA-200 family enhanced invasion and metastasis in lung cancer mouse models by regulating epithelial mesenchymal transition (EMT) [62]. In addition, the miR-17–92 cluster enhanced tumour growth by targeting two tumour suppressor genes—PTEN and RB2—in lung cancer, particularly in the aggressive form of small-cell lung cancer [63].

1.3.3 miR-126 in cancer

Transcriptional analysis and microarrays-based assays showed that there were significant differences between the total expressions of miRNA in tumour cells and that of normal cells. MiRNA-126 is one of these miRNAs that is down-regulated in breast cancer. Restoration of levels of miRNA in primary breast cancer cells suppressed tumour growth and metastasis to the lung and bone in nude mice [57]. Importantly, patients with primary breast cancer cells characterised by a low level of miR-126 exhibited a lower percentage survival than patients who displayed tumours with a high level of miR-126. Therefore, this suggests that there is a clinical correlation between the loss of miR-126 and survival of cancer patients [57]. Down-regulation or loss activity of miR-126 has also been reported for other cancers versus non-cancers, such as lung [64], cervix [65], prostate [66], and colon [67] cancers. The miR-126 function is not yet very well known in these types of cancers. However, down-regulation of miR-126 was correlated with an increased expression of VEGF-A in gastric cancer tissues [68, 69]. Sasahira et al. showed that the down-regulation of miR-126 induced angiogenesis and lymphangiogenesis by activation of VEGF-A.

This was strongly correlated with disease-free survival for oral cancer patients [70]. Volm et al. also explored the up-regulation of VEGF-A in non-small lung cancer; this reduced the sensitivity of lung cancer cells to apoptotic stimuli [71]. Liu's group reported that VEGF-A was down-regulated by miR-126 when lung cancer cells were transfected by lentivirus miR-126, suggesting that a down-regulation of VEGF-A was accompanied by cell cycle arrest and a decrease in tumour growth *in vivo* and *in vitro* [72].

1.3.4 MiRNA therapy approaches

A recent advance in the miRNA field has been the discovery of their role in the regulation of different cellular processes such as development, differentiation, proliferation and apoptosis, which are important in cancer formation. MiRNAs as oncogenes or suppressors are suitable therapeutic targets (**Figure 1.1**).

There are several advantages of miRNAs based therapeutics. Firstly, miRNAs can degrade the targets. Secondly, miRNAs can target multiple oncogenes simultaneously, which might reduce the need for combination therapies. If a certain miRNAs expression is reduced in the disease, miRNA mimics can be used for the treatment; the resulting mimics of miRNAs can minimise the effect of certain oncogenes as a form of replacement therapy. An example of miRNAs replacement therapy is the intra-tumoral introduction of the miRNA let-7 into mouse models of NSCLC, which reduced the tumor size [73]. In addition, an intra-tumoral injection of cholesterol-conjugated miR-99a mimics significantly decreased tumour growth in hepatocellular carcinoma-bearing nude mice [74].

By contrast with up-regulation of miRNA resulting in disease pathology, miRNA inhibition treatment can be used to decrease miRNAs expression. Antagonists of miRNAs can reduce the expression level of oncogenic miRNAs in tumours and in turn increase the level of specific tumour-suppressor genes. MiRNAs-21, an antagonist, was applied in glioma cell lines and stimulated the caspase-induced

apoptotic pathway [75]. MiRNAs can also be introduced into the therapeutic field as indirect miRNA-based therapy. For example some tumours have low levels of certain miRNAs compared with that of normal cells; thus introducing vectors that carry miRNA-regulated suicide genes into the tumour cells may lead to high abundance of the suicide gene in the cancer cells but not in the normal cells.

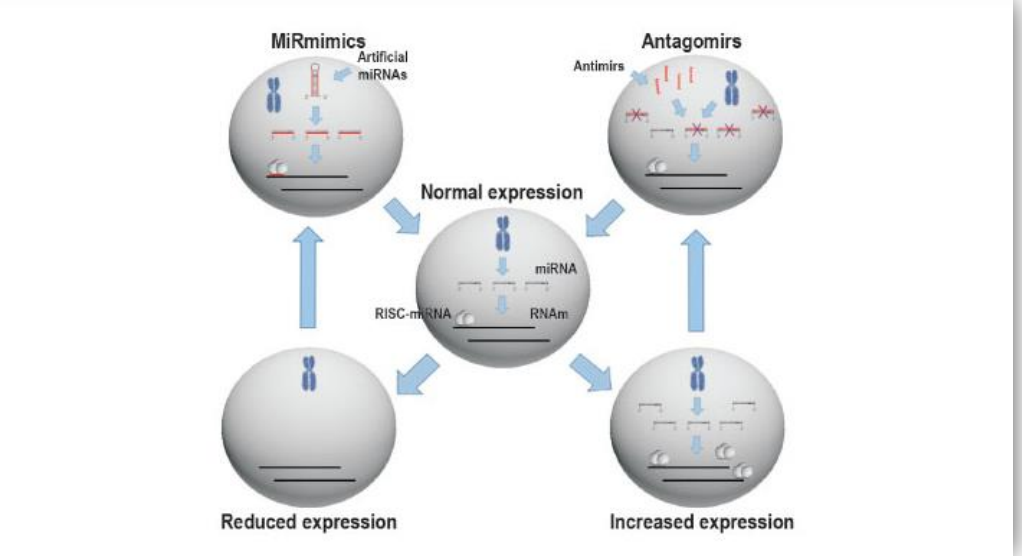

Figure 1.1: Schematic of miRNA treatment [76].

1.4 Synthetic materials for miRNA delivery

Synthetic materials are potentially effective carriers for DNA and siRNA [77-80]. Synthetic materials are cationic materials that condense the negative charge of nucleic acids through electrostatic interactions. They have advantages over viral-based vectors because of control over their composition, simplified manufacturing and low immunogenicity [81]. Viral-based vectors are currently more efficient than synthetic materials. However, the efficiency of synthetic systems has been improved by adjusting particle size and surface properties to give a greater bio-distribution *in vivo.*

Several synthetic materials have been used to deliver miRNAs. The most common materials are discussed in the next section.

1.4.1 Lipid-based delivery system

Liposomes are some of the most common transfection reagents used *in vitro*. However, these reagents are not often used *in vivo* as a result of high toxicity, unwanted immune response and non-specific uptake [82]. Recently, different lipid-based delivery systems have become commercially available, and considerable effort has been devoted to modifying the composition and chemical structure of liposomes. Some studies have been successful in delivering siRNAs [83]. Although siRNA and miRNA share certain similarities, the subtle difference between siRNA and miRNA is the former typically bind perfectly to their mRNA targets, whereas the latter have multiple targets [84].

Wu et al. (2011) introduced DOTMA: cholesterol: TPGS to deliver miRNAs 133b by adding miRNAs 133b to empty liposomes reagents. *In vitro*, liposomes transfected with miRNA 133b were more efficient in treating A549 non-small lung cancer than siPORT NeoFX. Approximately 50-fold more Cy5 labelled oligodeoxynucluotides lipoplexes accumulated in the lung than with the siPORT NeoFX reagent. Moreover, the mature miRNA level was 52% greater than that of untreated mice in lung post-transfection [85]. However, no inhibition of tumour growth was reported. DOTMA: cholesterol: TPGS was also used to deliver pre-miR-107 for head and neck squamous cell cancer treatment. There was a 42% reduction in tumour growth by lipoplexes containing pre-miR-107 compared with controls [86]. However, the clearance of lipoplexes was observed; there is limited information about the stability of miRNA lipoplexes following injection to blood fluidics, where high salt concentrations and protein can change the ionic complexes. Cationic liposomes are the most common reagent used for lipid-based systems. However, they are limited for *in vivo* application due to their toxicity [82].

To overcome this obstacle, a natural lipid emulsion (NLE), MaxSuppressor *in vivo* RNALancerII (BIOO Scientific, Inc.), has been developed. NLE was introduced to deliver miRNA34a and let-7 for

non-small lung cancer cell treatment. By contrast with the cationic liposome, NLEs accumulated in the lung more than in the liver. There was a decrease of tumour burden by approximately 40% in mice treated with miR-34a and let-7 compared with the miRNA control, and the expression of miR-34a and let-7 was greater than that in untreated mice [87]. Developing miRNA formulations combined with NLE is a novel therapy with considerable potential for lung cancer patients.

While lipid-based materials constitute one of the most important candidates to deliver miRNAs, they are not the only option available. Several alternative materials are presented below and offer advantages.

1.4.2 Polyethyleneimine (PEI)-based Delivery System

Polyethlenimine (PEI) is one of the most common polymers used for inclusion of a gene of therapeutic potential. PEI is positively charged as a protonation of amine groups. Therefore, it can be used to condense nucleic acids. The interaction between PEI and nucleic acids retains a net positive charge on their surfaces, resulting in the promotion of interactions with negatively charged polysaccharide on the cell surface.These interactions with the cell surface make the complexes undergo endocytosis. Many studies have used PEI to deliver both DNA and siRNAs in animal models [81, 88, 89]. However, the translation of PEI as a delivery system to clinical applications is still limited because of its greater activity than other polymers [90, 91].

Polyurethane-short branch polyethyleneimine (PU-PEI) has been introduced to deliver miR-145 to treat cancer stem cell (CSC) derived lung adenocarcinoma. The LAC-CSC did not respond to a combination of radiation and cisplatin during a 30-day experimental period. However, there was a significant reduction in tumour growth when miRNA delivery was combined with radiation and cisplatin [92]. In addition, when miR-145 PU-PEI was administered to orthotopic CSC-derived glioblastoma tumours, there was a significant tumour reduction, particularly when the miR-145 PU-

PEI delivery system was combined with radiation and temozolomide. The synergic effect improved the survival rate and showed that this potential miRNA treatment could overcome tumour chemo-radioresistance, inhibit tumour relapse and suppress cancer [93].

1.4.3 Dendrimers

Dendrimers have received considerable attention in gene delivery because of their defined architecture and a high ratio of surface moieties to molecular weight. Dendrimers have successfully been introduced to deliver miRNAs and siRNA, but few studies have reported their applications.

U251 glioblastoma cells were treated using co-delivery of anti-miR-21 and 5-fluorouracil (5-FU) by polyamidoamine dendrimers. This increased apoptosis and decreased the migration of tumour cells compared with treating with 5-FU only [94]. Anti-miR21 that was delivered by poly amidoamine dendrimers increased the chemo-sensitivity of glioblastoma cells to taxol [93]. Dendrimers have the ability to bind miRNAs, assisting in the entry of cells, but their entry is not precise. Eliciting the mechanism of the delivery system of cell entry has the potential to protect miRNAs by evading endosomal and lysosomal compartments [95].

1.4.4 Poly (lactic-co-glycolide) PLGA Particles

Polylactic-co-glycolide particles are a family of water insoluble polymers that are commonly used in biomedical applications [96]. These particles enable the formation of micro-particles and nanoparticles, which entrap the biologically active molecules [97, 98]. PLGA particles can protect nucleic acids from degradation, and have a high loading capacity and multiple surface modifications that generate potentially favourable pharmacodynamics [99]. These particles have been approved by the USA Food and Drug Administration (FDA) as biodegradable polymers for drug and gene delivery [100-102]. However, the disadvantage of PLGA—which limits their application for drug or gene

delivery, particularly for lung cancer—is its rapid clearance from the circulatory system. To overcome this issue, PEG-modified PLGA was synthesised, and the inclusion of the PEG moiety effectively increased the blood circulation time of the carrier molecule [103].

1.5 Cancer cells as 3D structures (spheroids)

Monolayer cultures have been commonly used in cancer research and anti-tumour drug development. However, they do not sufficiently reflect physiological conditions since monolayer cultures suffer from the loss of stroma components and the extracellular matrix. Aggregations of cells with a 3D structure (called "spheroids") have been subjected to different *in vitro* studies for a better understanding of the principles of morphogenesis and tissue formation. Multicellular spheroids thus are of paramount importance in biomedical science since they mimic the *in-vivo* tumour tissue structure and microenvironment. Stem cells or cancer cells from malignant cell lines or fragments of human tumours can be used to create 3D structures [104] that have been used in studies of cell-cell interactions and communication, position-dependent proliferation, metabolic gradients and gene expression.

Spheroids more effectively mimic the behaviour of tumours than do two-dimensional (2D) cell cultures because spheroids, very similar to tumours, usually contain both: surface-exposed and deeply buried cells; proliferating and non-proliferating cells; well-oxygenated and hypoxic cells [105]; and show a greater degree of variation in morphology [106], function [107] and differentiation than do 2D monolayer cell cultures.

Multicellular spheroids *in vitro* display growth kinetics, resistance to radiotherapy, metabolic rates, chemotherapy, express cell signalling, and new proteins that demonstrate tissue-like structures with more functions than individual cells [108]. A systematic study has identified the degree of differentiation as an important determinant of the response of radio-therapy in various spheroid types

of human origin [109]. As a result, multicellular spheroids are believed to mirror the radio-sensitivity of differentiating tumours *in vivo* more precisely than do monolayer cell cultures. For example, when tumour cells were isolated and grown as a monolayer, they lost their drug resistance to alkylating, while this could be fully recaptured when cells were cultured as multicellular spheroids [110, 111]. Spheroids can also be used to study the adhesive properties of tumour cells [112]. Tumour-induced angiogenic responses can be modelled using cultures in which tumour spheroids interact with vascular cells generated from ESCs, which made feasible the analysis of interactions between different cell types in spheroids [113].

Many efforts have been devoted to studying the different aspects of tumour cells since 3D multicellular spheroids highlighted the need for improved and more effective *in-vitro* system models that more closely resemble the *in-vivo* situation and the biological behaviour of the cells.

1.6 Generation of multicellular spheroids

1.6.1 Conventional methods

Many techniques have been used to produce spheroids, including liquid-overlay [114], spinner flask, hanging drop and gyratory rotation methods [115, 116]. In the liquid-overlay technique, trypsinised cells are placed on dishes covered with a thin film of agar. Because the coating prevents cell attachment to the dish, cells grow in 3D and individual cells give rise to aggregates or spheroids. In the gyratory rotation and spinner flask techniques, after trypsinisation cells are located in a culture container with a magnetic stirrer, precluding cell attachment to the substrate and favouring cell-cell adhesion. In the more recently developed hanging drop technique, spheroids are grown in an inverted micro-plate. However, all of these techniques are limited by tedious and laborious procedures and the spheroids produced are usually loosely aggregated or have irregular size. Thus researchers have been

motivated to create novel strategies as alternative approaches for the production of uniform multicellular spheroids.

1.4.2 Microfluidic devices

Recently, several microfluidic strategies have been offered for on-chip spheroid culture, including: microarray devices that immobilise cells on selectively adhesive patterned structures [117]; cell trapping barriers [118-120]; non-adhesive microwells [121-124]; bubble- and droplet-based methods, in which the cells are encapsulated within bubbles [12] or gelated capsules [125-127]; cell trapping in microwells by ultrasonic actuation [128]; and microwells in which is induced a rotational flow [129].

Microarray methods have the advantage creating uniformly sized cell aggregates, while the aggregate size is likely to be limited by the dimensions and geometry of the patterns. Large numbers of cells also need to be seeded, as any cells that are not immobilised tend to be washed away and lost [120]. Ultrasonic actuation needs custom-made microwells and the actuation heats up the solution in the microwell [128], which may damage cells that are sensitive to a temperature increase. Bubble and droplet methods have similar limitations, since the aggregate sizes are dependent on that of the capsule, which, in turn, is restricted by the surface properties and dimensions of the microfluidic system. In addition, a bubble method has limitations from low cell capture efficiencies. Rotational flow devices, on the other hand, allow cell aggregates of different sizes to be formed from microwells of a single dimension, thereby circumventing the need to fabricate different devices to vary aggregate size. However, the need for a filtration system to prevent cell clots from entering the device not only reduces the efficiency of the method due to loss of a large number of cells but also introduces a further complexity, the necessity for an additional channel shredder to break up large cell clots by shear [129]. In addition, the closed microfluidic device restricts practical sampling and collection of cell aggregates—for example, for plating the cell aggregates to stimulate cell differentiation [130].

1.6.3 Liquid marble bioreactor

The phenomenon of liquid marbles was presented in the pioneering work of Aussillous and Quere in 2001 [131]. Since then, extensive studies have been devoted to miniaturisation the technology [131-133]. Due to their unique physical and structural characteristics, liquid marbles have been subjected to a variety of practical applications during the past decade.

These applications included microfluidics [134, 135], electro-wetting [136] and water pollution [137]. A number of studies have also been dedicated to the use of liquid marbles as miniature reactors. Tian's group has reported the possibility of using liquid marbles for gas sensing [138]. Fujii et al. also proposed using modified liquid marbles for gas sensing. In this study, liquid marbles were made using PS latex particles carrying pH-sensitive PDEA hair (PDEA-PS particles). Finally, liquid marbles were rapidly disintegrated upon exposure to HCl gas, presumably due to desorption of the latex particles from the surface of the liquid marbles [139].

Liquid marbles have also been created from *Lycopodium* spores and used to encapsulate aqueous solutions of 9-fluorenylmethoxycarbonyl-diphenylalanine (Fmoc-FF). Self-assembly of ribbon-like peptide fibrils into an ultrathin peptide membrane resulted on acidification of the Fmoc-FF solution at the liquid/air interface, showing the potential of liquid marbles in micro-bio-reactors applications [140]. In addition, a liquid marble strategy was used effectively to detected polluted water with contaminants such as oils, petroleum and their derivatives that minimise the surface tension of water [137]. Polyvinylidene fluoride (PVDF) marbles floating on the surface of contaminated water with silicon oil or kerosene were destroyed due to the formation of a low surface tension film on the surface of the water. Therefore, liquid marbles have been proposed for determination of water pollution from oils and petroleum [137]. Furthermore, liquid marbles are covered by graphite powder, have a low evaporation rate compared with that of uncovered liquid marbles and have sufficiently long lifetimes to retain their spherical shape, which makes them an interesting choice for industrial

and biological applications such as microfluidic, genetic analysis and anti-fouling uses. Hence, liquid marbles are also effective storage devices [141]. In addition, a gas storage system was developed in which methane molecules were absorbed in the water of the marbles [142, 143].

Recently, liquid marbles have received considerable attention in the pharmaceutical industry. They have shown many advantages in drug delivery by offering the benefits of handling high drug loadings, production of spherical granules with excellent flow, simultaneous control of the size and structure of the granules, good compression properties, and fast drying periods [141, 144, 145]. Fatty acid crystals and triacylglycerol crystals have been used to form edible liquid marbles with useful applications in the food, cosmetic and medical areas [146]. Liquid marbles covered by solid particles (based on a copper substrate or a polystyrene latex) have been used to form capsules containing drug components that were stimulus-responsive [147, 148].

Recently, liquid marbles with unique properties have been employed to build micro-biological reactors for microorganism cultivation. A liquid marble bioreactor provided a more suitable environment for the growth of aerobes than McCartney bottles with shaking incubation. Cell concentration increased more rapidly in liquid marbles [149]. Some of the significant advantages of liquid marble bioreactors [134, 150] are that they minimise the consumption of chemical and biological reagents, accurately control reaction conditions, and have much shorter reaction times.

Furthermore, liquid marbles have been explored for the generation of cancer multicellular spheroids [151] and for immune-haematological assays [152]. Also, another important biological application for liquid marbles is their use to produce embryoid bodies (EBs) [153] and to differentiate cardiac tissue from ESCs [154]. These studies showed that liquid marbles constitute a promising approach for tissue engineering and biomedical applications. Studying cell behaviour becomes easier with small populations of cells, and small volumes significantly minimise waste when working with hazardous

biological materials. Since there is no direct contact between the liquid core and the underlying substrate bed, liquid marble bioreactors decrease the risk of contamination with biohazards.

Liquid marbles **(Figure 1.2)** also constitute a simple and effective method that does not require complicated equipment (except normal cell culture). In sum, the most significant properties of liquid marbles are permeability of the porous shell (which allows the possibility of gas exchange between the medium and the surrounding environment), non-adhesiveness of hydrophobic powder particles (which encourages cells to suspend in the medium and generate EBs and multicellular tumour spheroids more effectively) and a confined liquid core volume (which supports effective contact between cells). This has motivated efforts to exploit these advantages for living cell applications.

Figure 1.2: Preparation of Liquid Marble [152].

1.7 Tissue engineering and stem cells

Tissue engineering (TE) is a new technology that aims to produce or replace tissues and organs using combinations of cells, biomaterials, and biologically active molecules [155]. TE is an interdisciplinary field that combines biology, medicine and engineering in order to manipulate the biological functions of tissues in order to restore and replace injured tissues or organs and maintain normal tissue functions [15, 16]. The purpose of tissue engineering is also to develop novel and effective *in-vitro* biological methods and technologies that provide a better understanding of the normal function of tissues, in addition to functions similar to those found *in vivo* [156]. Therefore, the TE approach could revolutionise current therapies and significantly improve the quality of patients' lives.

TE started in 1933 when mouse tumour cells were transplanted into a polymer membrane and implanted into a pig's abdominal cavity. The cells remained viable for a long time without any rejection from the immune system [157]. Collagen or collagen-glycosaminoglycan (CG) composite sheets were used as a 2D means to culture cells and to generate a new skin during the late 1970s and 1980s [158, 159]. TE progressed to creating 3D structures composed of synthetic polymers to accommodate large cell numbers [160]. Interestingly, this discipline has only been defined in the last two decades, when Langer and Vacanti published an article that described how biological and engineering principles functioned to bring cells, biomolecules and scaffolding together to repair or grow new tissues [15]. The theory of construction of tissues in the laboratory seemed impossible. However, extensive studies have followed—for instance, the transplantation of a shaped human ear on to the back of a mouse opened a new way of thinking about generating new tissues [161].

Although significant advances have been reported [162-164], clinical applications have progressed much more slowly than expected. There are several difficulties associated with current implantation practice. The number of organs available for transplantation is far exceeded by the number of patients needing such procedures. Many tissues are not stored in banks and so supply problems exist and there is always a possibility of organ and tissue rejection.

The most important elements in the success of tissue engineering are expanding the cells of interest that are needed for biological functions and maintaining their normal phenotype, for instance producing an extracellular matrix, secreting cytokines and other signalling molecules, and interacting with neighbouring cells/tissues (as normal cell functions are considered indispensable).

In tissue engineering, biomaterials act as an artificial extracellular matrix (ECM) to replicate the biological and mechanical functions of native ECM. Thus, the biomaterials are designed to produce a microenvironment *ex vivo* for the generation of tissue-like constructs and regulation of cell function. In the promotion of tissue growth, biomaterials play important roles in producing the cell environment and giving mechanical support, leading to cell behaviour such as adhesion, proliferation, migration and differentiation. Biomaterials act as temporary mechanical supports for tissue to grow and for cells to undergo spatial reorganisation into tissues [15, 165].

1.8 Cell sources for cell therapy and tissue engineering approaches

1.8.1 Primary cells

Construction of an engineered tissue usually requires the use of cells to populate matrices. The source of donor tissue can be heterologous (such as bovine), allogeneic (same species, different individual), or autologous. Autologous cells are extracted from patients and then implanted into scaffolds under controlled culture conditions, delivering the resulting construct to the position wanted in the patient's body and directing the new tissue construct into the scaffold, which can be degraded over time [166, 167]. These cells have many advantages and are preferred over others because a biopsy can be obtained from the patient, expanded *in vitro* and then reimplanted in the same patient without any rejection from the immune system (avoiding side effects from immunosuppressive medications) [168]. Major advances have been to expand the use of several types of primary human cells to make it possible to use the autologous approach in clinical applications. However, the low proliferation of primary cells in the autologous approach limits their applications [168]. Although autologous cells are still used in tissue engineering as a type of primary cell, they have key drawbacks, including low yield and the probability of gene alterations associated with ageing. These problems have motivated researchers to develop or find an alternative source.

Stem cells can solve the problems encountered using primary cells released from explanted tissues. Stem-cell-based therapies are a promising tool to address the shortfall of tissue and organs in medicine [169, 170]. The potential uses of stem cells in tissue engineering and stem-cell-based therapeutics are well established. **Table 1.1** shows some of the common types of cells used in TE, which vary from autologous or allogeneic to differentiated to stem cell or progenitor origin, depending on the site where the seeding is required [171].

Table 1.1: Cells used in tissue engineering and cell therapy [171].

Cell type	**Human cell source, donor immunogenicity**	***Ex-vivo* manipulation and immunogenicity**	**Clinical experience**
Embryonic stem and progenitor cells	Embryonic tissue; tight ethical regulation, allogeneic, presumably with low immunogenicity	High expansion and differentiation capacity; potentially immunogenic culture supplements	Only preclinical studies (potential teratoma formation); require xeno-/ pathogen-free culture supplements.
Induced pluripotent stem cells	Autologous tissue biopsy (e.g. skin, fat, or muscle), require reprogramming	Limited expansion, but high differentiation capacity; epigenetic memory?	Only experimental and preclinical studies (potential teratoma formation)
Fetal, umbilical cord, and placenta-derived stem and progenitor cells	Aborted foetal tissue (e.g., foetal liver or marrow, umbilical cord, amniotic fluid and placental tissue)	High expansion capacity but unknown long-term risk of malignant formation; response to allergens?	Mostly preclinical studies; umbilical cord blood cells for cartilage
Adult stem and progenitor cells	Bone marrow aspiration, peripheral blood, adipose, and other adult tissues; usually autologous, but also allogeneic sources	Low to moderate risk of de-differentiation and unknown long-term risk of malignant transformation; potential immunological issues	Pulmonary valve and trachea (autologous EPCs/MSCs); acute GvHD (allogeneic MSCs)
Lineage-committed and differentiated adult tissue cells	Commonly tissue biopsy, but also peripheral blood; selection of cell types, autologous vs. allogeneic donor?	Limited expansion capacity; no immunogenicity expected but immune-response to allergens	Trachea; bladder; cartilage

1.8.2 Stem cells

Stem cells are pluripotent cells that are defined by two unique properties: they have the capacity to be self-renewing and they can generate differentiated cells by replicating themselves many times, by contrast with muscle, blood or nerve cells, under controlled conditions.

Stem cells can proliferate and produce a large number of cells in the laboratory. If these cells continue to be non-specific cell types with similar characters to those of parent stem cells, they are capable of long-term self-renewal. Stem cells are located in various areas of the human body, including the inner cell mass of the early embryo, some tissues of the foetus, the umbilical cord, the placenta and several other adult organs. The potential of stem cells was recognised in the late 1990s when pluripotent ESCs were isolated from early embryos and grown in the laboratory [172, 173]. One of the essential properties of stem cells is that they are not specialised. They can become specialised cells—including heart, muscle, blood and nerve cells— but they do not have any specific tissue structure with specific functions.

Differentiation of stem cells is a process in which unspecialised stem cells give rise to specialised cells through several stages. The degree of differentiation of stem cells to various other tissue types varies with the different types of stem cells. This phenomenon is referred to as plasticity. These cells can also be classified, according to their differentiation capacity, into totipotent, pluripotent, multipotent and unipotent stem cells (**Figure 1.3**).

Totipotent stem cells have the ability to differentiate into all specialised cell types in the body to generate a new embryo. These cells have the ability to develop a completely new embryo that can develop into a new organism. A fertilised egg is totipotent. None of the stem cells used in research appears to have this ability. Stem cells that are capable of differentiating into various cell types within the body are called pluripotent ESCs. These cells have the ability to form three germ layers consisting of the mesoderm (muscle, bone, etc.), ectoderm (neurons, skin, etc.) and endoderm

(hepatocytes, pancreatic beta cells, etc.). Multipotent stem cells can create different types of cells. However, they are limited to some tissues and organs. Hematopoietic stem cells are examples of multipotent stem cells that can differentiate into cell blood types, but not into brain or heart cells. Finally, unipotent stem cells can generate only one type of cell.

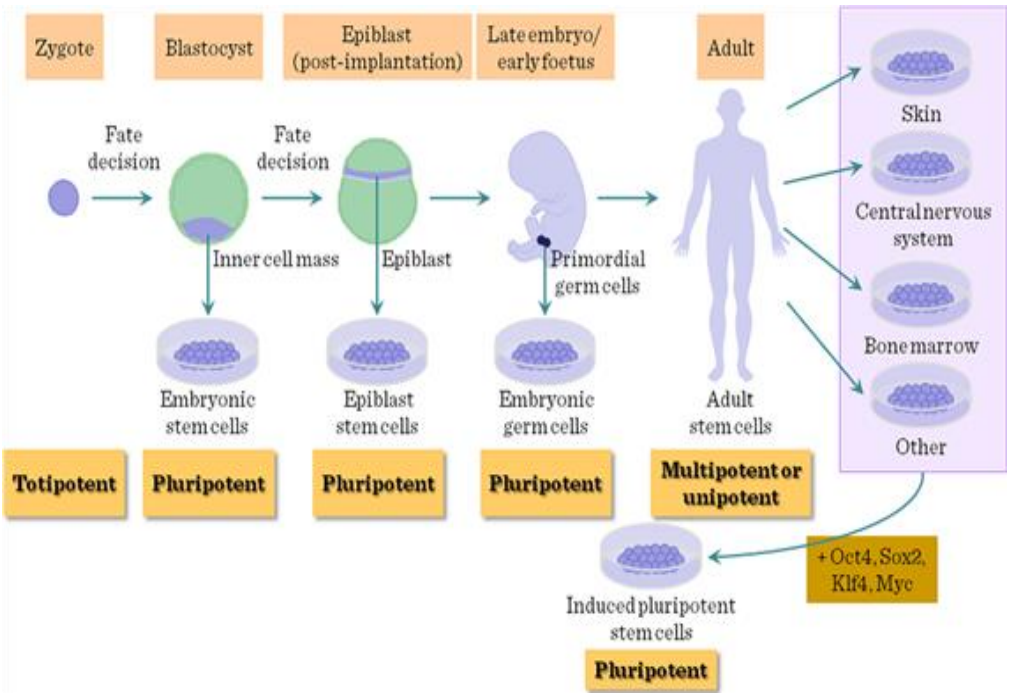

Figure 1.3: A schematic model of the origin of stem cells and reprogramming **[**182].

The unique properties of stem cells mentioned above mean that they offer many benefits in cell therapies, drug discoveries and tissue engineering [174-176]. Naturally, stem cells play a role in the human body by specifying the starting material for organs and tissues, as well as by their continuous maintenance, growth and renewal [177]. Due to their ability to generate a multitude of tissue types, stem cells have recently been considered as a primary cell source for tissue engineering, in which the focus is on developing alternative therapies for degenerative diseases and injuries by regenerating the damaged tissue and repairing their function in the affected individual. So far, the majority of the research has been carried out on two main groups of human and animal stem cells, including non-

embryonic (adult or somatic) stem cells and ESCs for stem cell therapy and tissue engineering. This is discussed in more detail in the next section.

1.8.2.1 Adult stem cells

Adult or somatic stem cells have been used clinically since the 1950s, when stem cells in bone marrow stroma and blood could rescue patients suffering from bone marrow failures [178]. These cells are an undifferentiated type of cells, found in different areas of the human body, including the bone marrow, skin, brain, liver, muscle and nervous tissues, as well as in the circulation [179] (as shown in **Figure 1.4**).

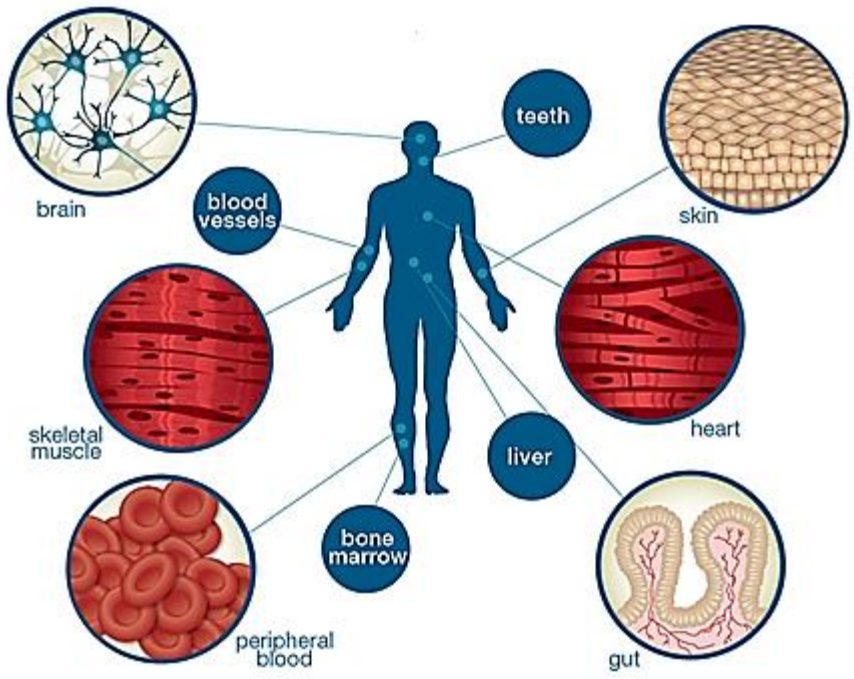

Figure 1.4: Locations of somatic stem cells in human body, Accessed in 2015 [180].

It was initially believed that stem cells were located only in the type of tissue that they generate. It was not expected that some components of blood were capable of developing an entirely different embryonic origin. For instance, the generation of muscle tissue and the development of neuron-like cells formed from stem cells in the bone marrow increased researchers' expectations about the ability

of hematopoietic stem cells (HSCs) to give rise to multiple cell types from all three germ layers [181-184]. For example, transplantation of hematopoietic stem cells (HSCs) into an irradiated mouse formed not only blood components (mesoderm layer), but also epithelial cells in the lungs, gut (endoderm layer) and skin (ectoderm layer) [184].

Adult stem cells can generate and replace old or damaged cells when they have been located (such as skin stem cells to generate new skin cells). However, their ability to differentiate is more limited than that of ESCs. Although ESCs can give rise to multiple lineages, adult stem cells are not pluripotent, and are less versatile compared to ESCs. The limitations of the use of adult stem cells and primary cells in tissue engineering are similar because of the difficulties in accessibility, low number of cells, limited differentiation potential and poor growth. The isolation and expansion of adult stem cells *in vitro* has been found to be challenging. However, these cells are still a promising strategy in stem-cell-based therapeutics to treat different diseases. By comparison with ESCs, they have not so far formed teratomas.

1.8.2.2 Embryonic stem cells (ESCs)

Tissue biopsy is a procedure used to extract cells from a patient's organ, and exists in the majority of existing tissue engineering strategies. However, there is insufficient generation of normal cells for many patients through tissue biopsy and it cannot be expanded from a particular organ (such as the pancreas). In this regard, ESCs are an alternative source of cell sources from which the desired tissue can be developed. ESCs are promising tools to enhance the understanding of normal development and disease for cell therapy applications, and to treat incurable and damaging disorders, including spinal cord injury, neurological disease, blindness and type 1 diabetes [185].

ESCs were initially derived from mice, and then from other species, including non-human primates and humans [172, 186]. These cells are isolated from the inner cell mass (ICM) of pre-implantation embryos after generation of the blastocyst, and cultured in the laboratory [18, 187]. Blastocyst

formation begins by the fertilisation of an ovum by a sperm, and results in a zygote, the earliest embryonic stage. Thirty hours after fertilization, the zygote starts to divide. By the 16-cell stage, the compacted embryo is termed a morula. The morula cells start to specialise by day three (E3.0) after fertilisation in the mouse and days five to six in humans, and forms a hollow sphere of cells called a blastocyst [188], as illustrated in **Figure 1.5**.

The outer layer of the blastocyst is called the trophoblast, and differentiates into the placenta and other tissues supporting foetus growth, whereas the inner cell mass develops into a foetus [18]. Pluripotent cells are derived from the inner cell mass and have the potential to proliferate *in vitro* and to maintain their undifferentiated state continuously while keeping the normal karyotype [18, 187, 189].

In addition, they have the ability to differentiate into all three somatic germ layers (mesoderm, ectoderm and endoderm), including cells of the hematopoietic [190, 191], cardiac [192, 193], endothelial [194] and neuronal tissues [195] under well-defined conditions *in vitro*. ESCs present certain advantages over somatic stem cells. They offer greater pluripotency and indefinite growth in culture [19, 196]. They give rise to a stable population of cells rather than a rare cell among other cell types, having been isolated from a relatively homogeneous population of cells within the ICM. Two main classes of ESCs—human and mouse embryonic stem cell—are discussed next.

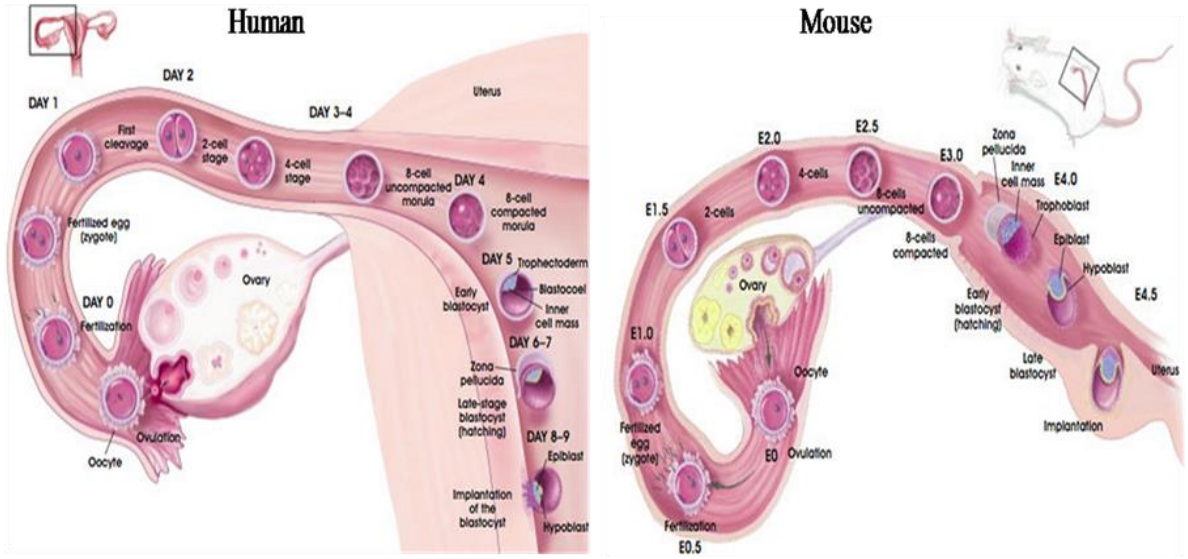

Figure 1.5: Pre-implantation blastocyst development in human and mouse [197].

1.8.2.2.1 Human embryonic stem cells (hESCs)

The first of the human ESCs derived in 1998 by Thomson and colleagues provided a tremendous boost to tissue engineering and stem cell biology [172]. These hESCs self-renew continuously under certain culture conditions. They also differentiate into cells representative of all three embryonic germ layers. Due to their properties, the discovery of hESCs marked the beginning of a new area of regenerative medicine and drug discovery.

Human ESCs have several distinct differences from murine ESCs. For example, hESCs have a slower proliferation rate (~24 h doubling times) and a flatter morphology. Cells are derived from embryos discarded from *in-vitro* fertilisation (IVF) techniques. They are also usually easy to dissociate into single cells, by contrast with murine ESCs (mESCs) [198]. Another differential property of hESCs is their ability to proliferate for more than two years while keeping a stable and normal complement of chromosomes. By contrast, mESCs need careful monitoring to note genetic mutations that occur over time.

Most hESCs obtained are grown on murine embryonic fibroblasts (MEFs) as feeder cells in media composed of Dulbecco's modified Eagle medium (DMEM) and serum replacement components that are not entirely free of animal ingredients. However, the feeder cells are inactive (i.e. they are not dividing and expanding) but still create the growth factors that sustain the ESCs.

One of the key concerns in tissue engineering is the need to grow human ESCs without any contamination by other cell lines or proteins. This problem, which was reported in January 2005, demonstrated the expression of a non-human protein when cell lines were grown on animal feeder layers [199]. Subsequently, different methods have been investigated to minimise the risk of the feeder layer, such as: adding a basic fibroblast growth factor to the culture medium [198, 200]; growing the cells on matrigel or laminin in feeder cell-conditioned medium [201]; or growing the cells in the presence of GSK-3-specific inhibitors such as 6-bromoindirubin-3´-oxime (BIO) [202]. However, all of these approaches are ineffective and at present it is not entirely possible to remove animal products. This problem in human embryonic cell culture still limits their applications in regenerative medicine.

More importantly, the potential use of human ESCs in regenerative medicine is at the centre of a cultural and religious ethical debate that varies by community. This is because different cultures and religious groups have their own ethical attitudes on the use of human ESC. For instance, in the UK, human ESC lines can only be derived legally under licence from the Human Fertilization and Embryology Authority, and the lines must be sited in the Medical Research Council's Stem Cell Bank. This is because the derivation of hESCs from embryos that are obtained from IVF procedures is not autologous. Therefore, the possibility of a patient's immune rejection is increased, which limits the efficacy of hESCs in clinical applications.

1.8.2.2.2 Mouse embryonic stem cells (mESCs)

ESCs were first established from the inner cell mass (ICM) of mouse blastocysts as cell lines in 1981 [18, 187]. Their development in mice starts with a single-cell zygote and results in a fairly complex structure—the blastocyst—with three distinct cell lineages. mESCs are characterized by a high proliferation rate and telomerase activity. It is thought that transcription factors play a key role in maintaining the pluripotent status of mESCs and their indefinite growth without resulting in genetic anomalies. For example, telomere shortening is prevented by KLF4, as the pluripotency transcription factor that controls telomerase reverse transcriptase (TERT) expression in mESCs [203].

The purpose of using non-human organisms as a model for human disorders is to recognise fundamental pathogenic mechanisms that provide a new way for developing novel therapeutic targets in order to evaluate the efficacy and safety of new drugs. Due to physiological, anatomical and genomic similarities between mice and humans, mice have historically been the most frequent model for the study of human diseases [204]. Mice have been used extensively as models in biological studies because mice and humans share approximately 99% of their genes and molecular pathways. Some of the other benefits of using mice are low costs, known age, known genetic background, easy handling and easy housing. Isolation of murine ESC lines provided biologists with a major tool. It was a simple model system to study the processes of early embryonic development and cellular differentiation.

It also paved the way for tissue engineering applications if similarly totipotent cells could be extracted from human blastocysts. Mice and humans have the same inherited diseases, such as heart disease, cancer, glaucoma, anaemia, hypertension, obesity, asthma and neurological disorders. Therefore, mice have become a good model for experiments to understand various diseases and discover new drugs for humans. Other animals share diseases with humans. However, mice are still the best model to address and cure human diseases because of their small size and low cost.

ESCs have the ability to differentiate into a wide variety of cell types. They also generate embryoid bodies, which contain three germ layers (ectoderm, mesoderm and endoderm) that can be used in a variety of experiments. *In vivo*, the evidence of pluripotency of mESCs is their generation of teratomas, which contain tissues originating from all three germ layers, after being transplanted in immune-deficient mice.

The possibility of inducing *in vitro* differentiation of ESCs into insulin-producing cells that can treat diabetes was explored. Transplantation of analogous mouse cells into mice that had diabetes resulted in the partial restoration of insulin regulation [205]. Furthermore, transplantation of mESCs into rodents with Parkinson's disease symptoms resulted in partial relief of these symptoms [206]. mESCs were also transplanted into animals with spinal cord injuries and partially renewed neural function [207].

Murine ESCs maintain their pluripotency in the presence of the cytokine Leukaemia Inhibitory Factor (LIF), but hESCs cannot [172]. The population doubling time of ESCs is about 12 hours, which is shorter than that of hESCs (24 hours). This could reflect the longer gestational period in humans than in mice.

If *in-vitro* culture of ESCs causes the production of a desired cell type, these cells can be tested for their potential to repair damaged or degenerating tissues. The ability to produce specific lineages from ESCs *in vitro* suggests that ESC-based cell replacement therapy might be possible for treating human degenerative diseases. However, the differences between hESCs and mESCs are still essential in clinical and human applications of ESCs [208]. Theoretically, an extensive range of human disorders could be treated using hESCs. The evidence supporting of this essential concept has principally been derived from the use of mouse ES cells.

The investigation of stem cell properties could be facilitated using systems of mESCs, because they are simple to culture, have a rapid growth rate, and can differentiate into multiple cell types. In addition, several specific factors that affect their self-renewal have been recognised. They can grow clonally. This allows many biological questions to be asked at the single cell level. The simple method of testing their pluripotency (using blastocyst injection) and the experimental accessibility to their tissue of origin lead to their ready availability to provide rigorous assays of their stem cell activity.

1.9 Embryonic stem cell application

Regenerative medicine, tissue engineering and bioengineering are new approaches in cell therapy. These methods allow researchers to generate and proliferate specific cells during the culture of different cells and tissues, and to investigate important functions that have changed in disease conditions. Thanks to ESCs' properties, ESCs have attracted considerable interest in the biopharmaceutical area for their use in drug discovery and cell replacement therapy. Progress in this area has created new potential in the studies of developmental biology, as well as in studies of gene functio on the level of the whole organism. All of this was accomplished after the isolation and identification of mESCs from mice [18, 187].

ESCs were isolated first from primates and then from human blastocysts; these cells were identified as promising sources for regenerative medicine and tissue engineering research [172, 186]. They could provide functional replacements for some diseased tissues—for example, Parkinson's disease or spinal cord injury [209, 210]. Adult and ESCs have provided materials for the development of regenerative medicine. However, ESCs exhibit many properties different from adult stem cells. An understanding of these properties could assist researchers in modifying adult stem cells to achieve better growth in culture and greater control of differentiation.

Due to their unlimited proliferation rate and pluripotency, ESCs have great potential in tissue transplantation, drug screening and cell therapy, as shown in **Figure 1.6**. Using ESCs in cell and organ transplantation has led to established treatments for a variety of diseases. ESCs are used in the development of the cell-based Alzheimer's disease screening assay, as well as in compound identification and optimisation [211]. Derivation of liver-like cells, from bone marrow and ESCs, is an alternative approach to liver transplantation, which is the only successful treatment modality for end-stage liver failure [212].

mESCs provide a valuable source of specific neuronal and glial cells for transplantation [213, 214]. ESCs can be differentiated into functional islet-like cells with the potential to rescue experimentally induced diabetes in mouse models [215]. Pancreatic endoderm produced from ESCs generated mature pancreatic cell types that functioned *in vivo* [216]. Both adult and embryonic stem have the potential to differentiate into appropriate cells for repair of damaged bones, cartilage and tendons [217, 218].

Using ESCs as models can improve protocols for the more successful application of ESCs in cartilage and bone tissue engineering. For example, mouse ESCs were used as a screening system to identify elements both required and sufficient for cartilage and bone generation [219, 220]. Moreover, differentiated ESCs were utilised for the evaluation of drug adsorption, metabolism and the toxicity of mutagenic, cytotoxic and embryo effects in toxicological studies [221, 222].

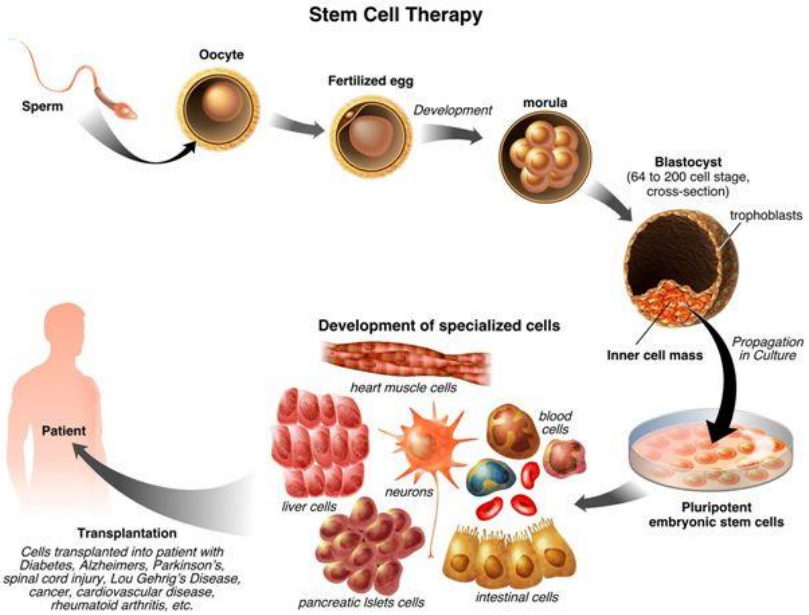

Figure 1.6: The potential use of stem cells in regenerative medicine, Accessed in 2015 [233]

An additional important potential of ESCs is their ability to differentiate into lung lineages, thus demonstrating a promising source for lung regenerative therapy because of their self-renewal capability. mESCs can also provide a novel approach for generation of infinite quantities of lung epithelial cells for lung repair.

1.10 Stem cell therapy

1.10.1 Mesenchymal stem cells for lung repair

Several studies have reported the feasibility of using mesenchymal stem cells (MSCs) cells to cure lung diseases. For example, mice were exposed to bleomycin followed by systemic MSCs administration, resulting in a major reduction in lung inflammation [223]. MSCs that were administered to animal models with acute lung injury/sepsis resulted in the animals having significantly greater survival, with less damage to the lung and less inflammation [224, 225]. The

administration of MSCs into damaged lung led to the discovery that some growth factors, such as keratinocyte growth factor and angiopoietin, can stimulate repair of the lung from injury. Moreover, delivering MSCs to animal models improved their survival and function in some sepsis-damaged organs such as kidney by producing circulating pro-inflammatory cytokines and chemokine levels , which has led to decrease bacterial inflammation [226, 227].

MSCs were also administrated to patients with moderate-severe COPD disease in the United States of America in 2008. The aim of the trial was to assess the safety of MSCs and to evaluate their efficiency in reducing the inflammation associated with disease. The outcomes were major reductions in the inflammatory marker C- reactive protein and improved quality of life for patients [228].

MSCs also produce anticancer agent(s), resulting reduced lung cancer [229, 230]. Airway and alveolar lung markers have been identified from embryonic and mesenchymal stem cells derived from umbilical cord or bone marrow [231-234]. For instance, when isolated MSCs from cystic fibrosis patients were co-cultured with those from airway CF patients, these cells give a rise to wild type CF trans-membrane conductance regulator (CFTR) and partly corrected defective CFTR-mediated chloride conductance, thus repairing the damaged CF cells,. This provided evidence for the potential of MSCs for therapeutic use [235]. In addition, mouse MSCs derived from bone marrow were pinpointed in the lung, provided a rise of airway and alveolar cell markers [236, 237]. Taken together, these studies suggest a bright future for the potential of MSC therapy for lung disease.

1.10.2 Embryonic stem cells for lung repair

Pluripotent ESCs (ESCs)—or induced pluripotent stem cells (iPS)—and endogenous pulmonary stem cells have been utilised in lung regeneration [238, 239]. iPS can be induced into forming definitive endoderm, and then, critically, airway and alveolar epithelium *in vitro* [240].

Growth factors, such as epidermal growth factor, retinoic acid and triiodothyronine, play a role in the differentiation of ESCs into lung epithelial cells [241]. Activin A induced ESCs to form lung epithelial cells [231]. ESCs have also been induced to form lung lineages by treatment with extracts of differentiated mature lung cells [242]. Rodents with acute lung injury (lipopolysaccharide injury) were treated by systemic injection with purified murine SPC-positive cells, but there was no resulting engraftment in the lung. Unpurified, differentiated ESCs showed only transient engraftment [243]. However, pulmonary epithelial cell delivery may be realistic, as shown in recent work using human ESC-derived AT2 cells in a bleomycin-induced lung injury model, in which hESC-AT2 cells engrafted in the lung after intra-tracheal delivery. They were then induced to differentiate into an AT1 phenotype, resulting in improved survival, reduced lung inflammation, fibrosis, and the generation of pulmonary epithelium—such as AT2 cells and airway epithelium—by several protocols [244]. ESC results can also be affected by the surrounding environment. For instance, ESCs can differentiate into lung epithelial when embryoid bodies are co-cultured with lung mesenchyma [245].

Differentiated human ESCs have several advantages for human health, including producing lung epithelial cells for treatment of pulmonary diseases and neurons for patients with Parkinson's disease. Furthermore, the potential of ESCs to differentiate into mature cells of all three germ layers makes them a promising tool for treatment of different diseases by controlling the differentiation of stem cells into linages of choice. For instance, if ESCs can be induced to differentiate into lung epithelial cells, they will assist in the therapy and treatment of patients with pulmonary diseases.

A schematic model showing endogenous, embryonic and adult stem cells that can contribute to lung development and repair [246] is illustrated in **Figure 2.7**.

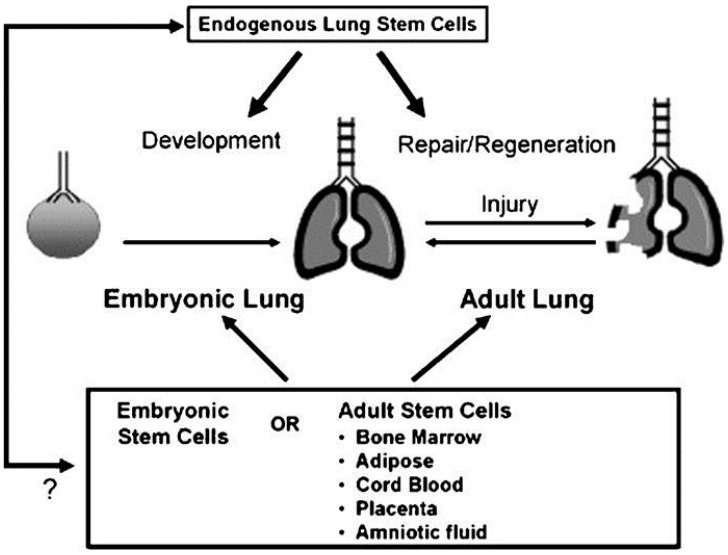

Figure 1.7: A schematic model showing the roles of endogenous, embryonic and adult stem cells in lung development, injury, repair and regeneration [246].

1.11 Stem cell delivery for pulmonary disease

Physical and life scientists have recently collaborated to discover novel routes for direct handling of living cells for precision placing or disposition in order to produce a viable microenvironment. A multicellular environment has many different applications in tissue engineering and regenerative medicine.

The tissues developed have been used, for example, for rapid wound healing. Several approaches have been used to deliver the cells, including ink jet printing [247], laser-guided cell writing [248], bio-electrospraying [249] and aerodynamically assisted bio-jetting [250]. Primary/immortalised embryonic and mesenchyme stem cells have been used in these processes. A jet-based technique was employed to process cell suspensions. This technique has received considerable attention due to its ability to direct cells in 3D architectures to generate functional tissue. Despite offering great promise, ink-jet printing and laser guided cell writing have some restrictions that prohibit their exploration.

These restrictions preclude the processing of concentrated multicellular suspensions and producing fine cell-bearing residues to the time taken for forming complex microenvironments [251]. Novel microfluidic technologies have been designed to overcome the drawbacks associated with these conventional techniques. Some of these technologies are discussed next.

1.11.1 Electrospraying

Bio-electrospraying function generates a monodispersed distribution of aerosol drops in the optimal size range. DC electrospraying has been used to produce aerosols of methylparahydroxybenzoate, which is an antibacterial and antifungal agent, as a preservative in pharmaceutical preparations, and of beclomethasone dipropionate, which is a glucocorticoid steroid used to treat allergies and asthma [252].

The procedure for electro-spraying is simply designed and consists of a liquid reservoir feeding into a capillary nozzle that is connected to a high-voltage source. This facilitates miniaturisation of the technology into a cheap and portable consumer device that has so far avoided the common problems of conventional nebulisation technologies.

Electrospraying or electrohydodynamic jetting is jet-based technology; the liquid suspension is charged using 1000 V and passed through a large-bore needle to be fragmented into drops [253]. Pioneering research has shown that suspensions of living cells can form micro-droplets with no effects on cell viability or phenotype, and electrospraying can generate finer droplets than others such as ink-jet printing and aerosol [249, 254]. Bio-electrospraying has been used to process mature cell types such as smooth muscle cells [255], kidney cells [256], lymphocytes [257] and neuronal cells [253] with more than 70% viability after one week of culture [255]. A few studies have attempted to electrospray stem cells [258]. A disadvantage is that, although bio-electrospraying forms fine cell-

bearing droplets and residues, the flow rate is low (approximately 6 mL/h). The advantage of this technique, however, is that it is an alternative and novel approach for cell handling.

1.11.2 Surface acoustic waves (SAW)

A surface acoustic wave is an acoustic wave that travels along a surface; the use of surface acoustic waves is an efficient approach for the generation of aerosol droplets [259, 260]. By contrast with electrospraying, SAW requires large voltages, similar to those of conventional ultrasonic atomisation, which requires bulky and cumbersome transducers necessitating tens of watts of power [261]. However, efficient fluid-structural coupling of SAW allow atomisation to be carried out with only 1 W of power, which is sufficiently small to be powered by small camera or watch batteries. Thus, an SAW nebuliser can be packaged into a low-cost compact portable format. An SAW device was used in an *in vitro* lung model by British Pharmacopeia; the SAW device yielded 70–80% lung dose efficiency for pulmonary delivery of the short-acting 2-agonist salbutamol®, an important improvement over the 20–30% efficiency obtained with currently available off-the-shelf inhalers [262].

The high frequency and low power of SAW play a significant role in minimising shear damage of drug molecules, both of which are serious concerns associated with the use of conventional ultrasonic transducers [263, 264]. SAW atomisation has also been employed to generate nanoparticles [265]. In this, the advantages of SAW devices is their ability to generate a large number of nanoparticles directly from the interfacial destabilisation and atomisation process, simultaneous particle generation and pulmonary delivery using the same micro-device can be carried out.

Protein particles of 50–100 nm can likewise be generated in this manner [266]. As this gives a one-step synthesis of nanoparticles and a device for direct pulmonary administration, it is a more attractive

method than other delivery pathways for protein and peptide delivery, given the low protolithic activity in the lung.

1.12 Tissue engineering for lung repair

Patients suffering from lung diseases are commonly treated using transplanted lung organs. However, the limited number of donors means that lung patients requiring organs die while waiting for transplants. Even if organs are available for transplants, the patients need lifelong use of immunosuppressive medications and these medications can interact with others, leading to complications. These problems focused attention on finding alternatives to organ transplantation, and thus tissue engineering was begun. Tissue engineering is the use of combinations of cells, scaffolds and other signals to construct living, functioning 3D tissues or organs [267].

The scaffolds for lung tissue need to be elastic, stretchable and compressible through inhalation. Ultimately, once new lung tissue has been generated, the scaffold should be degraded and the degraded scaffolds should not be toxic and disappear from the lung site. Many strategies have been developed to engineer lung tissue by utilising both natural and artificial polymeric scaffolds, including polyglycolic acid (PGA) polymer, Pluronic F-127 hydrogels [268], Matrigel [269] and Gelfoam [270].

Porous scaffolds with polyglycolic acid or pluronic (PF-127) were seeded with ovine somatic lung progenitor cells; once these had grown *in vitro*, they were implanted in the back of a nude mouse or into an ovine lung wedge resection site. PF-127 scaffolds implanted with somatic lung progenitor cells resulted in similar morphology to lung alveolar tissue but there was an inflammatory reaction as a response to the scaffold polymer. Despite this, these results hold promise for engineering distal lung tissue [268]. Alveolar-like structures were also achieved by using simple porous scaffolds [270]. In brief, foetal rat pneumocytes were seeded into gelfoam sponges and then injected into the healthy lung of a rat. Angiogenesis produced vascular structures in the sponges and these communicated with

native lung vessels; these results confirmed previous studies suggesting that native lung cells could generate a morphogenic lung structure [271].

Chen and co-workers obtained evidence of organised, ciliated, pseudo-stratified epithelium as well as presumptive developing alveoli by growing foetal rat pneumocytes on a collagen-glycosaminoglycan scaffold and seeded *in vitro* for up to 2 weeks [272]. Seeding foetal mouse pneumocytes on Matrigel for one week *in vitro* permitted the construction of alveolar structures, though these were not detected on poly-L-lactic acid (PLLA) or poly-lactic-co-glycolic acid (PLGA) matrices [273]. This indicated that stem cell culture in a 3D scaffold in medium conducive to lung epithelial development could provide an excellent environment for lung regeneration, much better than that accomplished with routine tissue culturing [273].

Coraux et al. in 2005 showed that ESCs seeded on different substrates such as collagen type I, collagen type IV, collagen type VI and gelatin in submerged cultures and air-liquid interface produced fully differentiated airway epithelium. At day 8, Clara cells were derived from cells grown on collagen type I with or without keratinocyte growth factor and retinoic acid; ciliated cells were obtained from ESCs grown on collagen type I after air-liquid interface culture. At day 15, Clara cells were obtained in other substrates [274]. This suggested that the structure and composition of the extracellular matrix were physiological requirements for these tissues [275].

In previous studies, the lung environment supported cell survival, and oxygen diffused through both natural and synthetic materials [276, 277]. Therefore the best matrix that can be used to support engineered lung tissue is decellularised matrix. Some limitations should be considered before selecting between natural matrix and decellularised matrix, though decellularised matrix may be degraded in the decellularisation process. Results obtained using decellularized tracheal matrix suggest that it may be the best matrix for lung regeneration in the future [278].

1.12.1 Hydrogels as extracellular matrix mimics for 3D cell culture

Although most knowledge in modern biology has been provided from classical 2D cell culture, cells reside, proliferate and differentiate in complex 3D microenvironments. Using 3D biodegradable scaffolds offers an alternative approach to finding an extracellular matrix (ECM) conducive to restructuring the cells, considered an important area of study in current tissue engineering.

Stem cells have unique functions; thus these cells need to reside in the specialised, 3D microenvironment that surrounds them in native tissues. The microenvironment components need to be positioned in their correct physiological and functional locations, since the interactions between those components are essential for the control of stem cell functions [279].

Several studies have demonstrated a role of the extracellular microenvironment (ECM) in controlling cellular behaviour [280-282]. A preferred scaffold with appropriate biochemical and biophysical signals can offer structural stability for developing tissues' cellular behaviour and function as well as providing a temporary platform for cell activities [283]. Because of the major role of matrix composition in ESC proliferation, differentiation and behaviour into specific lineages, extensive efforts have been devoted to producing biomaterials that behave more like natural extracellular matrix (ECM).

The similarities between hydrogels and natural ECM suggested that hydrogels would provide a 3D environment to cells in culture similar to that inside the body, and so is an attractive area for tissue engineering. Additionally, hydrogels have the best potential for allowing the proper diffusion of nutrients and waste to and from tissues due to their high water contents and so providing an ideal 3D platform for cell-cell and cell-material communications [284]. Hydrogels are defined as 3D stable networks of macroscopic dimensions formed from cross-linked hydrophilic polymers to form insoluble polymeric materials that have the ability to swell and retain large amounts of water [285].

Various special characteristics of hydrogels have been shown to guide and affect stem cell fate; these are their tuneable physical and chemical properties and spatially controlled distribution of bio-stimuli [286, 287]. As a result of offering highly hydrated 3D networks of polymers in which cells can attach, grow, proliferate and differentiate, hydrogel scaffolds offer interesting opportunities for cell delivery and tissue development. It is relatively easy to manipulate the mechanical properties of the hydrogel and so provide chemical signals to the cells through a combination of growth factors and mechanical signals. Currently, hydrogel scaffolds are being used in attempts to engineer a wide range of tissues such as cartilage, bone, muscle, fat, liver and neurons [288].

1.12.2 Biomaterials for synthesising hydrogels

Polymers are the most frequently used materials for tissue construction because of the ability to control their chemical and structural properties, and can be in general categorised into synthetically derived and naturally occurring polymers [289].

Greater understanding of the composition of the ECM in different stem cell niches has stimulated the production of synthetic materials and they are produced by the polymeriation of monomers with a wide range of properties. These materials offer advantages over natural ones but they also have limitations. Synthetic materials are inherently less bioactive but are mechanically strong and can be engineered with the desired macro- (shape) and micro-structure (pore size and porosity), as well as being modified to possess the desired bioactive properties that facilitate cellular growth and organogenesis in a biomimetic manner [290, 291]. The surface properties of synthetic polymers can also be engineered to suit specific functions and hence be more beneficial for tissue engineering applications. Moreover, degradation rate and mechanical strength are known for many synthetic polymers; hence degradation time should not change significantly between hosts.

The most popular synthetic polymer in the biomedical field is polyethylene glycol (PEG) due to its properties, which include biocompatibility, low immunogenic polymers, protein-resistance and good solubility in various solvents [292, 293]. Three dimensional degradable polyethylene glycol (PEG) and poly (lactic co-glycolic acid)/poly(l-lactic acid)-based hydrogels have been used in many studies for the maintenance and support of complex tissue structures, and for the formation of structures with the characteristics of neural tissues, cartilage and liver, in addition to a network of blood vessel-like tubules, and for the cultivation and differentiation of stem cells [294]. Moutos et al. in 2006 designed a 3D woven scaffold prepared from PGA to mimic the mechanical properties of a native articular cartilage [295]. In general, synthetic polymers are hydrophobic and mechanically strong and have slower degradation rates than natural polymers [283].

Polyacrylamide/acrylic acid copolymers and polyurethanes (PU) are examples of synthetic biomaterials with properties that can be highly modified to affect the behaviour of stem cells. Significantly, proteolytic sensitivity can be conferred in these materials by using small peptides with enzyme-specific cleavage sequences as cross-linkers in polymer synthesis [296]. Poly (acrylic amide) (PAAm), poly (acrylic acid) (PAA) and its derivatives, and poly (vinyl alcohol) (PVA) are synthetic polymers used for scaffold construction and have been approved by the USA Food and Drug Administration (FDA). PVA has been utilised in pharmaceutical and biomedical applications and controlled drug release tests, regeneration of artificial articular cartilage and for a hybrid artificial pancreas [297-299]. As implied by the term "synthetic", they are deficient in the biological components of the native extracellular matrix (ECM) [300, 301]. Moreover, during degradation of these polymers, weak acids could possibly be produced that could be toxic and cause an adverse reaction if they accumulate locally [302].

Biomaterials derived from natural sources are commonly applied materials in the earliest recorded cases of modern tissue engineering [303]. Collagen, fibrinogen, agarose, alginate, hyaluronic acid,

glycosaminoglycans (GAGs), hydroxyapatite (HA) etc. are examples of natural biomaterials being used in scaffold fabrication. These commonly consist of ECM components and therefore have the advantage of being bioactive, biocompatible and with mechanical properties similar to native tissue. The similarity between natural biomaterials and native extracellular matrix (ECM), permits the cells to interact with these polymers in a natural manner through receptors and signals, and to support the correct functioning of cells in attachment, growth, proliferation and differentiation. Agarose, alginate, chitosan, hyaluronic acid, gelatin, fibrin glue, collagen derivatives, and acellular tissue matrices are all natural materials that have supported ESC differentiation.

Polysaccharide and proteins are naturally derived polymers, are potentially recognised by the cells and support cell development. The use of polysaccharides for the fabrication of hydrogels is valuable not only from a biomimetic prospective but also from a scaffold-processing perspective. These polysaccharides have hydroxyl groups and carboxylic acid groups as abundant functional groups, and so are amenable to various types of chemical modifications. This composition offers the possibility of introducing cross-linkable, cell-specific ligands, or extracellular signalling molecules, such as peptides and oligosaccharides, into the polysaccharide precursors of hydrogels that accelerate tissue reorganisation. Collagen, hyaluronic acid (HA) and alginate are natural polymers being used for tissue engineering to improve surface chemistry and to support cell growth and differentiation of embryonic/adult stem cells as a natural polymers [284]. Fibrinogen, fibrin and hyaluronic acid (HA) are other examples of derived natural materials introduced for producing 3D scaffolds, mESCs differentiation, cellular behaviour and cell signalling [304, 305]. Hyaluronic acid hydrogels have been employed to maintain the pluripotency and undifferentiated state of hESCs, after which these cells could be differentiated into specific lineages by adding soluble factors into the scaffold [306].

HA has also been applied in a nano-structured self-assembling peptide scaffold to stimulate osteogenic differentiation of mESCs [307]. However, although fibrinogen, fibrin and HA are available commercially, they are usually very costly.

Alginate is a natural polysaccharide that has been used in a wide range of applications, including cell encapsulation and drug, antibody and growth factor delivery, due to its biocompatibility and low toxicity [308, 309]. Alginate has been used for cell encapsulation and differentiation of both hESCs and mESCs [310]. For example, after encapsulation of mESCs in alginate polyl-lysine (PLL), cells retained their ability to proliferate [311]. Porous alginates as 3D matrices have also been associated with enhanced proliferation of embryonic, mesenchymal and neural stem cells [284]. Indeed, alginate is considered to have the simplest as well as the most biocompatible gelling process; however, its lack of bio-active moieties and lack of diverse modifications limit its practical applications [312]. Furthermore, degradation of alginate causes loss of divalent ions into the surrounding medium, discourages protein adsorption and is uncontrollable and unpredictable, and so it is not the best biomaterial option [288].

Cellulose is a natural polysaccharide, consisting of glucose repeating units. Because cellulose and its derivatives can be degraded by microbial or fungal enzymes in nature, it is regarded as an environmentally friendly component. Cellulose is biocompatible and inexpensive [313, 314]. An early result with liver cells demonstrated superior adhesive properties of cellulose-based materials compared to most polymer surfaces [315]. Several studies have reported the applicability of cellulose-based materials for culturing cells and for implantation, such as for bone regeneration [316], hepatocyte culturing for an artificial liver [317], and expansion of progenitor hematopoietic cells in culture [318].

Cellulosic materials are desirable materials for tissue engineering applications because they are renewable, inexpensive, biodegradable, photo-cross-linkable, easy to functionalise, biocompatible to most stem cells, and have mechanical properties similar to those of soft tissues and organs. Moreover, cellulose-based materials have very low water solubility, therefore allowing for better control over scaffold design in pharmaceutical and biomaterials applications. These materials can be degraded and the products are water-soluble in the body and so disappear from the site where they have been implanted. Hydrogen bonds from the hydroxyl groups hold the cellulose chains together, and account for the high degree of crystallinity, low solubility and poor cellulose degradation *in vivo* [314].

Hydroxypropylcellulose (HPC), carboxymethycellulose (CMC) and hydroxypropylmethyl cellulose (HPMC) are commonly used cellulose derivatives [319]. HPC has been approved by the US Food and Drug Administration (FDA) as an agent for drug delivery. It is soluble in water and many organic solvents, and available abundantly at low cost, and this partly contributed to its use in biomedical and pharmaceutical applications. In addition, HPC has desirable properties such as biocompatibility, biodegradability and cell-responsiveness, which leads to its use as a hydrogel for tissue engineering applications.

Generally, materials derived from natural sources are advantageous due to their inherent properties of biological recognition, including presentation of receptor-binding ligands and susceptibility to cell-triggered proteolytic degradation and remodelling. By contrast, common disadvantages of natural polymers include variations in degradation rate, batch-to-batch inconsistency and poor mechanical strength [300, 302, 320]. Biomaterials play a significant role in cell behaviour. Most important, the scaffold must be biodegradable. Biodegradability of polymers is one of the most important factors in pharmaceutical and biomaterials, and is needed for functional clinical applications, because after implantation the scaffolds must be degradable by the body and changed by native tissue to replace the dying cells and so restore the original function. Therefore, scaffolds should support cell growth and

differentiation. Furthermore, they must be degraded into metabolites that do not have any toxicity effects or immunogenic responses.

Three dimensional scaffolds could collectively play an important role as *in-vitro* models to expand our knowledge about fundamental aspects of tissue biology or to generate systems for drug and cosmetics screening [321]. In this regard, the most common compositions of extracellular matrix *in vivo* include collagen, non-collagenous glycoprotein, amino-polysaccharides and proteoglycans, and elastin. For synthetic scaffolds to replace these, their biocompatibility has to be raised.

1.13 Outline of Thesis

This thesis is presented in a "thesis by chapters" format. Each chapter contains a brief introduction, relevant methods, results, and discussion. The outline of the present PhD thesis is as follows:

Chapter 1 gives a general introduction, an introduction to gene therapy, miRNAs and their therapeutics for cancers, information about stem cell types, stem-cell-based tissue engineering and their applications for different diseases, including lung tissue ailments and this thesis outline.

Chapter 2 provides a summary of the general materials and experimental methods used in this thesis.

Chapter 3 describes the potentially therapeutic use of miR-126 PEI nanoparticles for lung cancer spheroids. In addition, this chapter describes a novel application of liquid marbles in the formation of 3D structures inside liquid marbles made of polytetrafluoroethylene powder and cell culture medium. Liquid marbles are shown to be capable of accommodating A549 cells in a convenient growth condition. A case study is then conducted and includes an investigation of miRNA-126 PEI nanoparticle treatment for those spheroids.

Chapter 4 describes the rapid enhancement of multi-cellular spheroid assembly by acoustically driven micro-centrifugation. In this chapter, the ability of surface acoustic devices to generate multi-cellular spheroids that can be used in *in-vitro* experiments is examined. The advantages of this method over existing technologies are mentioned. The high efficiency of the method is highlighted. Finally, the potential of spheroids that are formed using SAW microfluidic devices for further applications is explored.

Chapter 5 describes SAW nebulised delivery of stem cells for the potential treatment of lung disease. In this chapter, a novel device constitutes an attractive tool for the delivery of stem cells via inhalation for treatment and repair of lung function.

Chapter 6 describes stem cell differentiation in hydrogel for lung tissue regeneration. In this chapter, a novel 3D scaffold is developed as an extracellular matrix, and used for the immobilisation of ESCs to allow them to differentiate into lung epithelial cells in air-liquid interface (ALI) conditions, for eventual injection into damaged lung to replace dying cells.

Chapter 7 discusses the major findings and recommends the scope for further exploration of these approaches to repair other organs.

CHAPTER TWO-General Materials & Methods

This chapter describes general methods used in this study. Specific methods are described in the relevant chapters. All materials used in this study are also listed in the appendixes.

2.1 General Procedures

All of the glassware used to store solutions was washed using Pyroneg® detergent and rinsed in tap water, with a final rinse in deionised water (dH_2O). All of the glassware, micropipettes, solutions, pipette tips and Eppendorf tubes were sterilised by autoclaving at standard conditions (121°C for 20 min) before being used. Solutions were prepared in dH_2O filtered through a Millipore Milli-Q® water system (Liquipure), unless otherwise specified. Small volumes of the solutions were dispensed with micropipettes from Finnpipette (Eppendorf Pty Ltd., Australia), using pipettes with ranges of the following volumes: 200 µL–1 mL, 20 µL–200 µL, 2.0 µL-20 µL, 0.1 µL–10 µL, and 0.1 µL–2.5 µL. Sodium hydroxide (NaOH) and hydrochloric acid (HCl) used to adjust pH were AnalaR grade or higher. Chemicals, consumables, software, reagents, commercial kits, antibodie, and common equipment'used during this study are itemised in the appendixes.

2.2 Solution Preparation

2.2.1 Phosphate-Buffered Saline (PBS)

One tablet of PBS was dissolved in 100 mL of dH_2O and sterilised by autoclaving under standard conditions.

2.2.2 Ethanol 70%

Ethanol 96% (74% v/v) was diluted with sterile dH_2O.

2.2.3 Tris-Acetic Acid-EDTA (TAE) Buffer (50X)

TAE buffer was prepared by dissolving a mixture of glacial acetic acid (5.17%, w/v), EDTA (1.86%, w/v) and Tris-base (24.2%, w/v) in sterile dH_2O, and diluting to 1X before use.

2.2.4 Agarose Gel Electrophoresis

2.2.4.1 Preparing Agarose Gel

For RNA or DNA gel electrophoresis, agarose powder (1.5%, w/v) was dissolved in 1X TAE buffer and boiled until completely liquefied. The prepared boiled agarose was allowed to cool on a shaker to reach approximately 55°C. It was then poured into a casting tray and allowed to solidify for 30 min before use.

2.2.4.2 DNA Loading Preparation

One volume of 11X loading dye was added to 10 volumes of cDNA sample and mixed with gel electrophoresis.

2.2.4.3 Electrophoresis

The mixture of RNA or cDNA samples and loading dye were loaded into the prepared gel wells. Electrophoresis was at 80 V for an appropriate time period.

2.2.4.4 Agarose Gel Staining

The RNA or DNA gel was stained in ethidium bromide solution with a concentration of 1 mg/mL for 10 min. The gel was then rinsed with tap water for at least 15 min before viewing.

2.2.4.5 Visualisation of RNA & DNA

RNA or DNA bands in the gel were visualised using ultraviolet (UV) light, and photographed using the Gel-Doc System (Biorad).

2.3 PEI Stock Solution Preparation (10 mg/mL)

The polyethyleneimine powder was dissolved in sterilised dH_2O. The pH of PEI solution was adjusted to 7.0 with HCl. The solution was then sterilized using 0.22 µm membrane, and stored at 4°C.

2.4 Preparation of Buffers for Mouse Embryonic Stem Cells (mESCs)

2.4.1 Gelatin Preparation (0.1%)

Gelatin (0.1%) was prepared by diluting 5 mL of 2% gelatin stock in 95 mL of sterilised phosphate buffer solution (PBS), filtered through a 0.22 µm membrane, aliquoted and stored at 4°C.

2.4.2 Collagenase Type I Solution (100 U/µl)

Collagenase type I was prepared by dissolving 1 g of collagenase powder in 1 mL Hank's salt solution (HSS). The solution was sterilised by filtration through a 0.22 µm filter, aliquoted and stored at -20°C.

2.4.3 Human/Mouse Activin A Stock Solution (50 µg/mL)

Activin A was prepared by dissolving 50 µg in 1 mL of 0.1% BSA/PBS, filtered through a 0.22 µm membrane, aliquoted into sterile Eppendorf tubes and stored at -20°C.

2.4.4 Mouse Wnt3a Stock Solution (40 µg/mL)

Wnt3a solution was prepared by dissolving 40 µg in 1 mL of 0.1% BSA/PBS, filtered through a 0.22 µm filter, aliquoted and stored at -20°C.

2.4.5 L-Ascorbic Acid Stock Solution (5mg/mL)

The L-ascorbic acid solution was prepared by dissolving 5 mg in 1 mL cold TC-H_2O and vortexing periodically until completely dissolved. The solution was sterilised by filtration, aliquoted and stored at 4°C.

2.4.6 Mono-Thioglycerol Stock Solution

Mono-thioglycerol was prepared by diluting 32 µL of 1-thioglycerol in 100 mL sterilised phosphate buffered solution (PBS). The stock solution was diluted immediately to the final working concentrations before use.

2.4.7 Heparin Sulphate Salt Solution (1 µg/mL)

Heparin sulphate salt powder (1 µg) was dissolved in 1 mL sterile dH_2O and filtered, aliquoted and stored at 4°C.

2.4.7 Preparation of Growth Factor (F0291)

Growth factor F0291 was reconstituted by dissolving 25 µg in 1 mL filtered 20 mM Tris, pH 7.0, aliquoted into sterile Eppendorf tubes and stored at -20°C. The stock solution was diluted immediately before use to the final working concentration.

2.5 Preparation of Buffer Solutions for Immunofluorescence Assays

3.5.1 Bovine Serum Albumin (BSA) solution (1%)

BSA was prepared by dissolving 1 g of BSA in 100 mL sterile phosphate buffer solution (PBS) and stored at 4°C.

2.5.2 Tween-20 (0.05%)

Tween-20 solution was prepared by diluting 50 µL Tween-20 in 100 mL sterilised phosphate buffer solution and stored at room temperature.

2.5.3 Triton -100X (0.5%)

Triton-100X was prepared by diluting 0.5 mL in 100 mL sterilised phosphate buffer solutions (PBS) and stored at room temperature.

2.5.4 DAPI Solution (1µg/mL)

DAPI powder (1 µg) was dissolved in 1 mL sterilised dH_2O, protected from the light, and stored at -20°C.

2.6 Inactivation of Foetal Bovine Serum (FBS)

The following procedure was performed to extinguish heat-labile complement prior to using FBS in a tissue culture cell line medium. An FBS (500 mL) bottle at -80°C was thawed at 4°C overnight. The following day, the FBS bottle was incubated in a water bath at 37°C until it thawed completely. The bottle was aliquoted into conical 50 mL tubes, which were incubated in a water bath at 56°C for 30 min. The tubes were removed from the water bath and allowed to cool down at room temperature for one hour. The FBS tubes were stored at -20°C and FBS was through a 0.22 µm membrane before use.

2.7 Cell Culture Techniques

All procedures for tissue culture were performed in a biological safety cabinet Class II to reduce the risk of contamination. All solutions and buffers were sterilised twice by autoclaving. All materials were wiped with 70% ethanol and sterilised with ultraviolet light for 20 min before use in the experiments.

All tissue culture media, non-essential amino acids, and TrypLE™ select enzyme were stored at 4°C. Foetal bovine serum (FBS), 0.05% trypsin-EDTA, growth factor supplements and penicillin-streptomycin were stored at -20°C unless specified otherwise.

2.7.1 Cell Culture Growth Conditions

All tissue culture protocols were performed carefully using sterile techniques with clean, detergent-free, sterile glassware. Before use, media and solutions were pre-warmed at 37°C in a water bath. All cell lines were routinely seeded in 25 cm^3 or 75 cm^3 tissue culture flasks, six-well microtitre plates or in 35 cm^2 area Petri dishes containing the appropriate medium.

Cell cultures were incubated at 37°C with 5% CO_2 overnight before being used in an experiment. The cell cultures were regularly tested and confirmed to be mycoplasma-free using a Mycofluor Detection Kit. No mycoplasma infection was identified in any of the cell cultures during the work in this thesis.

2.7.2 Cell Lines

Cell lines used in this project were lung cancer cells (A549), breast cancer cells (BT474), rat mesenchymal stem cells and mouse embryonic stem cells (E14TG2A). Cell cultures were monitored visually with an inverted phase-contrast microscope and each cell line was cultured as described in the relevant chapter.

2.7.2.1 Cell Counting

Cells were quantified using a Countess® Automated Cell Counter (Invitrogen, Australia) according to the manufacturer's protocol to determine the total number of cells and their viability. In brief, 10 µL of cells in suspension was added to 10 µL of 0.4% Trypan blue dye and 10 µL of this mixture was loaded into a counting chamber.

2.7.2.2 Cryopreservation of Cell Lines

Lung cancer cells A549, breast cancer cells BT474, rat mesenchymal stem cells (MSCs) and murine embryonic stem cell (E14TG2A) pellets were resuspended to a concentration of 2×10^6 cells/mL in freezing medium containing 30 % (v/v) FBS and 1% (v/v) penicillin/streptomycin or gentamicin and 10% (v/v) dimethyl sulfoxide (DMSO). Cells were aliquoted to polypropylene cryovials, stored at -80°C overnight in an isopropanol chamber and then placed in liquid nitrogen (-196ºC) for long-term storage.

2.7.2.3 Thawing Cell Lines

Frozen cells were removed from liquid nitrogen, sprayed with 70% ethanol and transferred to 10 mL tube containing complete medium. Cells were centrifuged for five minutes. The supernatants were aspirated and each cell pellet was resuspended in 1 mL of growth medium and then reseeded into 75 cm^2 tissue culture flasks.

CHAPTER THREE

Liquid marble micro-bioreactor for miRNA transfection

3.1 Introduction

Liquid marble (LM) is a soft solid-like droplet made from encapsulating aqueous liquid droplet with hydrophobic powder [322]. The flexible powder shell of LM allows the droplet to be split and merged, as well as allowing liquid to be introduced into or extracted from the LM. The unique properties of LM can be utilised to control chemical and biochemical reactions that occur within LM, making LM an attractive reactor vessel [154]. LM can act as a miniature bioreactor; with its non-adhesive shell promoting cell-to-cell interaction, thereby facilitating the formation of spheroids from cancer cells as well as the formation of embryoid bodies from ESCs [151, 153, 154]. Cancer spheroids are well regarded as *in-vitro* models for the evaluation of drugs, as the cell-cell and cell-extracellular matrix (ECM) interactions within three-dimensional (3D) spheroids better represent the *in-vivo* microenvironment than in conventional monolayer cultures. Compared with monolayer cultures, 3D spheroids allow longer observations periods, which is advantageous for studying time-dependent gene expression resulting from non-viral gene delivery vectors. In particular, this applies to polymeric gene delivery systems, which release genes slowly after their delivery inside cells or tissues [323].

MiRNAs are collectively a class of non-coding RNA; they consist of 20 – 25 nucleotides that function as gene regulators by cleaving and/or inhibiting the translation of target messenger RNA (mRNA) [4], as well as simultaneously regulating a broad set of genes of interest [5]. Due to their ability to trigger synergistic therapeutic effects in cancer, miRNAs have recently emerged as a new class of cancer therapeutic. MiRNAs are also involved in many cellular and physiological processes, including differentiation, proliferation and the maintenance of metabolic homeostasis [324-326].

Many applications of miRNA require miRNA to be transfected into cells. However, the use of miRNAs is limited due to their poor stability and integrity. Naked miRNAs are susceptible to nucleases and are often degraded in serum prior to transfection. In addition, miRNAs are expensive and are usually present in only small quantities. Many strategies have been devised to improve the transfection efficiency of miRNAs; for example, nanoparticle carriers are often used to deliver miRNAs [5]. However, little attention has been paid to developing and improving the vessel or 'reactor' where the transfection 'reaction' occurs.

In this study, the use of LM as a miniature reactor to generate an *in-vitro* tumour model, namely a cancer spheroid, was investigated, and its use as a miniature reactor to enhance miRNA transfection was evaluated.

3.2 Methods

3.2.1 Cell culture

The human non-small cell lung cancer line A549 was obtained from cryostored stocks in the School of Medical Sciences, RMIT University, and routinely cultured in RPMI 1640 medium containing 10% fetal bovine serum (Gibco, Australia) at 37°C in a humidified atmosphere containing 5% CO_2.

3.2.2 Generation of lung multicellular spheroids

LM micro-bioreactors containing human lung carcinoma cells (A549) were prepared according to previous protocols [151, 153]. In brief, a 300 μl drop of cell suspension was placed on a polytetrafluoroethylene (PTFE) powder bed and was swirled gently until a marble was formed (**Figure 3.1**). Cells were allowed to further incubate inside LM for another 7 days to obtain cancer spheroids. As a control, cancer spheroids were prepared using a liquid suspension (LS) method, in which A549 cells were allowed to aggregate to form spheroids in ultra-low attachment 96-well plates

(Corning® Costar®). In addition, an LM array was generated for use in different assays, as shown in **Figure 3.2**. Samples were taken from the LM at different times and compared with the control.

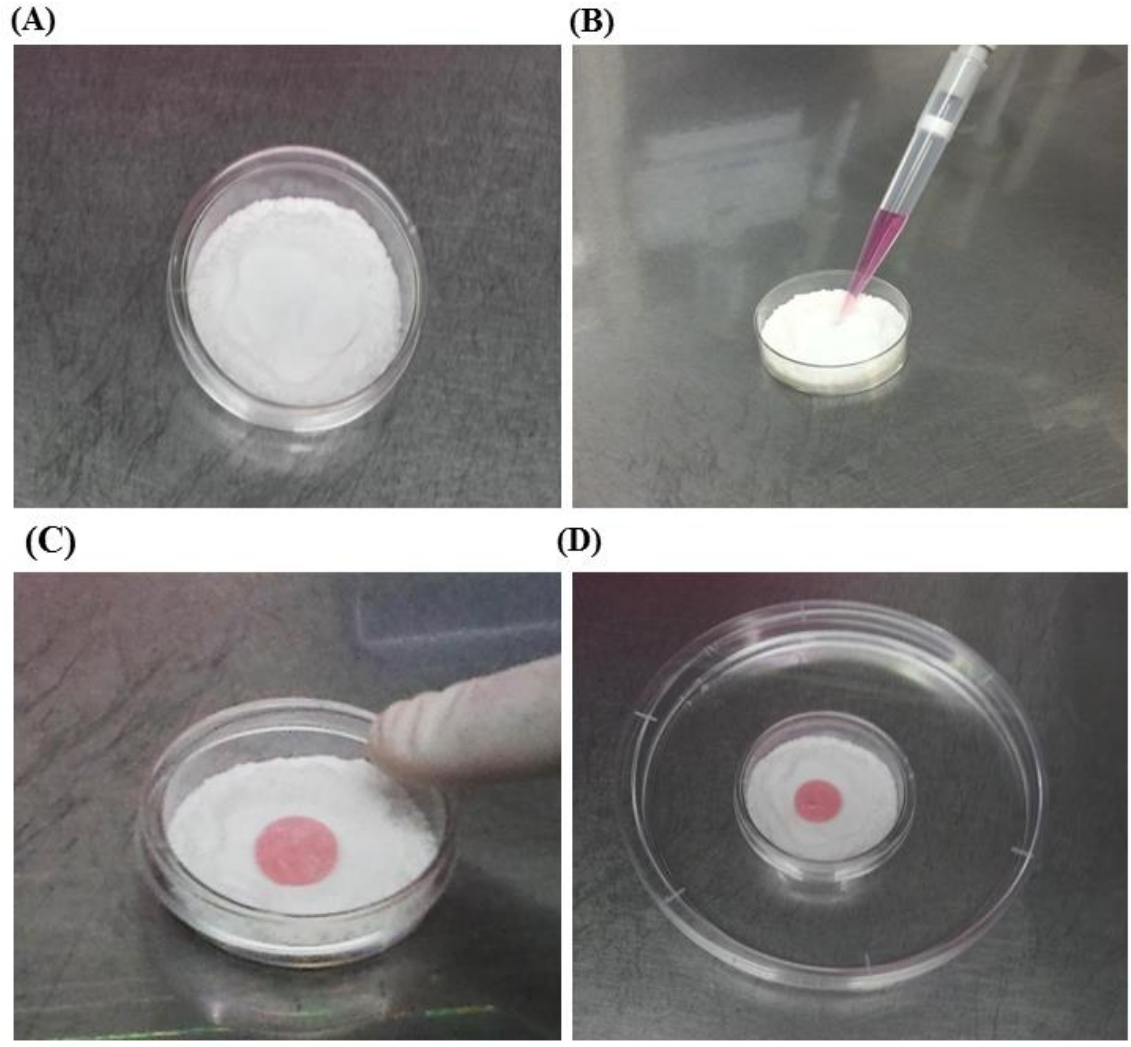

Figure 3.1: Preparation of lung spheroids using liquid marble. The liquid containing the suspended A549 cells in the growth medium was placed on the hydrophobic powder bed where the liquid beads up due to the high hydrophobicity of the powder. The drop was then rolled on the powder bed to cover it with the hydrophobic powder. The Petri dish containing the resulting liquid marble was then placed inside a second Petri dish that was half filled with sterile water and incubated at 37ºC for 7 days.

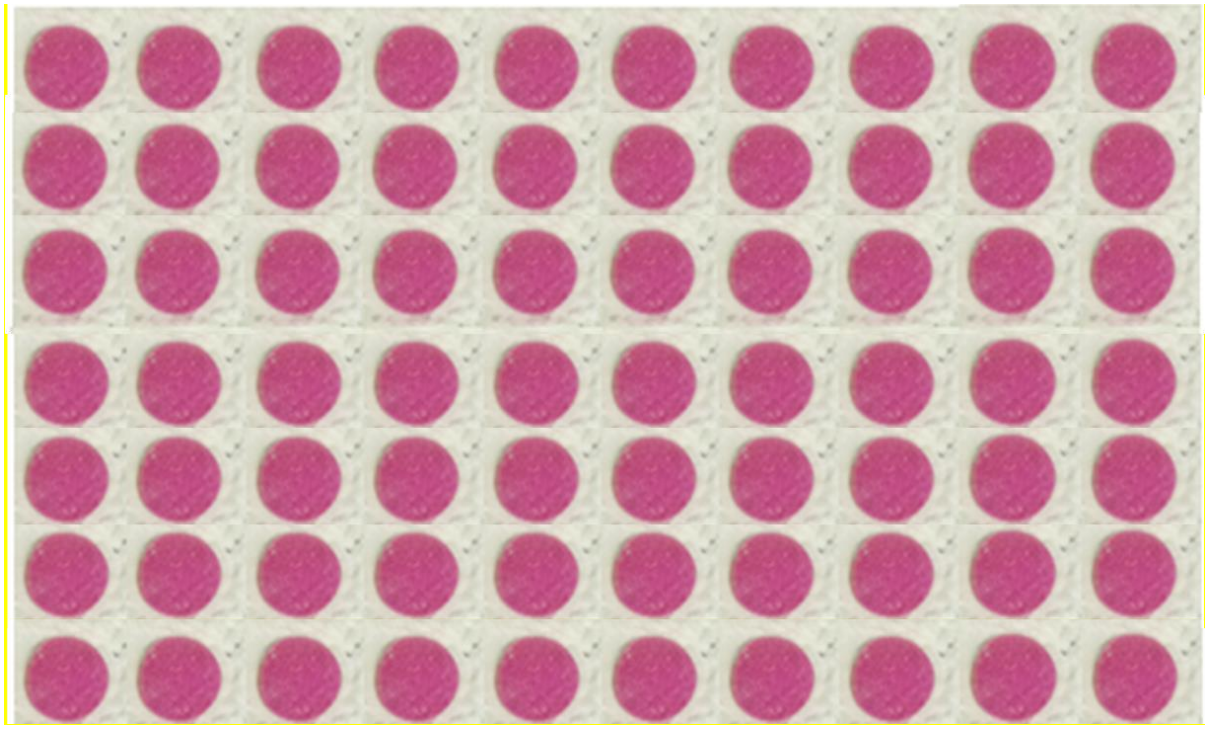

Figure 3.2: Liquid marble array for different assays.

3.2.3 Spheroid viability and morphology

A Live/Dead cytotoxicity kit (Life Technologies) containing Calcein-AM and propidium iodide (PI) was used to evaluate the viability of lung multicellular spheroids [327]. Liquid marble containing 10^5 cells/ ml was formed and incubated by adding 50 µl fresh medium every 2-3 days; liquid suspension cultures served as controls. Seven days later, spheroids were collected from the liquid marble and placed in a new Petri dish with a diameter 35 mm, and stained with Calcein and PI. Dead cells were imaged by the inclusion of the PI fluorophore in the medium. Images of live (green) and dead (red) cells were acquired by laser confocal fluorescence microscopy (Nikon A1R) using a Nikon Eclipse Ti Fluorescence Microscope.

The diameter of the spheroids was measured using ImageJ (National Institutes of Health, Bethesda, MD). The irregularity parameter *IP*, defined as the ratio of the diameter of the minimum circumscribed circle *D* to that of the maximum inscribed circle *d*, i.e. $IP \equiv D/d$ [328], was used as an

indicator to evaluate the circularity of a spheroid; an *IP* with a value of 1 indicates a perfect circle, whereas a larger *IP* value indicates that the spheroid exhibits irregular morphology [328].

3.2.4 Complexation of PEI and miR-126

MiR-126 with the sequences 5' UCGUACCGUGAGUAAUAAUGCG '3 and 5' CAUUAUUACUUUUGGUACGCG '3 [329] was employed as a model drug. To protect the miR-126 from nuclease degradation in serum, anionic charge miR-126 was complexed with either cationic charge Lipofectamine® RNAiMAX transfection reagent or cationic charge linear polyethylenimine (PEI, MW 25,000) at a Nitrogen/Phosphate (N/P) ratio of 33:1 to form nanoparticles via polyelectrolyte interaction. PEI and lipofectamine both served as delivery vehicles to protect miRNA against degradation by nucleases in serum.

PEI/miR-126 complexes were prepared essentially as described previously for siRNAs [330, 331]. In brief, 1 µg miRNA was dissolved in 75 µL 10 mol/L HEPES/150 mmol/L NaCl, pH 7.4, and incubated for 30 minutes on ice. Ten microliters of PEI (4.3 µg/µL) was dissolved in 75 µL of the same buffer, and after 10 minutes, pipetted into the miRNA solution. This resulted in an N/P ratio = 33, which was previously determined as optimal for siRNAs [330].

3.2.5 Measurement of size and charge of particles

Size and charge of miR-126 containing PEI were measured using a Zetasizer Nano ZS (Malvern Instruments, Malvern, UK). The samples for testing were prepared in triplicate and measured at 20°C. The surface charge of miR-126 containing PEI nanoparticles was measured using its Zeta potential in triplicate. Malvern software was used to calculate the Zeta potential and the mean ± standard deviation was calculated.

3.2.6 Transfection of mature miR-126 containing PEI nanoparticles

Lung cancer spheroids were formed using liquid marble and liquid suspension methods in RPMI 1640 medium supplemented with 10% FBS. The monolayer cells and multicellular spheroids were incubated at 37°C in a humidified incubator atmosphere containing 5% CO_2 overnight. The next day, Opti-MEM® I reduced serum medium was added along with miR-126 nanoparticles and lipofectamine and incubated for 24 hours; miR-126 delivered by Lipofectamine® RNAiMAX Transfection Reagent was used as a positive control. Transfection of miR-126 via Lipofectamine® RNAiMAX Transfection Reagent was performed according to the manufacturer's protocol. In brief, 4.5 µl of lipofectamine was mixed with 75 µl Opti-MEM medium and incubated for 10 min. Then 1 µg of miR-126 was mixed with 75 µl Opti-MEM medium. Diluted lipofectamine was added to diluted miR-126 and incubated for 5 min at room temperature. Ten microlitres of mature miR-126 lipofectamine 2000 complex was added to 100 µl of monolayer and spheroid cultures by following the same procedure as for miR-126 PEI nanoparticles. Untreated cells treated with scrambled miRNA precursor with no target transfected with PEI and lipofectamine 2000 served as a negative control.

3.2.7 Measurement of VEGF-A protein expression

Immunofluorescence staining was performed on monolayer and spheroid A549 cells to detect total VEGF-A. Spheroids were collected from liquid marble by pipetting into Eppendorf tubes and washed with PBS (2 x 5 min) by centrifugation to avoid losing the spheroids. The collected spheroids were fixed with 4% paraformaldehyde solution at room temperature for 30 min and subsequently washed twice by soaking the sample in washing buffer comprising 0.05% Tween-20 in PBS for 10 min each. The spheroids were next permeabilised using 0.5% Triton X-100 in PBS for 20 min at room temperature, followed by blocking in a solution containing 1% BSA in PBS for 1 hour at room temperature. The samples were then washed three times with washing buffer for 10 min each, followed by incubation for 1 hour at room temperature with vascular endothelial growth factor

(VEGF-A) primary antibody diluted in blocking solution (1:100). The samples were again washed three times with washing buffer for 10 min each. The samples were incubated with secondary antibodies (1:1000) for 1 hour at room temperature, followed by washing three times with washing buffer for 10 min each. The cell nuclei were then counterstained with 4',6-diamidino-2-phenylindole dihydrochloride (DAPI, blue)(1:2000) for 5 min. Finally, the sample was again washed three times with washing buffer for 10 min each time prior to analysis using laser scanning confocal microscopy (LSCM). Monolayer A549 cells served as the control, and were similarly stained using the immunofluorescence staining protocol. During imaging using laser scanning confocal microscopy (LSCM), PBS was replenished periodically to prevent drying of the spheroids.

3.2.8 Quantification of mature miR-126 and VEGF-A expression by TaqMan-qPCR assay

After transfection (24 hours), cells were washed with 1 X PBS and RNA was extracted using an RNeasy Mini Kit (Qiagen, Australia) according to the manufacturer's protocol. To determine miR-126 expression, total RNA was transcribed into cDNA using a TaqMan MicroRNA Reverse Transcription Kit (Applied Biosystems, 433596). The qPCR amplifications of cDNA were measured by TaqMan miRNA assay (Applied Biosystems, assay ID 000451). Mature miR-126 expression was measured by ΔΔCT and normalised to RNU44 (Applied Biosystems, assay ID 001094) as an endogenous control in the tested samples, relative to the untreated samples. To determine VEGF-A expression at the miRNA level, RNA was transcribed into cDNA by the QuantiTect reverse transcription kit (Qiagen, Australia). qPCR (Rotor-Gene, Qiagen Pty Ltd, Australia) with default settings was performed using an activation start cycle for 10 min at 95°C, followed by 40 cycles of 15 seconds at 95°C and 60 seconds at 60°C and 30 seconds at 72°C . The VEGF-A expression (Applied Biosystems, assay ID Hs00900055_m1) was normalised to GAPDH (Applied Biosystems, assay ID Hs02758991_g1) and the experiment was conducted in triplicate. Relative gene expression values were determined by the ΔΔCT method [332].

3.2.9 Cellular uptake of miR-126 PEI nanoparticles in A549 cells

The cellular uptake of mature miR-126 PEI nanoparticles was measured using LSCM. A549 cells, as a monolayer or spheroids, were transfected with fluorescently labelled miRNA (Dharmacon Miridian miRNA-Dy547) containing PEI for 24 hours to measure cell uptake efficiency. Monolayer cells were fixed with 4% paraformaldehyde, washed twice with washing buffer and permeabilised using 0.5% Triton X-100 in PBS for 2 min at room temperature, followed by blocking in a solution containing 1% BSA in PBS for 30 min at room temperature. Cells were then washed three times with washing buffer for 5 min each, followed by incubation for 1 hour at room temperature with Vinculin primary antibody (Millipore), diluted in blocking solution (1:100) and again washed three times with washing buffer for 5 min each. Cells were incubated with mouse secondary antibodies (1:1000) for 30 min at room temperature, followed by washing three times with washing buffer for 5 min each. The cell nuclei were then counterstained by DAPI (1:2000) for 5 min. Finally, cells were again washed three times with washing buffer for 5 min each prior to analysis using LSCM. Monolayer A549 cells served as a control. Calcein-AM was added to spheroids generated using liquid marble (LM) and liquid suspension (LS), incubated for 20 min and observed by LSCM.

3.2.10 Statistical analysis

The differences between the treatments were analysed for significance using one-way analysis of variance with post-hoc Duncan's multiple range tests at specific times and doses. A Student's t-test was used to analyse differences between two groups, using GraphPad Prism version 6.01 (GraphPad Prism software Inc., La Jolla, CA, USA). Experiments were performed independently at least three times. All values are expressed as mean ± standard deviation. Differences between treatments were considered significant at $p< 0.05$.

3.3 Results and Discussion

3.3.1 Cell culture, generation of spheroids and spheroid viability and morphology

Both liquid marble (LM) and liquid suspension (LS) methods resulted in cells aggregating to form spheroids. Consistent with a previous study [153], spheroids generated from LM were a spherical shape (**Figure 3.3A**), whereas spheroids generated from LS were more irregular shapes (**Figure 3.3B**). The irregular parameter (*IP*) value of LM spheroids was approximately half that of LS spheroids and the difference increased with period of culture (**Figure 3.3C).**

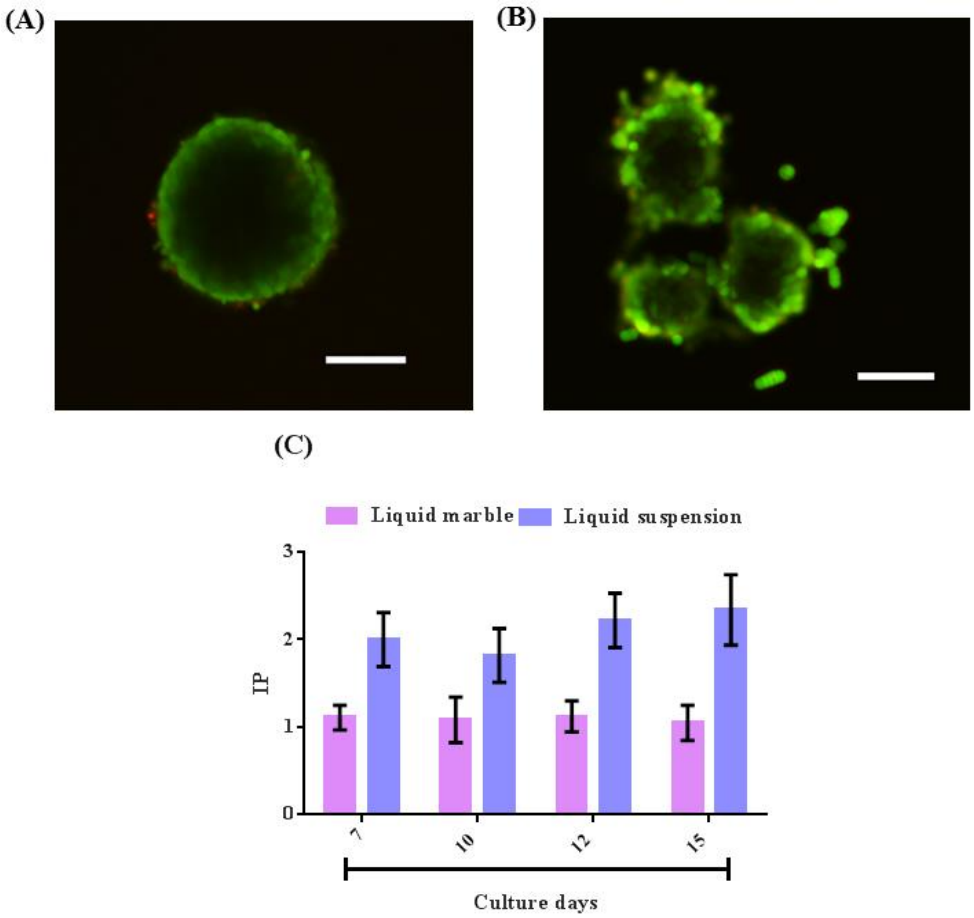

Figure 3.3: Generation of lung cancer A549 spheroids at 2×10^4/100 µl cell seeding density by liquid marble (A) and liquid suspension (B) methods after 7 days incubation. Scale bar represents 100 µm. C. Irregular parameter (*IP*) values for liquid marble and liquid suspension cells over time.

In both LM and LS generated spheroids, the periphery of the spheroids was populated by viable cells (stained green) in a viability assay using Calcein AM and propidium iodide (PI). PI is impermeable to live cells (hence they stain green), but penetrates through dead cells' leaky membranes and stains the nuclei red [333]. There was an absence of color in the spheroid core, whereas red staining was expected from previous research showing necrotic cores in spheroids [11, 323, 334]. Such necrotic cores are a typical feature of cancer tumors and spheroids, especially older and larger spheroids in which oxygen and nutrient transport is limited by diffusion, resulting in a core populated by dead cells [11, 334]. The anomalous absence of central spheroid staining found here is possibly because PI penetration into the spheroid core was blocked by tight cohesion of the live cells around the spheroid surface.

3.3.2 Complexation of PEI and miR-126 and measurement of size and charge of particles

MicroRNA-126 (miR-126) is a microRNA that is highly expressed in vascular endothelial cells [335]. A reduction in miR-126 was associated with increased capillary density in lung cancer, whereas the restoration of miR-126 suppressed lung cancer though down-regulating vascular endothelial growth factor A (VEGF-A) expression and microvessel density (MVD) [336].

The hydrodynamic size of PEI-miR-126 complexes was 234.7 ± 3.8 nm, and the Zeta potential was 14.2 ± 1.1 mV (**Figure 3.4**). By contrast, the Zeta potential of free miR-126 complexes was negative.

(A)

Nanoparticles	Size (nm)
miR-126 PEI	234.7 nm ± 3.81

(B)

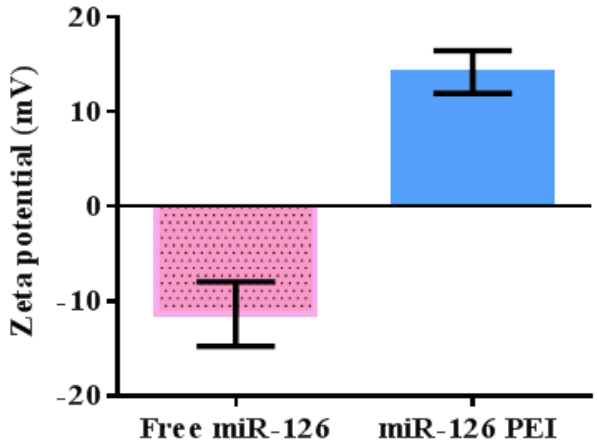

Figure 3.4: Mean size (nm) and Zeta potential (mV) of miR-126 PEI complexes (NP33) prepared using phosphate-buffered saline (PBS). A. Size of miR-126 PEI nanoparticles, B. Charge of free miR-126 and miR-126 PEI-nanoparticle complexes. The difference between treatments was analysed by Student's t-test and considered significant at p <0.05.

3.3.3 Transfection and Quantification of mature miR-126 containing PEI nanoparticles

To evaluate the performance of LM as a bioreactor, nanoparticles containing 1 μg of miR-126 were transfected to four groups of cells for comparison. The four groups were (1) spheroids generated using LM and transfected inside LM, (2) spheroids generated using LM and transferred to ultra-low attachment plates for transfection, (3) monolayer cells cultured on tissue culture plates (TCP), and (4) spheroids generated using the LS method and then transfected in ultra-low attachment plates. For miR-126 transfection in LM (1), the nanoparticles were introduced into the LM by simple injection

using a pipette. At 24 hours post-transfection, the miR-126 expression of cells inside spheroids was quantified using real-time polymerase chain reaction (qPCR). The VEGF-A expression from spheroids was also quantified using qPCR.

In general, spheroids treated with PEI nanoparticles showed greater miR-126 expression than in those treated with lipofectamine nanoparticles, indicating that PEI had greater transfection efficiency (**Figure 3.5)**.

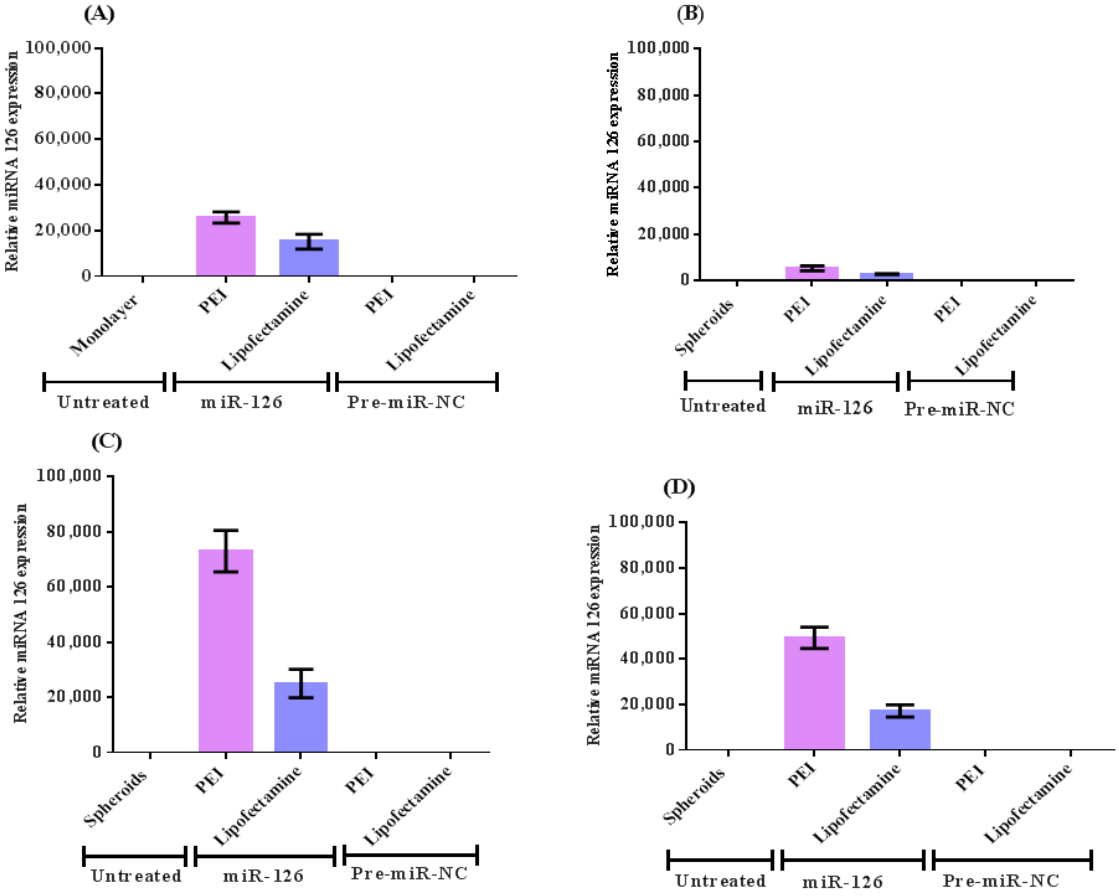

Figure 3.5: Mature miR-126 expression 24 hours after transfection with miR-126 PEI and lipofectamine. Data are mean ± standard deviation (n=3) and were analysed by unpaired Student's t-test (one-tailed). (A) Control cells, (B) Spheroids (LS), (C) Spheroids (LM), (D) Spheroids generated using liquid marble and then transferred into low adhesion 96-well plates for transfection.

In micro-bioreactor performance, LM-generated and transfected spheroids showed the greatest miR-126 expression, followed in turn by spheroids generated in LM but transfected in ultra-low attachment plates, cells in monolayers and lastly LS spheroids, with the least miR-126 expression.

To evaluate if the up-regulated miR-126 expression in LM was specific to nanoparticle-miR-126 delivery or is an artifact, spheroids were transfected separately with nanoparticles containing pre-miR™ (negative control). Pre-miR™ contains miRNA precursor with a scrambled sequence that does not target any human gene products specifically. As a second negative control, the miR-126 expression in untreated spheroids was also assessed.

There was negligible miR-126 expression from the two negative controls, namely untreated spheroids and spheroids that received scrambled miRNA, thus confirming that the miR-126 expression observed was specific to nanoparticle–miR-126 transfection. Cells in monolayers showed greater miR-126 expression than those in spheroids generated using LS.

Interestingly, miR-126 was highly expressed in spheroids generated using LM, and especially more highly in spheroids that were transfected inside LM. Yet spheroids are often reported to be more resistant to chemotherapeutic drug uptake than monolayer cells, due to a variety of reasons including differences in cell-cell communication, cell shape and/or ability of spheroid to repair damage [337]. A study by Saleh et al. reported that spheroids showed less plasmid DNA uptake than monolayer cells and suggested that the major barrier for DNA transfection was limited DNA penetration into deep regions of the spheroids [338]. By contrast, while most drugs are less effective in killing cancer cells in spheroids than in monolayers, some studies have reported that drugs such as Thiotepa (MW 189) and Bortezomib (PS341, MW 384.2) are equally or more effective against cells in spheroids than in monolayers [339, 340]. The effectiveness of such drugs is thought to be associated with their small molecular weight, and so these drugs penetrate better into spheroids [339].

The spheroid generation method may affect transfection efficiency. In these experiments, miR-126 was much smaller than plasmid DNA and many conventional drug systems. One would expect miR-126 to be able to penetrate deeply into spheroids and show equal or higher transfection than in monolayers. Interestingly, spheroids showed greater miR-126 expression than did monolayer cells (**Figure 3.5**), but only in spheroids generated using the LM method and not in spheroids generated using the LS method. These results indicate that small molecular weight is not the only factor that influences miRNA transection – the method used to generate spheroids also influences the subsequent transfection.

Spheroid shape may also affect miRNA uptake. The shape of LM-generated spheroids was more regular and spherical, and cell viability was greater, than in LS-generated spheroids. After transplantation, hepatocytes in the spheroid form showed longer survival and a greater survival rate than those with the conventional shape [341]. A previous study on embryoid bodies (EBs) - spheroids formed by aggregating ESCs – also observed that LM-generated EBs, which are homogeneous in size and shape, contained greater numbers of viable cells than LS-generated EBs, which were often irregular in size and shape [153], probably because regularly shaped spheroids have even nutrient diffusion, gas diffusion and waste removal. Therefore, the differences in miR-126 expression between LM spheroids and LS spheroids could be because cells in LM spheroids have greater viability, and only viable cells expressed miRNA after transfection.

For LM-generated spheroids, the miR-126 expression in those transfected in LM was greater than in those transfected in the ultra-low attachment plate, especially when the delivery vehicle being used was PEI ($p < 0.0098$). This suggests that the properties of transfection vessels also play a role in influencing miRNA transfection.

3.3.4 Cellular uptake

To better understand the reasons for the high miRNA transfection in LM-generated and transfected spheroids, fluorescently labelled miRNA (Dharmacon Miridian miRNA-Dy547) was used for transfection. Cellular uptake of PEI-miRNA-Dy547 was monitored at 24 hours post-transfection. Monolayer cells and LS spheroids were used as controls; both of these stained with Calcein AM (green) for visualisation.

Representative confocal microscopy images in **Figure 3.6** show that very little miRNA-Dy547s (red) had internalised into LS spheroids, and it was found only near the periphery of LS spheroids. By contrast, more miRNA-Dy547 internalised into LM-generated but ultra-low attachment plate-transfected spheroids; however, the internalized miRNA-Dy547 was again only localised at the periphery of the spheroids. As explained earlier, the high transfection in LM spheroids may be due to a more regular shape and thus greater viability than LS spheroids. Compared with the controls (LS spheroids and monolayer cells) and spheroids generated in LM but transfected in ultra-low attachment plates, more miRNA-Dy547 was taken up in LM-generated and transfected spheroids, both at the periphery and penetrating deeply into the core. These results revealed that the high miR-126 expression found in LM-generated and transfected spheroids was due to high miRNA uptake. The high miRNA uptake was only observed in LM-transfected spheroids and not in LM-generated but ultra-low attachment plate-transfected spheroids, indicating that LM, as a vessel, also plays a key role in transfection. Many studies have reported that PTFE, the materials that made up liquid marble shell, is non-adhesive. It is likely that such non-adhesive properties contribute to high miRNA transfection by not absorbing any miRNA, whereas ultra-low attachment plate comparatively absorbs more miRNA as shown in Figure 3.6, thus lead to lower miRNA uptake as less miRNA is available to the spheroid [151, 153, 342].

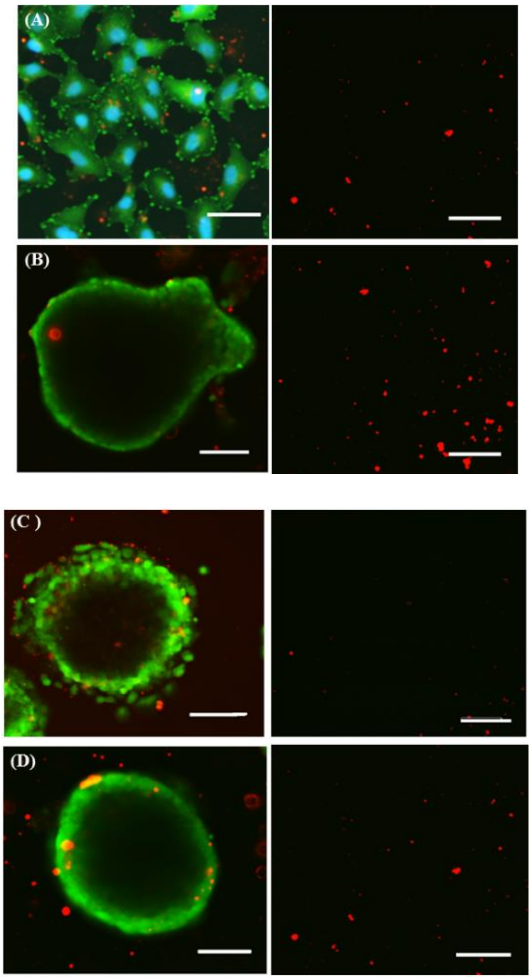

Figure 3.6: Confocal microscopy analysis of cellular uptake of miRNA-Dy547 containing PEI nanoparticles. Left side: A: Monolayer cells, B: Cells from liquid suspension method, C: Cells from liquid marble method transfected with miRNA-Dy547, D: spheroids formed using liquid marble and transferred to 96-well plate to be transfected. Right side: well plate only. Scale bar represent 100 μm.

PTFE, which constitutes the LM shell, resists protein adhesion due to its ultra-low surface free energy and high hydrophobicity, with a water contact angle of 108°[343, 344]. The anti-adhesive LM shell therefore inhibits non-specific absorption of miRNA into the shell and does not waste any miRNA in surface binding. The hydrophobic PTFE/water interface is negatively charged [345]. A statistical model proposed by England and Pande suggested that a hydrophobic and charged surface drives the surrounding water to reorganise; such forces may play a vital role in protein folding *in vivo* [346].

The PTFE interface of the LM, which presents as a 3D sphere, may drive reorganisation of its confined water molecules in a way that promotes movement of hydrophilic miRNA towards the LM

core where spheroids are located, and subsequently enhances spheroids' miRNA uptake. This can be demonstrated by the fact that more miRNA-Dy547 aggregated at the periphery of LM-generated and transfected spheroids than in LM-generated but ultra-low attachment plate-transfected spheroids, indicating that LM was a better transfection vessel than ultra-low attachment plates.

In addition, the spent medium collected at the end of the transfection experiment from the LM bioreactor had the least amount of un-transfected miRNA-Dy547, indicating that most of the miRNA-Dy547 had internalized into the spheroids; this explained why LM-generated and transfected spheroids showed the greatest miRNA expression. The spent medium from LS spheroids had the greatest amount of un-transfected miRNA-Dy547, as expected from the LS spheroids showing the least miRNA expression. Monolayer cells and LM-generated but low ultra-low attachment plate-transfected spheroids had similar amounts of un-transfected miRNA-Dy547 in their spent medium.

These results confirmed that LM performed better as a transfection vessel than ultra-low attachment plates. Ultra-low attachment plates have commonly been used for various gene transfection studies [347, 348] due to their biological inertness. The ultra-low attachment plates are covalently bonded with hydrophilic and neutrally charged hydrogel layers that inhibit cellular attachment and protein adsorption. Unlike the LM PTFE interface, which confines aqueous transfection reagents in a 3D context, the hydrogel layers on ultra-low attachment plates are only present at the bottoms and sides of the wells; these hydrogel layers are abundant in hydrogen bonds that do not distort the orientation of water molecules, unlike the hydrophobic PTFE interface.

3.3.5 Measurement of VEGF-A protein expression

Representative images of immunostaining in **Figure 3.7** show that after miR-126 transfection, the level of VEGF-A (green) was low in A549 cells, regardless of whether cells were cultured in monolayers or in spheroids. These results are similar to those of others, in which it was reported that

miR-126 transfection led to down-regulation of VEGF-A in A549 cells [349]. The greater the miR-126 transfection, the less was the resulting VEGF-A protein expression.

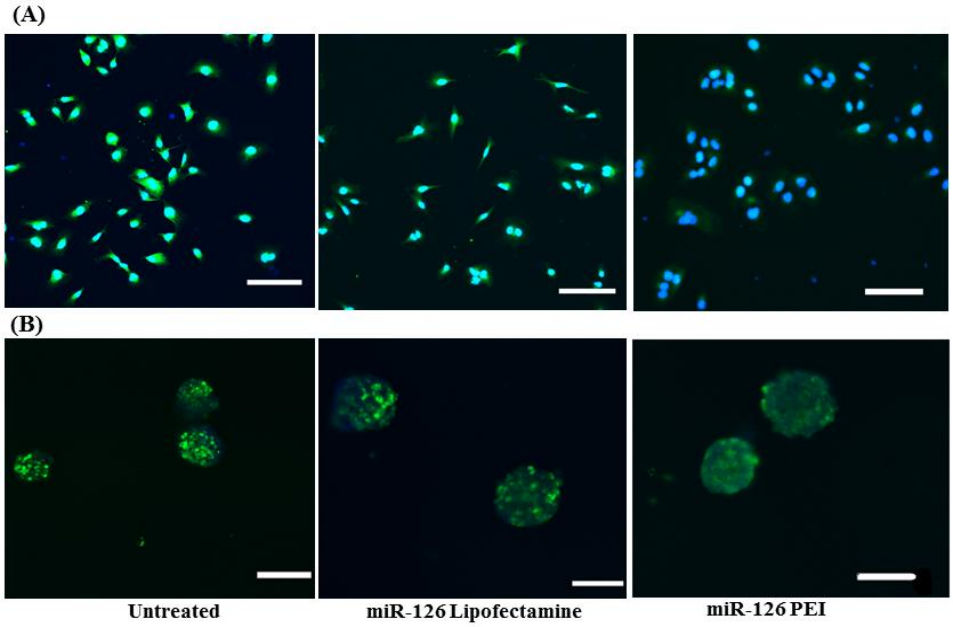

Figure 3.7: Immunostaining of VEGF-A expression 24 hours post-transfection**.** Monolayers (A) and spheroids (B) in the liquid marble method were transfected with miR-126 PEI complexes at NP=33 ratio, miR-Lipofectamine. Scale bar represents 100 µm.

3.3.6 Quantification of VEGF-A expression by TaqMan-qPCR assay

Quantitative qPCR analysis in **Figure 3.8** demonstrated that LM-generated and transfected spheroids showed the least VEGF-A expression, followed in turn by spheroids generated in LM but transfected in ultra-low attachment plates, cells in monolayers and then LS spheroids, in order of increasing VEGF-A expression. These results agree with the earlier miR-126 transfection results, where LM-generated and transfected spheroids showed the greatest miRNA transfection and expressed the least level of VEGF-A, compared with the controls.

Some studies suggested that miRNA and protein expression does not always correlated with each other. An increase in miRNA levels may not lead to increase protein levels because of various levels of post-transcriptional and post-translational regulation, the amount of transcript does not always correlate with the amount of protein produces. In addition, there is a huge variability in this correlation for different genes, where some correlate better than others. This may be the reason why the expression levels of VEGF-A and miR-126 do not correlate with each other [350-352]. This suggests again that LM is an ideal bioreactor vessel for miRNA transfection.

In addition, cells transfected by PEI-miR-126 expressed less VEGF-A level than those transfected by lipofectamine, confirming that PEI was more efficient in transfecting miR-126, thus leading to lower VEGF-A expression. Cells or spheroids that received scrambled miRNA showed negligible change in VEGF-A expression from the control.

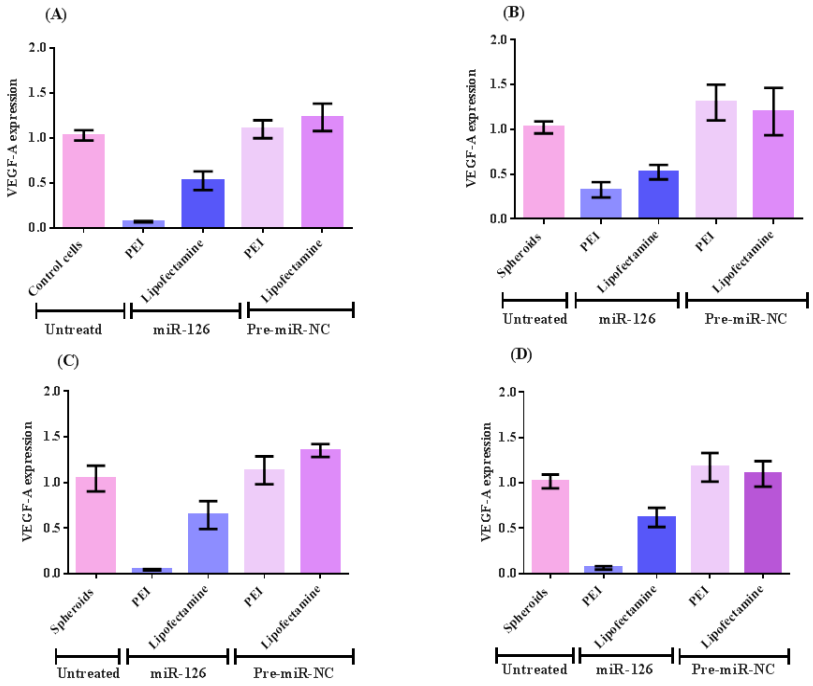

Figure 3.8: VEGF-A expression at 24 hours of A549 cells. Cells were transfected with miR-126 PEI complexes at N/P=33, miRNA-Lipofectamine, Negative Control polyethylenimine (NC-PEI), Negative Control Lipofectamine (NC-Lipofectamine), Data are shown as mean (n =3) ± standard error of the mean and were compared by Student's t-test with controls. A Monolayer cells, B

Spheroids (liquid suspension), C Spheroids (liquid marble), D Spheroids generated by liquid marble method and then transferred into well plates for transfection.

3.4 Conclusion

In summary, A549 lung cancer spheroids were generated by a LM microbioreactor and the spheroids were subjected to miR-126 transfection inside the LM. The miR-126 expression and the subsequent VEGF-A down-regulation in LM transfected spheroids reached a greater level than in various controls: monolayer cells, spheroids generated using the LS method, and LM-generated spheroids that were transfected in a conventional ultra-low attachment plate. There are multiple possible reasons for the greater miRNA expression observed in the LM bioreactor. First of all, miRNA is much smaller than many chemotherapeutic drugs and thus penetrated well into spheroids. Secondly, the PTFE shell possesses ultra-low surface free energy and so does not absorb and waste any miRNA through non-specific adsorption. Lastly, the hydrophobic interface present on the LM shell may play a role in promoting the movement of hydrophilic miRNA towards the centre of the LM where spheroids resided. Overall, this study demonstrates that LM can serve not only as a platform that produces tumour-like spheroids, but also as an efficient microbioreactor vessel that enhances miRNA transfection and outperforms conventional transfection vessels.

CHAPTER FOUR

Rapid Enhancement of Multicellular Spheroid Assembly by Acoustically-Driven Microcentrifugation

4.1 Introduction

Multicellular spheroids, comprising three-dimensional spherical cell aggregates displaying cell–cell and cell–matrix interactions, more closely mimic *in vivo* avascular tumor structure and functionality than conventional monolayer cultures, in which intercellular contact is often lost [9, 10]. They are therefore of fundamental importance to studies in cancer biology, metastasis and invasion, in addition to therapeutic screening [11, 12, 353]. Multicellular spheroids have also been shown to play a role in improving the differentiation efficiency of mesenchymal stem cells [354, 355].

Various techniques have been used to produce these spheroids, all of which involve first the formation of loose cell aggregates followed by their compaction into a tight spheroidal cluster [10]; the different approaches vary primarily in the way the cells are driven to aggregate, and the method by which intercellular adhesion is promoted by preventing cell adhesion to the surface of a tissue culture dish [153]. The most widely used spheroidal culture technique to date is the hanging drop method [116] in which cell suspensions are first dispensed onto the lid of a Petri dish followed by inversion of the lid to form a hanging drop, each of which leads to the formation of a single cell aggregate. This method, however, requires a careful balance between capillary and gravitational forces, is not practically amenable to medium exchange [356], and is difficult to translate to large-scale production since the maximum permissible drop size is limited to 50 μl [151]. Rotational bioreactors such as spinner flasks, on the other hand, have been employed for large-scale spheroid production and allow for medium exchange and cell sampling, although costly specialised culture equipment is required and the large shear stresses exerted lead to a tendency to fragment cells [153].

Liquid overlay methods; by contrast, involve culturing a cell suspension on a weakly adhesive surface such as a thin agarose layer, agar gel or temperature-responsive methylcellulose coating atop a tissue culture dish [114, 357]. Whilst simple, inexpensive and amenable to scale-up, these methods suffer from large variations in spheroidal quality [10]. Furthermore, agar performs poorly as a non-adhesive substrate [114]. Additionally, agarose preparation requires the reagent to be autoclaved for dissolution and sterilisation, followed by a long cooling period for the sol-gel transition. Temperature-responsive methylcellulose hydrogels, on the other hand, make medium exchange difficult due to their high viscosity and stringent temperature requirements [357].

More recently, various microfluidic strategies have been proposed for on-chip spheroid culture. These include microarray devices that immobilise cells on selectively-adhesive patterned structures [117], cell trapping barriers [118-120] or non-adhesive microwells [121-124]; bubble and droplet-based methods in which the cells are encapsulated within bubble [12] or gelated capsules [125-127]; cell trapping in microwells by ultrasonic actuation [358]; and microwells in which rotational flow of a cell suspension is induced [129, 359]. Microarray methods possess the advantage of large-scale production of uniformly sized cell aggregates, although the aggregate size tends to be limited by the dimensions and the geometry of the patterns. Large numbers of cells also need to be seeded, as any cells that are not immobilised tend to be washed away and lost [120]. Bulk ultrasonic actuation, on the other hand, typically requires large transducers and custom-made microwells that facilitate the transmission of sound energy into the wells, and the necessity for relatively high power is associated with considerable heating as well as long stabilisation times (typically 15 minutes), which can be detrimental to the cells [358]. Bubble and droplet methods possess similar limitations as the aggregate sizes are dependent on that of the capsule, which, in turn, is restricted by the surface properties and dimensions of the microfluidic system. In addition, bubble methods suffer from low cell capture efficiencies. The rotational flow device, on the other hand, allows cell aggregates of different sizes to be produced from microwells of a single dimension, therefore circumventing the need to fabricate different devices to obtain aggregate size variation. However, the requirement of a filtration system to

prevent cell clots from entering the device not only reduces the efficiency of the method due to loss of a large number of cells but also introduces further complexity embodied in the necessity for an additional channel shredder to break up large cell clots by shear [129]. In addition, the closed microfluidic device restricts practical sampling and collection of cell aggregates, for example, for plating the cell aggregates to stimulate cell differentiation [130].

Whichever approach is chosen, the low adoption of microfluidic technology at the bench has primarily been due to the inertia of practitioners such as laboratory technicians in adopting new and sophisticated technology, preferring instead to continue using familiar equipment and protocols even if these are inefficient and not cost-effective [360]. Another reason for their preference for existing laboratory formats in lieu of new technology is the existing compatibility of these methods to a vast array of ancillary laboratory technology, e.g. microscope stages, microplate readers, etc. that are already available without needing to invest in costly new equipment to accommodate the new format.

In this chapter, it is therefore proposed to interface a novel surface acoustic wave (SAW) microcentrifugation tool for rapid spheroid generation with a laboratory format with which practitioners are already intimately familiar and that has already been customised to fit a vast array of existing ancillary equipment for laboratory analysis, with the aim of exploiting the advantage of process improvement through new technology whilst allowing the user the benefit of retaining an existing format to which they are accustomed: the tissue culture microplate (**Figure 4.1**). Microcentrifugation driven by SAWs nanometer amplitude electromechanical waves localised on a chip-scale piezoelectric substrate [361] has already been demonstrated for a variety of purposes, e.g. chaotic micromixing [362], rapid particle concentration [363] and sorting [364], as well as driving the rotation of small disks on which microchannels for a wide range of microfluidic operations can be patterned—the so-called *Miniaturized Lab-on-a-Disc* [365]; this is in addition to the vast array of other microfluidic manipulations enabled by the SAW [366-371]. Unlike high-shear rotational bioreactors or other bulk ultrasonic devices which typically operate below 1 MHz, the 10–100 MHz

order frequency SAWs, which operate at very low (< 1 W) power given the efficiency of the device, have significantly less tendency to denature large biomolecules and cells, as there is insufficient time between the field reversal at these frequencies compared with the shear relaxation time of molecules or cells. Furthermore, cavitation—a common cause of biomolecular or cellular damage in ultrasonic devices—is also suppressed at these high frequencies and low powers [372].

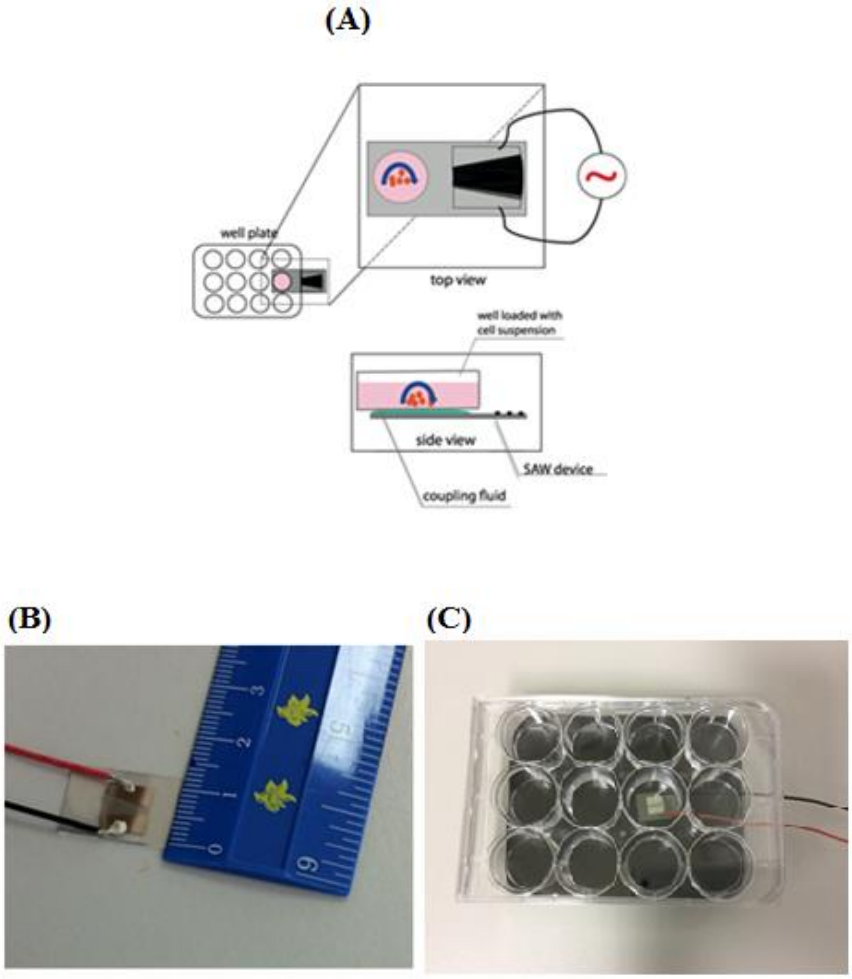

Figure 4.1: (A) Schematic depiction of the setup used for rapid spheroid generation in a microwell on a well plate. The surface acoustic wave **(**SAW) device is interfaced from beneath using a fluid coupling layer. (A) Representative images of (B) the SAW device and (C) the arrangement used. For clarity, a 12-well plate is shown in (C), although the SAW micro-centrifugation technique was demonstrated in a 96-well plate.

The aggregation of cells using the microcentrifugation flow induced in the microwells by the SAW device is complemented by a low-adhesive coating in the well plate using fast-gelling carboxymethyl cellulose (CMC)-based hydrogel, namely carboxylmethyl cellulose tyramine (CMC-TYR). CMC is a cellulose derivative approved by the Food and Drug Administration (FDA) and has been commonly used as a degradable pharmaceutical material; it is commercially available at low cost, and is non-fouling in addition to possessing low cell-adhesive properties [373]. Another advantage of the use of CMC-TYR is its fast gelation rate, which minimises the preparation time for coating the tissue culture surface. Altogether, the fast (1–10 s) SAW-driven microcentrifugation together with the use of the CMC-TYR coating facilitates rapid production of uniform tumour cell spheroids—here demonstrated with BT-474 cells—using standard tissue culture plasticware and allowing easy access for medium exchange and sampling, thus constituting a promising platform for studies in cancer biology and drug screening. Although SAWs have previously been coupled into superstrates on which sessile drops are manipulated [374-376], the use of SAWs to drive micro-centrifugation in a standard tissue culture well plate has yet to be demonstrated. Moreover, spheroid dimension can potentially be simply controlled by modulating the power input to the SAW, therefore removing the need, for example, for elaborate fabrication of different microstructures.

4.2 Methods

4.2.1 SAW Device Fabrication

The electrodes of the SAW device were fabricated using standard UV photolithography according to a method modified from Qi et al. [377]. Briefly, a 5 nm thick layer of chromium, followed by a 1.5 μm thick layer comprising 99% aluminium and 1% copper, were sputtered on a 127.68° *Y*-axis rotated, *X*-axis propagating lithium niobate wafer (Roditi Ltd., London, UK). A thin (~3 μm) layer of AZ4562 photoresist (Microchemicals GmBH, Ulm, Germany) was then spun coated onto the wafer, followed by UV exposure through a glass mask, development of the photoresistant layer and wet etching for

electrode pattern generation, using a commercially available aluminium etchant (ANPE 5-5-80-10, Microchemicals GmBH, Ulm, Germany). Here, elliptical single-phase unidirectional transducers (SPUDT) [363] were used for the Rayleigh SAW generation with an electrode finger width and spacing corresponding to a resonance frequency of ~30 MHz. The substrate wafer containing the SPUDT was then diced into chips approximately 180 mm long and 120 mm wide.

4.2.2 Hydrogel Synthesis and Preparation

CMC-TYR was synthesized according to Al-Abboodi et al. [130]. In brief, 5 g CMC and 0.864 g TYR were first dissolved in 250 ml of Milli-Q® water (Millipore; Merck Pty. Ltd., Kilsyth, VIC, Australia), followed by the addition of 0.573 g NHS and 0.955 g EDC, and overnight agitation at room temperature and pH 4.7. For purification, the mixture was then transferred to dialysis tubing and dialysed against 100 mM NaCl, 25% ethanol, and Milli-Q® water in sequence for 2 days each. The product was then lyophilised for storage.

CMC-TYR hydrogel was used as a low-adhesion coating of the tissue culture well plate. The lyophilized CMC-TYR was first dissolved in PBS at a final concentration of 5% (v/v) and filter-sterilised using a 0.22 μm sterile syringe filter. Filter-sterilised HRP and dilute H_2O_2 were added to this solution at final concentrations of 224 units/l and 2.88 mM, respectively. Next, 125 μl/cm^2 of this solution was vortex-mixed for 4 s and immediately transferred to the inner walls of each well in the well plate and allowed to cross-link enzymatically to form the coating.

4.2.3 Hydrogel Characterisation

The conjugation of TYR on CMC was assessed in deuterium oxide (D_2O) using NMR operating at 300 MHz (ACF300, Bruker Pty. Ltd., Alexandria, NSW, Australia). The gelation time of CMC-TYR was estimated using an inverted tube test method according to Gupta et al. [378]. Briefly, HRP and H_2O_2 at final concentrations of 224 units/l and 2.88 mM, respectively, were added to a 2 ml

microcentrifuge tube (Axygen Scientific, VWR International Pty. Ltd., Murarrie, QLD, Australia) containing 5% (v/v) CMC-TYR in PBS. The mixture was vortex-mixed for 4 s with the tube reverted in 30 s intervals to observe for flow. The gelation time was recorded as the time when the gel ceased to flow.

The swelling ratio of the CMC-TYR hydrogel was measured using a conventional gravimetric method according to Hoo et al. [379]. In brief, sterilised hydrogels were prepared from 5% (v/v) CMC and HRP at a final concentration of 245 units/l with varying amounts of H_2O_2 to give final concentrations of 3.2, 12.8, and 28.8 mM.

The hydrogels were subsequently cut into round disks using a sterile circular mould that was then swollen by immersion in sterile PBS for 3 days at 37°C. Excess liquid was wiped off by gently blotting the hydrogel with laboratory wipes. The swollen weight W_s of the hydrogel disks was then measured, followed by lyophilisation, after which the dry weight W_d was measured. The swelling ratio was calculated as $(W_s - W_d)/W_d \times 100\%$ [380].

4.2.4 Cell Culture

The human mammary gland carcinoma BT-474 cell line was used as a model cancer cell line and was obtained from the School of Health Sciences, RMIT University (Bundoora, VIC, Australia).
Cells were maintained in a cell culture medium consisting of DMEM supplemented with 10% (v/v) FBS and 100 μg/ml penicillin-streptomycin at 37°C in a 5% CO_2 humidified incubator. Cells were trypsinised using 0.25% trypsin–EDTA after reaching 80–90% confluence.

4.2.5 Spheroid Generation

A cell suspension was first prepared by suspending BT-474 cells with the desired cell density (2×10^3, 4×10^3, 5×10^3, or 6×10^3 cells/ml) in cell culture medium, followed by the addition of 1% gelatin to the cell culture medium as an intercellular linker to assist cell aggregation. The feasibility of generating spheroids using SAW microcentrifugation was investigated in both 12-well and 96 well-plates. Specifically, the microwells of the microplate were coated with a thin layer of CMC-TYR (167 μl/cm^2) that functioned as a low-adhesive coating and were subsequently filled with 20 μl of cell suspension. Acoustic energy was then transmitted into the microwell to induce the microcentrifugation flow within it for the purpose of driving the cells to aggregate. This was achieved by placing the SAW device beneath the microwell, sandwiching a thin layer of fluid couplant consisting of KY Jelly (Chemists Warehouse, Virginia, QLD, Australia) in between. This technique for acoustic energy coupling from the SAW device into a superstrate layer was first demonstrated by Hodgson et al. [374] and later employed for a variety of acoustomicrofluidic operations on superstrates [375, 376].

The microcentrifugation flow was generated by introducing asymmetry in the delivery of the acoustic wave with respect to the geometry of the drop or microwell [381], achieved most easily here by simply offsetting the drop or microwell with respect to the SPUDT. The SAW device was activated by supplying an oscillating electrical signal at a resonance frequency of 30 MHz to the SPUDT for 1 min using a multifunction synthesiser (Wave Factory WF1966 2CH, NF Corporation, Yokohama, Japan) and coaxial amplifier (Mini-Circuits ZHL-1-2W, RS Components Pty. Ltd., Sunshine West, VIC, Australia) to induce the microcentrifugation flow within the well in order to drive the cell aggregation. Once the cell aggregate was formed, 100 μl of medium was carefully added to the well. The position of the SAW device beneath the well plate was then moved under other wells in order to repeat the same spheroid generation process as required, although multiple SAW devices, one under each well, can also be employed in order to parallelise the process for high throughput operation.

Spheroids were also produced using a liquid overlay method for comparison. In brief, 20 μl of cell suspension containing the intercellular linker was prepared in the same manner and with the same seeding density as those used for the SAW microcentrifugation. The cell suspension was further mixed with 100 μl of medium and added to microwells that were pre-coated with a thin layer of CMC-TYR (167 $\mu l/cm^2$). In both cases, the microwell plates were then transferred to a 5% CO_2 humidified incubator for further spheroid cultivation at 37°C. Wells that were not subjected to the acoustic irradiation were used as controls.

4.2.6 Characterization of Spheroid Viability, Morphology and Proliferation

After the SAW irradiation, cells were incubated for 2 hours. Cell viability was then evaluated using a LIVE/DEAD® Cell Viability Assay (Life Technologies, Mulgrave, VIC, Australia) according to the manufacturer's protocol.

To investigate the cell distribution within the spheroid, the spheroids produced were cultured for 10 days and then collected by centrifuging at 300 rpm. The collected spheroids were subsequently fixed with 4% paraformaldehyde followed by rinsing in PBS, and finally subjected to Tissue Tex® O.C.T. embedding. Histochemical analysis was performed on 5 μm sections of the spheroid. The sections were further stained by hematoxylin and eosin (H&E) using standard procedures [382]. The morphology of the H&E, calcein AM and propidium iodide (PI)-stained spheroids was visualised using optical microscopy (CKX41, Olympus Pty. Ltd., Notting Hill, VIC, Australia) and laser scanning confocal microscopy (LSCM; Eclipse Ti Confocal Microscope, Nikon Instruments Inc., Melville, NY), respectively. The diameter, cross-sectional area, and perimeter of the spheroids were measured using ImageJ (National Institutes of Health, Bethesda, MD). The irregularity parameter *IP*, defined as the ratio of the diameter of the minimum circumscribed circle *D* to that of the maximum inscribed circle *d*, i.e. $IP \equiv D/d$ [328], was used as an indicator to evaluate the circularity of a

spheroid; an *IP* with a value of 1 indicates a perfect circle, whereas a large *IP* value indicates that the spheroid exhibits irregular morphology [328].

For the spheroid proliferation studies, the spheroids were cultured and subsequently monitored for a period of 10 days after being exposed to the SAW. The same viability and morphology characterisation studies were employed as that detailed above. The spheroids were collected for trypsinisation at different time intervals, and the number of cells proliferating within spheroids was determined by measuring the DNA content using a Quanti-iT PicoGreen dsDNA Assay (Life Technologies, Mulgrave, VIC, Australia) according to Hoo et al. [383]. For the control, cells were allowed to aggregate using the conventional liquid overlay method on a CMC-TYR coated well plate and monitored in the same way.

4.2.7 F-actin Organisation

The F-actin organisation in the spheroids was examined using an Actin Cytoskeleton and Focal Adhesion Staining Kit (Merck Millipore, Bayswater, VIC, Australia). Firstly, 20-day-old spheroids were removed from the CMC-TYR coated well plate by pipetting and were subsequently centrifuged for 3 min at 500 rpm in order to concentrate the spheroids at the bottom of a centrifuge tube, with the supernatant then decanted to remove most of the medium. The spheroids were next embedded according to a method modified from Al-Abboodi et al. [384] to prepare the spheroids for staining. Finally, a small drop of sample containing the spheroids was pipetted from the centrifuge tube onto a separate well plate. CMC-TYR was employed as the embedding substrate, the high water content of the hydrogel allowing the stain to penetrate through the hydrogel. Briefly, freshly prepared hydrogel precursor solution (100 μl) containing 5% (v/v) CMC-TYR, 245 units/l HRP and 3.2 mM H_2O_2 were immediately added into the wells of the well plate containing the spheroids to form a thin liquid layer. The spheroids were embedded simultaneously with the precursor crosslinking to form a hydrogel layer. The embedded spheroids were further fixed with 4% formaldehyde solution at room temperature for 1 hour and subsequently washed twice by soaking the sample in wash buffer

comprising 0.05% Tween-20 in PBS for 10 min each. The spheroids were next permeabilised using 0.5% Triton X-100 in PBS for 20 min at room temperature, followed by blocking in a solution containing 1% BSA in PBS for 1 hour at room temperature. The samples were then washed three times with wash buffer for 10 min each, followed by incubation with anti-vinculin primary antibody diluted in blocking solution (1:100) for 1 hour at room temperature and a similar washing step in the buffer solution.

For double labelling, the sample was incubated with FITC-conjugated secondary antibodies (1:1000) and tetramethylrhodamine isothiocyanate (TRITC)-conjugated phalloidin (1:200) for 1 hour at room temperature, followed by washing three times with wash buffer for 10 min each. The cell nuclei were then counterstained by DAPI (1:2000) for 5 min. Finally, the sample was again washed three times with buffer solution for 10 min each time prior to analysis using LSCM. Monolayer BT-474 cells were employed as the control, and were stained using the Actin Cytoskeleton and Focal Adhesion Staining Kit according to the manufacturer's protocol. During imaging with LSCM, ten representative cells were selected from each specimen and the mean fluorescence intensity (MFI) of FITC was quantified using ImageJ; PBS was replenished periodically to prevent drying of the sample.

4.2.8 Statistical Analysis

All experiments were performed with at least three replicates and results reported as the average value ± standard deviation. Multiple groups of data were compared using One-Way Analysis of Variance (ANOVA). Two groups of data were compared using the Student's *t*-test. Differences were considered statistically significant when $p < 0.05$.

4.3 Results and Discussion

4.3.1 Hydrogel Characterisation

CMC-TYR conjugate synthesis via mediated coupling according to the scheme illustrated in **Figure 4.2** was confirmed by ^{1}H NMR spectroscopy. **Figure 4.3** shows the typical spectrum of CMC-TYR; the signal of aromatic protons of tyramine appeared at δ = 6.8 and 7.2. CMC-TYR conjugates were enzymatically cross-linked with HRP to form an irreversible hydrogel in approximately 3 min; HRP-mediated oxidative coupling of phenol derivatives gives rise to a C–O linkage between the ortho–carbon and the phenolic oxygen groups or a C–C linkage between the ortho-carbons of the aromatic ring [130, 385], thereby cross-linking CMC-TYR conjugates to form a hydrogel. The hydrogel obtained was clear and insoluble in aqueous solution. The fast gelation time of CMC-TYR, which can be modulated via the enzyme concentration [130, 386], also contributes to a significant reduction in the preparation time of the non-adhesive coating compared to the conventional methods in which agarose gel is used, which requires at least 20 min to gel [387].

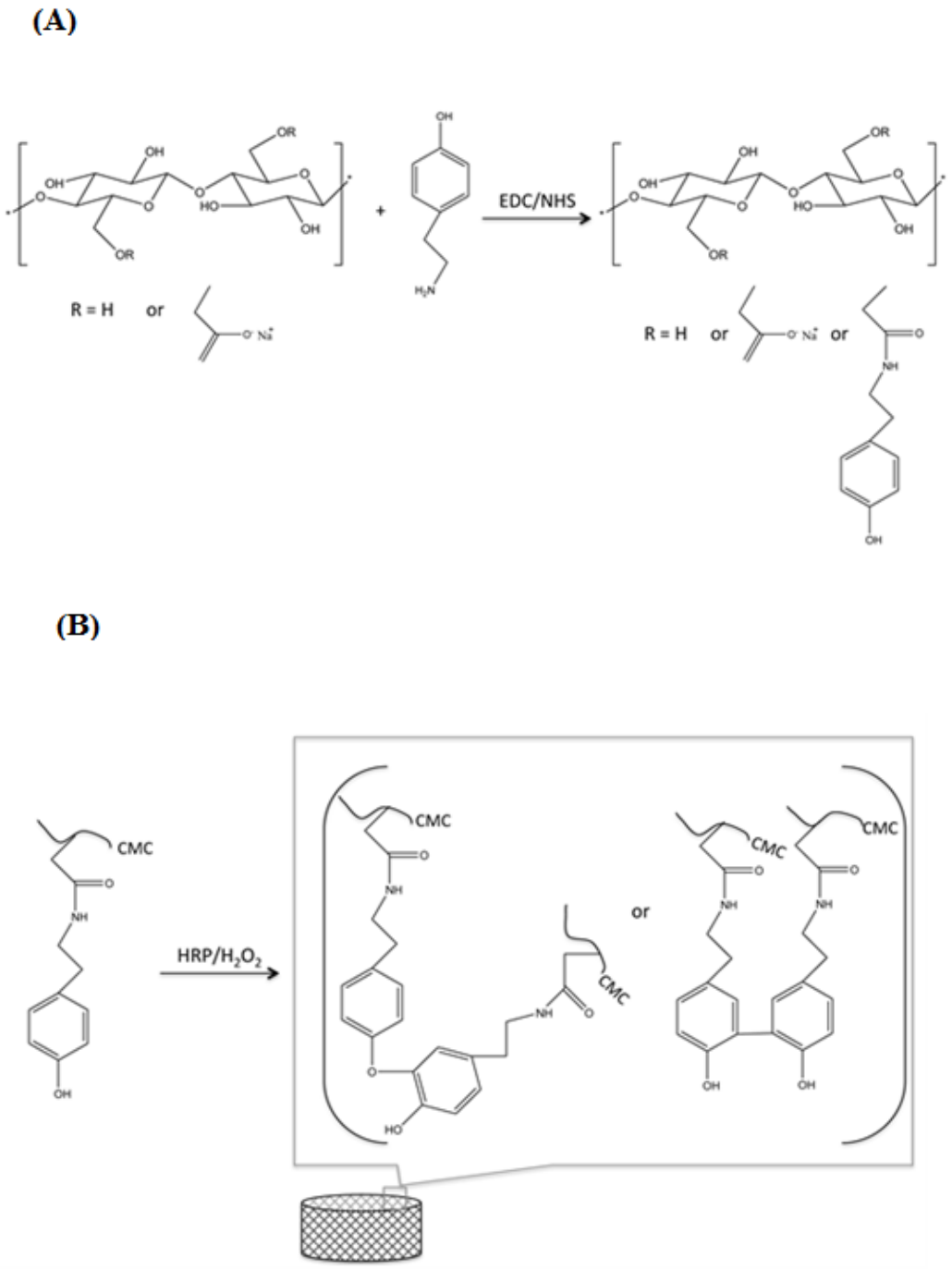

Figure 4.2: Synthesis scheme for (A) CMC-TYR, and (B) CMC-TYR hydrogel cross-linking.

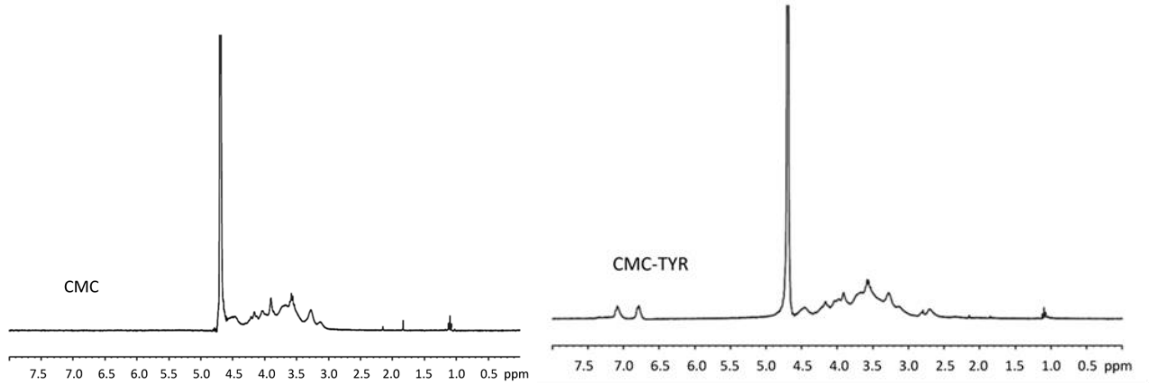

Figure 4.3: 1H NMR spectra of CMC and CMC-TYR

Figure 4.4 summarises the swelling ratios of the CMC-TYR hydrogel at different H_2O_2 concentrations. The swelling ratio is a measure of the material wettability; hydrogels with high swelling ratios are highly hydrophilic and highly permeable, which facilitates the transport of water-soluble molecules through the pores [379, 388] and minimises cell adhesion, whereas long-range non-covalent interactions between cells and the hydrophobic surface promotes cell surface adhesion [380]. As expected, the swelling ratio decreased with increasing H_2O_2 concentration ($p < 0.0001$, $n = 3$), from 85.5% ± 1.1% to 70.4% ± 1.5% and 47.5% ± 3.2% for hydrogels prepared from 3.2, 12.8 and 28.8 mM H_2O_2, respectively. The increasing H_2O_2 concentration led to a greater number of cross-linking bonds per unit volume (cross-linking density) within the hydrogel, which reduces the infiltration of water molecules into the densely cross-linked network, thereby resulting in a lesser swelling ratio [389]. The high swelling ratios exhibited by the CMC-TYR hydrogels thus revealed that these hydrogels were highly hydrophilic due to the presence of numerous hydroxyl groups on the CMC backbone, therefore constituting the required low-adhesive surface coating.

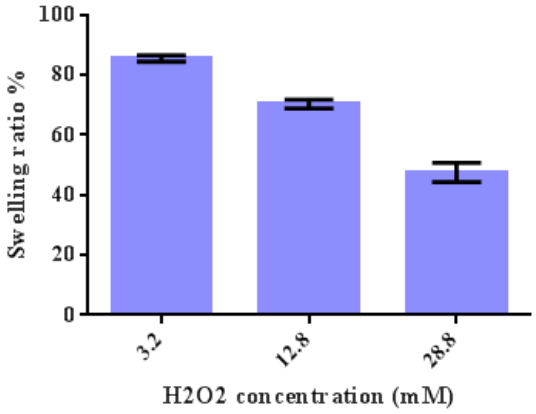

Figure 4.4: Swelling ratio of CMC-TYR, prepared from 5% (v/v) CMC-TYR and HRP at a final concentration of 245 units/l and various concentrations of H_2O_2. The error bars represent the standard deviation (n = 3).

4.3.2 SAW Microcentrifugation Driven Cell Aggregation as a Precursor to Spheroid Formation

Figure 4.5 shows representative images of the spheroids generated using the SAW device compared with those from the control experiment, in which acoustic irradiation and hence microcentrifugation flow were absent. Also shown are representative results when the hydrogel low-adhesive coating was absent. In the uncoated microwells (top row of images in **Figure 4.5**), cells were more concentrated as a result of the microcentrifugation flow in the well from the acoustic irradiation than in the control experiment, in which no external force was applied and the cells simply sedimented under gravity. The relationship between the numbers of cells in the aggregate and the input power is discussed below. Nevertheless, a large number of cells remained in a spoke-like pattern instead of being concentrated into a tight pallet at the centre of each well. This pattern is due to standing waves that arise as a consequence of the reflection of sound waves from the walls of the well; in other words, the well forms an effective acoustic cavity. Particles and cells with densities greater than the surrounding fluid are easily trapped at the nodes of standing waves, where the acoustic radiation pressure is at its minimum [390]. In addition, the absence of a weakly adhesive coating meant that the cells tended to adhere to the bottom of the well.

It can, however, be seen from the bottom row of images in **Figure 4.5** that these difficulties in attempting to drive the cells into a tightly-packed aggregate were circumvented by coating the microwell with the hydrogel, which had a direct effect on the quality of the spheroids formed . In the presence of the coating, the cells were concentrated into a tight central aggregate in each well; a larger aggregate cell density was achieved when the cells were concentrated by the SAW-driven microcentrifugation flow. The disappearance of the spoke-like cell patterns with the use of the hydrogel coating suggests that the hydrogel plays a two-fold role in not only preventing cell adhesion along surfaces but also in absorbing the sound wave and thus preventing its reflection and hence the generation of standing waves in the well.

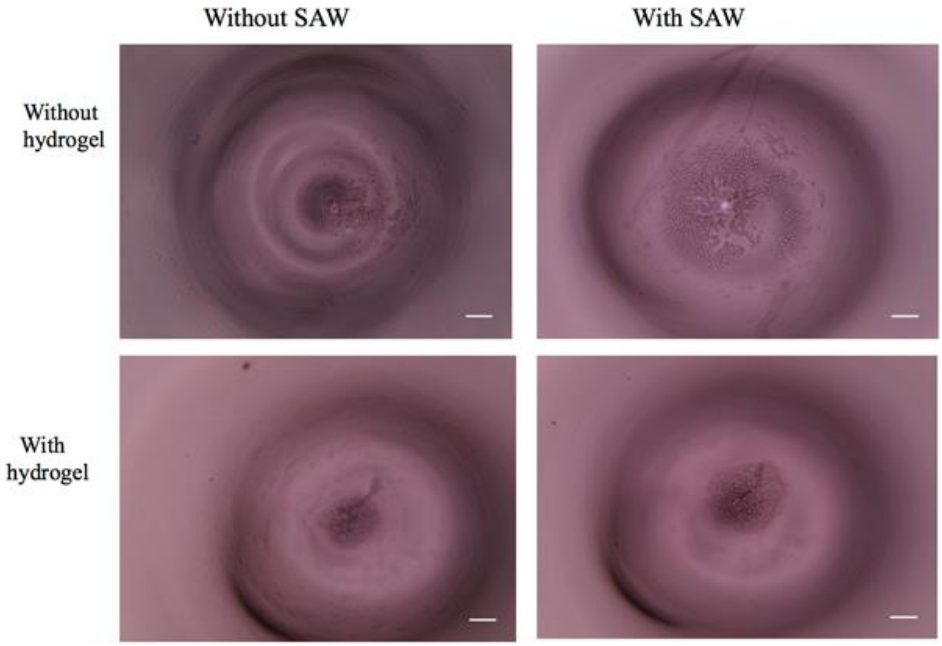

Figure 4.5: Representative microscopy images showing the cells in a microwell of a 96-well plate in both the presence (right) and absence (left) of the microcentrifugation flow induced by the acoustic radiation. The effect of the hydrogel low-adhesive coating in the well is also shown in the bottom row. The solution in each well contained BT-474 cells at a seeding density of 5 x10^3cells/ml. The scale bar represents a length of 0.5 mm.

The effect of the SAW power applied, which has a direct effect on the velocity of the induced microcentrifugation flow in the well, is shown in **Figure 4.6**. The cells all remained viable (stained green with Calcein AM); no PI stained cells (dead cells) were observed. This was consistent with previous findings on the lack of effect of SAW irradiation on cell viability [372].

The morphology of the cell aggregates and hence the subsequent spheroid formation, however, depends intimately on the power applied as well as the cell seeding densities ($2 \times 10^3 - 6 \times 10^3$ cells/mL) employed. In order to obtain quantitative morphometric characterization, both the spheroid cross-sectional area and irregularity parameter *IP* were examined as a function of these system parameters. The former is a measure of the compactness of the spheroid formed, whereas the latter is a measure of the circularity of the spheroid (*IP* values close to 1 correspond to more circular spheroids).

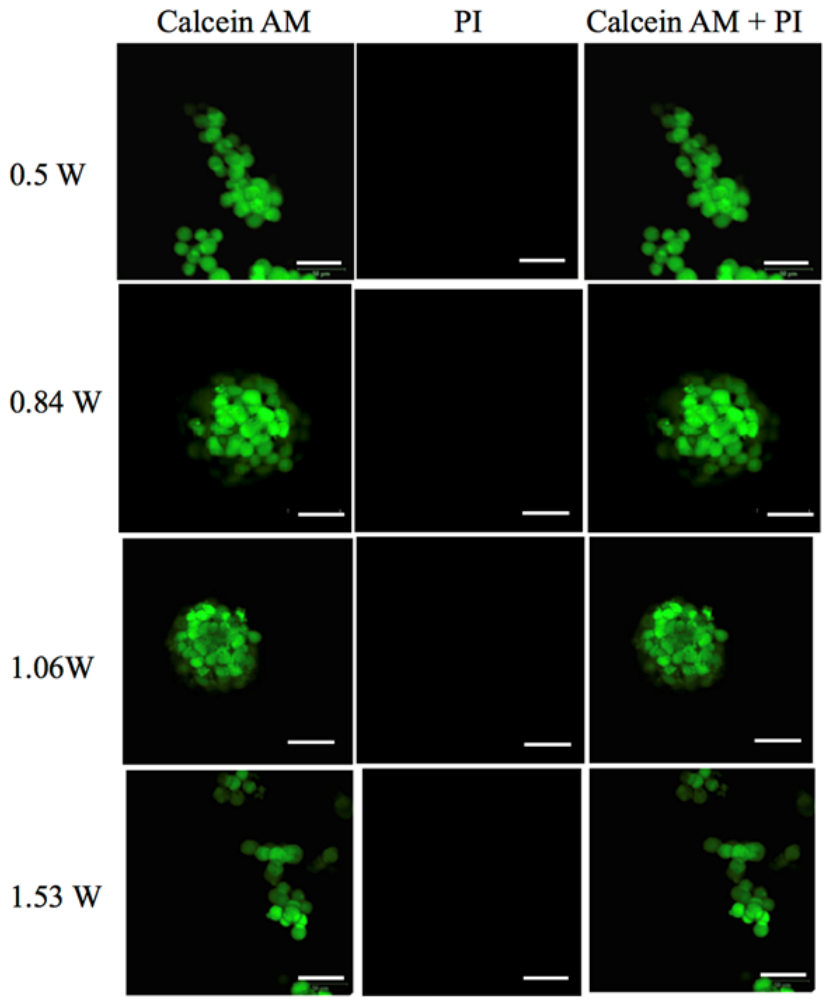

Figure 4.6: Effect of applied SAW power on the morphology of the cell aggregates prepared from a seeding density of 5 x 10^3cells/ml. These representative confocal microscopy images were obtained 2 hours after the SAW was applied to drive the microcentrifugation flow. The cells were then stained using a live/dead cell viability assay. Live cells are stained by Calcein AM and appear green; no cell is stained by propidium iodide (PI). Scale bars represent 50 μm in length

Figure 4.7 shows that the smallest spheroid cross-sectional area, i.e. the most compact spheroids, and the most circular spheroids were obtained at intermediate powers of about 1 W. This was consistent with previous findings on SAW microcentrifugation-driven particle concentration, which found that the tendency for particles to concentrate increased with the power applied and hence the intensity of the microcentrifugation flow up to a point beyond which the increasingly rapid convective flow overcame the diffusion-driven particle concentration dynamics, thereby leading to re-dispersion of the particles [381]. The existence of an optimum at intermediate applied powers is also true for the formation of spherical spheroids with *IP* values close to 1, given that excessive convective dispersion at high microcentrifugation velocities leads to increasingly chaotic flow [362] that promotes increasing irregularity in the cell aggregates. Furthermore, the optimum for spheroid shape shifted slightly to higher powers for larger cell seeding densities. This suggests that greater microcentrifugation velocity thresholds are necessary to concentrate and also to disperse larger numbers of cells, given the increase in the intrinsic viscosity with greater cell concentrations [391].

The ability to achieve some degree of control over spheroid uniformity for different cell densities using the SAW device is a significant advantage because of importance of spheroid uniformity, especially for many cell-based assays [118]. Non-uniform spheroids commonly lead to non-uniformities in the exposure and diffusion of reagents to the cells, thus resulting in large variations in the observed cell behaviour [392]. In addition, image analysis in these studies is also complicated by irregularity in spheroid morphology. By contrast, other microfluidic techniques such as the microarray- and microcapsule-based approaches only yield spheroids of a fixed size range for a given system geometry, therefore requiring expensive and laborious steps in tailoring different photomasks for the fabrication of different microstructures for each cell seeding density and desired size range.

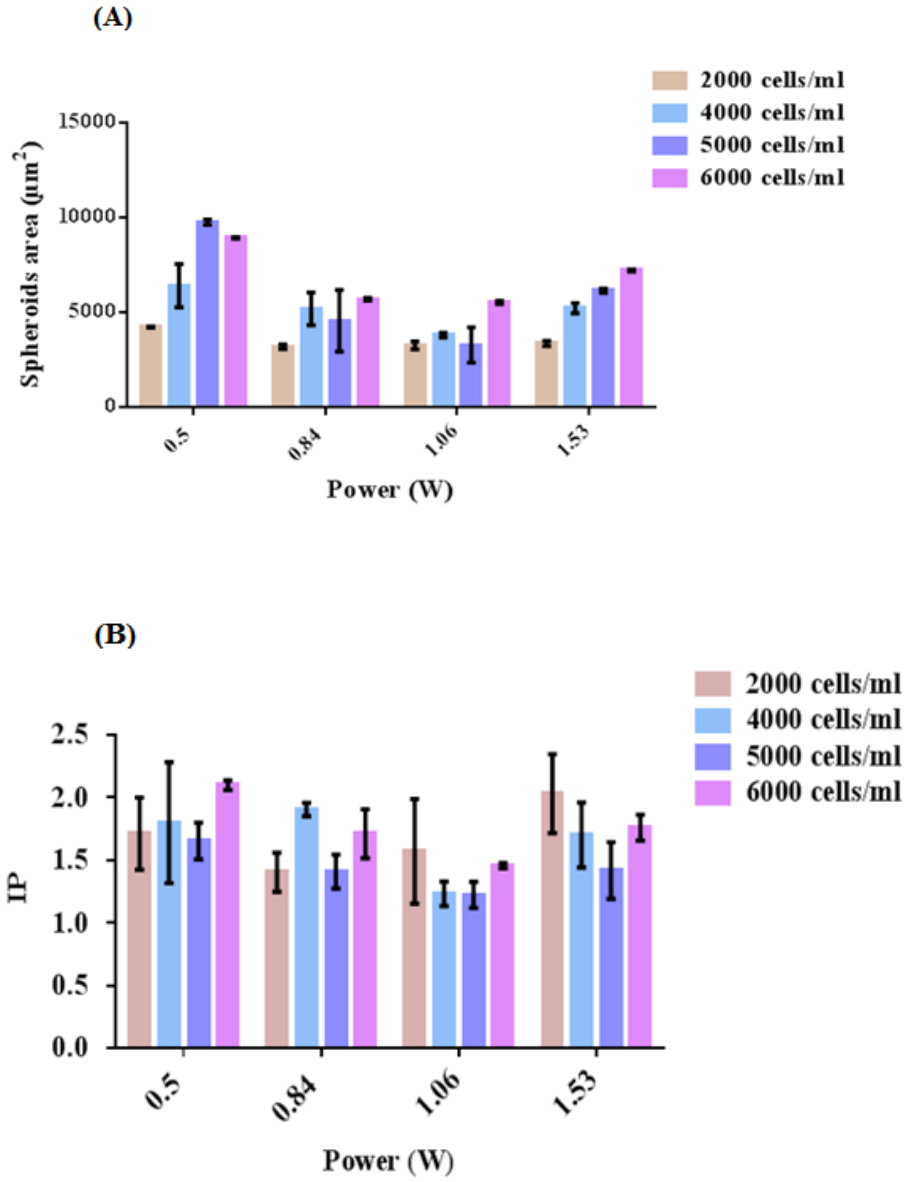

Figure 4.7: Effect of the SAW applied on the spheroid (A) cross-sectional area, and (B) irregularity parameter IP. The spheroids were obtained 2 hours after the SAW was applied to drive the microcentrifugation flow. The error bars represent the standard deviation (n = 3).

4.3.3 Spheroid Proliferation

The representative confocal microscopy images in **Figure 4.8** show that the size of the spheroids generated by both the SAW microcentrifugation method and the liquid overlay method (control) increased over time, indicating the proliferation of cells. The vast majority of cells on the periphery of the spheroids remained viable (stained green by Calcein AM) and formed a shell around a poorly stained core, but there was little evidence of necrotic or dead cells (stained red by PI). This lack of central staining may be because PI is impermeable to live cells and did not penetrate through the outer viable cell layer to reach the cells at the centres of the spheroids, as discussed earlier as other studies on tumor spheroid also observe similar phenomenon [11, 323]. Necrotic cores are common in spheroids, especially in older and larger spheroids, in which the cells in the centre of the spheroid are deprived of oxygen and nutrients due to diffusion limitations [11, 334].

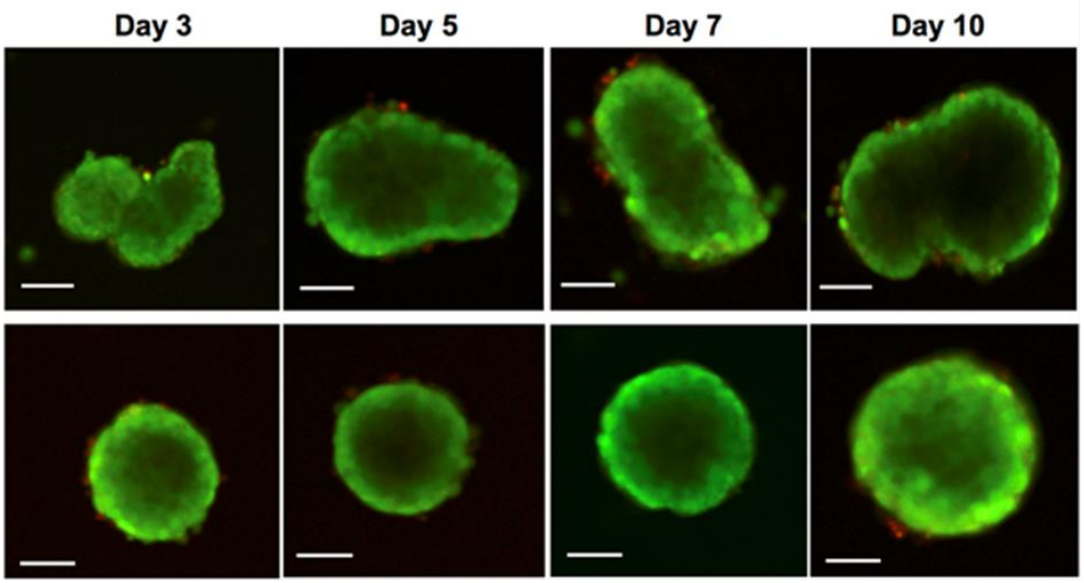

Figure 4.8: Representative confocal microscopy images showing the viability of spheroids cultured using both the liquid overlay (LO, top panel) and SAW microcentrifugation (SAW, bottom panel) methods over a period of 10 days. In both cases, the spheroids were prepared from a seeding density of 5 x 10^3cells/ml and stained using a live/dead cell viability assay. Live cells, which appear green, are stained by Calcein AM; dead cells, which appear red, are stained by propidium iodide. Scale bars represent 100 μm in length.

Proliferation of the cells forming the spheroids was assessed by determining the DNA content, given that DNA is a cellular component that accurately reflects the cell number. **Figure 4.9** shows that the number of cells in the spheroids cultured using both the SAW microcentrifugation method (p = 0.01, n =3) and liquid overlay method (p < 0.001) increased gradually over a 7 day period, indicating that the cells proliferated within the spheroids.

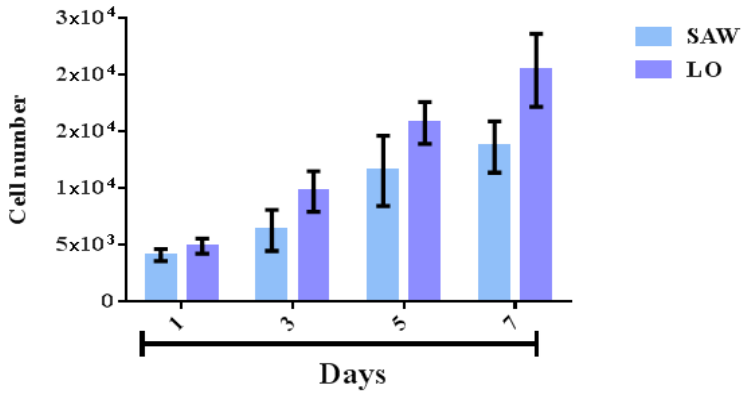

Figure 4.9: Gradual increase in the proliferation of BT-474 cells in spheroids cultured using both the liquid overlay and SAW microcentrifugation methods over a period of 7 days, as assessed by increase in DNA content. In both cases, the spheroids were prepared from a seeding density of 5 x 10^3cells/ml. The error bars represent the standard deviation (n = 3).

This proliferation was also by the quantitative data in **Figure 4.10** showing that the mean diameter for spheroids produced from the SAW microcentrifugation method (p < 0.0001, n = 5) increased over time, although spheroid shape became more irregular. Spheroids produced using the liquid overlay method exhibited relatively large variation in diameter within the same treatment due to their more irregular shapes. Spheroids produced using the SAW microcentrifugation method had a smaller size and a lesser irregularity parameter (IP) (closer to a value of 1) than did spheroids obtained with the liquid overlay method, suggesting the possibility of using the SAW microcentrifugation method to synthesise more uniform and compact spheroids, allowing them to be potentially more useful for cell-based assays.

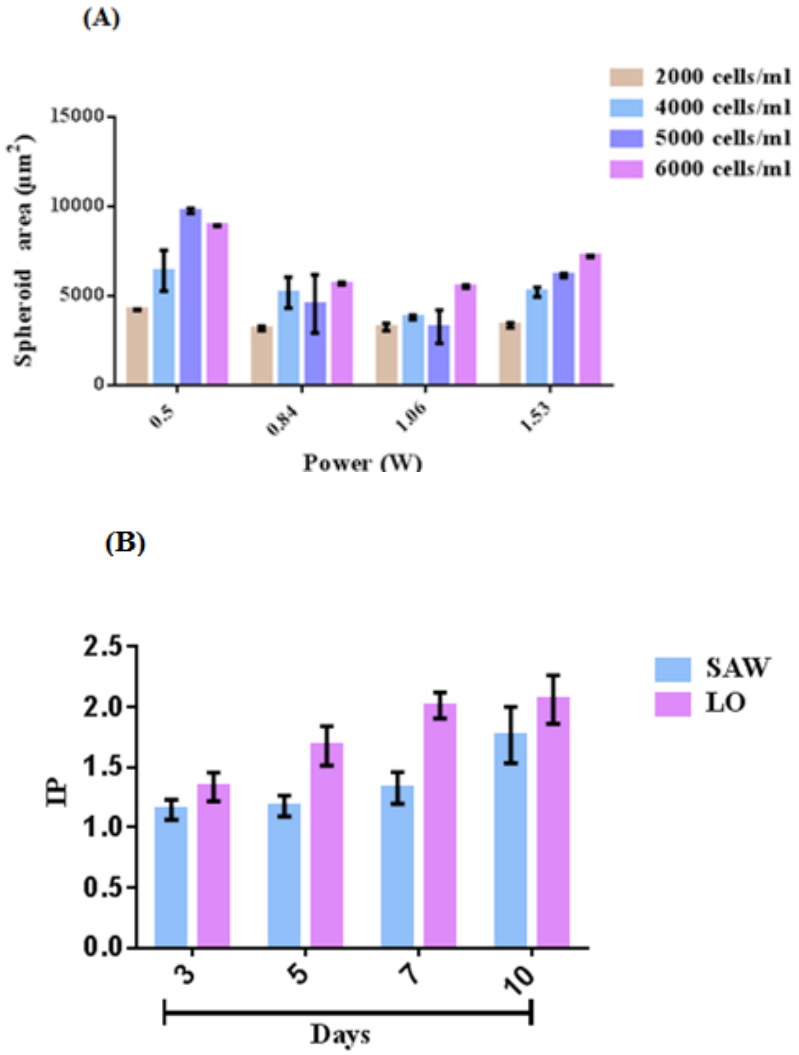

Figure 4.10: (A) Diameter and (B) irregularity parameter (IP) of spheroids obtained using both the conventional liquid overlay (LO) and SAW microcentrifugation (SAW) methods with a seeding density of 5 x 10^3cells/ml. The error bars represent the standard deviation (n = 3).

Figure 4.11 is a representative histological section of a spheroid produced with the SAW microcentrifugation method showing the distribution of cells; nuclei appear in violet from the H&E staining. A large number of cells are tightly packed within the spheroid, typical of tumor morphology [11]. It is this tight packing that limits nutrient and oxygen diffusion into the spheroid interior, thus resulting in the necrotic cores observed in **Figure 4.8** and may explain the lack of stain penetration in live/dead staining. Indeed, such concentric heterogeneous cell populations of spheroids mimic the

avascular stage of tumours *in vivo* [393], making the *in-vitro* spheroid model a useful tool for cancer biology studies.

The spheroids produced by both methods exhibited heterogeneous cell subpopulations that contained viable cells at their periphery and non-viable cells in their core. Such necrotic cores are common in spheroids, especially in older and larger spheroids, in which the cells in the centre of the spheroid are deprived of oxygen and nutrients due to limitations on diffusion [11, 334].

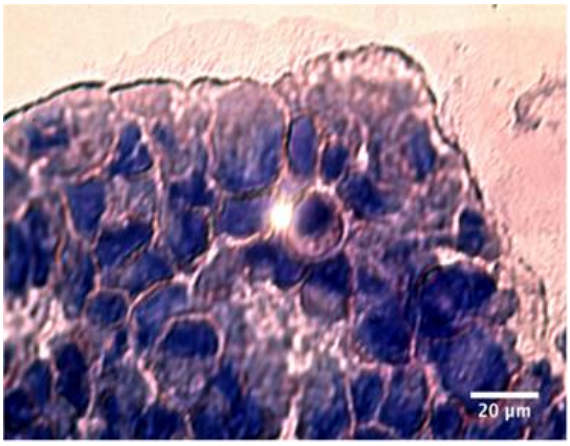

Figure 4.11: Representative image showing the histological section of a spheroid generated using the SAW microcentrifugation device with a seeding density of 5 x 10^3cells/ml. The 20-day old spheroid was stained by H&E and visualized using light microscopy.

4.3.4 F-actin Organisation

The cytoskeletal organisation and focal adhesion of the spheroids generated using the SAW microcentrifugation method compared with those of monolayer cells are shown by the representative images in **Figure 4.12**. Actin filaments in the cytoskeleton of the spheroids were stained red by TRITC-conjugated phalloidin, while the focal adhesion marker vinculin was stained green by fluorescently labeled anti-vinculin monoclonal antibody. Monolayer cells exhibited the usual spindle morphology and displayed more well-spread actin filaments and typical cell–substrate adhesion. By

contrast, in the spheroids the organisation of the actin filaments was more irregular whereas the vinculin appears more aggregated, especially at the centre of the spheroids. As shown in **Figure 4.13,** compared with monolayer cells, the mean flourscent intensity (MFI) of vinculin expressed by the spheroids produced using the SAW microcentrifugation method was significantly greater ($p < 0.0001$, $n = 20$), again indicating that the vinculin in spheroids was more aggregated than that in monolayer cells. Together, these suggest the formation of tight cell–cell interfaces in the spheroid, thus suggesting again the possibility of the production of tumour-like spheroids by the SAW microcentrifugation method.

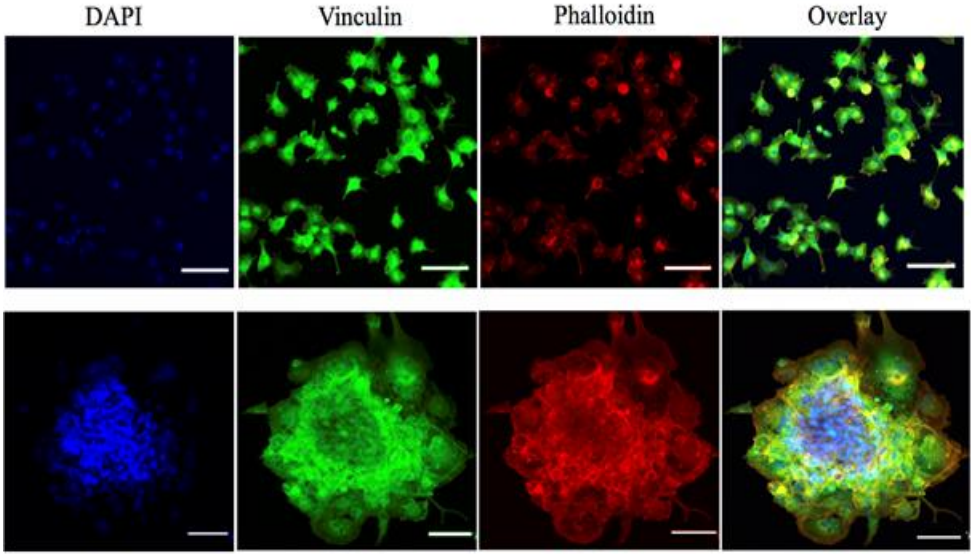

Figure 4.12: Representative confocal microscopy images revealing the focal adhesion points and nuclei of monolayer BT-474 cells (top panel, control) and that of a 20-day old BT-474 spheroids generated using the SAW microcentrifugation device (bottom panel). Nuclei were stained blue by DAPI, focal contacts were stained green by anti-vinculin antibody, and F-actin was stained red by TRITC-conjugated phalloidin. Images were overlaid in the last column. The scale bars represent 100 μm in length.

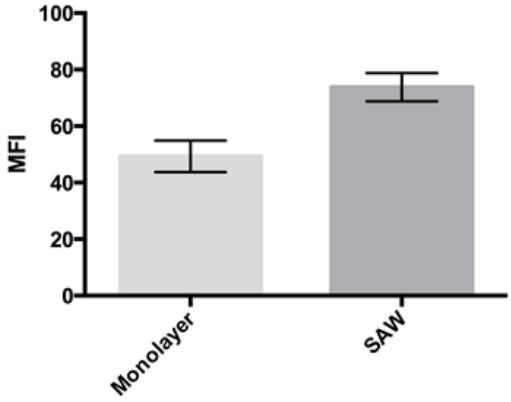

Figure 4.13: The mean fluorescence intensity (MFI) of vinculin expressed in monolayer BT474 cells (control) and 20-day old BT-474 spheroids generated using the SAW microcentrifugation device. The error bars represent the standard deviation (n = 20).

4.4 Conclusion

In summary, this chapter has presented evidence of the feasibility of interfacing a SAW microfluidic device with a superstrate, such as a tissue culture dish or a microarray well plate, for the controlled generation of uniform multicellular spheroids. This has considerable advantages over other microfluidic devices for spheroid production, as it uses existing laboratory formats already highly familiar to biologists and laboratory technicians and for which ancillary equipment such as microscopes and plate readers have been designed to fit are retained, without requiring further investment into new analytical equipment. Furthermore, the chip-scale dimensions of the SAW device, as well as its low cost, by exploiting the economies of scale associated with large volume nanofabrication, facilitate scale-out (i.e. numbering up) for high-throughput operation. Whilst this study has demonstrated the use of a SAW device to enhance spheroid production in a single microwell on a standard tissue culture microplate, it is equally feasible to envisage the use of multiple SAW devices in parallel, for example one under each well.

The acoustic irradiation was coupled into the microwell through a fluid couplant layer sandwiched in between. Through symmetry breaking of the sound waves in the liquid, an intense microcentrifugation

flow was induced in the microwell, which drove the cells into a tight aggregate. This was aided by the use of a low-adhesive hydrogel coating on the microwell walls, which prevented cell adhesion to the wall and suppressed standing sound waves, which trap cells at nodal positions away from the centre. This study has shown the generation of compact and circular spheroids, the size of which was controlled by modulating the input power of the SAW; the most compact and uniform (in terms of circularity) spheroids were obtained at intermediate powers, since a trade-off existed between the increasing concentration and aggregation of cells with more intense microcentrifugation flow as the power was increased and the increasingly dispersive nature of the intense chaotic flow at high power. This optimum power depended on the cell seeding density. The ability to control spheroid size simply through the input power represents a distinct improvement on current processes, since it circumvents the need for the fabrication of multiple devices with various geometric designs. Moreover, the cell concentration process was rapid, requiring only a minute, compared with conventional methods such as liquid overlay methods, which require at least a day. The fast gelation rate of the CMC-TYR hydrogel also considerably reduced the preparation time for coating of the tissue culture surface. Compared with the conventional hanging drop method, the SAW microcentrifugation method had the advantage of being able to handle larger fluid volumes. Furthermore, the resulting spheroids exhibited a concentric heterogeneous cell population arrangement and the tight cell-to-cell interfaces typically observed in solid tumors *in vivo*, thus demonstrating the usefulness of the platform for improving investigations of cancer biology and drug screening.

CHAPTER FIVE

Assessment of the Potential of a High Frequency Acoustomicrofluidic Nebulisation Platform for Inhaled Stem Cell Therapy

5.1 Introduction

There is growing evidence that demonstrates the efficacy of stem cell-based therapies for the treatment of a variety of lung diseases, including: chronic obstructive pulmonary disease (COPD); pulmonary and cystic fibrosis; and pulmonary hypertension [13, 14]. This is especially timely given the recognition of the urgency for new approaches to treat lung diseases in light of its increasing prevalence, in particular of COPD, which is anticipated to be among the leading causes of global mortality in the next 5 years. Motivated by the shortage of donor lungs and the extremely high mortality rate (almost 50%) following lung transplantation, there is an increasing number of studies examining the potential of stem cell administration to injured lungs, for both an immodulatory role to attenuate inflammation and a regenerative role for injury repair [394].

There are, however, far fewer studies on the development of methods to administer stem cells to the lung. While there have been investigations that show recruitment of stem cells to the lung following systemic (e.g. intravenous) administration, recruitment depends on many critical factors [395]. Direct lung delivery via aerosol inhalation, on the other hand, not only facilitates local targeting of the disease- or injury-specific region, but also allows easy and painless administration, involves fewer side effects and avoids the need for anaesthesia.

Nevertheless, there remain considerable challenges associated with stem cell aerosolisation, in particular the stem cell survival and retention of function during the nebulisation process. Their fragility rules out the use of a wide number of commonly-used nebulisation techniques, particularly those that subject the aerosols to intense stresses (e.g. shear, cavitation and heat) such as jet (compressed air) and conventional ultrasonic nebulisers [396-398]. By contrast, electrohydrodynamic atomisation is a viable method for stem cell delivery [399-402], although the necessity for large (kV) DC potentials typically renders electrospray impractical as a portable consumer inhalation device from a safety viewpoint.

MSCs possess multi-lineage potential to differentiate into a number of cell types including osteocytes, adipocytes and chondrocytes. They express surface markers CD29, CD44 and CD106, these markers often being considered indicators for MSC isolation as well as differentiation [403-406], and therefore used to assess the pluripotent phenotype and integrity of the MSCs prior to and after nebulisation at different time intervals.

In this chapter, the aim was to develop and evaluate a novel high frequency acoustic nebulisation platform as an effective aerosolisation technique for inhaled mesenchymal stem cell (MSC) therapy. This is the first study that has investigated the viability of stem cells under surface acoustic wave (SAW) nebulisation. SAWs [366, 368] operate at much higher frequencies (10–100 MHz) [407] than conventional bulk ultrasonic nebulisers (10 kHz – 1 MHz) [408] and so the vibrational excitation to which the cells are subjected occurs over a much shorter period than their hydrodynamic shear relaxation time scales, thus eliminating the risk of cell lysis [264, 409]. Additionally, the low power (about 1 W) is one to two orders of magnitude less than that required by conventional ultrasonic nebulisers and so not only eliminates the possibility of cavitation but also makes feasible the development of miniaturised options, such as battery-powered portable handheld devices [410]. While the efficacy of the SAW nebulisation has been demonstrated for proteins, e.g. monoclonal

antibodies for lung tumour inhibition [411] and nucleic acids, e.g. plasmid DNA for influenza vaccination [412], as well as for microfluidic mass spectrometry interfacing [413-415] and protein substrate patterning [416], there has yet to be a demonstration of the efficacy of the SAW nebulisation platform for pulmonary stem cell delivery. Stem cells did retain their viability and functionality under SAW excitation, but the intensity of the vibration to which the cells were subjected (typically 100 mW) were far below the critical levels required for nebulisation [417].

5.2 Methods

5.2.1 Cell culture

GIBCO® rat (SD) MSCs from the bone marrow of Sprague Dawley rats (Life Technologies, Mulgrave, VIC, Australia) were maintained in cell culture medium comprising D-MEM with GlutaMAX™ supplemented with 10% MSC qualified FBS and 5 μg/ml gentamicin at 37°C in a humidified 5% CO_2 incubator. Cells were rinsed with DPBS, followed by trypsinisation with TrypLE™ after reaching 80% confluence. The harvested cells were rinsed with cell culture medium and reconstituted to a cell suspension solution containing 2×10^6 cells/ml.

5.2.2 SAW nebuliser device fabrication and setup

A 0.5 mm thick 127.68° Y-axis rotated, X-axis propagating lithium niobate wafer (Roditi Ltd, London, UK), which constituted the piezoelectric substrate on which the SAWs were generated, was first cleaned according to standard procedures [365]. The electrodes were then fabricated on the wafer using standard UV photolithography according to a protocol modified from Qi et al. [377]. In brief, the clean wafer was sputtered with a 5 nm thick layer of chromium followed by a 1.5 μm thick layer comprising 99% aluminium and 1% copper using

an electron beam evaporator (Nanochrome II, Intlvac Corp., Niagara Falls, NY, USA). The wafer was then spun-coated with a thin layer (approximately 3 μm thick) of AZ4562 photoresist (Microchemicals GmBH, Ulm, Germany) followed by exposure to UV through a glass mask. The next step comprised the development of the photoresist layer and wet etching using an aluminium etchant, ANPE 5-5-80-10 (Microchemicals GmBH, Ulm, Germany) to generate the IDT patterns, which consisted of elliptical single-phase unidirectional transducers (SPUDT) [363] with an electrode finger width and spacing corresponding to a resonance frequency of approximately 30 MHz. The wafer containing the SPUDT was subsequently diced into microchips, each of approximately 18 mm length and 12 mm width.

A two-dimensional spatial distribution of the surface displacement amplitude near the focal point of the elliptical SPUDT was measured with a laser Doppler vibrometer (LDV) (UHF-120, Polytec GmBH, Waldbronn, Germany); an in-depth analysis of the surface displacement patterns produced by various IDT designs can be found in Shilton et al.[363]

To affect the nebulisation process in order to generate the aerosol-laden MSCs, the edge of a SAW microchip was partially immersed into the MSC suspension contained in a Petri dish, as depicted in **Figure 5.1**. Rayleigh SAWs were then generated by applying an input oscillating electrical signal to the SPUDT at the resonant frequency using a signal generator (SML01, Rhode & Schwarz, Munich, Germany) and amplifier (10W1000C, Amplifier Research, Souderton, PA, USA). Above a critical power of 1.5 W, nebulisation ensued and the resultant aerosol mist containing the MSCs was collected for further characterisation.

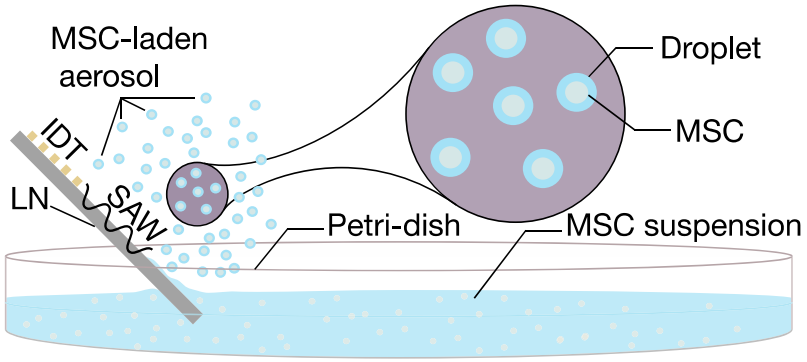

Figure 5.1: Schematic depiction of the SAW nebulisation setup for rapid aerosolisation of MSCs (not to scale). Power is supplied as an oscillating electrical signal to the SPUDT electrodes photolithographically patterned onto a lithium niobate (LN) substrate. This causes the generation of a SAW, which, when in contact with the MSC suspension in the Petri dish, nebulises the fluid to form an aerosol mist, each droplet of which contains MSCs.

5.2.3 Aerosol characterisation

The SAW device was characterised to determine its nebulisation rate and the aerosol sizes under ambient conditions. The nebulisation flow rate of the SAW nebuliser device was first modulated by adjusting the input power (1.5–3 W) and the time for a fixed volume of solution to completely nebulise was subsequently measured. Aerosol droplet sizes were determined using laser diffraction (Spraytec, Malvern Instruments, Malvern, UK), specified as a median diameter from a volume-based size distribution; a mean value across five replicates was calculated.

5.2.4 Characterisation of cell morphology, viability and proliferation

For preliminary testing, the nebulised MSCs were first collected and stained with trypan blue to assess their viability. Cells were counted immediately to quantify the stained and unstained cells using an automated cell counter (Countess®, Life Technologies Pty. Ltd., Mulgrave, VIC, Australia).

The nebulised MSCs were transferred to a new tissue culture well-plate at a seeding density of 5×10^3 cells/ml for re-culturing for 2 and 24 hours in order to determine their viability, metabolic activity and proliferation ability. The morphology of the cells was monitored using phase contrast microscopy and images were captured at various time points. The viability of the re-cultured MSCs was examined by staining the cells with Calcein AM and PI according to the manufacturer's instructions; viable cells stained green, while inviable cells stained red. The stained MSCs were re-cultured for 2 hours and visualised using laser scanning confocal microscopy (LSCM) (Eclipse Ti, Nikon Instruments Inc., Melville, NY, USA) without further rinsing. The stained MSCs that were re-cultured for 24 hrs were rinsed using phosphate buffered saline (PBS) before LSCM visualisation.

For quantification, in a separate experiment MSCs were nebulised as described above and collected. Some of these MSCs were immediately stained with Calcein AM and PI according to the manufacturer's instructions while others were transferred to a new tissue culture well-plate at a seeding density of 5×10^3 cells/ml and re-cultured for 24 hours. The recultured cells were then trypsinised and stained with Calcein AM and PI. The stained cells were analysed using flow cytometry (FACSCanto™ II, BD Biosciences, North Ryde, NSW, Australia). As a positive control, MSCs were treated with 0.1% Triton X-100 for 2-3 min prior to staining.

The metabolic activity of the re-cultured MSCs was quantified using an AlamarBlue® assay according to Hoo et al. [380]. In brief, spent medium was removed from each well prior to rinsing with Dulbecco's Phosphate-Buffered Saline (DPBS). AlamarBlue® dye (10%) diluted with cell culture medium was added into each well and incubated at 37°C in humidified 5% CO_2 for 4 h. Fluorescence was visualised using a multi-mode microplate reader with an excitation wavelength of 570 nm and an emission wavelength of 600 nm (SpectraMax® Paradigm, Molecular Devices LLC, Sunnyvale, CA, USA).

The ability of the nebulised MSCs to proliferate was determined by quantifying the deoxyribonucleic acid (DNA) content using a Picogreen® assay according to Hoo et al. [380]. In brief, the MSCs were trypsinised after re-culturing for 1, 3, 5 and 7 days. The cells were then washed twice using cold DPBS, followed by centrifugation for 5 min at 152 g The resultant cell pellet was subsequently collected for lysis using a NP40 cell lysis buffer for 30 min on ice and vortexed every 10 min; the cell lysates were subjected to a freeze-thaw cycle prior to centrifugation at 13000 rpm for 10 min at 4°C. Each 100 µl of clear lysate was aliquoted to a new 96-well plate and incubated for 5 min with 100 µl of PicoGreen® reagent. Fluorescence was subsequently analysed using a multi-mode microplate reader at an excitation wavelength of 480 nm and an emission wavelength of 520 nm. The number of cells in each sample was determined by correlating the DNA content with a standard curve, obtained using cell lysates containing a known number of MSCs. Non-nebulised cells were used as control for all of the experiments.

5.2.5 Reverse-transcription polymerase chain reaction (RT-PCR) and real-time polymerase chain reaction (qPCR)

The gene expression of nebulised MSCs and control MSCs were determined qualitatively using RT-PCR and quantitatively using qPCR with CD29, CD44, and CD106 as markers. Ribonucleic acid (RNA) was isolated from the MSCs using an RNAeasy Mini Kit (Qiagen, Chadstone, VIC, Australia) according to the manufacturer's instructions. The RNA quality and concentration were examined using a spectrophotometer (ND-1000, NanoDrop Technologies, Thermo Fisher Scientific Inc., Waltham, MA, USA). To eliminate any contaminating genomic DNA, the isolated RNA was treated with a DNA-free™ kit (Life technologists, Australia) according to the manufacturer's protocol. Complementary DNA (cDNA) was generated using a QuantiTect Reverse Transcription kit (Qiagen, Chadstone, VIC, Australia) according to the manufacturer's instructions and subjected to PCR amplification using primers obtained from Geneworks Pty. Ltd. (Thebarton, SA, Australia); the primer sequences are listed in **Table 5.1**. Glyceraldehyde-3-phosphate dehydrogenase (GAPDH) was used as the housekeeping gene. For RT-PCR, the PCR products were size-fractionated using 1.5% agarose gel electrophoresis.

The qPCR analysis was performed on a Rotor-Gene Q (Qiagen, Chadstone, VIC, Australia) using a QuantiTect SYBR® Green PCR kit (Qiagen, Chadstone, VIC, Australia). After 10 min of denaturation at 95°C, 40 PCR cycles were carried out: 95°C for 15 s, 60°C for 30 s, and 72°C for 15 s. The relative mRNA levels were calculated using the $\Delta\Delta C_T$ method according to Sarvi et al. [418]. The results were reported as fold change values compared with the non-nebulised cells.

Table 5.1: PCR primer sequences:

Gene	Forward/reverse (5' 3')	Ref.
ITGB (CD29 protein)	AATGGAGTGAATGGGACAGG / TCTGTGAAGCCCAGAGGTTT	[419]
CD44	TTGGCATCCCTCCTGGCGCTGG / AAGGAGGAACTGGAAGAGACCC	[420]
CD106	CCTCACTTGCAGCACTACGGGCT / TTTTCCAATATCCTCAATGACGGG-	[421]
GAPDH	CAAGGTCATCCATGACAACTTTG / GTCCACCACCCTGTTGCTGTAG	[422]

5.2.6 Immunophenotyping

MSCs possess multi-lineage potential to differentiate into a number of cell types including osteocytes, adipocytes and chondrocytes. They are known to express surface markers CD29, CD44, and CD106 positively, these markers often being considered indicators for MSC isolation as well as differentiation [403-406], and therefore used to assess the pluripotent phenotype and integrity of the MSCs prior to and after nebulisation at different time intervals. MSCs were nebulised as described previously and collected for further cultivation. After 24 h of cultivation, the cells were harvested and aliquoted at a concentration of 1×10^6 cells per sample. The cells were washed with PBS and centrifuged at 1500 rpm three times and subsequently re-suspended in buffer [0.1% bovine serum albumin (BSA) in PBS] containing antibodies and incubated on ice for 25–30 min. The MSCs were labelled with one of Alexa Fluor 488®-conjugated integrin beta-1/CD29 antibody (Life Technologies, Mulgrave,

VIC, Australia), FITC-conjugated anti-CD44 antibody (Merck Millipore, Bayswater, VIC, Australia) or PE mouse-conjugated anti-rat CD106 antibody (BioLegend, San Diego, CA, USA), followed by labelling with FITC-conjugated goat anti-mouse IgG secondary antibodies (Merck Millipore, Mulgrave, VIC, Australia); the antibodies were diluted according to the manufacturer's protocols. The labelled MSCs were then washed twice in buffer (3% BSA in PBS), followed by resuspension in 500 µl of buffer (3% BSA in PBS) and analysed by flow cytometry; 10,000 events were acquired from each sample and the results were plotted using flow cytometry data analysis software (Flowing Software, v2.5.1, www.flowingsoftware.com). The surface marker expression of the nebulised cells was compared with that of the non-nebulised cells (control).

5.2.7 Statistical analysis

All experiments were performed with at least three replicates. Unless otherwise stated, the results were reported as the average value ± standard deviation. Multiple groups of data were compared using One-Way Analysis of Variance (ANOVA), while two groups of data were compared using Student's t-test; differences were considered statistically significant when $p < 0.05$.

5.3 Results and Discussion

5.3.1 Aerosol characterisation

As shown in **Figure 5.2**, the applied SAW power had a direct influence on the nebulisation rate, which increased as the power was ramped to approximately 350 µL/min at 3 W ($p < 0.0001$, $n = 3$).

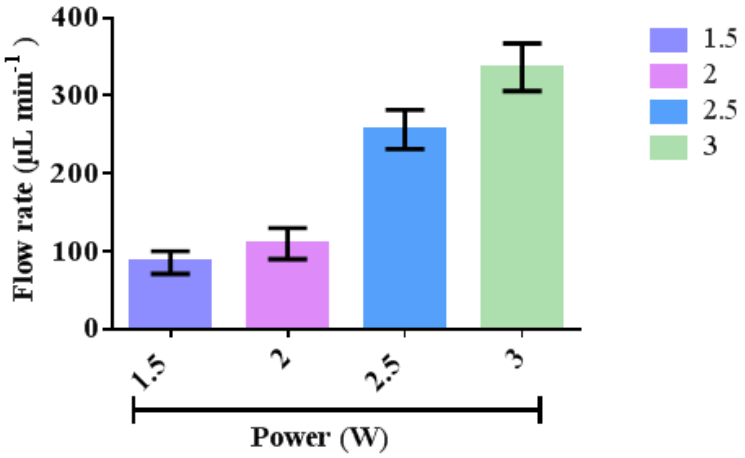

Figure 5.2: SAW nebulisation rate (µL/min) as a function of the power applied to the device. The data are represented as mean value ($n = 3$) ± standard error.

The corresponding surface displacement amplitude of the SAW is plotted in **Figure 5.3**, which shows a linear response in the magnitude of the surface displacement with an increase in the power input, indicating that the device has not reached its power saturation limit**.** These observations are consistent with previous findings that as more acoustic energy is transmitted into the fluid to drive both streaming and destabilisation of its interface, this, in turn, leads to its disintegration into aerosol droplets that constitute the nebulised mist [410].

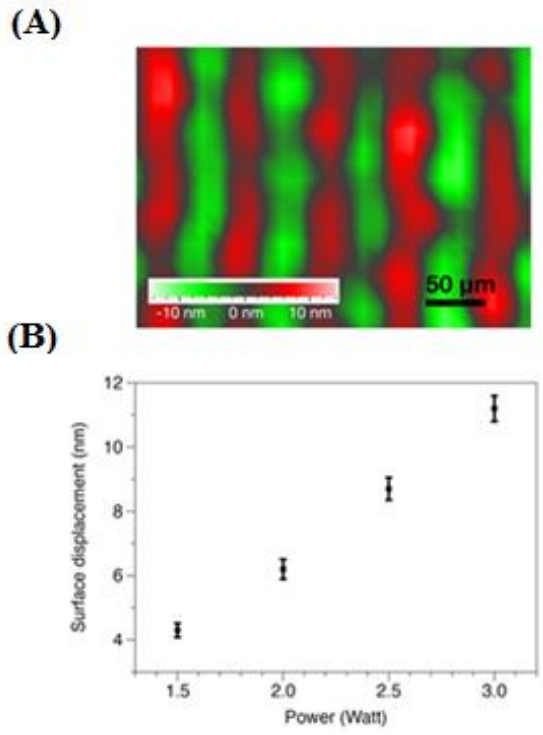

Figure 5.3: (A) Representative two-dimensional spatial distribution of the surface displacement at the focal region of the SPUDT, obtained using laser doppler vibrometry at an input power of 2.5 W, (B) Average surface displacement as a function of the input power to the device that corresponds to the nebulisation rates.

Table 5.2 shows that the mean aerosol size across all input powers was about 13 µm, which is similar to the size of a single MSC, thus indicating that most of the droplets contained a single cell. Aerosols with droplet sizes >5 µm would be expected to deposit due to inertial impaction in the upper respiratory tract [357, 423]. Therefore there is potential for the use of the SAW device in inhaled stem cell delivery for tissue repair and regeneration within the extra-thoracic (pharyngeal and laryngeal) regions.

Table 5.2: Median aerosol drop size as a function of the input power to the SAW device measured using laser diffraction.

Applied power (W)	Median droplet size (μm)
1.5	13.17 ± 0.29
2.0	13.33 ± 0.29
2.5	13.50 ± 0.50
3.0	13.50 ± 0.50

5.3.2 Cell morphology and viability

In a preliminary study to optimise the SAW nebulisation (in terms of maximising retention of the cell viability post-nebulisation). Cell viability was judged by Trypan blue assay and (cells were examined using Trypan blue immediately after being nebulised and cell viability were calculated by normalising the number of viable cells in the nebulised samples against the viable cells in the untreated samples). Cell viability decreased with increasing applied power (**Figure 5.4)**, possibly due to the increase in the stresses to which the cells are subjected with increasing levels of acoustic radiation pressure. This observation is consistent with a previous study using SAW radiation to drive osteoblast perfusion into tissue scaffolds (although not via nebulisation), in which cell viability decreased as the power applied increased [372]. Cell viability (normalised by that of the control cells) remained relatively high—close to 90% even at 1.5 W, which, together with the 100 μL/min delivery at this power (**Figure 5.2**), is adequate for most stem cell therapeutic applications and demonstrates the potential efficacy of the device as a platform for pulmonary stem cell delivery. To minimise the loss in stem cell viability, the device was henceforth operated at the optimum applied power of 1.5 W.

The minimum power need to drive microcentrifugation is 1.5 W, below this power, no microcentrifugation was observed.

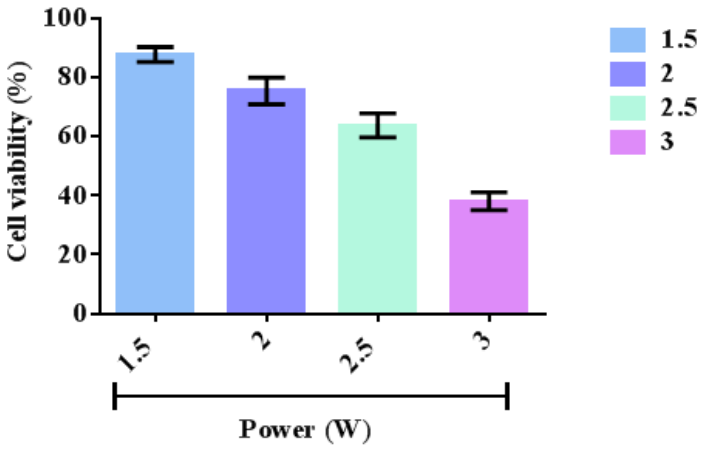

Figure 5.4: Post-nebulisation MSC viability as a function of the power applied to the SAW device, measured immediately after nebulisation using a trypan blue assay. The data are represented as mean value (n = 3) ± standard error.

Figure 5.5 shows representative LSCM images of the cells stained with Calcein AM and PI after being seeded on a new well-plate and incubated for 2 and 24 hours. At 2 hours post-nebulisation, most of the MSCs were stained by Calcein AM (green), indicating that they remained viable after nebulisation. These MSCs had started to attach on to the well-plate. At 24 hours post-nebulisation, the nebulised MSCs exhibited spindle-like morphology similar to that of untreated cells, indicating the retention of their structural integrity post-nebulisation. Furthermore, most of the cells were viable (stained green with Calcein AM) and there were relatively few inviable cells (stained red with PI).

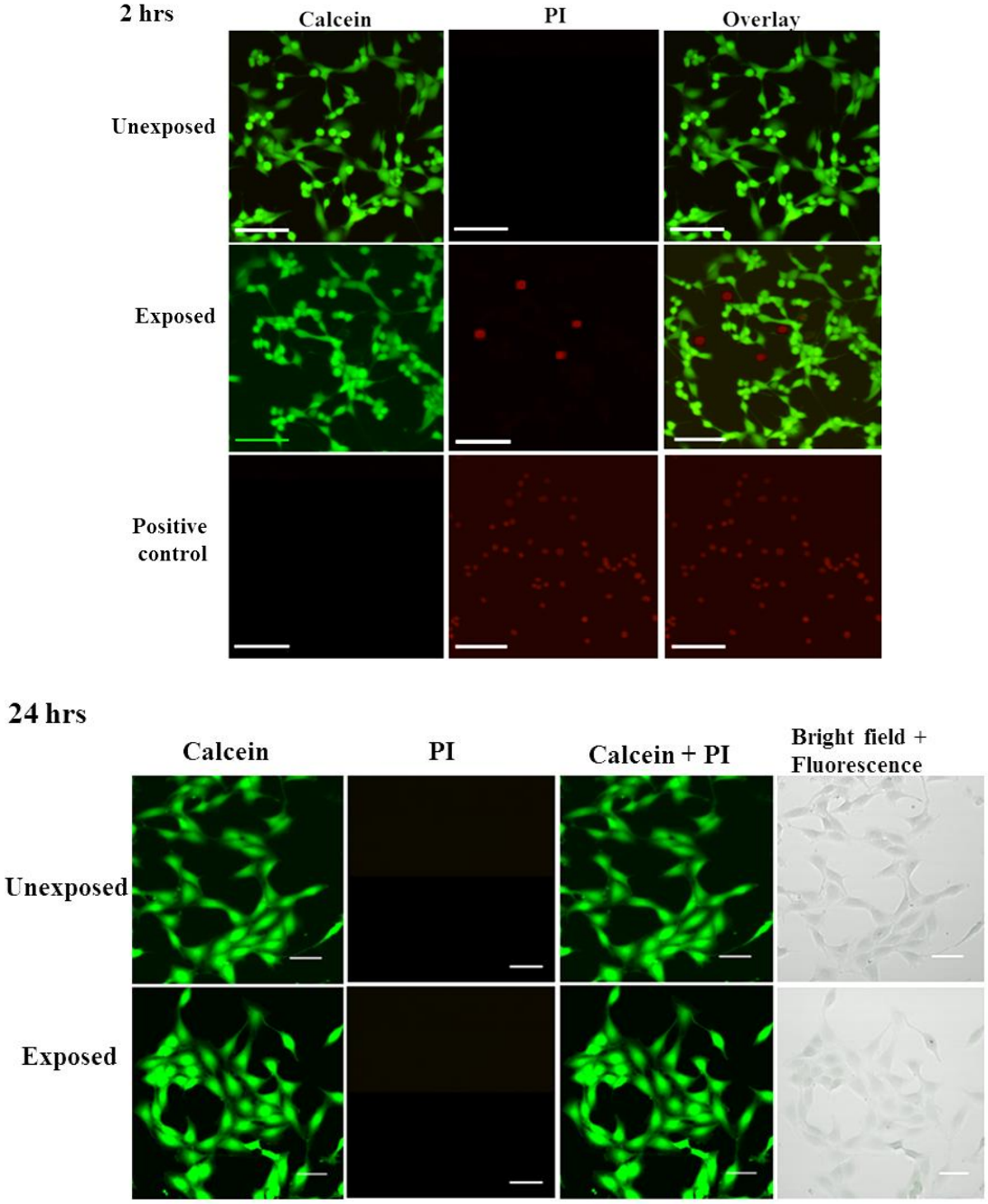

Figure 5.5: Viability of unexposed and nebulised MSCs, as indicated by Calcein AM and PI staining. The cells were examined 2 hours and 24 hours post-nebulisation. Live cells stained by Calcein AM appear green and dead cells stained by PI appeared red. For the positive control, cells were treated with 0.1% Trition X-100 prior to staining. The scale bars represent a length of 50 μm.

The high cell viability was confirmed by flow cytometry, in which representative dot plots of Calcein AM intensity against PI intensity (**Figure 5.6)** showed that the majority of nebulised cells was stained with Calcein AM. MSCs nebulised at 1.5 W exhibited a viability of 86.0 ± 4.2% immediately after nebulisation. Nonetheless, MSC growth recovered after re-culturing for another 24 hours, to the extent that there was no significant difference in cell viability between nebulised MSCs and untreated MSCs ($p = 0.026$, $n = 4$). Thus, SAW nebulisation did not change MSC viability.

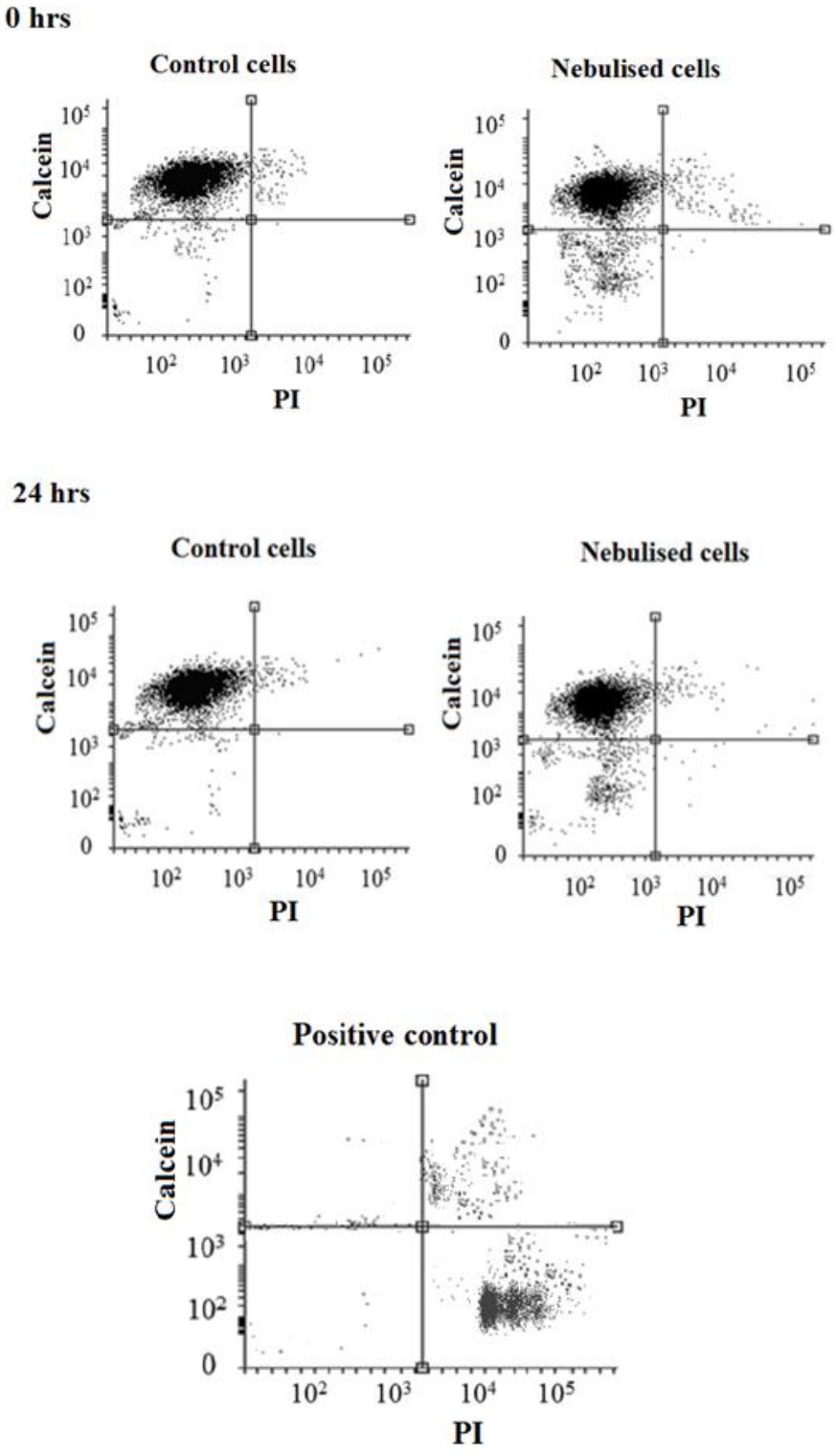

Figure 5.6: Flow cytometry analysis indicating the viability in the population of unexposed and nebulised MSCs stained with Calcein AM and PI immediately after nebulisation and at 24 hours after nebulisation. For the positive control, cells were treated with 0.1% Trition X-100 prior to staining**.**

5.3.3 Cell metabolic activity and proliferation

When MSCs were seeded into a well-plate and cultured over 7 days, as shown in the representative phase-contrast optical microscope images in **Figure 5.7**, both nebulised and untreated MSCs expanded and occupied more of the substrate area over time. In addition, the morphology of nebulised MSCs remained similar to that of untreated MSCs.

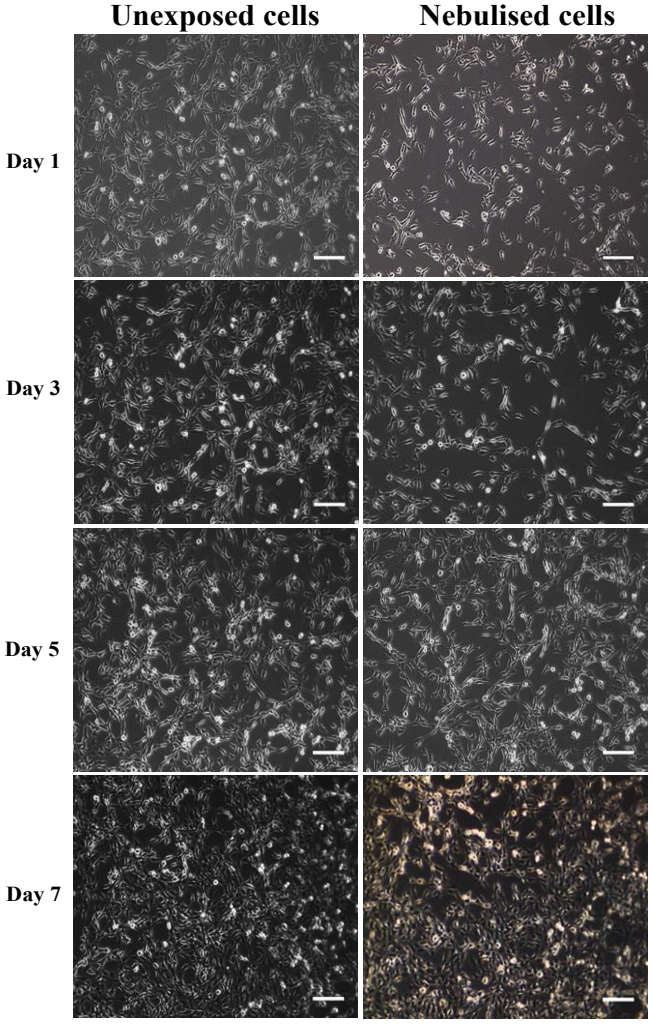

Figure 5.7: Phase contrast images of unexposed (left column) and nebulised (right column) MSCs acquired at different incubation times. The majority of cells exhibited a spindle-like morphology. Scale bars represent a length of 100 µm.

Figure 5.8 shows the metabolic activity of the nebulised MSCs over a period of 7 days, calculated by normalising the extent of AlamarBlue® reduced by the nebulised cells compared with that reduced by the untreated cells. The metabolic activity of the nebulised MSCs increased over time, regardless of the power at which the cells were nebulised, but decreased as the power applied increased. The metabolic activity of MSCs nebulised at 1.5 W was the greatest amongst the range of applied power that was tested. This observation is not surprising, given the decrease in cell viability with increasing power (**Figure 6.3**) which was expected to influence the metabolic rate proportionally.

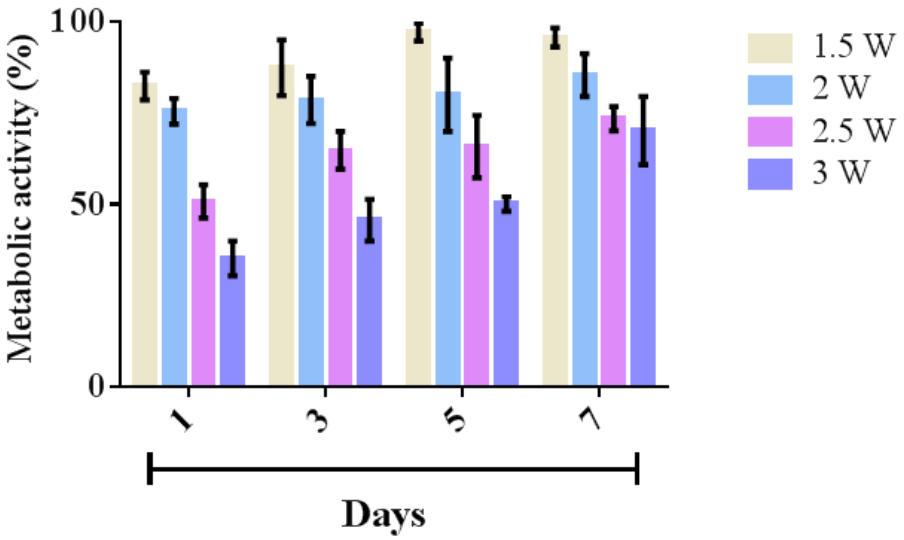

Figure 5.8: Metabolic activity of nebulised MSCs at day 1, 3, 5, and 7 days, determined using an AlamarBlue® assay, the results of which were normalised against the activity of the control, i.e. the unexposed cells (100% activity). The data are represented as mean (n = 3) ± standard error.

The strong correlation between the number of cells and DNA content allowed the cellular proliferation rate to be determined with high accuracy by measuring the DNA content of the MSCs over time using a Quant-iT PicoGreen® dsDNA assay. **Figure 5.9** shows that the number of MSCs increased gradually over a 7 day period in both the nebulised (p < 0.0001, n = 3) and untreated (p < 0.0001, n = 3) samples. This study note though that the nebulised

cells proliferated slightly slower from day 5 (p = 0.16, n = 3); nonetheless, the nebulised cells were observed to maintain their proliferation ability throughout the entire test duration.

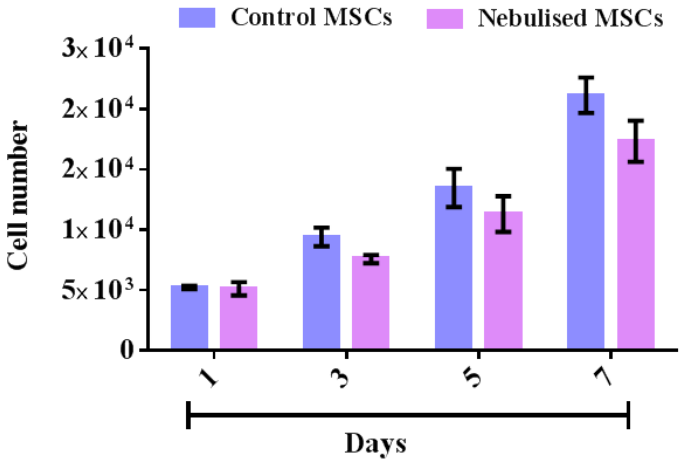

Figure 5.9: MSC proliferation after nebulisation at 1.5 W. Cell proliferation was determined by quantifying the DNA content using a Quant-iT PicoGreen® dsDNA assay. The data are represented as mean (n = 3) ± standard error.

5.3.4 Gene and protein expression

MSCs possess multi-lineage potential to differentiate into a number of cell types including osteocytes, adipocytes and chondrocytes. They express the surface markers CD29, CD44 and CD106. RT-PCR analysis of the expression of these three genes showed no significant different between control and nebulised MSCs at either 24 or 72 hours, and no significant trend with time, suggesting that nebulised cells were phenotypically similar to control cells (**Figure 5.10A)**.

Gene expression of the nebulised MSCs was further quantified using qPCR at different time points as shown in **Figure 5.10B**. Compared to the control, the nebulised MSCs continued to express similar levels of CD29, CD44 and CD106 after 24 hours (p = 0.92, n = 4; p = 0.6, n =

4 and p = 0.49, n = 4, respectively) and 72 hours (p = 0.5, n = 4; p = 0.65, n = 4; p = 0.98, n = 4, respectively), suggesting that SAW nebulisation did not alter the expression of these genes in the MSCs.

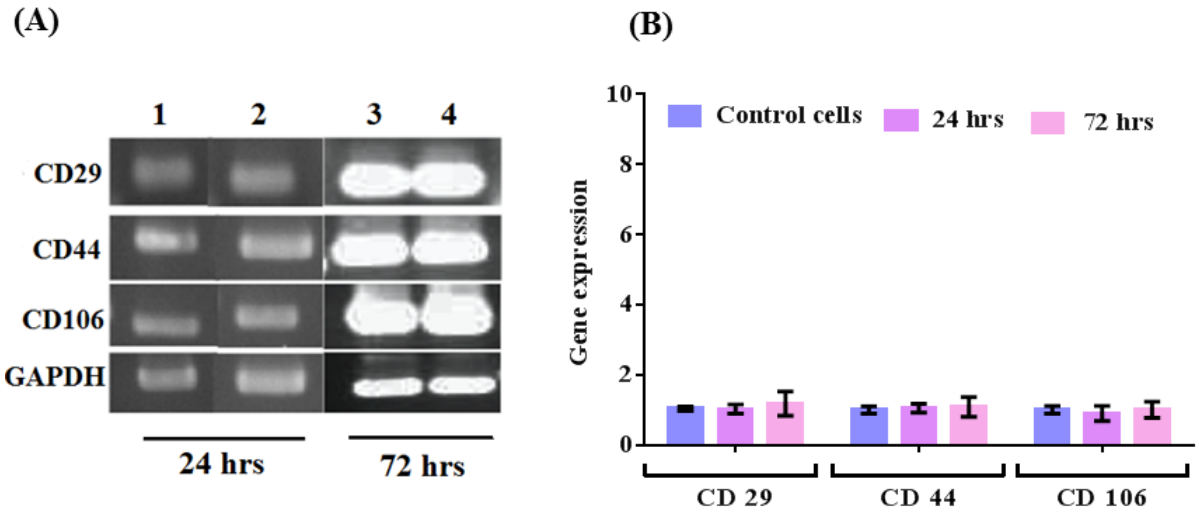

Figure 5.10: (A) RT-PCR and (B) qPCR analysis of nebulised MSCs, showing the lack of change in expression of three genes relative to unexposed MSCs after 24 and 72 hours. The error bars indicate the standard deviation (n = 3). In (A), lanes 1 and 3 are from unexposed cells (control) whereas lanes 2 and 4 are from nebulised cells.

This lack of change in gene expression was further verified by flow cytometry analysis, used to determine the expression of these proteins in cells. **Figure 5.11** shows that the nebulised MSCs had similar CD29, CD44 and CD106 positive cell counts to their their controls after 24 hours (p = 0.30, n =3; p = 0.69, n = 3 and p = 0.16, n =3, respectively) and 72 hours (p = 0.72, n =3; p = 0.32, n = 3 and p = 0.83, n = 3, respectively). Taken together, these results suggest that SAW nebulisation caused no detrimental effect to the phenotype and integrity of the MSCs, even after taking into account the longer culture period post-nebulisation. The SAW device is therefore a promising platform for stem cell nebulisation.

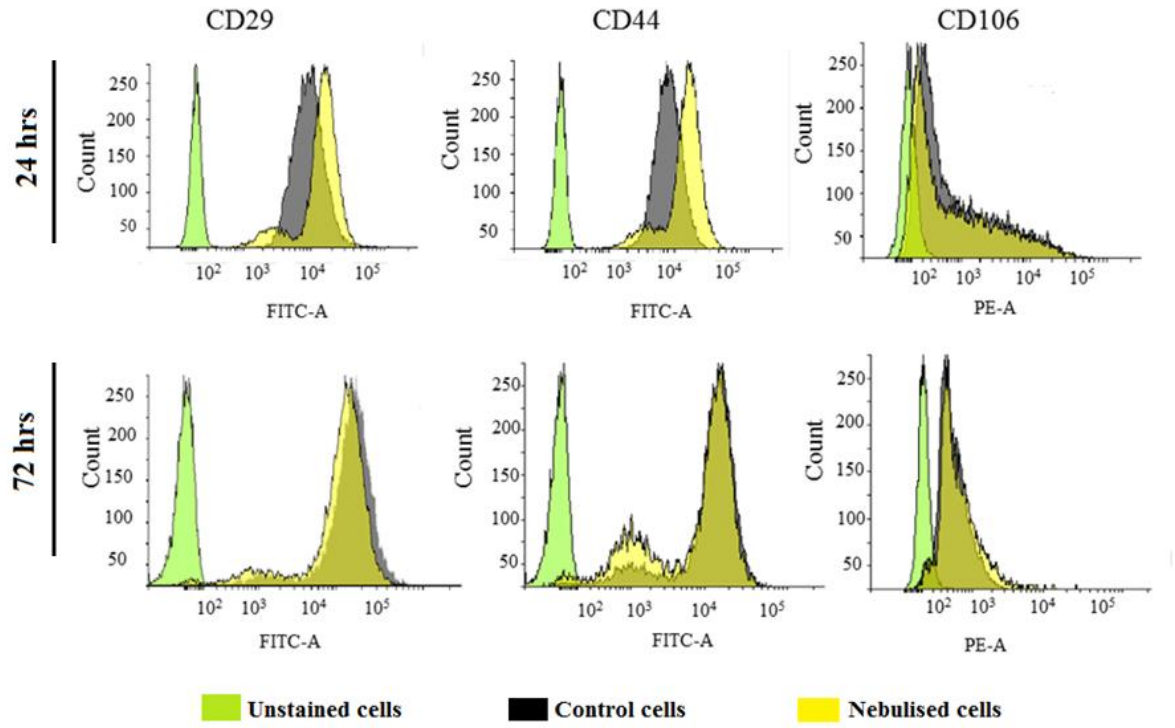

Figure 5.11: Immunophenotypic profile of unexposed (control) and nebulised MSCs after incubation periods of 24 and 72 hours.

5.4 Conclusions

This study demonstrates the feasibility of generating MSC-laden aerosols using a SAW nebulisation platform without deleterious effects on the cells. An optimum power level of 1.5 W yielded a balance between maximising cell viability at an acceptable level of approximately 90% after re-culturing for 24 hours whilst maintaining a practically useable delivery rate of 100 µL/min for inhalation. This was verified by post-nebulisation assessment of the structure, metabolic activity, proliferation and genetic makeup of the MSCs, which indicated that the SAW nebulisation process did not have any significant adverse effects on the cell metabolic rate, proliferation ability, or genotypic and phenotypic characteristics compared with their non-nebulised counterparts. Given the novelty of inhaled stem cell therapy, comparisons with other delivery methods

are difficult at present due to lack of comparable studies. More data for benchmarking are likely to become available in the near future due to the increasing interest in stem cell therapy, given the absence of viable alternative treatment regimes for respiratory ailments to date. Nonetheless, the results in this work provide compelling evidence that the SAW nebulisation platform, with its inherent benefits of low cost and portability, constitutes an attractive tool for the delivery of stem cells via inhalation for the treatment and repair of lung function.

CHAPTER SIX

Stem cell differentiation in hydrogel for lung tissue regeneration

6.1 Introduction

Lung diseases are major causes of morbidity and mortality worldwide. Currently, there is no effective therapy for many lung diseases including chronic obstructive pulmonary disease (COPD), idiopathic pulmonary fibrosis (IPF) and cystic fibrosis. Lung transplantation is the only option for patients with end-stage lung diseases however; there are limited donor lungs available for transplantation. Typically, transplantation recipients have suffered immune response problems, resulting in only 50% survival.

Currently, there is increasing interest in using hydrogels as either a drug- or protein-delivery system along with cell therapies and this may offer new treatment options for a wide range of diseases. The use of injectable and biodegradable hydrogels encapsulated with desired cells for implantation is attractive, as the implantation can be administrated by simple needle injection. Nevertheless, there is a need to develop new injectable hydrogels as well as optimising hydrogel performance. Such injectable hydrogels can be used to regenerate lung tissues as well as many other tissue types. Many chemical cross-linking processes have been utilised to cross-link hydrogel tissue scaffolds. However; many of these processes involve the use of toxic reagents or can cause unwanted side effects, making them not suitable for biomedical applications [424]. It is therefore very important to identify biocompatible cross-linking mechanisms using non-toxic catalysts such as enzymes that can occur under mild conditions [425]. Laccases are enzymes produced by fungi, higher plants, bacteria and insects. They are multi-copper oxidases that have the ability to catalyse the oxidation of several phenol-like compounds, aromatic amines and some inorganic compounds [426]. Due to their ability to catalyse the oxidation of an aromatic substrate in the presence of molecular oxygen, which is then reduced to

water after the reaction, laccases are widely used in various applications such as pulp delignification, bio-bleaching, treatment of industrial plant wastewater, fibre modifications, fruit juice processing and biosensor and biofuel cell construction [427, 428]. Kato et al. have reported the encapsulation of laccase in an aluminium silicate nanotube hydrogel as a new technology for stable biocatalysis [429]. Mano's group has reported the synthesis and characterisation of a laccase-mediated redox hydrogel for efficient catalysis of O_2 electroreduction [430].

Also, for tissue regeneration, Bletchley et al. have developed a hybrid hydrogel system comprised of two polymer backbones, gelatin and dextran, for functional vascular morphogenesis *in vitro*. The polymer precursors in this system were cross-linked through a laccase-mediated reaction [431]. Rocasalbas et al. developed a bioactive hydrogel dressing for chronic wound treatment containing plant polyphenols, chitosan and gelatin, that were cross-linked by laccase [432]. Park and Gerecht have reported a new hypoxia-inducible (HI) hydrogel containing gelatin and ferulic acid that forms hydrogel networks through a laccase-mediated reaction. Laccase successfully cross-linked gelatin polymers to form hydrogels that promote the formation of vascular networks and establish neovasculature that is functional and anastomoses with the host network during subcutaneous wound healing [433].

Cell-based tissue engineering using hydrogel scaffolds offers great promise for repairing lung tissue. Embryonic stem cells (ESCs) are a promising cell source for cell therapy applications and the treatment of incurable and damaging disorders, including spinal cord injury, neurological disease, blindness and Type 1 diabetes [185]. ESCs are isolated from the inner mass of the blastocyst during embryological development. These cells have a pluripotent nature and differentiate into three germ layers: endoderm, mesoderm and ectoderm, and they can also renew themselves while maintaining an undifferentiated state [434]. They have received great attention due to their ability to provide the biomedical community with an unlimited source of all cell types for tissue replacement [435].

A review of the literature suggests that an air-liquid interface closely mimics the lung microenvironment that cells experience *in vivo* for lung tissue engineering. Airway epithelial cells de-differentiate as a flat non-ciliated morphology in routine culture conditions: however, when the cultures are exposed to an air–liquid interface that mimics the *in vivo* conditions, the cells differentiate into pseudo-stratified columnar epithelium that creates high-resistance barriers [436, 437]. Rippon and co-workers have shown that induced pluripotent stem cells (iPSCs) differentiated into definitive endoderm and then fully differentiated into airway epithelia when raised in an air-liquid interface medium by culturing in transwell inserts coated with a combination of fibronectin, laminin and collagen or in six-well plates coated using Matrigel [243]. Wong et al. developed a protocol to induce the differentiation of stem cells into definitive endoderm and then into airway epithelium cells by culturing ESC and iPSC cells in transwell inserts pre-coated with human placental collagen Type IV with the addition of Activin-A and WNT3A to drive their differentiation into definitive endoderm and then promote polarisation in apical expression for CFTR in bronchial-air liquid interface (B-ALI, Lonza) medium in the presence of a growth factor (FGF18) [438]. Firth et al. have also developed a step-wise differentiation protocol ending in an air–liquid interface to generate a pseudo-stratified polarized layer of endodermal-derived epithelial cells from human induced pluripotent stem cells by culturing iPSCs cells in transwell inserts coated with a combination of fibronectin, laminin and collagen or six-well plates coated Matrigel [439].

Growing stem cells in tissue engineering constructs in air-liquid interface conditions instead of in tissue culture plasticware may offer a better solution for lung tissue regeneration, since the whole tissue engineering construct can be transplanted into the patient directly as a piece of 3D tissue instead of needing to retrieve differentiated cells from tissue culture wells, which often results in distortion of the cell-cell bonding. For example, Shojaie et al. demonstrated the differentiation of pluripotent cells cultured in a decellularized mouse and rat lung scaffold under air-liquid interface conditions into mature airway epithelia, complete with ciliated cells, club cells and basal cells with morphological and functional similarities to native airways, with specific lung epithelia markers and compared them

with 2D culture [440]. They showed the development of 3D scaffolds that mimicked the 3D architecture of lung tissues synthesized from DHHA and gelatin; such synthetic scaffolds are more economical than decellularized tissue scaffolds, which need expensive enzymes to remove cells.

The overall aim of the current study was to develop an injectable tissue scaffold capable of improving the differentiation of embryonic stem cells in air-liquid interface culture conditions. Cytotoxicity studies using murine embryonic stem cells were carried out to examine the biocompatibility of the scaffold. The hydrogel was investigated as a support for the proliferation and differentiation of mESCs into lung epithelial cells at air-liquid interface culture (ALI).

6.2 Methods

6.2.1 Synthesis and characterisation of Gtn-DHHA

Gelatin and 3,4-dihydroxyhydrocinnamic acid (Gtn-DHHA) conjugates (**Figure 6.1**) were synthesized using a general carbodiimide ester-mediated coupling reaction. In brief, DHHA (1.66 g) and NHS (1.6 g) were dissolved in 75 mL MilliQ water and 50 mL dimethylformamide (DMF); the solution was purged with N_2 gas for 20 min. To this solution, 1-ethyl-3-(3-dimethylaminopropyl)-carbodiimide hydrochloride (EDC) (1.91 g) was added immediately. The reaction was stirred at room temperature for 5 hours at pH 4.7 and N_2 gas was purged in the solution during the synthesis. Then 5 g of gelatin was dissolved in 150 mL MilliQ water. The dissolved gelatin was added to the mixture and was stirred overnight at room temperature. The mixture was transferred to dialysis tubes with a molecular cut-off of 1,000 Da.

The final product was dialysed against 100 mM NaCl, 25% ethanol, and Milli-Q water for 2 days each in sequence, with N_2 gas purging the dialysed solutions. The products were then lyophilised. Conjugation of 3, 4-dihydroxyhydrocinnamic acid to gelatin was confirmed by 1H NMR (D_2O). In brief, the conjugation of DHHA on gelatin was assessed in D_2O using an NMR operating at 300 MHz (ACF300, Bruker Pty Ltd, Alexandria, NSW, and Australia).

The gelation time of Gtn-DHHA was estimated using an inverted tube test method according to Gupta et al.[378]. Briefly, laccase at concentrations of 2.27, 4.16 and 5.76 units/mL were added to 2 ml microcentrifuge tubes (Axygen Scientific, VWR International Pty Ltd, Murarrie, QLD, Australia) containing 5%, 10% and 15% (v/v) Gtn-DHHA in PBS. The mixture was vortexed and mixed with the tube reverted every 30 s interval to observe flow. The gelation time was recorded as the time when the gel ceased to flow.

The swelling ratio of the Gtn-DHHA hydrogel was measured using a conventional gravimetric method according to Hoo et al. [383]. In brief, sterilised hydrogels were prepared at 5%, 10% and 15% (v/v) Gtn-DHHA with 2.27 units/mL laccase concentrations. The hydrogels were subsequently cut into round disks using a sterile circular mould and were swollen by immersion in sterile PBS for 3 days at 37^{o}C. Excess liquid was wiped off by gently blotting the hydrogel with laboratory wipes. The swelling ratio, SR, of the scaffold was calculated according to the equation below:

$$SR = \frac{Wh - Wd}{Wd}$$

where Wh is the weight of the scaffold in the swollen equilibrium and Wd is the weight of the dried scaffold. Each sample was measured three times from triplicate specimens and the average value of the measurement was taken. Rheological measurements of the hydrogel formation were performed using an HR3 Discovery Hybrid stress-controlled rheometer (TA Instruments, USA). The instrument was calibrated before the experiments by using Poly Dimethyl Siloxane (PDMS) as a calibration standard; cross-over frequency was well within the limits as per standards provided by the instrument suppliers. The cone and plate geometry of 50 mm diameter and 0.04^{o} cone angles used were according to Wang et al. [441]. The shear rheological measurements were conducted at room temperature in the dynamic oscillatory mode with a constant deformation of 1% and frequency of 1 Hz. Laccase was added at different concentrations of an aqueous solution of Gtn-DHHA (5%, 10% and 15% in 1 mL of PBS). This solution was vortexed and then immediately applied to the bottom plate. The upper cone was then lowered to a measurement gap of the truncated value provided by the

instrument supplier). A layer of silicon oil was carefully applied around the cone to prevent solvent evaporation during the experiment.

A solvent trap was used to cover the rheometer to avoid further change in phase change. The measurement parameters were determined to be within the linear viscoelastic region in preliminary experiments. A compression test was carried out to assess the mechanical properties of Gtn-DHHA scaffolds at different polymer concentrations using a dynamic mechanical analyser (TQ Instruments, Q800) at a frequency of 1 Hz and a preload 0.01 N according to [442].

The test was performed at room temperature (22°C) and at 298 K. The testing was performed in quadruplicate. To measure degradation rate, hydrogels were prepared at 5%, 10% and 15% (w/v) polymer concentrations, and the hydrogels were then immersed in 10 mL of PBS containing 0.61 units/ml of type I collagenase and incubated at 37°C in an orbital shaker at 100 rpm. The degradation rate of the hydrogels was assessed by measuring the residual hydrogel weight. To measure the residual weight, the hydrogels were removed from the solution, blotted dry and weighed at different time points [441].

6.2.2 Cell culture

E14TG2A cells were cultured on 0.1% gelatin-coated tissue culture plates in Dulbecco's modified Eagle's medium supplemented with 10% fetal bovine serum-embryonic stem cell-qualified (Gibco), 1% non-essential amino acids (Gibco), 1% L-glutamine (Gibco), 0.1 mM 2-mercaptoethanol, 1% penicillin-streptomycin and 1000 U mL^{-1} murine leukemia inhibitory factor (mLIF, Chemicon, Australia). Cells were maintained in a humidified atmosphere of 5% CO_2/95% air at 37ºC.

6.2.3 Cell viability

ESCs were immobilized in the enzymatically cross-linked hydrogels in 24-well plates. Cells cultured on 0.1% gelatin-coated tissue culture plates served as controls. After 24 hours, a live/dead cytotoxicity kit (Life tTechnologies) containing calcein-AM and propidium iodide were used to evaluate viability of pluripotent embryonic stem cells [327].

Confocal laser scanning microscopy was used to visualize the live (green) and dead (red) cells, dead cells were imaged by the inclusion of the propidium iodide fluorophore in the medium and then visualised by laser confocal fluorescence microscopy (Nikon A1R equipped with a Nikon Eclipse Ti Fluorescence Microscope).

6.2.4 Cell proliferation assay

Cells were immobilized in the enzymatically cross-linked hydrogels in 24-well plates and compared with those cultured on 0.1 gelatin-coated plates as control. For the control, mESCs at a cell density of 1×10^5 cells/ml were seeded in 6-well coated plates and maintained in culture medium while 3D cell cultures in hydrogel mESCs were mixed with 1 mL of Gtn-DHHA solution (10% w/w) in 6-well plates at a final concentration of 1×10^5cells/ml. To initiate gel formation, 2.27 units/mL of laccase (Sigma Aldrich, Australia) was added to the solution. The hydrogels were allowed to set for 2 hours before the addition of culture medium. For both 2D and 3D studies, the culture medium was changed every day.

The total number of cells within Gtn-DHHA hydrogel was quantified using a Quant-iT™ PicoGreen® dsDNA Assay Kit by measuring the DNA content, as DNA is the cellular component that most precisely reflects cell number [443]. PicoGreen assay was performed according to the manufacturer's instructions (Life Technologies). Fluorescence of the samples was measured using a plate reader and compared with that of a lambda DNA standard, provided with the kit.

In brief, the cells were trypsinised from the substrate and centrifuged for 5 min at 140×g. The cell pellet was washed with cold PBS twice, each followed by centrifugation for 5 min at 140×g. The resulting cell pellet was collected by discarding the supernatant. The cells were lysed using 100 µL of NP40 cell lysis buffer (Life Technologies, Australia) for 30 min on ice and vortexed at 10 min intervals. The extract was transferred to microcentrifuge tubes and centrifuged at 13000 rpm for 10 min at 4°C.

The clear lysate was aliquoted to clean microcentrifuge tube, 100 µL of PicoGreen reagent was added and allowed to incubate for 5 min at room temperature in the dark. The final solution was transferred into a 96-well plate, and the fluorescence was read using a fluorescence plate reader (FLUOstar Omega microplate reader, BMG Labtech Pty, Ltd, Australia) at standard fluorescein wavelengths (excitation~ 480 nm, emission ~ 520 nm). The unknown DNA results were compared with that of a DNA standard curve.

6.2.5 Differentiation of embryonic stem cells into lung epithelial cells

To investigate the ability of embryonic stem cells to differentiate into definitive endoderm and further into lung epithelial cells, the cells were trypsinised with TrypLE™ Express Enzyme (1X) (Life Technologies, Australia), and then seeded at a cell density 1×10^5 cells/mL in maintaining medium composed of DMEM and 10% fetal bovine serum, 1% non-essential amino acid, 1% L-glutamine, 0.1 mM 2-mercaptoethanol and 1% penicillin-streptomycin in 24-well plates without leukaemia inhibitor factor (LIF) in the presence or absence of growth factors in an air-liquid interface and submerged medium for immunofluorescence and qPCR analysis.

After 1 day of culture, the spent medium was changed with a differentiation medium containing 75% (v/v) Iscove's Modified Dulbecco's Medium (Life Technologies, Australia), and 25% (v/v) Ham's F12 Medium (Life Technologies, Australia), 1% FBS (Life Technologies, Australia) supplemented with 0.5 x B27, 50% U/mL penicillin, 50% µg/mL streptomycin, 0.05% BSA, 2 mM glutamine

(Life Technologies, Australia), 0.5 mM ascorbic acid, 4.5 x 10^{-4} M 1-thioglycerol (Sigma Aldrich, Australia), 20 ng/ml Activin; also 1 ng/ml Wnt3a (Bio-Scientific, Australia) was added to the differentiation medium. Cells were allowed to grow for 7 and 14 days in the differentiation medium for 2D and 3D culture respectively. Medium exchange was carried out every 2 days.

To better mimic the lung microenvironment, cells were maintained in Gtn-DHHA hydrogel under air-liquid interface (ALI) culture conditions, spent medium was removed after 7 days and 14 days for 2D and 3D culture, respectively. Fresh differentiation medium supplemented with 1 µg/mL heparin sulphate salt and 500 ng/mL FGF2 (F0291, Sigma Aldrich, Australia) replaced the spent medium and cells were incubated for a further 14 and 30 days for the control and hydrogel samples respectively.

6.2.6 Immunofluorescence assays

A. Immunofluorescence assays for endoderm markers

Endoderm markers were evaluated for both control and 3D cells in the presence of growth factors after 7 and 14 days respectively. For immunofluorescence assay, control cells (2D) and cells in 3D scaffolds were fixed in 4% paraformaldehyde for 10 min and 30 min respectively and washed 3 times with PBS. Cells were blocked with 1% BSA (bovine serum albumin) for 30 and 60 min respectively. E-Cadherin and Foxa2 primary antibodies (Santa Cruz Biotechnology, USA) were added to cells (1:100) and incubated for 1 hour and 48 hours (to allow for antibodies to penetrate within the hydrogel) respectively. Cells were then washed three times with PBS for 5 minutes each for the control and 15 min each for the 3D scaffold cells. Goat anti-rabbit secondary antibody (Sapphire Bioscience, Australia) and Donkey anti goat antibody (Life Technologies, Australia) were added to cells (1:1000) and then incubated for 30 min and 4 hours for control and 3D scaffold cells respectively. Cells were rinsed 3 times with PBS for 5 min and 15 min respectively. Then 4', 6-diamidino-2-phenylindole (DAPI) 1:2000 was added to the cells and incubated for 3 min and 20 min for control and 3D scaffold cells respectively at terminal stages of the technique.

Prior to determining endoderm markers, cells were immersed in 300 µL of PBS to prevent cell drying. Images of cells were acquired by laser confocal fluorescence microscopy (Nikon A1R with a Nikon Eclipse Ti Fluorescence Microscope).

B. Immunofluorescence assays for lung cell markers

Control cells and 3D cells were fixed in 4% paraformaldehyde for 10 and 30 min respectively and rinsed three times with 1X PBS. Cells were blocked with 1% BSA (bovine serum albumin) for 30 min and 60 min respectively. Pep2 and Sema4f primary antibodies (Santa Cruz Biotechnology, USA) were added to cells (1:100) and incubated for 1 hour and 48 hours respectively. Cells were rinsed three times with PBS for 5 min and 15 min for control and 3D cultures respectively. Goat anti-rabbit secondary antibody (Sapphire Bioscience, Australia) was added to cells (1:1000) and cells incubated for 30 min and 4 hours for control and 3D cultures respectively. Cells were rinsed 3 times with PBS for 5 min and 15 min, respectively and then 4', 6-diamidino-2-phenylindole (DAPI) (1:2000) was added to cells and incubated for 3 min and 20 min respectively at terminal stages of the technique. Prior to determining lung epithelial cells, cells were immersed in 300 µL of PBS to prevent cell drying. Images of cells were acquired by laser confocal fluorescence microscopy (Nikon A1R with a Nikon Eclipse Ti Fluorescence Microscope).

6.2.7 TaqMan quantitative PCR

The gene expression of Sox17, Fox2a for endoderm markers and Ttf1, Unc5b, Pept2 and Sema4f for lung markers in 2D control and 3D scaffolds were quantified using qPCR. Pou5f1 and GAPDH were used as negative and positive controls respectively. Ribonucleic acid (RNA) was isolated from cells using an RNAeasy Mini Kit (Qiagen, Australia) according to the manufacturer's instructions. The RNA quality and concentration were examined using a NanoDrop ND-1000 spectrophotometer (NanoDrop Thermofisher, Australia). To eliminate any contaminating genomic DNA, the isolated RNA was treated with a DNA-free™ kit according to the manufacturer's instructions. Complementary DNA (cDNA) was generated using QuantiTect Reverse Transcription kit (Qiagen,

Australia) according to the manufacturer's instructions. The cDNA samples were subjected to PCR amplification using probes obtained from Applied Biosystems (Australia). The qPCR analysis was performed using a Rotor-Gene Q (Qiagen, Australia) with a TaqMan transcription kit (Life Technologies, Australia) using TaqMan assays, Sox17 (Mu00488363_m1), Foxa2 (Mm01976556_s1) and Pou5f1 (Mm03053917_g1), and Ttf1 (Mm00657018_m1), Unc5bMm00504054_m1), Pept2(Mm00451610_m1) and Sema4f(Mm01181883_m1). All gene expressions were normalised to GAPDH (Mm99999915_g1) as a reference in corresponding samples. After 10 min of denaturation at 95°C, 40 PCR cycles were carried out at 95°C for 15 s, 60°C for 30 s, and 72°C for 15 s. The relative mRNA levels were calculated using the $\Delta\Delta C_T$ method [332]. The results were reported as fold change values compared to 2D monolayer cells.

6.2.8 Statistical analysis

All experiments were performed with at least 3 replicates and results were reported as the average value ± standard deviation. Multiple groups of data were compared using One Way Analysis of Variance (ANOVA). Two groups of data were compared using Student's t-test. Differences between groups of data were considered statistically significant when $p < 0.05$.

6.3 Results and Discussion

This study attempted to examine the proliferation and differentiation potential of murine embryonic stem cells in Gtn-DHHA scaffold hydrogels via an *in vitro* experiment in the presence and absence growth factors and with or without provision of air-liquid interface. The ability of mESCs to differentiate into endoderm and subsequently lung epithelial cells was evaluated.

6.3.1 Gtn-DHHA characterisation and hydrogel preparation

DHHA conjugate was synthesized according to the scheme illustrated in **Figure 6.1**; the conjugation was confirmed using ^{1}H NMR spectroscopy as shown in **Figure 6.2**. ^{1}H NMR spectra of Gtn-DHHA were compared with DHHA and gelatin as controls to determine if there was a change. The ^{1}H NMR spectra showed that the difference between the DHHA control spectrum (**Figure 6.2A**) and gelatin as controls (data not shown), and the Gtn-DHHA conjugate spectrum (**Figure 6.2B**); original peaks appearing in the control either changed or disappeared from the conjugate spectrum. All four peaks present in the DHHA control spectra were no longer present, or had changed in the conjugate spectra. **Figure 6.2B** shows a typical spectrum of Gtn-DHHA; the cluster peaks at δ = 7.2 and 7.5 confirmed the conjugation of DHHA with Gtn. The Gtn-DHHA conjugate with 5%, 10% and 15% at various concentrations of laccase was used to determine optimum gel precursor/cross-linker ratio. This test found that all concentrations could be crosslinked by laccase, with gelation time decreasing as gel Gtn-DHHA concentration increased, and the gelation time decreased with increased availability of O_2 by purging O_2 in the hydrogel liquid with air (**Figure 6.3**).

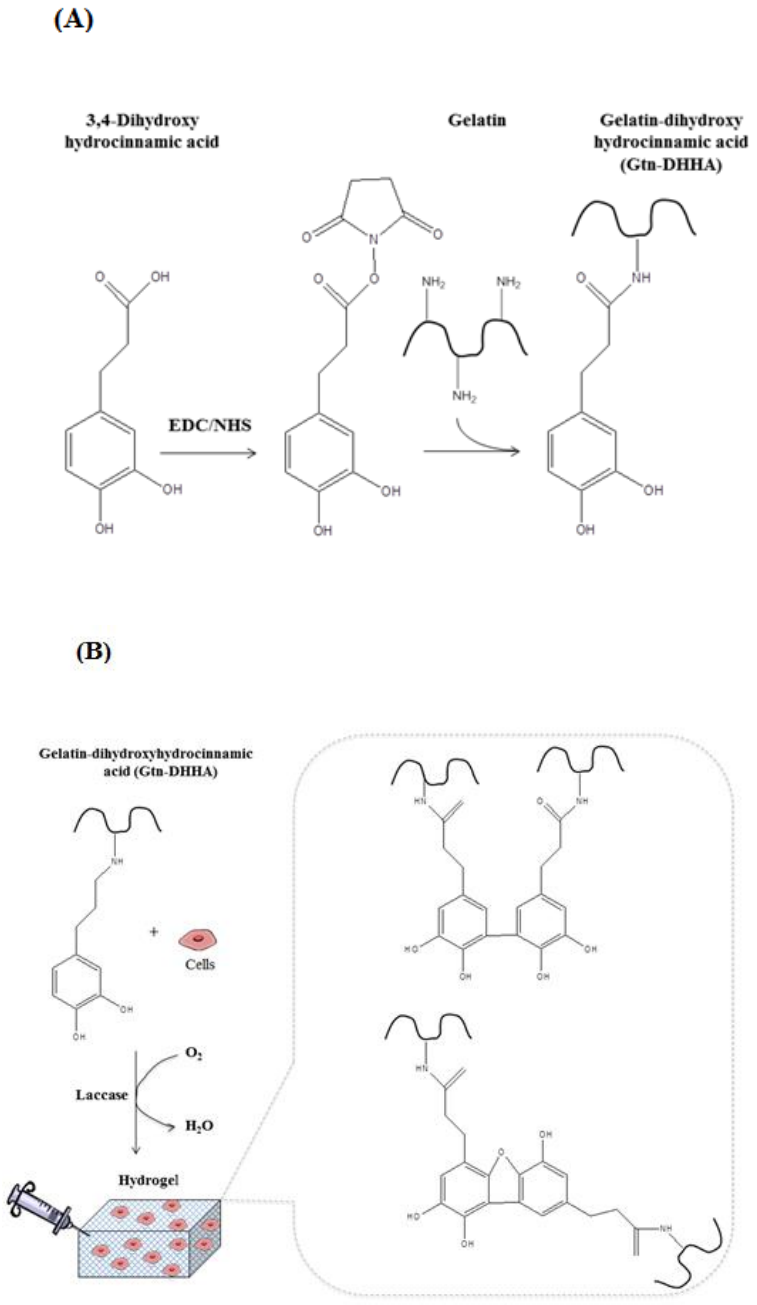

Figure 6.1: Synthesis scheme for (A) 3,4-dihydroxyhydrocinnamic acid, and (B) gelatin-3,4-dihydroxyhydrocinnamic hydrogel crosslinking.

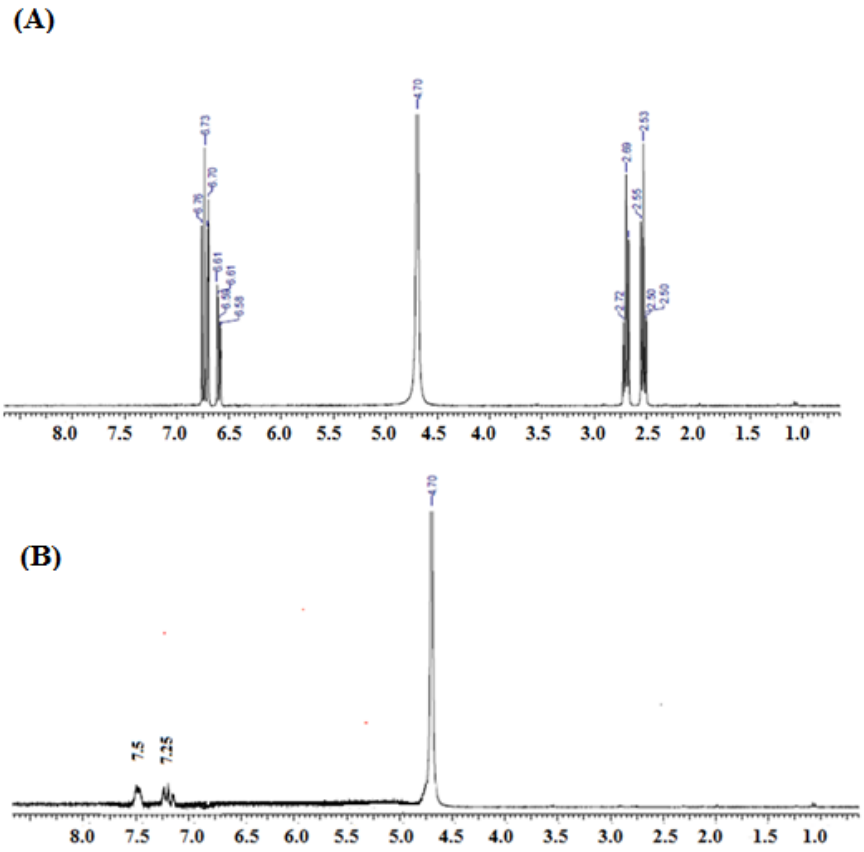

Figure 6.2: ^{1}H NMR spectrum of (a) 3, 4-Dihydroxyhydrocinnamic acid, b. gelatin-3,4-dihydroxyhydrocinnamic acid conjugate.

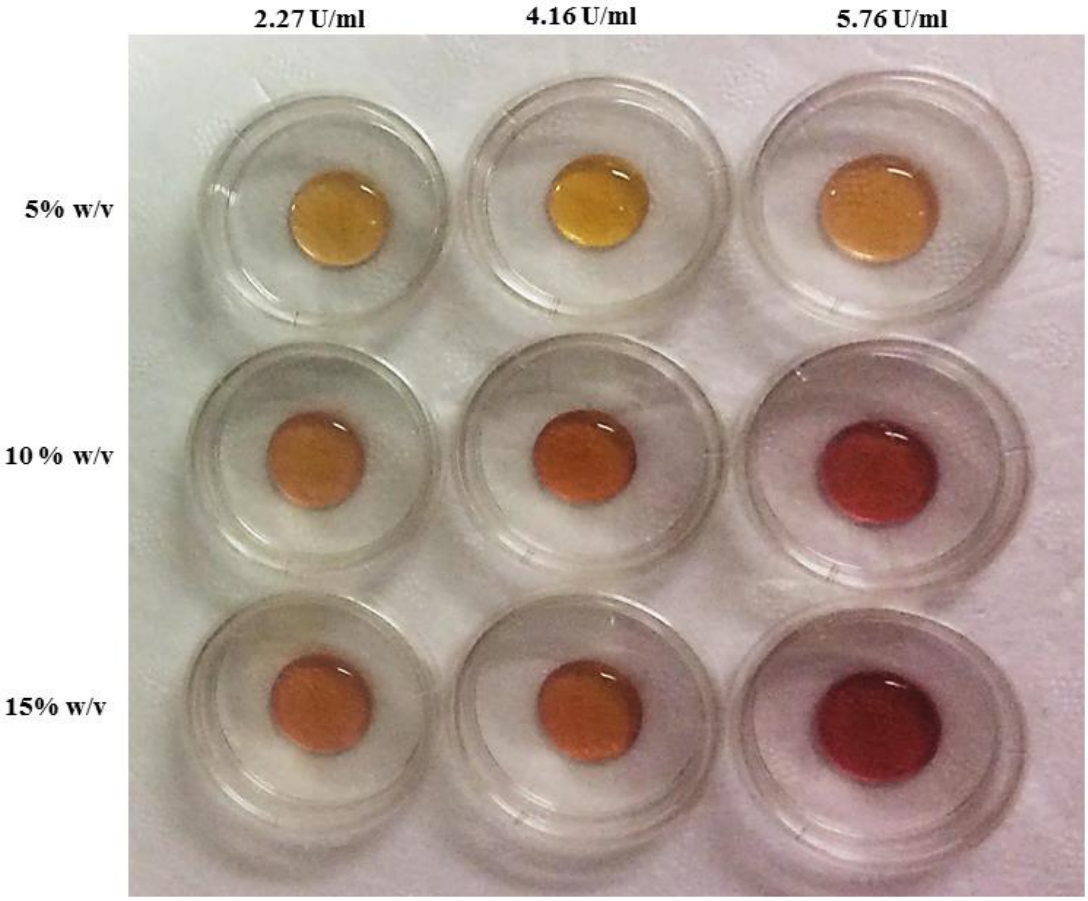

Figure 6.3: Images of Gln-DHHA hydrogel gelation at various concentrations of laccase (2.27, 4.16, and 5.76 units/ml).

6.3.2 Swelling ratio and mechanical properties

Figure 6.4A summarises the swelling ratios of different concentrations of Gtn-DHHA hydrogel cross-linked by a fixed amount of laccase at 2.27 U/ml. The swelling ratio is a measure of the material wettability; hydrogels with high swelling ratios are highly hydrophilic and highly permeable, which facilitates the transport of water-soluble molecules, oxygen, nutrients and the exchange of metabolites within the hydrogel [441]. As expected, the swelling ratios decreased with increasing polymer concentration ($p < 0.05$, n = 3), and were 36.03% ± 4.30, 25.16 ± 3.25 and 18.7 ± 3.5 for 5%, 10% and 15% Gtn-DHHA hydrogels respectively. From rheological measurement, the crossover of G" and G', also known as gel point, occurred within 533.76 s for 5% Gtn-DHHA hydrogel cross-linked by

2.27 U/ml of laccase **(Table 6.1).** The gel point is known as the transition point from the liquid state to the solid state [444]. The effects of various concentration of polymer on gel point were also studied; the time required to reach gel point decreased as polymer concentrations increased while keeping laccase concentration constant. The gel points were 248.52 s and 121.54 s for 10% and 15% Gtn-DHHA respectively, indicating that the gel point was dependent on polymer concentration. These results are in good agreement with previous reports on the independent tuning of hydrogel mechanical properties and gelation rates [441, 445-447]. For tissue regeneration to be successful, it was expected that the mechanical properties of the scaffold had to be similar to those of *in vivo* tissue in order to provide cells with an instructive microenvironment. The storage modulus values of 5%, 10% and 15% Gtn-DHHA were 1.29 ± 0.14, 3.43 ± 0.18 and 10.17 ± 0.62 kPa respectively.

As predicted, the storage moduli increased as Gtn-DHHA polymer precursor concentration increased ($p < 0.05$, n=4), as shown in **Figure 6.4B**. It is well known that the hydrogels with greater precursor masses display stronger mechanical properties. The storage moduli of the Gtn-DHHA hydrogels were comparable to those of soft tissues and organs, for example thyroid, fibrotic liver, breast and kidney [448]. These results demonstrate that the swelling ratio and the mechanical strength of the hydrogel could be modulated by changing the hydrogel concentration.

Table 6.1: Gelation time for 3D hydrogel by rheology testing.

Gln-DHHA concentration (w/v)	Laccase concentration (U/mL)	Gelation time (s)
5%	2.27	533.76
10%	2.27	248.52
15%	2.27	121.54

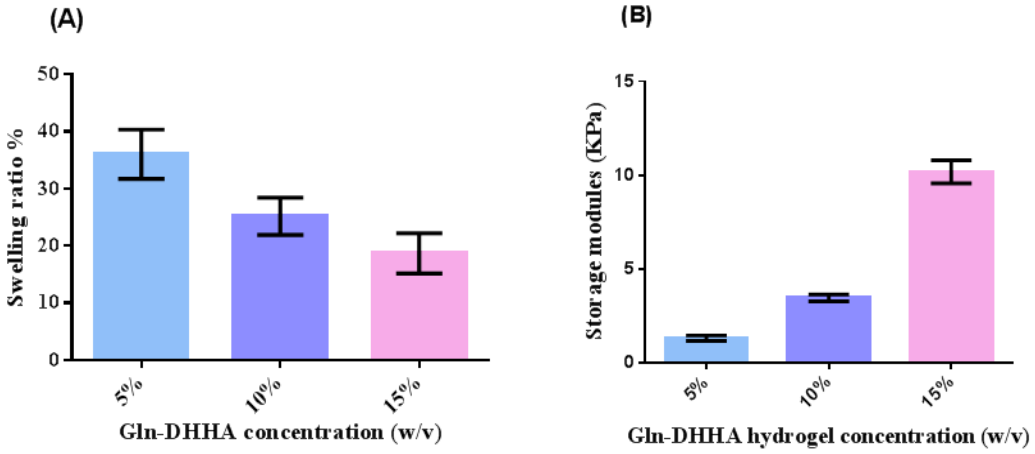

Figure 6.4: Swelling ratio (A) and storage modulus (KPa) (B) of Gln-DHHA-5 wt%, 10 wt% and 15 wt% at 2.27 unit/ml laccase. The data are represented as mean values with standard deviation as error bars in the form of mean value ± standard deviation.

6.3.3 Degradation rate

Figure 6.5 shows that the rate of hydrogel degradation decreased with increased hydrogel concentration due to the lower water accessibility (therefore slower degradation rate) and this result demonstrated that the enzymatic degradability of Gtn-DHHA hydrogels could be modulated by varying polymer concentration.

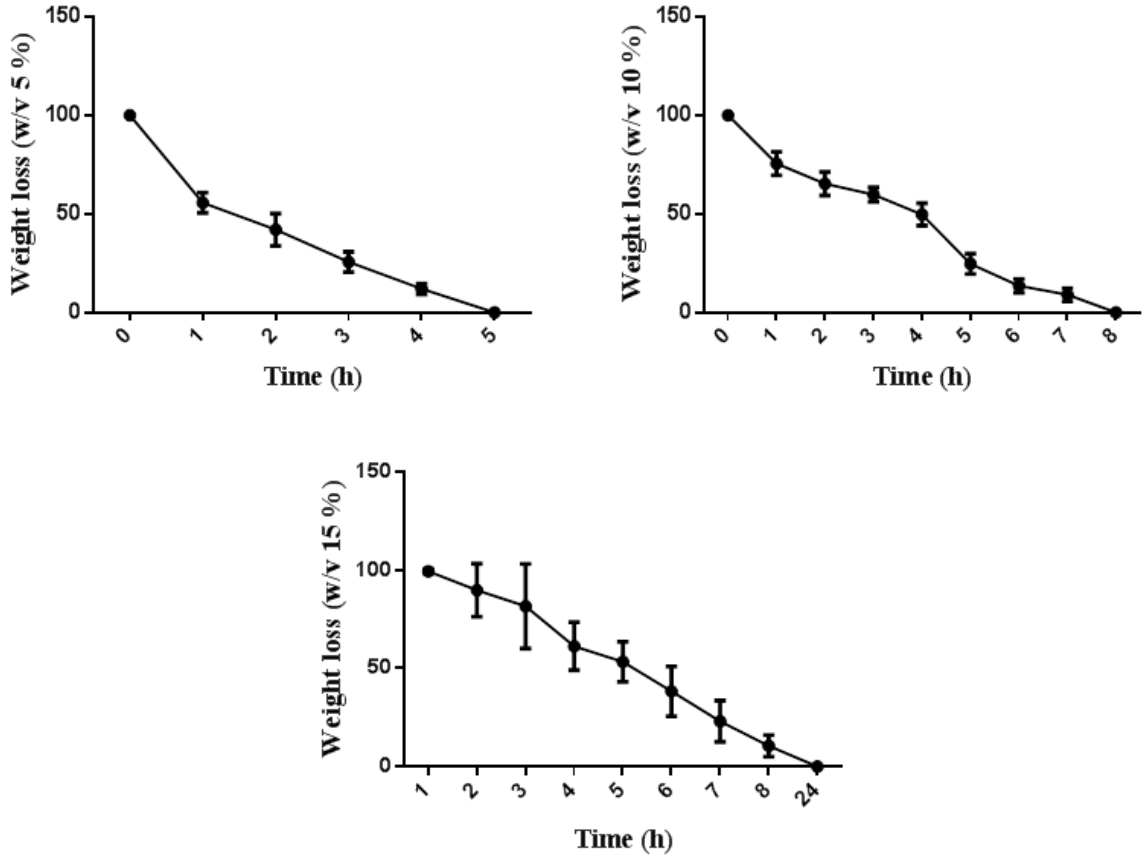

Figure 6.5: Degradation rate of swelling ratio of scaffold hydrogels prepared at 5%, 10% and 15% (w/v). The data are shown as mean values ± standard deviation.

6.3.4 Cell viability and proliferation

The viability of ESCs was around 90% as measured by counting the number of Calcein AM-stained cells. At 24 hours after immobilisation, cells encapsulated within the hydrogels displayed a rounded morphology; cells need to degrade the hydrogel by secreting proteinase such as MMP prior to spreading out (**Figure 6.6**).

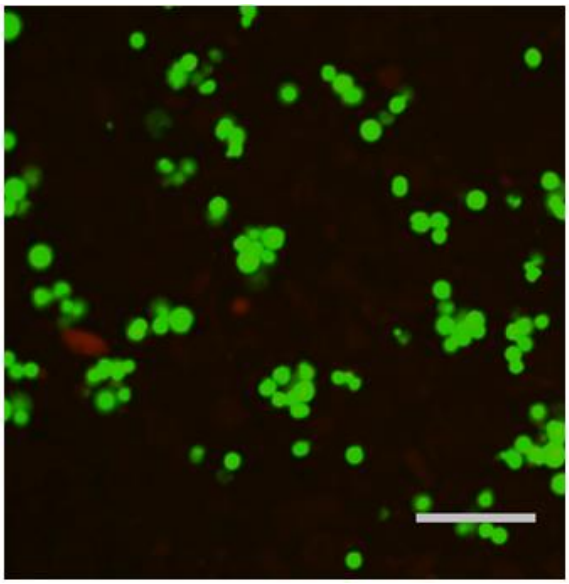

Figure 6.6: The effect of scaffold hydrogel on embryonic stem cell viability (E14TG2A). Cells were embedded in scaffold hydrogel. Cells were stained with Calcein-AM and propidium iodide. Viable cells stained with Calcein at 24 hours after culturing are shown. Scale bars represent 100 µm.

The cell DNA content was no significantly increased over a 7-day period; the cell number in scaffolds changed more slowly than those in the controls at day 7, probably because cells in hydrogel need to secret proteinase to degrade the 3D hydrogel before they can propagate, which takes longer than propagation on a 2D surface (**Figure 6.7)**. Nonetheless, these results indicate that the Gtn-DHHA encapsulated cells remained viable and possibly capable of proliferation, and confirmed that Gtn-DHHA hydrogel was suitable for tissue engineering applications.

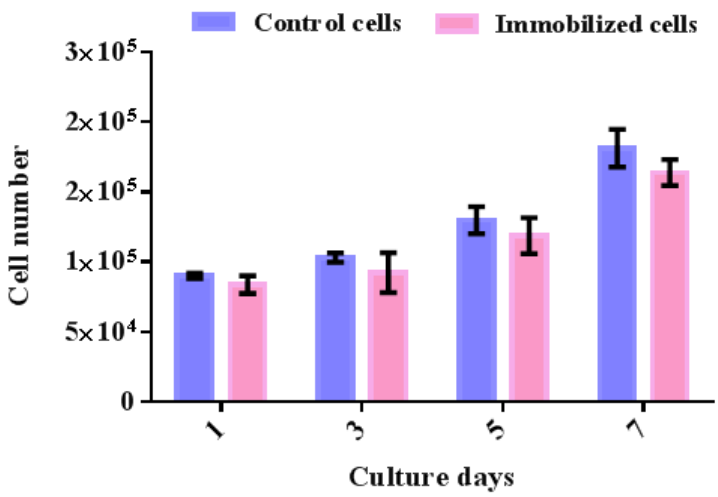

Figure 6.7: Cell proliferation of embryonic stem cells (E14TG2A) in coated well plates and scaffold hydrogels. Data are represented as mean (n = 3) ± standard error of the mean and were compared by Student t-test with control cells.

6.3.5 Gene expression and immunostaining profile for endoderm markers

Various factors should be considered in attempt to develop lung distal airways cells as the presence of biomolecules may direct the differentiation of ES cells into lung epithelium, for example molecular signalling associated with fibroblast growth factor (FGF2), B-27 without retinoic acid, Activin, WNT3 signalling, heparin salts, bovine serum albumin and ascorbic acid [449, 450].

Figure 6.8 shows a schematic of the protocol used to differentiate mESCs into cells with phenotypic characteristics of alveolar epithelial cells, in which fibroblast growth factor (FGF-2) was added to drive the differentiation of mESCs into lung epithelial cells.

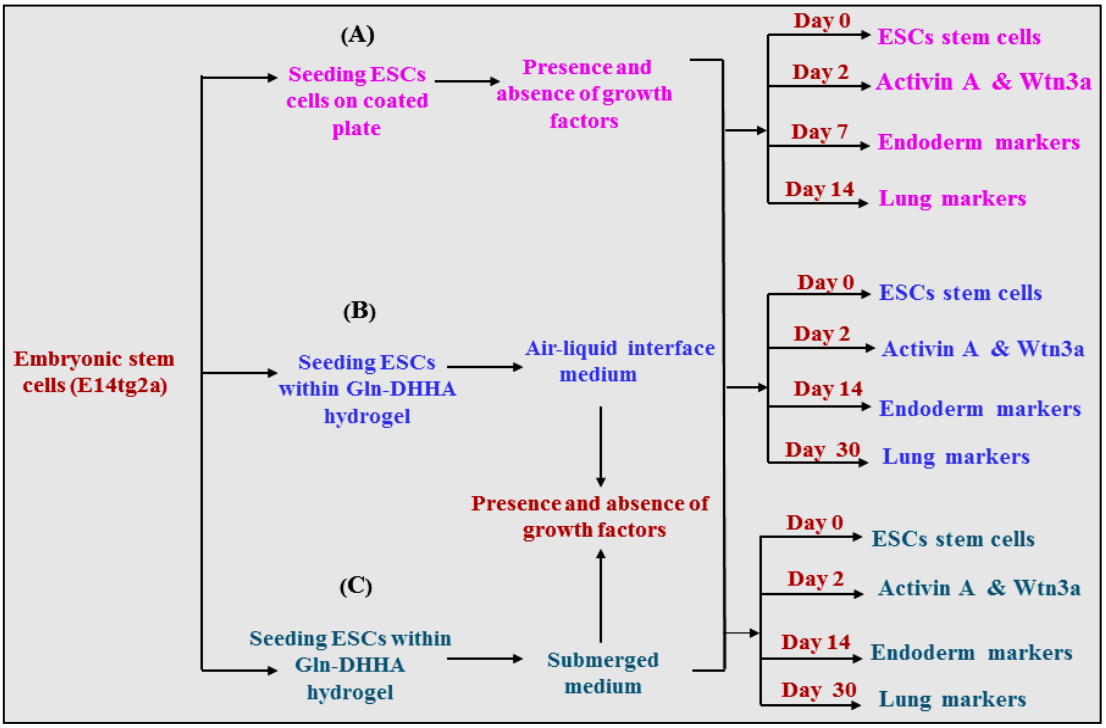

Figure 6.8: Schematic of protocol utilised to differentiate murine embryonic stem cells (E14tg2a) into cells with phenotypic characteristics of lung epithelial cells. A. Control, B. Immobilised cells at air-liquid interface medium, C. immobilised with submerged medium in the presence and absence of growth factors.

Lung cells are differentiated from endoderm. Definitive endoderm was first produced from mESCs by adding growth factors Activin A and WNT3 [451]. In the study in this thesis, over periods of 7 days and 14 days, the endoderm transcription factors Foxa2 and Sox17 of 3D culture cells exhibited greater expression than 2D monolayer cells, in particular for those cells that were embedded in 3D hydrogel in an air-liquid interface (8.46±1.10, 4.73± 0.85) fold change respectively, compared with submerged medium (6.40 ± 0.72, 5.90 ± 0.91) fold change respectively, and control cells (3.40 ± 0.75, 3.16 ± 0.30) fold change respectively in the presence of growth factors (**Figure 6.9A**). These results support prior investigations, which suggested that Sox17 and Foxa2 expression initially was increased with Activin A treatment [451]. A lesser expression was shown in the absence of growth factors (**Figure 6.9B**).

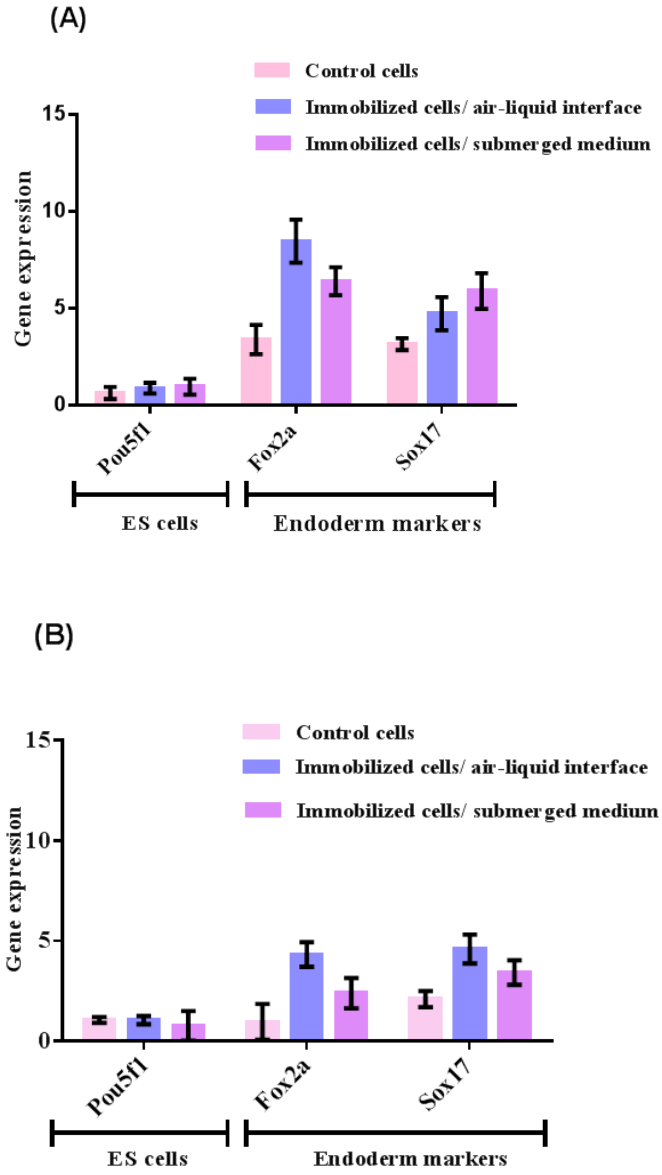

Figure 6.9: Fold change of gene expression of differentiated embryonic stem cells into endoderm relative to undifferentiated ESCs in the presence (A) and (B) absence of growth factors compared with their controls. Cells were assessed after 7 days and 14 days for control and embedded scaffolds respectively. Data are represented as mean (n = 3) ± standard error of the mean and were compared by Student t-test to control cells. Differences were considered significant at $p<0.05$.

Differentiated cells were analysed by immunostaining using confocal microscopy for all tested conditions to assess if the up regulation of E-caderin and Fox2a was correlated with Gtn-DHHA scaffolds. The immunostaining pattern of E-cadherin and Fox2a showed that there was a difference in protein distribution between 2D and 3D culture cells; the expression of E-cadherin and Fox2a of 3D cells appeared brighter and more uniformly distributed in cells exposed to air-liquid interfaces compared with those in submerged scaffold. E-cadherin is a glycoprotein and cell adhesion molecule that plays a role in the process of cell-to-cell adhesion; Fox2a and E-cadherin are also good indicators for definitive endoderm [452], as shown in **Figure 6.10 A, B**.

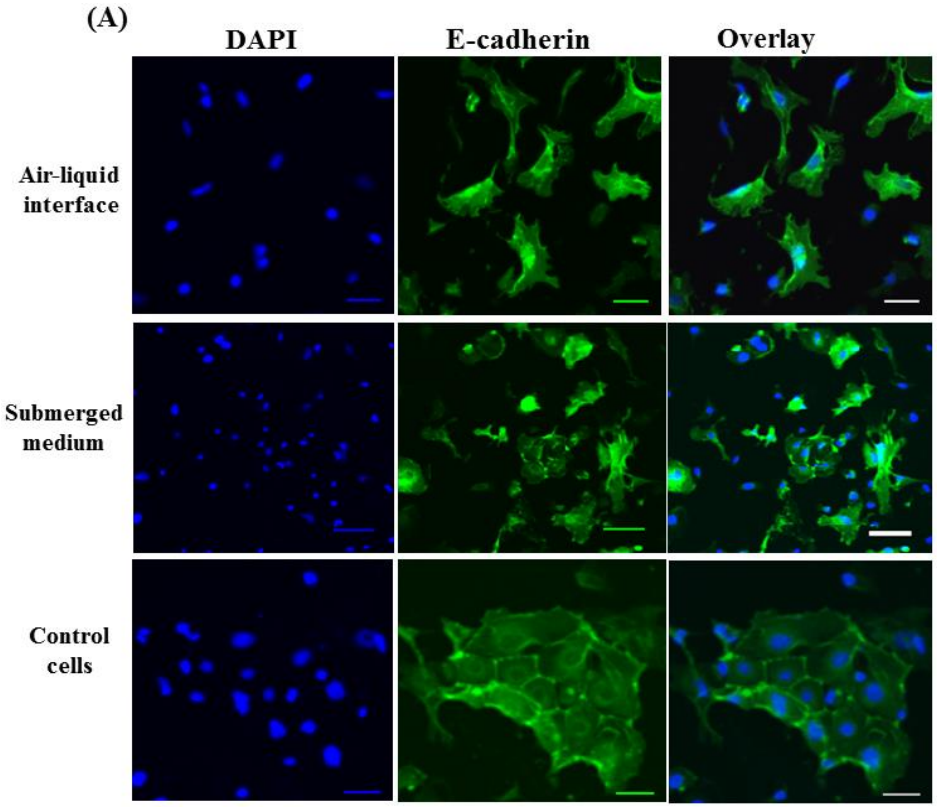

Figure 6.10A: Immunofluorescence analysis of endoderm expression (E-Cadherin). These images were taken for cells embedded in scaffolds in the presence of growth factor compared with the control. Nucleated cells are in Blue (DAPI). The E-cadherin marker is shown by a green colour and is an indicator for endoderm. Expression for this marker was brighter in cells embedded in scaffolds and control. Scale bar represents 100 µm.

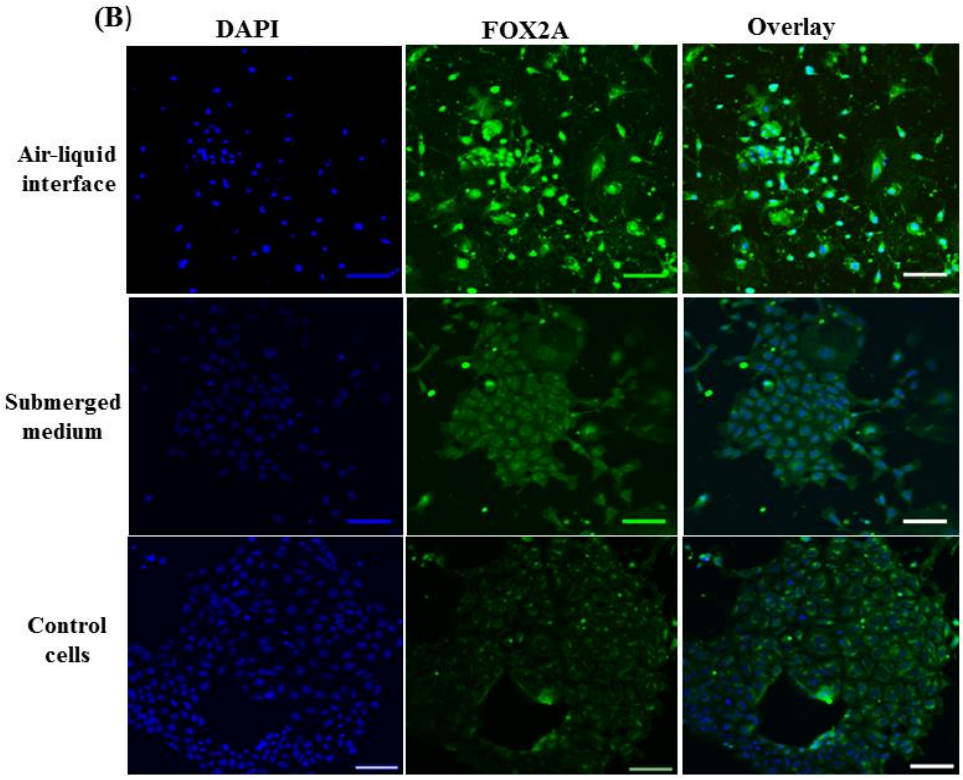

Figure 6.10B: Immunofluorescence analysis of endoderm expression (Fox2a). These images were taken for cells embedded in scaffolds in the presence of growth factors compared with controls (cells were cultured on gelatin-coated plates). Nucleated cells are in Blue (DAPI). The Fox2a marker is shown by a green colour and is an indicator for endoderm. Expression for this marker was brighter in cells embedded in scaffolds than in the control. Scale bar represents 100 µm.

6.3.6 Gene expression and immunostaining profile for lung epithelial markers

Relative to control and submerged cells, cells incubated in an air-liquid interface for 30 days showed evidence of differentiation, with greater Pept2, Sema4f, Unc5b and Ttf-1 gene expression (8.70 ± 1.80, 5.90 ± 0.52, 6.43 ± 0.35, 3.80 ± 1.38)-fold changes compared with cells grown in submerged medium (4.43 ± 0.68, 2.93 ± 0.49, 2.53 ± 0.45, 1.36 ± 0.251)-fold changes, and control cells (1.83 ± 0.709, 3.36 ± 1.70, 3.20 ± 0.55, 3.13 ± 0.95)-fold changes respectively, in the absence of growth factors (**Figure 6.11A**). By contrast, in the presence of growth factors, there was significantly

greater Pep2, Sema4f, Unc5b and Ttf-1 gene expression for 3D cells in an air-liquid interface (12.03 ± 1.95, 5.83 ± 1.64, 6.03 ± 0.30, 4.03 ± 0.85)-fold changes than in 3D cells in submerged medium (6.90 ± 1.56, 4.00 ± 1.30, 2.73 ± 0.50, 1.96 ± 0.15)-fold changes, and in control cells (6.20 ± 0.36, 3.76 ± 0.90, 3.24 ± 1.05, 2.90 ± 1.73)-fold changes, as shown in **Figure 6.11B**.

These differences may be because the scaffold cells are grown in an environment similar to the *in vivo* airway epithelia, both grown in ALI (air-liquid interface) conditions [453, 454]. Ttf-1 is the earliest marker known for lung expression and was more greatly expressed in scaffold cells exposed to ALI conditions than in those not so exposed, probably because the combination of both 3D and ALI provide a suitable extracellular matrix environment that mimics that *in vivo*, and such conditions are not present in monolayer cultures. Pep2 plays an important role in nitric oxide precursor uptake and is localised in alveolar type II cells and highly expressed in lung epithelial cells [455-457]. There was up-regulation of Pept2 after 30 days of culture on scaffolds, under ALI culture. Semaphorin 4F has been identified as a cell surface marker specific for lung bud [458]. Similarly, the present study demonstrated that Semaphorin 4F exhibited greater expression in immobilised cells with growth factor and in the presence of ALI than the control, as shown by qPCR results.

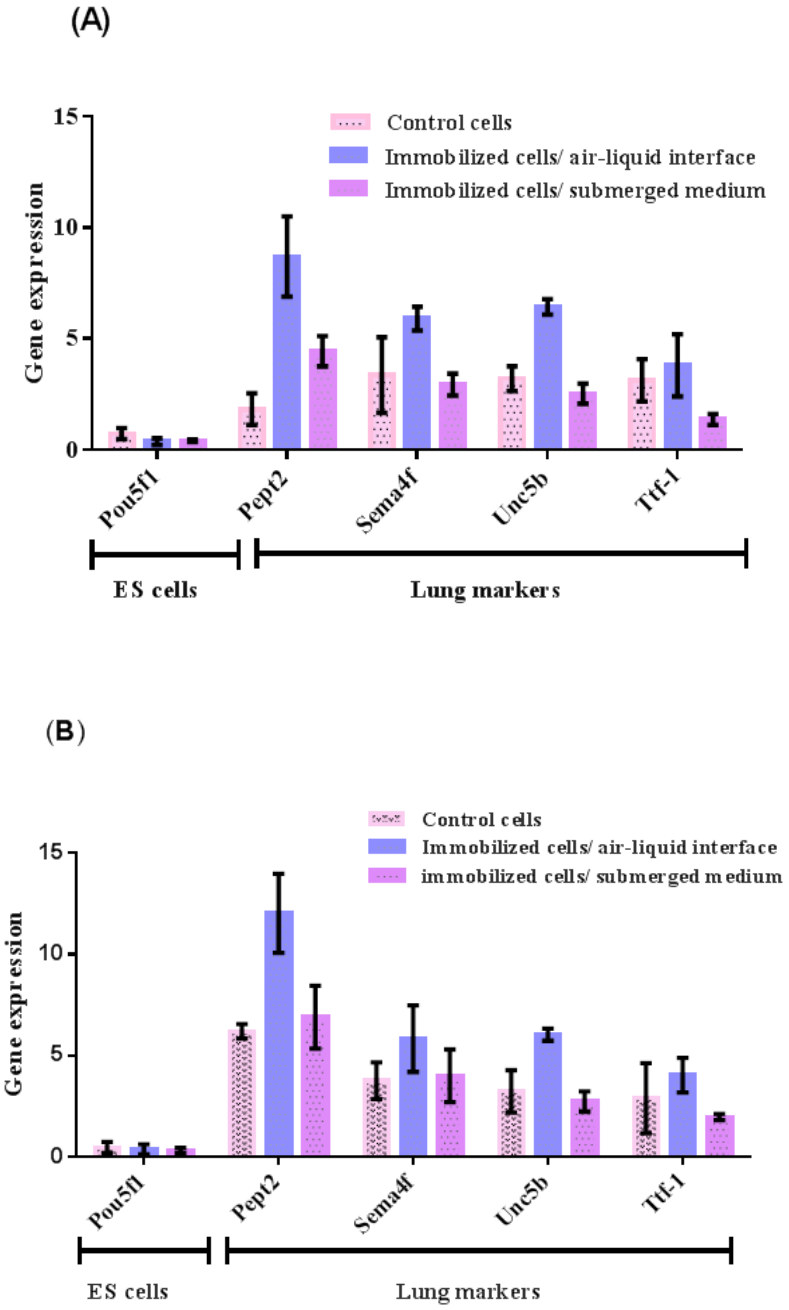

Figure 6.11: Fold change in gene expression during differentiation of embryonic stem cells into lung epithelial cells relative to undifferentiated ESCs in the absence (A) and presence (B) of growth factors compared with their controls. Cells were assessed after 14 days and 30 days for control and embedded scaffolds respectively. Data are represented as mean (n = 3) ± standard error of the mean and were compared by Student t-test with control cells. Differences were considered significant at $p<0.05$.

Protein expression, anti Pept2 and Sema4f antibodies were used to detect the expression of their corresponding lung epithelial markers using immunostaining at selected times. There was greater Pept2 and Sema4f protein expression in scaffold cells at 30 days following exposure to an air-liquid interface than in submerged and control cells (**Figure 6.12 A and B**). This study demonstrated that the use of a 3-dimensional (3D) scaffold was advantageous compared with 2-dimensional (2D) monolayer culture in terms of generating lung epithelial cells, since 3D systems closely mimic the *in-vivo* microenvironment, especially in an air-liquid interface [440]. As predicted, the embryonic stem cells maintained their viability and further differentiated in Gtn-DHHA hydrogel; therefore, this hydrogel is a suitable and promising scaffold candidate for use in lung tissue regeneration.

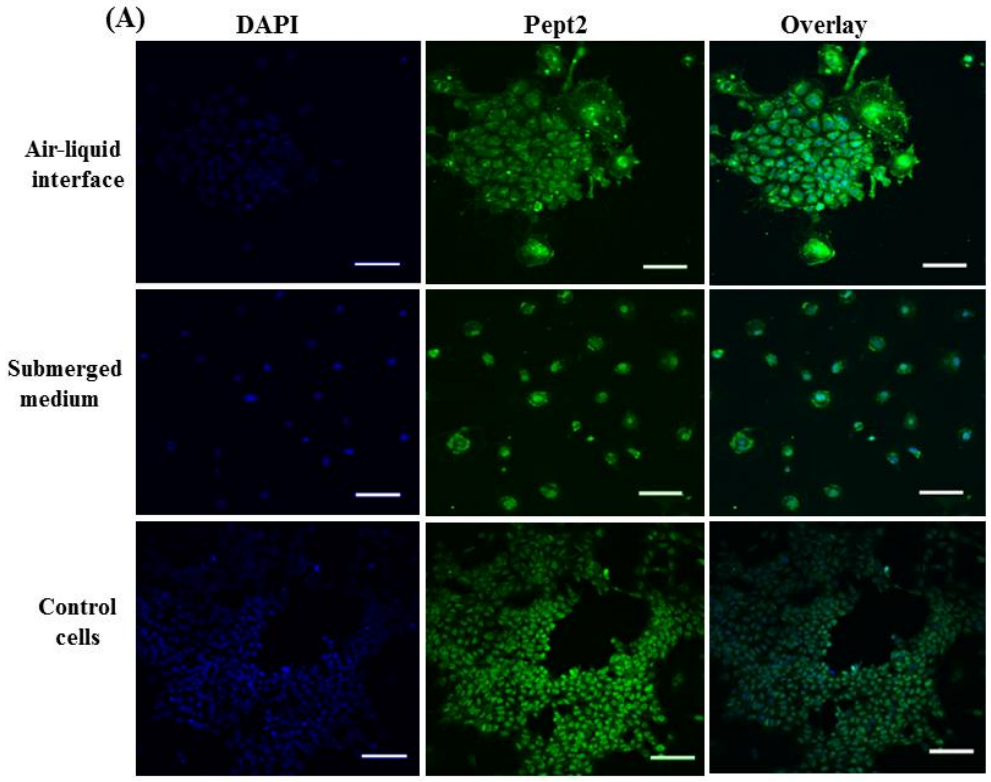

Figure 6.12A: Immunofluorescence analysis of lung epithelial cells (Pept2). These images were taken of cells embedded in scaffolds in the presence of growth factors compared with the control. Nucleated cells are in blue (DAPI). Pep2 marker staining (green colour) is an indicator for lung epithelium cells. Expression for this marker was greater in cells embedded in scaffolds in air-liquid medium compared with that in submerged and control cells. Scale bar represents 100 µm.

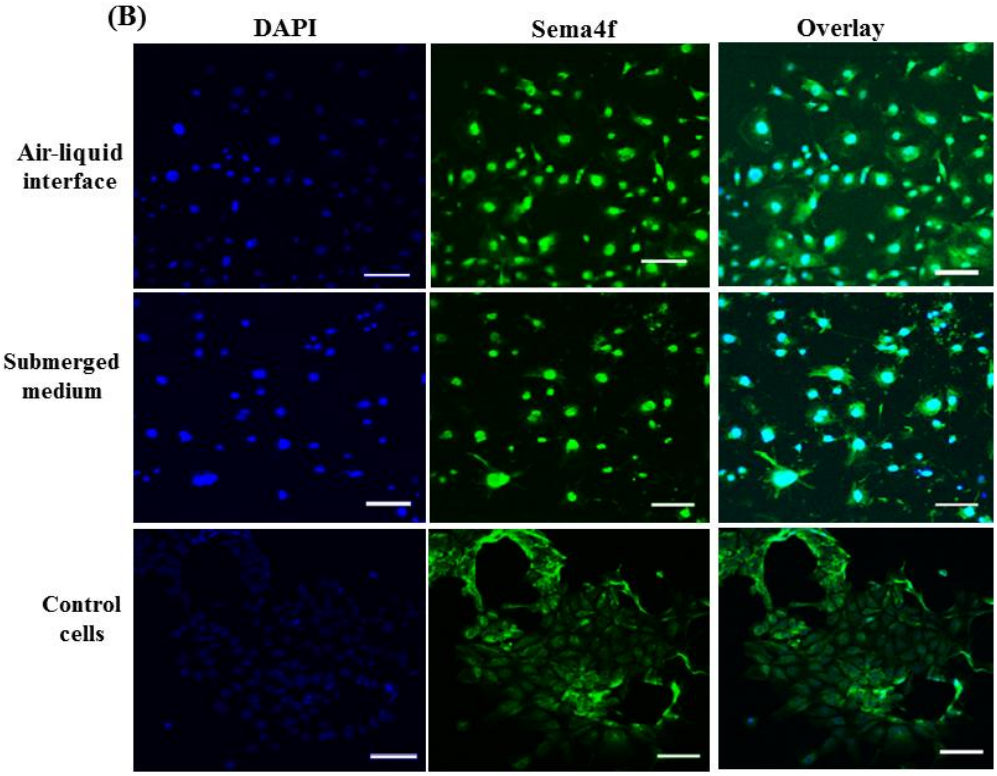

Figure 6.12B: Immunofluorescence analysis of lung epithelial cells (Sema4f). These images were taken of cells embedded in scaffolds in the presence of growth factors. Nucleated cells are in blue (DAPI). Sema4f marker (green colour) is an indicator for lung epithelium cells. Expression for this marker was greater in cells embedded in scaffolds compared with that in submerged and control cells. Scale bar represents 100 μm.

6.4 Conclusions

In the current study, a novel injectable biodegradable hydrogel composed of Gtn and DHHA cross-linked by laccase was designed for lung tissue engineering. Gtn-DHHA hydrogel displayed a high swelling ratio, biodegradability, high biocompatibility and mechanical integrity. Gtn-DHHA hydrogel enhanced ESCs proliferation and differentiation toward lung epithelial cells in both the presence and absence of growth factors. Gene expression and immunostaining results suggested that Gtn-DHHA hydrogel supported stem cell differentiation and allowed growth factors to diffuse within the scaffold to reach cells, in particular under air-liquid interface (ALI) culture compared with submerged and control cells. This study suggests that Gtn-DHHA hydrogel is suitable for lung tissue repair and regenerative medicine for lung regeneration and may be applicable to other tissue regeneration uses. The combination of Gtn-DHHA hydrogel and air-liquid (ALI) culture provided a useful tool for the *in-vitro* differentiation of murine embryonic cells and provided structural support for lung epithelial cell survival and growth.

CHAPTER SEVEN

7. General Discussion, Conclusion and Future Directions

7.1 General Discussion

There are many different types of lung disease that currently have no effective cure. This study attempted to develop novel tools with the ultimate goal of treating lung disease. For lung cancer, liquid marble (LM) and SAW microcentrifugation methods were developed to generate a valid tumour model to enhance miRNA transfection.

Lung spheroids generated from the LM method had a spherical shape while spheroids generated from the liquid monolayer (LS) method exhibited more irregular shapes. This observation is consistent with previous studies [153]. In both LM- and LS- generated spheroids, the periphery was populated with viable cells, as tested by vital staining with Calcein AM and propidium iodide (PI). There was an absence of colour in the spheroid core, possibly because the core was populated with dead cells or because the stains did not penetrate through the tightly knit peripheral cells. PI is impermeable to live cells but can penetrate through a dead cell's leaky membrane and stain the nuclei [333]. PEI and lipofectamine as delivery vehicles both protected miRNA against degradation by nucleases in serum.

A major objective of the first approach was to evaluate miR-126 expression in both monolayer cultures and spheroids. miR-126 was highly expressed in spheroids generated using LM, especially in spheroids transfected inside LM. Spheroids are often more resistant to chemotherapeutic drug uptake than monolayer cells, due to a variety of reasons, including differences in: cell-cell communication, cell shape and/or the ability to repair damage [337]. More miRNA-Dy547 internalised into LM-generated spheroids than into LS-generated spheroids. However, the internalised miRNA-Dy547 was localised at the only the periphery of the spheroid. The high transfection rate in LM-generated spheroids may be due to a more regular shape and greater viability than that of LS-generated

spheroids. However, following transfection in ultra-low attachment plates, miRNA-Dy547 was localised at the periphery as well as penetrating deeply into the core of the LM-generated and transfected spheroids. These results suggested that the high miR-126 expression found in LM-generated and transfected spheroids was due to high miRNA uptake. The greatest miRNA uptake was observed in LM-transfected spheroids but not in ultra-low attachment plates, suggesting that LM as a transfection vessel also played a key role in transfection. PTFE, which makes up the LM, resists protein adhesion due to its ultra-low surface free energy and high hydrophobicity with a water contact angle of 108°[343, 344]. The anti-adhesive LM shell inhibits non-specific absorption of miRNA to the shell and therefore reduces loss of miRNA by adsorption. The level of VEGF-A reduced in A549 cells, regardless of whether cells were cultured in monolayers or in spheroids. These results agree with previous results by others that miR-126 transfection leads to down-regulation of VEGF-A in A549 [349]. Overall, this study demonstrated that LM could serve not only as a platform that produces tumour-like spheroids, but also as an efficient microbioreactor vessel that enhances miRNA transfection and outperforms conventional transfection vessels.

Most cells found on the periphery of the spheroids generated by SAW microcentrifugation remained viable and formed a shell around an unstained, possibly necrotic core. Necrotic cores are common in spheroids, especially in older and larger spheroids, where the cells in the centre of the spheroid are deprived of oxygen and nutrients due to limitations in diffusion [11, 334]. The spheroids produced via liquid overlay (LO) and SAW microcentrifugation methods also exhibited heterogeneous cell subpopulations that contained viable cells at their periphery and possibly inviable cells in their core.

The SAW device also had the advantage of being able to handle larger fluid volumes than the conventional hanging drop method [459]. The cell concentration process was rapid, requiring only a minute, compared with other conventional methods such as liquid overlay, which require at least a day. The resulting spheroid displayed the concentric heterogeneous cell population arrangement and the tight cell-to-cell interfaces characteristically observed in solid tumors *in vivo*. This demonstrated the usefulness of the platform for improving cancer biology and drug screening investigations.

Spheroids generated using both liquid marble and SAW microcentrifugation methods in **Chapter 3 and 4** could be used as an effective tumour model to study miRNA transfection.

A study in **Chapter 5** attempted to spray stem cells into a model of small lung damage. A preliminary study optimised the SAW nebulisation for the retention of cell viability post-nebulisation. The proportion of viable cells decreased as power applied increased, probably due to the increase in stresses to which the cells were subjected, with increasing levels of acoustic radiation. This observation is consistent with a previous study on using SAW radiation to drive osteoblast perfusion into tissue scaffolds, in which cell viability decreased with increasing applied power [372]. RT-PCR analysis of both control and nebulised MSCs expressed CD29, CD44 and CD106 markers at both 24 and 72 hours. These suggested that the nebulised cells were phenotypically similar to the control cells. The nebulised MSCs continued to express similar levels of these markers to controls after 24 hours, suggesting that SAW nebulisation did not alter these genes' expression in the MSCs. Similarly, tests of protein expression in whole cells showed that nebulised MSCs and controls had similar CD29, CD44 and CD106 positive cell counts after 24 hours. This suggests that nebulised cells functioned in the same manner as cells held in culture without exposure to SAW. Given the novelty of inhaled stem cell therapy, comparisons with other delivery methods is difficult, although more benchmarking data are anticipated in the future due to the increasing interest in stem cell therapy because of the absence of viable current alternative treatments for respiratory ailments. However, these results provide evidence that the SAW nebulisation platform, with its inherent benefits of low cost and portability, constitutes an attractive tool for the delivery of stem cells via inhalation for the treatment and repair of lung function, and can be a novel inhaled stem cell therapy for lung ailments.

For lung tissues damaged by accident, the study in **Chapter 6** attempted to create large lung tissue scaffolds as replacements. Embryonic stem cells (ESCs) survived in a 10% Gtn-DHHA hydrogel cross-linked with 2.27 unit/mL of laccase, as ESC viability was about 90% as measured by counting

Calcein AM stained cells. Cell DNA content did not change over a 7 day period in hydrogel. This suggests that the cell number in hydrogel scaffolds grew more slowly than in the control, possibly because the cells needed to secret proteinase to degrade the 3-dimensional (3D) 3D hydrogel before they could propagate, unlike growth on two-dimensional (2D) surfaces. These results suggested that the Gtn-DHHA encapsulated cells were viable and capable of proliferation, and that Gtn-DHHA hydrogel is suitable for tissue engineering applications.

The formation of definitive endoderm was assessed by qPCR and immunostaining assays. Over periods of 7 and 14 days, the endoderm transcription factors Foxa2 and Sox17 exhibited higher expression in 3D culture cells in the hydrogel scaffolds than in the 2D monolayer cells, in particular in cells embedded in 3D hydrogel in an air-liquid interface compared with submerged and control cells. These results support prior investigations, which suggested that Sox17 and Foxa2 expression initially increased on Activin A treatment [451]. Qualitative and quantitative assays were performed to evaluate the differentiation of stem cells into lung epithelial cells. Relative to control and submerged cells, cells incubated in the air-liquid interface for 30 days showed evidence of differentiation, as judged by their greater Pept2, Sema4f, Unc5b and Ttf-1 gene expression. This was as expected, because the scaffold cells are grown in air-liquid interface (ALI) conditions similar to those of *in-vivo* airway epithelia [453, 454].

These results were confirmed by evaluation of the expression of lung epithelial markers. There was greater expression of Pept2 and Sema4f in cells in scaffolds at 30 days following their exposure in the air-liquid interface than in submerged and control cells. This study demonstrated that a 3D scaffold was advantageous over a 2D monolayer culture for generating lung epithelial cells, since 3D systems more closely mimicked the *in-vivo* microenvironment, especially in forming an air-liquid interface [440]. Gtn-DHHA hydrogel and air-liquid interface (ALI) culture thus provides a useful tool for the *in vitro* study of embryonic cells, by increasing their differentiation and the formation of cells resembling lung epithelial cells both structurally and functionally.

The experimental evidence suggests that both liquid marble and SAW microcentrifugation enhanced spheroid formation and miRNA transfection, and that cells grown in 3D scaffolds and delivered by SAW nebuliser could be used to cure lung ailments.

7.2 General Conclusion

The four parts of this thesis have improved the knowledge of: gene therapy, microfluidic device assisted stem cell delivery and stem-cell-based tissue engineering for lung diseases.

The first part demonstrated the feasibility of a simple, effective and successful strategy called liquid marble (LM) to form lung spheroids compared with a conventional method. Liquid marbles made of liquid growth medium wrapped by non-adhesive powder particles were presented as efficient microbioreactors capable of supplying a convenient medium for cells to grow and aggregate. A549 lung cancer spheroids were generated in a LM microbioreactor; the spheroids were subjected to miR-126 transfection inside the LM. The miR-126 expression and the subsequent VEGF-A down-regulation in LM-transfected spheroids reached a level that could not be achieved in various controls, including monolayer cells, spheroids generated using the LS method, and spheroids transfected in conventional ultra-low attachment plates. Overall, this study demonstrated that LM could serve not only as a platform that produces tumour-like spheroids, but also as an efficient microbioreactor vessel that enhanced miRNA transfection and outperformed conventional transfection vessels.

The second part of this thesis investigated the feasibility of using surface acoustic waves (SAW) to generate multicellular spheroids. The results showed that the surface acoustic device had advantages over other microfluidics for the formation of uniform multicellular spheroids by driving cells into a tight aggregate. The SAW device also enhanced the production of spheroids in microwells of standard tissue culture microplates. Multiple SAW devices could be used in parallel to produce multiple spheroids simultaneously. Spheroid size could be controlled by varying the input power of the SAW device. This represents a distinct improvement on current methods, since it circumvents the need for

the fabrication of multiple devices with various geometric designs. Spheroid generation required only one minute, compared with that of the liquid overlay method, which takes at least a day.

The third part of the thesis was concerned with investigating the feasibility of generating MSC-laden aerosols via SAW without causing harmful effects on cells. An optimum power level of 1.5 W yielded a balance between maximising cell viability at an acceptable level (about 90%). The data demonstrated that the SAW nebuliser had no deleterious effects in rat mesenchymal stem cell viability, proliferation, or cell surface marker integrity and expression.

The fourth part of this thesis was concerned with developing a novel injectable biodegradable hydrogel for lung tissue engineering. Gtn-DHHA displayed a high swelling ratio, biodegradability, high biocompatibility and mechanical integrity. Gtn-DHHA enhanced ESC survival and proliferation. A comprehensive study investigated the feasibility of lung differentiation in mouse ESCs within 3D scaffolds. Gene expression studies suggested the differentiation of the ESCs into cells characteristic of lung epithelia. This was demonstrated by the expression of endoderm-specific markers, followed by the expression of lung-specific transcription markers and the immunological detection of lung markers (Sema4f and Pept2) in cells. This suggests that Gtn-DHHA hydrogel is a suitable tissue-engineered scaffold that could be used for lung tissue repair and presents a new pathway for regeneration of lung as well as possibly other tissue types.

7.3 Future Perspectives

Due to the success of this miRNA-based gene therapy, stem-cell delivery and fabrication of Gtn-DHHA scaffolds for lung regeneration and repair, other applications are now possible.

- PEI and lipofectamine significantly influenced the delivery of miRNA 126 into spheroids of lung cancer cells in the liquid marble method. Microarray devices and cell trapping barriers should be developed to make more effective and uniformly sized cellular spheroids to test the delivery of miRNA 126 coupled with PEI and lipofectamine [118-120].

- The most significant properties of liquid marbles are the permeability of the porous shell, which allows the possibility of gas exchange between the medium and the surrounding environment, and the non-adhesiveness of the hydrophobic powder particles, which encourages cell suspension in the medium. A multicellular lung spheroid was successfully formed in **Chapter 3**. The unique properties of liquid marble to form spheroids are applicable to both embryoid bodies and multicellular tumour spheroid formation [151, 153]. As a result, liquid marble should be explored for lung differentiation from embryonic stem cells, as another important biological application.

- The micro-centrifugation flow by the SAW microfluidic device rapidly enhanced the concentration of BT-474 cells into tight aggregates within a minute in **Chapter 4**. This is considerably faster than the conventional liquid overlay method. Therefore, the SAW device should be studied for its ability to generate embryoid bodies. This would be another vital area for future study.

- Liquid marble and SAW microcentrifugation should be used together to form uniform-sized, highly-reproducible, massive spheroids by encapsulating different kinds of cancer cells – this would compare well with droplet-based microfluidics [460].

- The concept of using 3D biodegradable scaffolds as alternatives to the extracellular matrix (ECM) more closely mimics cells' native environment and is an interesting area of study in current tissue engineering. The fourth section of this thesis (**Chapter 6**) focused the feasibility of producing lung epithelial cells using novel 3D scaffolds. This scaffold was biodegradable and was prepared by conjugating gelatin with 3, 4-dihydroxyhydrocinnamic acid. The observation of lung epithelial cells inside the hydrogel implied that the murine stem cells survived and proliferated well. Gtn-DHHA hydrogel allowed the formation of more lung epithelial cells at the ensuing air-liquid interface with medium conditions than did submerged and monolayered cultures. The biocompatibility, strength and mechanical properties of the Gtn-DHHA hydrogel are comparable to those of soft tissues and organs such as the thyroid, liver and breast [448]. Hence, Gtn-DHHA hydrogels should be tested as tissue scaffolds that mimic these soft tissues too.

REFERENCES

1. Orens, J.B. and E.R. Garrity, Jr., *General overview of lung transplantation and review of organ allocation.* Proc Am Thorac Soc, 2009. **6**(1): p. 13-9.
2. Jungebluth, P. and P. Macchiarini, *Stem cell-based therapy and regenerative approaches to diseases of the respiratory system.* Br Med Bull, 2011. **99**: p. 169-87.
3. Foronjy, R.F. and S.M. Majka, *The potential for resident lung mesenchymal stem cells to promote functional tissue regeneration: understanding microenvironmental cues.* Cells, 2012. **1**(4): p. 874.
4. Chitkara, D., A. Mittal, and R.I. Mahato, *miRNAs in pancreatic cancer: Therapeutic potential, delivery challenges and strategies.* Advanced Drug Delivery Reviews, 2015. **81**: p. 34-52.
5. Chen, Y., D.-Y. Gao, and L. Huang, *In vivo delivery of miRNAs for cancer therapy: Challenges and strategies.* Advanced Drug Delivery Reviews, 2015. **81**: p. 128-141.
6. Ortholan, C., et al., *MicroRNAs and lung cancer: new oncogenes and tumor suppressors, new prognostic factors and potential therapeutic targets.* Curr Med Chem, 2009. **16**(9): p. 1047-61.
7. Chen, C.Z., *MicroRNAs as oncogenes and tumor suppressors.* New England Journal of Medicine, 2005. **353**(17): p. 1768-1771.
8. Garzon, R., G. Marcucci, and C.M. Croce, *Targeting microRNAs in cancer: rationale, strategies and challenges.* Nature Reviews Drug Discovery, 2010. **9**(10): p. 775-789.
9. Korff, T. and H.G. Augustin, *Integration of Endothelial Cells in Multicellular Spheroids Prevents Apoptosis and Induces Differentiation.* The Journal of Cell Biology, 1998. **143**(5): p. 1341-1352.
10. Lin, R.-Z. and H.-Y. Chang, *Recent advances in three-dimensional multicellular spheroid culture for biomedical research.* Biotechnology Journal, 2008. **3**(9-10): p. 1172-1184.
11. Khaitan, D., et al., *Establishment and characterization of multicellular spheroids from a human glioma cell line; Implications for tumor therapy.* Journal of Translational Medicine, 2006. **4**(1): p. 12.
12. Agastin, S., et al., *Continuously perfused microbubble array for 3D tumor spheroid model.* Biomicrofluidics, 2011. **5**(2): p. 024110.
13. Lau, A.N., et al., *Stem Cells and Regenerative Medicine in Lung Biology and Diseases.* Mol Ther, 2012. **20**(6): p. 1116-1130.
14. Gomperts, B.N. and R.M. Strieter, *Stem Cells and Chronic Lung Disease.* Annual Review of Medicine, 2007. **58**(1): p. 285-298.
15. Langer, R. and J.P. Vacanti, *Tissue Engineering.* Science, 1993. **260**(5110): p. 920-926.
16. Vacanti, J.P. and R. Langer, *Tissue engineering: the design and fabrication of living replacement devices for surgical reconstruction and transplantation.* Lancet, 1999. **354 Suppl 1**: p. SI32-4.
17. Polak, D.J., *The use of stem cells to repair the injured lung.* British Medical Bulletin 2011. **99**(198-197).
18. Evans, M.J. and M.H. Kaufman, *Establishment in Culture of Pluripotential Cells from Mouse Embryos.* Nature, 1981. **292**(5819): p. 154-156.
19. Smith, A.G., *Embryo-derived stem cells: Of mice and men.* Annual Review of Cell and Developmental Biology, 2001. **17**: p. 435-462.
20. Lewin, A.S. and W.W. Hauswirth, *Ribozyme gene therapy: applications for molecular medicine.* Trends Mol Med, 2001. **7**(5): p. 221-8.
21. Richardson, P.D., et al., *Gene repair and transposon-mediated gene therapy.* Stem Cells, 2002. **20**(2): p. 105-18.

22. Mulligan, R.C., *The basic science of gene therapy.* Science, 1993. **260**(5110): p. 926-32.
23. Prasad, G., et al., *Recent advances in experimental molecular therapeutics for malignant gliomas.* Curr Med Chem Anticancer Agents, 2004. **4**(4): p. 347-61.
24. Tseng, J.F. and R.C. Mulligan, *Gene therapy for pancreatic cancer.* Surg Oncol Clin N Am, 2002. **11**(3): p. 537-69.
25. Prieto, J., et al., *Gene therapy of liver diseases.* Expert Opin Biol Ther, 2004. **4**(7): p. 1073-91.
26. Reid, T., R. Warren, and D. Kirn, *Intravascular adenoviral agents in cancer patients: lessons from clinical trials.* Cancer Gene Ther, 2002. **9**(12): p. 979-86.
27. Peng, Z., *Current status of gendicine in China: recombinant human Ad-p53 agent for treatment of cancers.* Hum Gene Ther, 2005. **16**(9): p. 1016-27.
28. Pulkkanen, K.J. and S. Yla-Herttuala, *Gene therapy for malignant glioma: current clinical status.* Mol Ther, 2005. **12**(4): p. 585-98.
29. Malaeb, B.S., et al., *Elevated activated partial thromboplastin time during administration of first-generation adenoviral vectors for gene therapy for prostate cancer: identification of lupus anticoagulants.* Urology, 2005. **66**(4): p. 830-4.
30. Vattemi, E. and P.P. Claudio, *Gene therapy for lung cancer: practice and promise.* Ann Ital Chir, 2004. **75**(3): p. 279-89.
31. Welfare, A.I.o.H.a., *Lung Cancer in Australia: An overveiw* CANCER SERIES 2011. **Cat. no. CAN 58**(64).
32. Ferlay, J., et al., *Estimates of worldwide burden of cancer in 2008: GLOBOCAN 2008.* Int J Cancer, 2010. **127**(12): p. 2893-917.
33. Welfare, A.I.o.H.a., *Cancer in Australia: an overview.* Cancer series, 2014. **no. 78. Cat. no. CAN 75. Canberra: AIHW.**
34. Travis, W.D., E. Brambilla, and G.J. Riely, *New pathologic classification of lung cancer: relevance for clinical practice and clinical trials.* J Clin Oncol, 2013. **31**(8): p. 992-1001.
35. Centers for Disease Control and Prevention, *Lung Cancer: Screening.* http://www. cdc.gov/cancer/lung/basic_info/screening.htm, 2009.
36. Centers for Disease Control and Prevention, *Lung Cancer: Diagnosis and Treatment.* http://www.cdc.gov/cancer/lung/basic_info/diagnosis_treatment.htm, 2009.
37. Lee, R.C., R.L. Feinbaum, and V. Ambros, *The C. elegans heterochronic gene lin-4 encodes small RNAs with antisense complementarity to lin-14.* Cell, 1993. **75**(5): p. 843-54.
38. Hutvagner, G. and P.D. Zamore, *A microRNA in a multiple-turnover RNAi enzyme complex.* Science, 2002. **297**(5589): p. 2056-2060.
39. Zeng, Y., R. Yi, and B.R. Cullen, *MicroRNAs and small interfering RNAs can inhibit mRNA expression by similar mechanisms.* Proceedings of the National Academy of Sciences of the United States of America, 2003. **100**(17): p. 9779-9784.
40. Houbaviy, H.B., M.F. Murray, and P.A. Sharp, *Embryonic stem cell-specific MicroRNAs.* Developmental Cell, 2003. **5**(2): p. 351-358.
41. Hatfield, S.D., et al., *Stem cell division is regulated by the microRNA pathway.* Nature, 2005. **435**(7044): p. 974-978.
42. Reinhart, B.J., et al., *The 21-nucleotide let-7 RNA regulates developmental timing in Caenorhabditis elegans.* Nature, 2000. **403**(6772): p. 901-906.
43. Brennecke, J., et al., *Bantam encodes a developmentally regulated microRNA that controls cell proliferation and regulates the proapoptotic gene hid in Drosophila.* Cell, 2003. **113**(1): p. 25-36.
44. Chen, C.Z., et al., *MicroRNAs modulate hematopoietic lineage differentiation.* Science, 2004. **303**(5654): p. 83-86.
45. Cheng, A.M., et al., *Antisense inhibition of human miRNAs and indications for an involvement of miRNA in cell growth and apoptosis.* Nucleic Acids Research, 2005. **33**(4): p. 1290-1297.

46. Cimmino, A., et al., *miR-15 and miR-16 induce apoptosis by targeting BCL2.* Proceedings of the National Academy of Sciences of the United States of America, 2005. **102**(39): p. 13944-13949.
47. Tanno, B., et al., *Silencing of endogenous IGFBP-5 by micro RNA interference affects proliferation, apoptosis and differentiation of neuroblastoma cells.* Cell Death and Differentiation, 2005. **12**(3): p. 213-223.
48. Lu, Y., et al., *Transgenic over-expression of the microRNA miR-17-92 cluster promotes proliferation and inhibits differentiation of lung epithelial progenitor cells.* Developmental Biology, 2007. **310**(2): p. 442-453.
49. Abelson, J.F., et al., *Sequence variants in SLITRK1 are associated with Tourette's syndrome.* Science, 2005. **310**(5746): p. 317-320.
50. Alvarez-Garcia, I. and E.A. Miska, *MicroRNA functions in animal development and human disease.* Development, 2005. **132**(21): p. 4653-4662.
51. Meltzer, P.S., *Cancer genomics - Small RNAs with big impacts.* Nature, 2005. **435**(7043): p. 745-746.
52. Volinia, S., et al., *A microRNA expression signature of human solid tumors defines cancer gene targets.* Proceedings of the National Academy of Sciences of the United States of America, 2006. **103**(7): p. 2257-2261.
53. Li, X., et al., *Survival prediction of gastric cancer by a seven-microRNA signature.* Gut, 2010. **59**(5): p. 579-85.
54. Hu, Y., et al., *Prognostic significance of differentially expressed miRNAs in esophageal cancer.* Int J Cancer, 2011. **128**(1): p. 132-43.
55. Zhang, H., et al., *MicroRNA patterns associated with clinical prognostic parameters and CNS relapse prediction in pediatric acute leukemia.* PLoS One, 2009. **4**(11): p. e7826.
56. Lu, J., et al., *MicroRNA expression profiles classify human cancers.* Nature, 2005. **435**(7043): p. 834-838.
57. Tavazoie, S.F., et al., *Endogenous human microRNAs that suppress breast cancer metastasis.* Nature, 2008. **451**(7175): p. 147-U3.
58. Mitchell, P.S., et al., *Circulating microRNAs as stable blood-based markers for cancer detection.* Proceedings of the National Academy of Sciences of the United States of America, 2008. **105**(30): p. 10513-10518.
59. Suarez, Y., et al., *Dicer-dependent endothelial microRNAs are necessary for postnatal angiogenesis.* Proc Natl Acad Sci U S A, 2008. **105**(37): p. 14082-7.
60. Hayashita, Y., et al., *A polycistronic microRNA cluster, miR-17–92, is overexpressed in human lung cancers and enhances cell proliferation.* Cancer Res. , 2005. **65**: p. 9628–9632.
61. Takamizawa, J., et al., *Reduced expression of the let-7 microRNAs in human lung cancers in association with shortened postoperative survival.* Cancer Research, 2004. **64**(11): p. 3753-3756.
62. Schliekelman, M.J., et al., *Targets of the Tumor Suppressor miR-200 in Regulation of the Epithelial-Mesenchymal Transition in Cancer.* Cancer Research, 2011. **71**(24): p. 7670-7682.
63. Lewis, B.P., et al., *Prediction of mammalian microRNA targets.* Cell, 2003. **115**(7): p. 787-98.
64. Yanaihara, N., et al., *Unique microRNA molecular profiles in lung cancer diagnosis and prognosis.* Cancer Cell, 2006. **9**(3): p. 189-98.
65. Wang, X.H., et al., *Aberrant Expression of Oncogenic and Tumor-Suppressive MicroRNAs in Cervical Cancer Is Required for Cancer Cell Growth.* Plos One, 2008. **3**(7).
66. Saito, Y., et al., *Epigenetic therapy upregulates the tumor suppressor microRNA-126 and its host gene EGFL7 in human cancer cells.* Biochemical and Biophysical Research Communications, 2009. **379**(3): p. 726-731.
67. Guo, C.G., et al., *The noncoding RNA, miR-126, suppresses the growth of neoplastic cells by targeting phosphatidylinositol 3-kinase signaling and is frequently lost in colon cancers.* Genes Chromosomes & Cancer, 2008. **47**(11): p. 939-946.

68. Chen, H.X., et al., *Reduced miR-126 expression facilitates angiogenesis of gastric cancer through its regulation on VEGF-A.* Oncotarget, 2014. **5**(23): p. 11873-11885.
69. Yupeng, L., et al., *miR-126 regulates angiogenesis by target vascular endothelial growth factor-A in gastric adenocarcinoma.* RNA & DISEASE 2015. **2**(e523).
70. Sasahira, T., et al., *Downregulation of miR-126 induces angiogenesis and lymphangiogenesis by activation of VEGF-A in oral cancer.* British Journal of Cancer, 2012. **107**(4): p. 700-706.
71. Volm, M., et al., *Angiogenic growth factors and their receptors in non-small cell lung carcinomas and their relationships to drug response in vitro.* Anticancer Research, 1997. **17**(1A): p. 99-103.
72. Liu, B., et al., *MiR-126 restoration down-regulate VEGF and inhibit the growth of lung cancer cell lines in vitro and in vivo.* Lung Cancer, 2009. **66**(2): p. 169-175.
73. Trang, P., et al., *Regression of murine lung tumors by the let-7 microRNA.* Oncogene, 2010. **29**(11): p. 1580-1587.
74. Li, D., et al., *MicroRNA-99a inhibits hepatocellular carcinoma growth and correlates with prognosis of patients with hepatocellular carcinoma.* J Biol Chem, 2011. **286**(42): p. 36677-85.
75. Chan, J.A., A.M. Krichevsky, and K.S. Kosik, *MicroRNA-21 is an antiapoptotic factor in human glioblastoma cells.* Cancer Research, 2005. **65**(14): p. 6029-6033.
76. Oliveira-Carvalho, V., et al., *MicroRNAs: a new paradigm in the treatment and diagnosis of heart failure?* Arq Bras Cardiol, 2012. **98**(4): p. 362-9.
77. Whitehead, K.A., R. Langer, and D.G. Anderson, *Knocking down barriers: advances in siRNA delivery.* Nature Reviews Drug Discovery, 2009. **8**(2): p. 129-138.
78. Kim, W.J. and S.W. Kim, *Efficient siRNA delivery with non-viral polymeric vehicles.* Pharm Res, 2009. **26**(3): p. 657-66.
79. Khatri, N., et al., *In vivo delivery aspects of miRNA, shRNA and siRNA.* Crit Rev Ther Drug Carrier Syst, 2012. **29**(6): p. 487-527.
80. Pereira, D.M., et al., *Delivering the promise of miRNA cancer therapeutics.* Drug Discov Today, 2013. **18**(5-6): p. 282-9.
81. Park, T.G., J.H. Jeong, and S.W. Kim, *Current status of polymeric gene delivery systems.* Advanced Drug Delivery Reviews, 2006. **58**(4): p. 467-486.
82. Lv, H., et al., *Toxicity of cationic lipids and cationic polymers in gene delivery.* J Control Release, 2006. **114**(1): p. 100-9.
83. Tseng, Y.C., S. Mozumdar, and L. Huang, *Lipid-based systemic delivery of siRNA.* Adv Drug Deliv Rev, 2009. **61**(9): p. 721-31.
84. Lam, J.K., et al., *siRNA Versus miRNA as Therapeutics for Gene Silencing.* Mol Ther Nucleic Acids, 2015. **4**: p. e252.
85. Wu, Y., et al., *MicroRNA delivery by cationic lipoplexes for lung cancer therapy.* Mol Pharm, 2011. **8**(4): p. 1381-9.
86. Piao, L., et al., *Lipid-based nanoparticle delivery of Pre-miR-107 inhibits the tumorigenicity of head and neck squamous cell carcinoma.* Mol Ther, 2012. **20**(6): p. 1261-9.
87. Trang, P., et al., *Systemic Delivery of Tumor Suppressor microRNA Mimics Using a Neutral Lipid Emulsion Inhibits Lung Tumors in Mice.* Molecular Therapy, 2011. **19**(6): p. 1116-1122.
88. de Fougerolles, A., et al., *Interfering with disease: a progress report on siRNA-based therapeutics.* Nat Rev Drug Discov, 2007. **6**(6): p. 443-53.
89. Ibrahim, A.F., et al., *MicroRNA Replacement Therapy for miR-145 and miR-33a Is Efficacious in a Model of Colon Carcinoma.* Cancer Research, 2011. **71**(15): p. 5214-5224.
90. BioCancell, *Phase 2b, Trial of Intravesical DTA-H19/PEI in Patients With Intermediate-Risk Superficial Bladder Cancer.* ClinicalTrials.gov(Internet), National Library of Medicine (US),Bethesda, MD, 2013 (Cited July 18,2013).NLM identified NCT00595088, 2008.

91. BioCancell, *Pilot Study of BC-819/PEI and BCG in Patients With Superficial Transitional Cell Bladder Carcinoma.* ClinicalTrials.gov (Internet), National Libray of Medicine (US),Bethesda,MD,2013, (Cited July 18,2013).NLM Identifier: NCT01878188, 2013.
92. Chiou, G.Y., et al., *Cationic polyurethanes-short branch PEI-mediated delivery of Mir145 inhibited epithelial-mesenchymal transdifferentiation and cancer stem-like properties and in lung adenocarcinoma.* Journal of Controlled Release, 2012. **159**(2): p. 240-250.
93. Yang, Y.P., et al., *Inhibition of cancer stem cell-like properties and reduced chemoradioresistance of glioblastoma using microRNA145 with cationic polyurethane-short branch PEI.* Biomaterials, 2012. **33**(5): p. 1462-1476.
94. Ren, Y., et al., *Co-delivery of as-miR-21 and 5-FU by Poly(amidoamine) Dendrimer Attenuates Human Glioma Cell Growth in Vitro.* Journal of Biomaterials Science-Polymer Edition, 2010. **21**(3): p. 303-314.
95. Hong, S.P., et al., *Interaction of poly(amidoamine) dendrimers with supported lipid bilayers and cells: Hole formation and the relation to transport.* Bioconjugate Chemistry, 2004. **15**(4): p. 774-782.
96. Kulkarni, R., E. Moore, and et al., *Biodegradable polylactic acid) polymers.* Journal of Biomedical Materials Research, 1971. **5196-181**.(PudMed:5560994).
97. Blum, J.S. and W.M. Saltzman, *High loading efficiency and tunable release of plasmid DNA encapsulated in submicron particles fabricated from PLGA conjugated with poly-L-lysine.* Journal of Controlled Release, 2008. **129**(1): p. 66-72.
98. Chaudhari, K.R., et al., *Bone metastasis targeting: A novel approach to reach bone using Zoledronate anchored PLGA nanoparticle as carrier system loaded with Docetaxel.* Journal of Controlled Release, 2012. **158**(3): p. 470-478.
99. Uchegbu, I.F., *Pharmaceutical nanotechnology: polymeric vesicles for drug and gene delivery.* Expert Opin Drug Deliv, 2006. **3**(5): p. 629-40.
100. Jain, R.A., *The manufacturing techniques of various drug loaded biodegradable poly(lactide-co-glycolide) (PLGA) devices.* Biomaterials, 2000. **21**(23): p. 2475-2490.
101. Ruhe, P.Q., et al., *rhBMP-2 release from injectable poly(DL-lactic-co-glycolic acid)/calcium-phosphate cement composites.* Journal of Bone and Joint Surgery-American Volume, 2003. **85A**: p. 75-81.
102. Bouissou, C., et al., *The influence of surfactant on PLGA microsphere glass transition and water sorption: Remodeling the surface morphology to attenuate the burst release.* Pharmaceutical Research, 2006. **23**(6): p. 1295-1305.
103. Akbarzadeh, A., et al., *Preparation and in vitro evaluation of doxorubicin-loaded Fe3O4 magnetic nanoparticles modified with biocompatible copolymers.* International Journal of Nanomedicine, 2012. **7**: p. 511-526.
104. Kunz-Schughart, L.A., et al., *The use of 3-D cultures for high-throughput screening: The multicellular spheroid model.* Journal of Biomolecular Screening, 2004. **9**(4): p. 273-285.
105. Frieboes, H.B., et al., *An integrated computational/experimental model of tumor invasion.* Cancer Research, 2006. **66**(3): p. 1597-1604.
106. Sutherland, R.M., et al., , *Oxygenation and Differentiation in Multicellular Spheroids of Human-Colon Carcinoma*. Cancer Research, 1986. **46**(10): p. 5320-5329.
107. Grover, A., R.G. Oshima, and E.D. Adamson, *Epithelial Layer Formation in Differentiating Aggregates of F9 Embryonal Carcinoma-Cells.* Journal of Cell Biology, 1983. **96**(6): p. 1690-1696.
108. Nederman, T., *Effects of Vinblastine and 5-Fluorouracil on Human Glioma and Thyroid-Cancer Cell Monolayers and Spheroids.* Cancer Research, 1984. **44**(1): p. 254-258.
109. Stuschke, M., et al., *Heterogeneity in the fraction sensitivities of human tumor-cell lines - studies in a 3-dimensional model system* International Journal of Radiation Oncology Biology Physics, 1995. **32**(2): p. 395-408.

110. Kobayashi, H., et al., *Acquired multicellular- mediated resistance to alkylating -agents in cancer* Proceedings of the National Academy of Sciences of the United States of America, 1993. **90**(8): p. 3294-3298.
111. Graham, C.H., et al., *Rapid acuisition of multicellular drug-resistance after a single exposure of mammary-tumor cells to antitumor alkylating-agents* Journal of the National Cancer Institute, 1994. **86**(13): p. 975-982.
112. Winters, B.S., S.R. Shepard, and R.A. Foty, *Biophysical measurement of brain tumor cohesion.* International Journal of Cancer, 2005. **114**(3): p. 371-379.
113. Wartenberg, M., et al., *Tumor-induced angiogenesis studied in confrontation cultures of multicellular tumor spheroids and embryoid bodies grown from pluripotent embryonic stem cells.* Faseb Journal, 2001. **15**(6): p. 995-1005.
114. Carlsson, J. and J.M. Yuhas, *Liquid-Overlay Culture of Cellular Spheroids*, in *Spheroids in Cancer Research*, H. Acker, et al., Editors. 1984, Springer Berlin Heidelberg. p. 1-23.
115. Sutherland, R.M. and R.E. Durand, *Growth and cellular characteristics of multicell spheroids. Recent results in cancer research.* Fortschritte der Krebsforschung Progres dans les recherches sur le cancer, 1984. **95**: p. 24-49.
116. Kelm, J.M., et al., *Method for generation of homogeneous multicellular tumor spheroids applicable to a wide variety of cell types.* Biotechnology and Bioengineering, 2003. **83**(2): p. 173-180.
117. Hardelauf, H., et al., *Microarrays for the scalable production of metabolically relevant tumour spheroids: a tool for modulating chemosensitivity traits.* Lab on a Chip, 2011. **11**(3): p. 419-428.
118. Jin, H.-J., et al., *A multicellular spheroid formation and extraction chip using removable cell trapping barriers.* Lab on a Chip, 2011. **11**(1): p. 115-119.
119. Yu, L., M.C.W. Chen, and K.C. Cheung, *Droplet-based microfluidic system for multicellular tumor spheroid formation and anticancer drug testing.* Lab on a Chip, 2010. **10**(18): p. 2424-2432.
120. Kuo, C.-T., et al., *Configurable 2D and 3D spheroid tissue cultures on bioengineered surfaces with acquisition of epithelial-mesenchymal transition characteristics.* NPG Asia Mater, 2012. **4**: p. e27.
121. Fukuda, J. and K. Nakazawa, *Hepatocyte spheroid arrays inside microwells connected with microchannels.* Biomicrofluidics, 2011. **5**(2): p. 022205.
122. Kim, T., I. Doh, and Y.-H. Cho, *On-chip three-dimensional tumor spheroid formation and pump-less perfusion culture using gravity-driven cell aggregation and balanced droplet dispensing.* Biomicrofluidics, 2012. **6**(3): p. 034107.
123. Hsiao, A.Y., et al., *Microfluidic system for formation of PC-3 prostate cancer co-culture spheroids.* Biomaterials, 2009. **30**(16): p. 3020-3027.
124. Lee, K., et al., *Gravity-oriented microfluidic device for uniform and massive cell spheroid formation.* Biomicrofluidics, 2012. **6**(1): p. 014114.
125. Alessandri, K., et al., *Cellular capsules as a tool for multicellular spheroid production and for investigating the mechanics of tumor progression in vitro.* Proceedings of the National Academy of Sciences, 2013. **110**(37): p. 14843-14848.
126. Chan, H.F., et al., *Rapid formation of multicellular spheroids in double-emulsion droplets with controllable microenvironment.* Sci. Rep., 2013. **3**.
127. Kim, C., et al., *Generation of core-shell microcapsules with three-dimensional focusing device for efficient formation of cell spheroid.* Lab on a Chip, 2011. **11**(2): p. 246-252.
128. Vanherberghen, B., et al., *Ultrasound-controlled cell aggregation in a multi-well chip.* Lab on a Chip, 2010. **10**(20): p. 2727-2732.
129. Ota, H. and N. Miki, *Microfluidic experimental platform for producing size-controlled three-dimensional spheroids.* Sensors and Actuators A: Physical, 2011. **169**(2): p. 266-273.
130. Al-Abboodi, A., et al., *Injectable 3D Hydrogel Scaffold with Tailorable Porosity Post-Implantation.* Advanced Healthcare Materials, 2014. **3**(5): p. 725-736.

131. Aussillous, P. and D. Quere, *Liquid marbles.* Nature, 2001. **411**(6840): p. 924-7.
132. Nguyen, T.H., K. Hapgood, and W. Shen, *Observation of the liquid marble morphology using confocal microscopy.* Chemical Engineering Journal, 2010. **162**(1): p. 396-405.
133. Bhosale, P.S. and M.V. Panchagnula, *On synthesizing solid polyelectrolyte microspheres from evaporating liquid marbles.* Langmuir, 2010. **26**(13): p. 10745-10749.
134. Xue, Y., et al., *Magnetic Liquid Marbles: A "Precise" Miniature Reactor.* Advanced Materials, 2010. **22**(43): p. 4814-+.
135. Bormashenko, E., et al., *New investigations on ferrofluidics: ferrofluidic marbles and magnetic-field-driven drops on superhydrophobic surfaces.* Langmuir, 2008. **24**(21): p. 12119-22.
136. Newton, M.I., et al., *Electrowetting of liquid marbles.* Journal of Physics D-Applied Physics, 2007. **40**(1): p. 20-24.
137. Bormashenko, E. and A. Musin, *Revealing of water surface pollution with liquid marbles.* Applied Surface Science, 2009. **255**(12): p. 6429-6431.
138. Tian, J.F., et al., *Liquid marble for gas sensing.* Chemical Communications, 2010. **46**(26): p. 4734-4736.
139. Fujii, S., et al., *pH-Responsive Hairy Particles Synthesized by Dispersion Polymerization with a Macroinitiator as an Inistab and Their Use as a Gas-Sensitive Liquid Marble Stabilizer.* Macromolecules, 2012. **45**(6): p. 2863-2873.
140. Braun, H.-G. and A.Z. Cardoso, *Self-assembly of Fmoc-diphenylalanine inside liquid marbles.* Colloids and Surfaces B-Biointerfaces, 2012. **97**: p. 43-50.
141. Forny, L., et al., *Storing water in powder form by self-assembling hydrophobic silica nanoparticles.* Powder Technology, 2007. **171**(1): p. 15-24.
142. Wang, W., et al., *Methane storage in dry water gas hydrates.* Journal of the American Chemical Society, 2008. **130**(35): p. 11608-+.
143. Carter, B.O., et al., *Gas Storage in "Dry Water" and "Dry Gel" Clathrates.* Langmuir, 2010. **26**(5): p. 3186-3193.
144. Hapgood, K.P., L. Farber, and J.N. Michaels, *Agglomeration of hydrophobic powders via solid spreading nucleation.* Powder Technology, 2009. **188**(3): p. 248-254.
145. Hapgood, K.P. and B. Khanmohammadi, *Granulation of hydrophobic powders.* Powder Technology, 2009. **189**(2): p. 253-262.
146. Kawamura, Y., H. Mayama, and Y. Nonomura, *Edible Liquid Marbles and Capsules Covered with Lipid Crystals.* Journal of Oleo Science, 2012. **61**(9): p. 477-482.
147. McEleney, P., et al., *Liquid marble formation using hydrophobic powders.* Chemical Engineering Journal, 2009. **147**(2-3): p. 373-382.
148. Dupin, D., S.P. Armes, and S. Fujii, *Stimulus-Responsive Liquid Marbles.* Journal of the American Chemical Society, 2009. **131**(15): p. 5386-+.
149. Tian, J., et al., *Respirable liquid marble for the cultivation of microorganisms.* Colloids and Surfaces B-Biointerfaces, 2013. **106**: p. 187-190.
150. Zhao, Y., et al., *Magnetic Liquid Marbles: Manipulation of Liquid Droplets Using Highly Hydrophobic Fe3O4 Nanoparticles.* Advanced Materials, 2010. **22**(6): p. 707-+.
151. Arbatan, T., et al., *Tumor inside a pearl drop.* Adv Healthc Mater, 2012. **1**(4): p. 467-9.
152. Arbatan, T., et al., *Liquid Marbles as Micro-bioreactors for Rapid Blood Typing.* Advanced Healthcare Materials, 2012. **1**(1): p. 80-83.
153. Sarvi, F., et al., *A novel technique for the formation of embryoid bodies inside liquid marbles.* Rsc Advances, 2013. **3**(34): p. 14501-14508.
154. Sarvi, F., et al., *Cardiogenesis of Embryonic Stem Cells with Liquid Marble Micro-Bioreactor.* Advanced Healthcare Materials, 2015. **4**(1).
155. Vacanti, C.A., *The history of tissue engineering.* Journal of Cellular and Molecular Medicine, 2006. **10**(3): p. 569-576.
156. Alsberg, E., et al., *Engineering growing tissues.* Proceedings of the National Academy of Sciences of the United States of America, 2002. **99**(19): p. 12025-12030.

157. Bisceglie , V., *Uber die antineoplasticsche Immunitat; heterologe Einpflanzung von Tumoren in Huhner-embryonen.* Z Krebsforsch, 1933. **40**: p. 122–40.
158. Bell, E., et al., *Living tissue formed in vitro and accepted as skin-equivalent tissue of full thickness.* Science, 1981. **211**(4486): p. 1052-1054.
159. Burke, J.F., et al., *Successful Use of a Physiologically Acceptable Artificial Skin in the Treatment of Extensive Burn Injury.* Annals of Surgery, 1981. **194**(4): p. 413-428.
160. Vacanti, J.P., et al., *Selective cell trasplantation using bioabsorbable atrificial polymers as matrices* Journal of Pediatric Surgery, 1988. **23**(1): p. 3-9.
161. Griffith, L.G. and G. Naughton, *Tissue engineering - Current challenges and expanding opportunities.* Science, 2002. **295**(5557): p. 1009-+.
162. Atala, A., et al., *Tissue-engineered autologous bladders for patients needing cystoplasty.* Lancet, 2006. **367**(9518): p. 1241-1246.
163. Macchiarini, P., et al., *Clinical transplantation of a tissue-engineered airway.* Lancet, 2008. **372**(9655): p. 2023-2030.
164. Khademhosseini, A., J.P. Vacanti, and R. Langer, *Progress in tissue engineering* Scientific American, 2009. **300**(5): p. 64-+.
165. Place, E.S., N.D. Evans, and M.M. Stevens, *Complexity in biomaterials for tissue engineering.* Nature Materials, 2009. **8**(6): p. 457-470.
166. Stock, U.A. and J.P. Vacanti, *Tissue engineering: current state and prospects.* Annu Rev Med, 2001. **52**: p. 443-51.
167. Gomes, M.E. and R.L. Reis, *Tissue engineering: Key elements and some trends.* Macromolecular Bioscience, 2004. **4**(8): p. 737-742.
168. Amiel, G. and A. Atala, *Current and future modalities for functional renal replacement.* Urologic Clinics of North America, 1999. **26**(1): p. 235-+.
169. Lavik, E. and R. Langer, *Tissue engineering: current state and perspectives.* Applied Microbiology and Biotechnology, 2004. **65**(1): p. 1-8.
170. Cascalho, M. and J.L. Platt, *New technologies for organ replacement and augmentation.* Mayo Clinic Proceedings, 2005. **80**(3): p. 370-378.
171. Jungebluth, P., et al., *Tissue-Engineered Airway: A Regenerative Solution.* Clinical Pharmacology & Therapeutics, 2012. **91**(1): p. 81-93.
172. Thomson, J.A., et al., *Embryonic stem cell lines derived from human blastocysts.* Science, 1998. **282**(5391): p. 1145-1147.
173. Reubinoff, B.E., et al., *Embryonic stem cell lines from human blastocysts: somatic differentiation in vitro.* Nature Biotechnology, 2000. **18**(5): p. 559-559.
174. Lou, Y.J. and X.G. Liang, *Embryonic stem cell application in drug discovery.* Acta Pharmacol Sin, 2011. **32**(2): p. 152-9.
175. Pouton, C.W. and J.M. Haynes, *Pharmaceutical applications of embryonic stem cells.* Adv Drug Deliv Rev, 2005. **57**(13): p. 1918-34.
176. Gorba, T. and T.E. Allsopp, *Pharmacological potential of embryonic stem cells.* Pharmacol Res, 2003. **47**(4): p. 269-78.
177. Zandstra, P.W. and A. Nagy, *Stem cell bioengineering* Annu. Rev. Biomed. Eng., 2001. **3**: p. 275-305.
178. Pillow, R.P., et al., *Treatment of bone-marrow failure by isogeneic marrow infusion.* N Engl J Med, 1966. **275**(2): p. 94-7.
179. Presnell, S.C., B. Petersen, and M. Heidaran, *Stem cells in adult tissues.* Semin Cell Dev Biol, 2002. **13**(5): p. 369-76.
180. http://learn.genetics.utah.edu/content/stemcells/quickref/, *Locations of somatic stem cells in the body.* Stem Cell Quick Reference.
181. Lagasse, E., et al., *Purified hematopoietic stem cells can differentiate into hepatocytes in vivo.* Nature Medicine, 2000. **6**(11): p. 1229-1234.
182. Bittner, R.E., et al., *Recruitment of bone-marrow-derived cells by skeletal and cardiac muscle in adult dystrophic mdx mice.* Anatomy and Embryology, 1999. **199**(5): p. 391-396.

183. Orlic, D., et al., *Transplanted adult bone marrow cells repair myocardial infarcts in mice.* Ann N Y Acad Sci, 2001. **938**: p. 221-9; discussion 229-30.
184. Krause, D.S., et al., *Multi-organ, multi-lineage engraftment by a single bone marrow-derived stem cell.* Cell, 2001. **105**(3): p. 369-77.
185. Puri, M.C. and A. Nagy, *Concise Review: Embryonic Stem Cells Versus Induced Pluripotent Stem Cells: The Game Is On.* Stem Cells, 2012. **30**(1): p. 10-14.
186. Thomson, J.A., et al., *Isolation of a primate embryonic stem-cell line* Proceedings of the National Academy of Sciences of the United States of America, 1995. **92**(17): p. 7844-7848.
187. Martin, G.R., *Isolation of a Pluripotent Cell-Line from Early Mouse Embryos Cultured in Medium Conditioned by Teratocarcinoma Stem-Cells.* Proceedings of the National Academy of Sciences of the United States of America-Biological Sciences, 1981. **78**(12): p. 7634-7638.
188. Fong, C.Y., et al., *Blastocyst transfer after enzymatic treatment of the zona pellucida: improving in-vitro fertilization and understanding implantation.* Human Reproduction, 1998. **13**(10): p. 2926-2932.
189. Ulloa-Montoya, F., C.M. Verfaillie, and W.S. Hu, *Culture systems for pluripotent stem cells.* Journal of Bioscience and Bioengineering, 2005. **100**(1): p. 12-27.
190. Palacios, R., E. Golunski, and J. Samaridis, *In-Vitro Generation of Hematopoietic Stem-Cells from an Embryonic Stem-Cell Line.* Proceedings of the National Academy of Sciences of the United States of America, 1995. **92**(16): p. 7530-7534.
191. Wiles, M.V. and G. Keller, *Multiple Hematopoietic Lineages Develop from Embryonic Stem (Es) Cells in Culture.* Development, 1991. **111**(2): p. 259-&.
192. Mummery, C., et al., *Cardiomyocyte differentiation of mouse and human embryonic stem cells.* Journal of Anatomy, 2002. **200**(3): p. 233-242.
193. Maltsev, V.A., et al., *Cardiomyocytes Differentiated in-Vitro from Embryonic Stem-Cells Developmentally Express Cardiac-Specific Genes and Ionic Currents.* Circulation Research, 1994. **75**(2): p. 233-244.
194. Wang, R., R. Clark, and V.L. Bautch, *Embryonic stem cell-derived cystic embryoid bodies form vascular channels: an in vitro model of blood vessel development.* Development, 1992. **114**(2): p. 303-16.
195. Bain, G., et al., *Embryonic Stem-Cells Express Neuronal Properties in-Vitro.* Developmental Biology, 1995. **168**(2): p. 342-357.
196. Stojkovic, M., et al., *Derivation, growth and applications of human embryonic stem cells.* Reproduction, 2004. **128**(3): p. 259-267.
197. Stem cell information National Institues of Health, 2001.
198. Laslett, A.L., A.A. Filipczyk, and M.F. Pera, *Characterization and culture of human embryonic stem cells.* Trends in Cardiovascular Medicine, 2003. **13**(7): p. 295-301.
199. Martin, M.J., et al., *Human embryonic stem cells express an immunogenic nonhuman sialic acid.* Nature Medicine, 2005. **11**(2): p. 228-232.
200. Xu, R.H., et al., *Basic FGF and suppression of BMP signaling sustain undifferentiated proliferation of human ES cells.* Nature Methods, 2005. **2**(3): p. 185-190.
201. Xu, C.H., et al., *Feeder-free growth of undifferentiated human embryonic stem cells.* Nature Biotechnology, 2001. **19**(10): p. 971-974.
202. Sato, N., et al., *Maintenance of pluripotency in human and mouse embryonic stem cells through activation of Wnt signaling by a pharmacological GSK-3-specific inhibitor.* Nature Medicine, 2004. **10**(1): p. 55-63.
203. Wong, C.-W., et al., *Kruppel-Like Transcription Factor 4 Contributes to Maintenance of Telomerase Activity in Stem Cells.* Stem Cells, 2010. **28**(9): p. 1510-1517.
204. Ehrnhoefer, D.E., et al., *Mouse models of Huntington disease: variations on a theme.* Disease Models & Mechanisms, 2009. **2**(3-4): p. 123-129.
205. Lumelsky, N., et al., *Differentiation of embryonic stem cells to insulin-secreting structures similar to pancreatic islets.* Science, 2001. **292**(5520): p. 1389-1394.

206. Studer, L., V. Tabar, and R.D.G. McKay, *Transplantation of expanded mesencephalic precursors leads to recovery in parkinsonian rats.* Nature Neuroscience, 1998. **1**(4): p. 290-295.
207. McDonald, J.W., et al., *Transplanted embryonic stem cells survive, differentiate and promote recovery in injured rat spinal cord.* Nature Medicine, 1999. **5**(12): p. 1410-1412.
208. Guasch, G. and E. Fuchs, *Mice in the world of stem cell biology.* Nature Genetics, 2005. **37**(11): p. 1201-1206.
209. Bjorklund, L.M., et al., *Embryonic stem cells develop into functional dopaminergic neurons after transplantation in a Parkinson rat model.* Proceedings of the National Academy of Sciences of the United States of America, 2002. **99**(4): p. 2344-2349.
210. Aboody, K., et al., *Translating Stem Cell Studies to the Clinic for CNS Repair: Current State of the Art and the Need for a Rosetta Stone.* Neuron, 2011. **70**(4): p. 597-613.
211. Dawson, T.M. and V.L. Dawson, *Neuroprotective and neurorestorative strategies for Parkinson's disease.* Nature Neuroscience, 2002. **5**: p. 1058-1061.
212. Navarro-Alvarez, N., A. Soto-Gutierrez, and N. Kobayashi, *Stem Cell Research and Therapy for Liver Disease.* Current Stem Cell Research & Therapy, 2009. **4**(2): p. 141-146.
213. Dinsmore, J., et al., *Embryonic stem cells differentiated in vitro as a novel source of cells for transplantation.* Cell Transplantation, 1996. **5**(2): p. 131-143.
214. Liu, S., et al., *Embryonic stem cells differentiate into oligodendrocytes and myelinate in culture and after spinal cord transplantation.* Proceedings of the National Academy of Sciences of the United States of America, 2000. **97**(11): p. 6126-6131.
215. Blyszczuk, P., et al., *Expression of Pax4 in embryonic stem cells promotes differentiation of nestin-positive progenitor and insulin-producing cells.* Proceedings of the National Academy of Sciences of the United States of America, 2003. **100**(3): p. 998-1003.
216. Shim, J.H., et al., *Directed differentiation of human embryonic stem cells towards a pancreatic cell fate.* Diabetologia, 2007. **50**(6): p. 1228-1238.
217. Wakitani, S., et al., *Autologous bone marrow stromal cell transplantation for repair of full-thickness articular cartilage defects in human patellae: Two case reports.* Cell Transplantation, 2004. **13**(5): p. 595-600.
218. Cohen, I., et al., *Use of a novel joint-simulating culture system to grow organized ex-vivo three-dimensional cartilage-like constructs from embryonic epiphyseal cells.* The Iowa orthopaedic journal, 2005. **25**: p. 102-7.
219. Ikeda, T., et al., *The combination of SOX5, SOX6, and SOX9 (the SOX trio) provides signals sufficient for induction of permanent cartilage.* Arthritis and Rheumatism, 2004. **50**(11): p. 3561-3573.
220. Ohba, S., et al., *Identification of a potent combination of osteogenic genes for bone regeneration using embryonic stem (ES) cell-based sensor.* Faseb Journal, 2007. **21**(8): p. 1777-1787.
221. Rohwedel, J., et al., *Embryonic stem cells as an in vitro model for mutagenicity, cytotoxicity and embryotoxicity studies: present state and future prospects.* Toxicology in Vitro, 2001. **15**(6): p. 741-753.
222. Sinz, M.W. and S. Kim, *Stem cells, immortalized cells and primary cells in ADMET assays.* Drug Discovery Today: Technologies, 2006. **3**(1): p. 79-85.
223. Ortiz, L.A., et al., *Mesenchymal stem cell engraftment in lung is enhanced in response to bleomycin exposure and ameliorates its fibrotic effects.* Proceedings of the National Academy of Sciences of the United States of America, 2003. **100**(14): p. 8407-8411.
224. Mei, S.H.J., et al., *Prevention of LPS-induced acute lung injury in mice by mesenchymal stem cells overexpressing angiopoietin 1.* Plos Medicine, 2007. **4**(9): p. 1525-1537.
225. Xu, J.G., et al., *Prevention of endotoxin-induced systemic response by bone marrow-derived mesenchymal stem cells in mice.* American Journal of Physiology-Lung Cellular and Molecular Physiology, 2007. **293**(1): p. L131-L141.

226. Németh, K., et al., *Bone marrow stromal cells attenuate sepsis via prostaglandin E(2)-dependent reprogramming of host macrophages to increase their interleukin-10 production.* Nat Med., 2009. **15**(1): p. 42-9.
227. Mei, S.H.J., et al., *Mesenchymal Stem Cells Reduce Inflammation while Enhancing Bacterial Clearance and Improving Survival in Sepsis.* American Journal of Respiratory and Critical Care Medicine, 2010. **182**(8): p. 1047-1057.
228. <http://investor.osiris.com/relaesedetail.cfm?ReleaseID=311598>.
229. Loebinger, M.R. and S.M. Janes, *Stem cells as vectors for antitumour therapy.* Thorax, 2010. **65**(4): p. 362-369.
230. Studeny, M., et al., *Mesenchymal stem cells: Potential precursors for tumor stroma and targeted-delivery vehicles for anticancer agents.* Journal of the National Cancer Institute, 2004. **96**(21): p. 1593-1603.
231. Rippon, H.J., et al., *Derivation of distal lung epithelial progenitors from murine embryonic stem cells using a novel three-step differentiation protocol.* Stem Cells, 2006. **24**(5): p. 1389-1398.
232. Samadikuchaksaraei, A., et al., *Derivation of distal airway epithelium from human embryonic stem cells.* Tissue Eng, 2006. **12**(4): p. 867-75.
233. Wang, D., et al., *A pure population of lung alveolar epithelial type II cells derived from human embryonic stem cells.* Proc Natl Acad Sci U S A, 2007. **104**(11): p. 4449-54.
234. Sueblinvong, V., et al., *Derivation of lung epithelium from human cord blood-derived mesenchymal stem cells.* Am J Respir Crit Care Med, 2008. **177**(7): p. 701-11.
235. Wang, G.S., et al., *Adult stem cells from bone marrow stroma differentiate into airway epithelial cells: Potential therapy for cystic fibrosis.* Proceedings of the National Academy of Sciences of the United States of America, 2005. **102**(1): p. 186-191.
236. Weiss, D.J., et al., *Stem cells and cell therapies in lung biology and lung diseases.* Proc Am Thorac Soc, 2011. **8**(3): p. 223-72.
237. Neuringer, I.P. and S.H. Randell, *Lung stem cell update: promise and controversy.* Monaldi Arch Chest Dis, 2006. **65**(1): p. 47-51.
238. Weiss, D.J. and C. Finck, *Embryonic Stem Cells and Repair of Lung Injury.* Molecular Therapy, 2010. **18**(3): p. 460-461.
239. Majka, S.M., et al., *Identification of novel resident pulmonary stem cells: Form and function of the lung side population.* Stem Cells, 2005. **23**(8): p. 1073-1081.
240. Sommer, C.A., et al., *Induced Pluripotent Stem Cell Generation Using a Single Lentiviral Stem Cell Cassette.* Stem Cells, 2009. **27**(3): p. 543-549.
241. Samadikuchaksaraei, A. and A.E. Bishop, *Effects of growth factors on the differentiation of murine ESC into type II pneumocytes.* Cloning and Stem Cells, 2007. **9**(3): p. 407-416.
242. Qin, M., et al., *Cell extract-derived differentiation of embryonic stem cells.* Stem Cells, 2005. **23**(6): p. 712-718.
243. Rippon, H., et al., *Embryonic Stem Cells as a Source of Pulmonary Epithelium In Vitro and In Vivo.* Proc Am Thorac Soc 2008. **5**: p. 717–722.
244. Roszell, B., et al., *Efficient derivation of alveolar type II cells from embryonic stem cells for in vivo application.* Tissue Eng Part A, 2009. **15**(11): p. 3351-65.
245. Van Vranken, B.E., et al., *Coculture of embryonic stem cells with pulmonary mesenchyme: A microenvironment that promotes differentiation of pulmonary epithelium.* Tissue Engineering, 2005. **11**(7-8): p. 1177-1187.
246. Jeffery, P.K., *Remodeling in asthma and chronic obstructive lung disease.* American Journal of Respiratory and Critical Care Medicine, 2001. **164**(10): p. S28-S38.
247. Heule, M., S. Vuillemin, and L.J. Gauckler, *Powder-based ceramic meso- and microscale fabrication processes.* Advanced Materials, 2003. **15**(15): p. 1237-1245.
248. Nahmias, Y., et al., *Laser-guided direct writing for three-dimensional tissue engineering.* Biotechnology and Bioengineering, 2005. **92**(2): p. 129-136.

249. Jayasinghe, S.N., P.A. Eagles, and A.N. Qureshi, *Electric field driven jetting: an emerging approach for processing living cells.* Biotechnol J, 2006. **1**(1): p. 86-94.
250. Arumuganathar, S., et al., *A novel direct aerodynamically assisted threading methodology for generating biologically viable microthreads encapsulating living primary cells.* Journal of Applied Polymer Science, 2008. **107**(2): p. 1215-1225.
251. Hartman, R.P.A., et al., *Jet break-up in electrohydrodynamic atomization in the cone-jet mode.* Journal of Aerosol Science, 2000. **31**(1): p. 65-95.
252. Ijsebaert, J.C., K.B. Geerse, and J.C.M. Marijnissen, *Electrohydrodynamic atomization of drug solutions for inhalation purposes.* J. Appl. Physiol, 2001. **6**: p. 2735 –2741.
253. Eagles, P.A., A.N. Qureshi, and S.N. Jayasinghe, *Electrohydrodynamic jetting of mouse neuronal cells.* Biochem J, 2006. **394**(Pt 2): p. 375-8.
254. Jayasinghe, S.N., A.N. Qureshi, and P.A. Eagles, *Electrohydrodynamic jet processing: an advanced electric-field-driven jetting phenomenon for processing living cells.* Small, 2006. **2**(2): p. 216-9.
255. Stankus, J.J., et al., *Microintegrating smooth muscle cells into a biodegradable, elastomeric fiber matrix.* Biomaterials, 2006. **27**(5): p. 735-744.
256. Kwok, A., et al., *A hybrid bio-jetting approach for directly engineering living cells.* Biomedical Materials, 2008. **3**(2).
257. Kempski, H., et al., *Pilot study to investigate the possibility of cytogenetic and physiological changes in bio-electrosprayed human lymphocyte cells.* Regenerative Medicine, 2008. **3**(3): p. 343-349.
258. Mongkoldhumrongkul, N., J.M. Flanagan, and S.N. Jayasinghe, *Direct jetting approaches for handling stem cells.* Biomedical Materials, 2009. **4**(1).
259. Qi, A., L.Y. Yeo, and J.R. Friend, *Interfacial destabilization and atomization driven by surface acoustic waves.* Physics of Fluids, 2008. **20**(7).
260. Yeo, L.Y. and J.R. Friend, *Ultrafast microfluidics using surface acoustic waves.* Biomicrofluidics, 2009. **3**(1).
261. Yeo, L.Y., et al., *Ultrasonic nebulization platforms for pulmonary drug delivery.* Expert Opinion on Drug Delivery, 2010. **7**(6): p. 663-679.
262. Qi, A.S., et al., *Miniature inhalation therapy platform using surface acoustic wave microfluidic atomization.* Lab on a Chip, 2009. **9**(15): p. 2184-2193.
263. Li, H.Y., et al., *Effect of surface acoustic waves on the viability, proliferation and differentiation of primary osteoblast-like cells.* Biomicrofluidics, 2009. **3**(3).
264. Qi, A., et al., *The extraction of liquid, protein molecules and yeast cells from paper through surface acoustic wave atomization.* Lab on a Chip, 2010. **10**(4): p. 470-476.
265. Friend, J.R., et al., *Evaporative self-assembly assisted synthesis of polymeric nanoparticles by surface acoustic wave atomization.* Nanotechnology, 2008. **19**(14).
266. Alvarez, M., J. Friend, and L.Y. Yeo, *Rapid generation of protein aerosols and nanoparticles via surface acoustic wave atomization.* Nanotechnology, 2008. **19**(45).
267. Polak, J., S. Mantalaris, and S.e. Harding, *Advances in Tissue Engineering.* London: Imperial College Press, 2008.
268. Cortiella, J., et al., *Tissue-engineered lung: An in vivo and in vitro comparison of polyglycolic acid and pluronic F-127 hydrogel/somatic lung progenitor cell constructs to support tissue growth.* Tissue Engineering, 2006. **12**(5): p. 1213-1225.
269. Mondrinos, M.J., et al., *In vivo pulmonary tissue engineering: contribution of donor-derived endothelial cells to construct vascularization.* Tissue Eng Part A, 2008. **14**(3): p. 361-8.
270. Andrade, C.F., et al., *Cell-based tissue engineering for lung regeneration.* Am J Physiol Lung Cell Mol Physiol, 2007. **292**(2): p. L510-8.
271. Hoganson, D.M., H.I. Pryor, 2nd, and J.P. Vacanti, *Tissue engineering and organ structure: a vascularized approach to liver and lung.* Pediatr Res, 2008. **63**(5): p. 520-6.
272. Chen, P., et al., *Formation of lung alveolar-like structures in collagen-glycosaminoglycan scaffolds in vitro.* Tissue Eng, 2005. **11**(9-10): p. 1436-48.

273. Mondrinos, M.J., et al., *Engineering three-dimensional pulmonary tissue constructs.* Tissue Eng, 2006. **12**(4): p. 717-28.
274. Coraux, C., et al., *Embryonic stem cells generate airway epithelial tissue.* American Journal of Respiratory Cell and Molecular Biology, 2005. **32**(2): p. 87-92.
275. Badylak, S.E., *The extracellular matrix as a scaffold for tissue reconstruction.* Seminars in Cell & Developmental Biology, 2002. **13**(5): p. 377-383.
276. Valentin, J., et al., *Oxygen diffusivity of biologic and synthetic scaffold materials for tissue engineering.* J Biomed Mater Res A, 2009. **91**(4): p. 1010-7.
277. Androjna, C., et al., *Oxygen diffusion through natural extracellular matrices: Implications for estimating "Critical thickness" values in tendon tissue engineering.* Tissue Engineering Part A, 2008. **14**(4): p. 559-569.
278. Gilbert, T.W., T.L. Sellaro, and S.F. Badylak, *Decellularization of tissues and organs.* Biomaterials, 2006. **27**(19): p. 3675-83.
279. Scadden, D.T., *The stem-cell niche as an entity of action.* Nature, 2006. **441**(7097): p. 1075-1079.
280. Cukierman, E., R. Pankov, and K.M. Yamada, *Cell interactions with three-dimensional matrices.* Current Opinion in Cell Biology, 2002. **14**(5): p. 633-639.
281. Battista, S., et al., *The effect of matrix composition of 3D constructs on embryonic stem cell differentiation.* Biomaterials, 2005. **26**(31): p. 6194-6207.
282. Streuli, C., *Extracellular matrix remodelling and cellular differentiation.* Current Opinion in Cell Biology, 1999. **11**(5): p. 634-640.
283. Tabata, Y., *Biomaterial technology for tissue engineering applications.* Journal of the Royal Society Interface, 2009. **6**: p. S311-S324.
284. Dawson, E., et al., *Biomaterials for stem cell differentiation.* Advanced Drug Delivery Reviews, 2008. **60**(2): p. 215-228.
285. Park, K., K.R. Kamath, and H. Park, *Biodegradable hydrogel for delivery of protein drugs* Abstracts of Papers of the American Chemical Society, 1993. **205**: p. 474-POLY.
286. Hwang, N.S., S. Varghese, and J. Elisseeff, *Controlled differentiation of stem cells.* Advanced Drug Delivery Reviews, 2008. **60**(2): p. 199-214.
287. Salinas, C.N. and K.S. Anseth, *The enhancement of chondrogenic differentiation of human mesenchymal stem cells by enzymatically regulated RGD functionalities.* Biomaterials, 2008. **29**(15): p. 2370-2377.
288. Drury, J.L. and D.J. Mooney, *Hydrogels for tissue engineering: scaffold design variables and applications.* Biomaterials, 2003. **24**(24): p. 4337-4351.
289. Lee, J., M.J. Cuddihy, and N.A. Kotov, *Three-dimensional cell culture matrices: State of the art.* Tissue Engineering Part B-Reviews, 2008. **14**(1): p. 61-86.
290. Safinia, L., A. Mantalaris, and A. Bismarck, *Nondestructive technique for the characterization of the pore size distribution of soft porous constructs for tissue engineering.* Langmuir, 2006. **22**(7): p. 3235-3242.
291. Stevens, M.M. and J.H. George, *Exploring and engineering the cell surface interface.* Science, 2005. **310**(5751): p. 1135-1138.
292. Gitsov, I. and C. Zhu, *Amphiphilic hydrogels constructed by poly(ethylene glycol) and shape-persistent dendritic fragments.* Macromolecules, 2002. **35**(22): p. 8418-8427.
293. Drumheller, P.D. and J.A. Hubbell, *Densely cross-linked polymer networks of poly(ethylene glycol) in trimethylolpropane triacrylate for cell-adhesion-resistant surfaces* Journal of Biomedical Materials Research, 1995. **29**(2): p. 207-215.
294. Levenberg, S., et al., *Differentiation of human embryonic stem cells on three-dimensional polymer scaffolds.* Proceedings of the National Academy of Sciences of the United States of America, 2003. **100**(22): p. 12741-12746.
295. Moutos, F.T., L.E. Freed, and F. Guilak, *A biomimetic three-dimensional woven composite scaffold for functional tissue engineering of cartilage.* Nature Materials, 2007. **6**(2): p. 162-167.

296. Kim, S. and K.E. Healy, *Synthesis and characterization of injectable poly(N-isopropylacrylamide-co-acrylic acid) hydrogels with proteolytically degradable cross-links.* Biomacromolecules, 2003. **4**(5): p. 1214-1223.
297. Peppas, N.A., et al., *Physicochemical, foundations and structural design of hydrogels in medicine and biology.* Annual Review of Biomedical Engineering, 2000. **2**: p. 9-29.
298. Kobayashi, M. and M. Oka, *Characterization of a polyvinyl alcohol-hydrogel artificial articular cartilage prepared by injection molding.* Journal of Biomaterials Science-Polymer Edition, 2004. **15**(6): p. 741-751.
299. Burczak, K., E. Gamian, and A. Kochman, *Long-term in vivo performance and biocompatibility of poly(vinyl alcohol) hydrogel macrocapsules for hybrid-type artificial pancreas.* Biomaterials, 1996. **17**(24): p. 2351-2356.
300. Barnes, C.P., et al., *Nanofiber technology: Designing the next generation of tissue engineering scaffolds.* Advanced Drug Delivery Reviews, 2007. **59**(14): p. 1413-1433.
301. Yang, F., et al., *Electrospinning of nano/micro scale poly(L-lactic acid) aligned fibers and their potential in neural tissue engineering.* Biomaterials, 2005. **26**(15): p. 2603-2610.
302. Zarkoob, S., et al., *Structure and morphology of electrospun silk nanofibers.* Polymer, 2004. **45**(11): p. 3973-3977.
303. Vacanti, C.A., *History of tissue engineering and a glimpse into its future.* Tissue Engineering, 2006. **12**(5): p. 1137-1142.
304. Willerth, S.M., et al., *Optimization of fibrin scaffolds for differentiation of murine embryonic stem cells into neural lineage cells.* Biomaterials, 2006. **27**(36): p. 5990-6003.
305. Liu, H., S.F. Collins, and L.J. Suggs, *Three-dimensional culture for expansion and differentiation of mouse embryonic stem cells.* Biomaterials, 2006. **27**(36): p. 6004-6014.
306. Gerecht, S., et al., *Hyaluronic acid hydrogen for controlled self-renewal and differentiation of human embryonic stem cells.* Proceedings of the National Academy of Sciences of the United States of America, 2007. **104**(27): p. 11298-11303.
307. Garreta, E., et al., *Fabrication of a three-dimensional nanostructured biomaterial for tissue engineering of bone.* Biomolecular Engineering, 2007. **24**(1): p. 75-80.
308. Glicklis, R., et al., *Hepatocyte behavior within three-dimensional porous alginate scaffolds.* Biotechnology and Bioengineering, 2000. **67**(3): p. 344-353.
309. Perets, A., et al., *Enhancing the vascularization of three-dimensional porous alginate scaffolds by incorporating controlled release basic fibroblast growth factor microspheres.* Journal of Biomedical Materials Research Part A, 2003. **65A**(4): p. 489-497.
310. Dean, S.K., et al., *Differentiation of encapsulated embryonic stem cells after transplantation.* Transplantation, 2006. **82**(9): p. 1175-1184.
311. Maguire, T., et al., *Alginate-PLL microencapsulation: Effect on the differentiation of embryonic stem cells into hepatocytes.* Biotechnology and Bioengineering, 2006. **93**(3): p. 581-591.
312. Magyar, J.P., et al., *Mass production of embryoid bodies in microbeads.* Bioartificial Organs Iii: Tissue Sourcing, Immunoisolation, and Clinical Trials, 2001. **944**: p. 135-143.
313. Martson, M., et al., *Biocompatibility of cellulose sponge with bone.* European Surgical Research, 1998. **30**(6): p. 426-432.
314. Miyamoto, T., et al., *Tissue biocompatibility of cellulose and its derivatives.* Journal of Biomedical Materials Research, 1989. **23**(1): p. 125-133.
315. De Bartolo, L., et al., *Evaluation of cell behaviour related to physico-chemical properties of polymeric membranes to be used in bioartificial organs.* Biomaterials, 2002. **23**(12): p. 2485-2497.
316. Takata, T., H.L. Wang, and M. Miyauchi, *Migration of osteoblastic cells on various guided bone regeneration membranes.* Clinical Oral Implants Research, 2001. **12**(4): p. 332-338.
317. Risbud, M.V. and R.R. Bhonde, *Suitability of cellulose molecular dialysis membrane for bioartificial pancreas: In vitro biocompatibility studies.* Journal of Biomedical Materials Research, 2001. **54**(3): p. 436-444.

318. LaIuppa, J.A., et al., *Culture materials affect ex vivo expansion of hematopoietic progenitor cells.* Journal of Biomedical Materials Research, 1997. **36**(3): p. 347-359.
319. Mastropietro, D.J. and H. Omidian, *Prevalence and trends of cellulosics in pharmaceutical dosage forms.* Drug Development and Industrial Pharmacy, 2013. **39**(2): p. 382-392.
320. Chamberlain, G., et al., *Concise review: Mesenchymal stem cells: Their phenotype, differentiation capacity, immunological features, and potential for homing.* Stem Cells, 2007. **25**(11): p. 2739-2749.
321. Canton, I., et al., *Real time detection of stress in 3D tissue engineered constructs using NF-kB activation in transiently transfected human dermal fibroblasts.* Tissue Engineering, 2007. **13**(7): p. 1750-1750.
322. Aussillous, P. and D. Quere, *Liquid marbles.* Nature, 2001. **411**(6840): p. 924-927.
323. Han, M., et al., *Transfection study using multicellular tumor spheroids for screening non-viral polymeric gene vectors with low cytotoxicity and high transfection efficiencies.* Journal of Controlled Release, 2007. **121**(1–2): p. 38-48.
324. Liang, D., et al., *miRNA-204 drives cardiomyocyte proliferation via targeting Jarid2.* International Journal of Cardiology, 2015. **201**: p. 38-48.
325. Li, X., et al., *miRNAs are required for the terminal differentiation of white matter astrocytes in the developing CNS.* Neuroscience, 2016. **312**: p. 99-107.
326. Hartig, S.M., et al., *The miRNA Interactome in Metabolic Homeostasis.* Trends in Endocrinology & Metabolism, 2015. **26**(12): p. 733-745.
327. Lim, T.C., et al., *The effect of injectable gelatin-hydroxyphenylpropionic acid hydrogel matrices on the proliferation, migration, differentiation and oxidative stress resistance of adult neural stem cells.* Biomaterials, 2012. **33**(12): p. 3446-3455.
328. Yu, H., et al., *Functional Morphometric Analysis in Cellular Behaviors: Shape and Size Matter.* Advanced Healthcare Materials, 2013. **2**(9): p. 1188-1197.
329. Zhu, X., et al., *miR-126 enhances the sensitivity of non-small cell lung cancer cells to anticancer agents by targeting vascular endothelial growth factor A.* Acta Biochimica et Biophysica Sinica, 2012. **44**(6): p. 519-526.
330. Hobel, S., et al., *Polyethylenimine/small interfering RNA-mediated knockdown of vascular endothelial growth factor in vivo exerts anti-tumor effects synergistically with Bevacizumab.* Journal of Gene Medicine, 2010. **12**(3): p. 287-300.
331. Grzelinski, M., et al., *RNA interference-mediated gene silencing of pleiotrophin through polyethylenimine-complexed small interfering RNAs in vivo exerts antitumoral effects in glioblastoma xenografts.* Human Gene Therapy, 2006. **17**(7): p. 751-766.
332. Livak, K.J. and T.D. Schmittgen, *Analysis of relative gene expression data using real-time quantitative PCR and the 2(T)(-Delta Delta C) method.* Methods, 2001. **25**(4): p. 402-408.
333. McGahon, A.J., et al., *The end of the (cell) line: methods for the study of apoptosis in vitro.* Methods in cell biology, 1995(46): p. 153-85.
334. Sutherland, R.M., *Cell and environment interactions in tumor microregions: the multicell spheroid model.* Science, 1988. **240**(4849): p. 177-184.
335. Sasahira, T., et al., *Downregulation of miR-126 induces angiogenesis and lymphangiogenesis by activation of VEGF-A in oral cancer.* Br J Cancer, 2012. **107**(4): p. 700-706.
336. Chen, H., et al., *Reduced miR-126 expression facilitates angiogenesis of gastric cancer through its regulation on VEGF-A.* Oncotarget, 2014. **5**(23): p. 11873-11885.
337. Olive, P. and R. Durand, *Drug and radiation resistance in spheroids: cell contact and kinetics.* Cancer and Metastasis Reviews, 1994. **13**(2): p. 121-138.
338. Saleh, A.F., et al., *Improved Tat-mediated plasmid DNA transfer by fusion to LK15 peptide.* Journal of Controlled Release, 2010. **143**(2): p. 233-242.
339. Knuchel, R., et al., *Sensitivities of Monolayers and Spheroids of the Human Bladder Cancer Cell Line MGH-U1 to the Drugs Used for Intravesical Chemotherapy.* Cancer Research, 1989. **49**(6): p. 1397-1401.

340. Frankel, A., et al., *Lack of Multicellular Drug Resistance Observed in Human Ovarian and Prostate Carcinoma Treated with the Proteasome Inhibitor PS-341*. Clinical Cancer Research, 2000. **6**(9): p. 3719-3728.
341. Okada, Y., et al., *Adenovirus-mediated viral IL-10 gene transfer prolongs survival of xenogeneic spheroidal aggregate-cultured hepatocytes.* Transplant International, 2000. **13**(1): p. S485-S493.
342. McHale, G. and M.I. Newton, *Liquid marbles: principles and applications.* Soft Matter, 2011. **7**(12): p. 5473-5481.
343. Lin, A., et al., *Preparation and characterization of a new negatively charged polytetrafluoroethylene membrane for treating oilfield wastewater.* Journal of Membrane Science, 2011. **371**(1–2): p. 286-292.
344. Zhang, J., J. Li, and Y. Han, *Superhydrophobic PTFE Surfaces by Extension.* Macromolecular Rapid Communications, 2004. **25**(11): p. 1105-1108.
345. Tian, C.S. and Y.R. Shen, *Structure and charging of hydrophobic material/water interfaces studied by phase-sensitive sum-frequency vibrational spectroscopy*. Proceedings of the National Academy of Sciences, 2009. **106**(36): p. 15148-15153.
346. England, J.L. and V.S. Pande, *Charge, hydrophobicity, and confined water: putting past simulations into a simple theoretical frameworkThis paper is one of a selection of papers published in this special issue entitled "Canadian Society of Biochemistry, Molecular & Cellular Biology 52nd Annual Meeting — Protein Folding: Principles and Diseases" and has undergone the Journal's usual peer review process.* Biochemistry and Cell Biology, 2010. **88**(2): p. 359-369.
347. Zhang, X.-Q., et al., *Sustained transgene expression via citric acid-based polyester elastomers.* Biomaterials, 2009. **30**(13): p. 2632-2641.
348. Rosser, M.P., et al., *Transient transfection of CHO-K1-S using serum-free medium in suspension: a rapid mammalian protein expression system.* Protein Expression and Purification, 2005. **40**(2): p. 237-243.
349. Liu, B., et al., *MiR-126 restoration down-regulate VEGF and inhibit the growth of lung cancer cell lines in vitro and in vivo.* Lung Cancer, 2009. **66**(2): p. 169-175.
350. Caruso, P., et al., *Dynamic Changes in Lung MicroRNA Profiles During the Development of Pulmonary Hypertension due to Chronic Hypoxia and Monocrotaline.* Arteriosclerosis Thrombosis and Vascular Biology, 2010. **30**(4): p. 716-U182.
351. Giordano, S. and A. Columbano, *MicroRNAs: new tools for diagnosis, prognosis, and therapy in hepatocellular carcinoma?* Hepatology, 2013. **57**(2): p. 840-7.
352. Hooten, N.N., et al., *microRNA Expression Patterns Reveal Differential Expression of Target Genes with Age.* Plos One, 2010. **5**(5).
353. Mueller-Klieser, W., *Multicellular spheroids.* Journal of Cancer Research and Clinical Oncology, 1987. **113**(2): p. 101-122.
354. Bosnakovski, D., et al., *Chondrogenic differentiation of bovine bone marrow mesenchymal stem cells (MSCs) in different hydrogels: Influence of collagen type II extracellular matrix on MSC chondrogenesis.* Biotechnology and Bioengineering, 2006. **93**(6): p. 1152-1163.
355. Frith, J.E., B. Thomson, and P.G. Genever, *Dynamic Three-Dimensional Culture Methods Enhance Mesenchymal Stem Cell Properties and Increase Therapeutic Potential.* Tissue Engineering Part C: Methods, 2009. **16**(4): p. 735-749.
356. Kurosawa, H., *Methods for inducing embryoid body formation: in vitro differentiation system of embryonic stem cells.* Journal of Bioscience and Bioengineering, 2007. **103**(5): p. 389-398.
357. Yang, M.-J., et al., *Novel Method of Forming Human Embryoid Bodies in a Polystyrene Dish Surface-Coated with a Temperature-Responsive Methylcellulose Hydrogel.* Biomacromolecules, 2007. **8**(9): p. 2746-2752.
358. Vanherberghen, B., et al., *Ultrasound-controlled cell aggregation in a multi-well chip.* Lab on a Chip, 2010. **10**: p. 2727-2732.

359. Kwapiszewska, K., et al., *A microfluidic-based platform for tumour spheroid culture, monitoring and drug screening.* Lab on a Chip, 2014. **14**: p. 2096-2104.
360. Yeo, L.Y., et al., *Microfluidic Devices for Bioapplications.* Small, 2011. **7**(1): p. 12-48.
361. Friend, J. and L.Y. Yeo, *Microscale acoustofluidics: Microfluidics driven via acoustics and ultrasonics.* Reviews of Modern Physics, 2011. **83**(2): p. 647-704.
362. Shilton, R.J., L.Y. Yeo, and J.R. Friend, *Quantification of surface acoustic wave induced chaotic mixing-flows in microfluidic wells.* Sensors and Actuators B: Chemical, 2011. **160**(1): p. 1565-1572.
363. Shilton, R., et al., *Particle concentration and mixing in microdrops driven by focused surface acoustic waves.* Journal of Applied Physics, 2008. **104**(1): p. 014910.
364. Rogers, P.R., J.R. Friend, and L.Y. Yeo, *Exploitation of Surface Acoustic Waves to Drive Size-Dependent Microparticle Concentration Within a Droplet.* Lab on a Chip, 2010. **10**: p. 2979-2985.
365. Glass, N.R., et al., *Miniaturized Lab-on-a-Disc (miniLOAD).* Small, 2012. **8**(12): p. 1881-1888.
366. Ding, X., et al., *Surface acoustic wave microfluidics.* Lab on a Chip, 2013. **13**(18): p. 3626-3649.
367. Yeo, L.Y. and J.R. Friend, *Ultrafast microfluidics using surface acoustic waves.* Biomicrofluidics, 2009. **3**(1): p. 012002.
368. Yeo, L.Y. and J.R. Friend, *Surface Acoustic Wave Microfluidics.* Annual Review of Fluid Mechanics, 2014. **46**(1): p. 379-406.
369. Dung Luong, T. and N. Trung Nguyen, *Surface Acoustic Wave Driven Microfluidics - A Review.* Micro and Nanosystems, 2010. **2**(3): p. 217-225.
370. Franke, T., et al., *Surface acoustic wave actuated cell sorting (SAWACS).* Lab on a Chip, 2010. **10**: p. 789-794.
371. Frommelt, T., et al., *Microfluidic Mixing via Acoustically Driven Chaotic Advection.* Physical Review Letters, 2008. **100**: p. 034502.
372. Li, H., et al., *Effect of surface acoustic waves on the viability, proliferation and differentiation of primary osteoblast-like cells.* Biomicrofluidics, 2009. **3**(3): p. 034102.
373. Sarvi, F., et al., *Surface-functionalization of PDMS for potential micro-bioreactor and embryonic stem cell culture applications.* Journal of Materials Chemistry B, 2013. **1**(7): p. 987-996.
374. Hodgson, R., et al., *Transmitting high power rf acoustic radiation via fluid couplants into superstrates for microfluidics.* Applied Physics Letters, 2009. **94**: p. 024102.
375. Bourquin, Y., et al., *Tuneable surface acoustic waves for fluid and particle manipulations on disposable chips.* Lab on a Chip, 2010. **10**: p. 1898-1901.
376. Wilson, R., et al., *Phononic crystal structures for acoustically driven microfluidic manipulations.* Lab on a Chip, 2011. **11**: p. 323-328.
377. Qi, A., et al., *Template-free Synthesis and Encapsulation Technique for Layer-by-Layer Polymer Nanocarrier Fabrication.* ACS Nano, 2011. **5**(12): p. 9583-9591.
378. Gupta, D., C.H. Tator, and M.S. Shoichet, *Fast-gelling injectable blend of hyaluronan and methylcellulose for intrathecal, localized delivery to the injured spinal cord.* Biomaterials, 2006. **27**(11): p. 2370-2379.
379. Hoo, S.P., et al., *Preparation of a soft and interconnected macroporous hydroxypropyl cellulose methacrylate scaffold for adipose tissue engineering.* Journal of Materials Chemistry B, 2013. **1**(24): p. 3107-3117.
380. Hoo, S.P., et al., *Thermoresponsive Cellulosic Hydrogels with Cell-Releasing Behavior.* ACS Applied Materials & Interfaces, 2013. **5**(12): p. 5592-5600.
381. Li, H., J. Friend, and L. Yeo, *Surface acoustic wave concentration of particle and bioparticle suspensions.* Biomedical Microdevices, 2007. **9**(5): p. 647-656.
382. Fischer, A.H., et al., *Hematoxylin and Eosin Staining of Tissue and Cell Sections.* Cold Spring Harbor Protocols, 2008. **2008**(5): p. pdb.prot4986.

383. Hoo, S., et al., *Thermoresponsive Cellulosic Hydrogels with Cell-Releasing Behavior.* ACS Applied Materials and Interfaces, 2013. **5**: p. 5592-5600.
384. Al-Abboodi, A., et al., *Three-dimensional nanocharacterization of porous hydrogel with ion and electron beams.* Biotechnology and Bioengineering, 2013. **110**(1): p. 318-326.
385. Wang, L.-S., et al., *Injectable biodegradable hydrogels with tunable mechanical properties for the stimulation of neurogenesic differentiation of human mesenchymal stem cells in 3D culture.* Biomaterials, 2010. **31**(6): p. 1148-1157.
386. Fon, D., et al., *Effects of GDNF-Loaded Injectable Gelatin-Based Hydrogels on Endogenous Neural Progenitor Cell Migration.* Advanced Healthcare Materials, 2014. **3**(5): p. 761-774.
387. Xiong, J.-Y., et al., *Topology Evolution and Gelation Mechanism of Agarose Gel.* The Journal of Physical Chemistry B, 2005. **109**(12): p. 5638-5643.
388. Korsmeyer, R.W. and N.A. Peppas, *Effect of the morphology of hydrophilic polymeric matrices on the diffusion and release of water soluble drugs.* Journal of Membrane Science, 1981. **9**(3): p. 211-227.
389. Qi, A., et al., *Hydroxypropyl Cellulose Methacrylate as a Photo-Patternable and Biodegradable Hybrid Paper Substrate for Cell Culture and Other Bioapplications.* Advanced Healthcare Materials, 2014. **3**(4): p. 543-554.
390. Lee, Y.-H. and C.-A. Peng, *Nonviral Transfection of Suspension Cells in Ultrasound Standing Wave Fields.* Ultrasound in Medicine & Biology, 2007. **33**(5): p. 734-742.
391. Mueller, S., E.W. Llewellin, and H.M. Mader, *The rheology of suspensions of solid particles.* Proceedings of the Royal Society A: Mathematical, Physical and Engineering Science, 2010. **466**(2116): p. 1201-1228.
392. Carlo, D.D., L.Y. Wu, and L.P. Lee, *Dynamic single cell culture array.* Lab on a Chip, 2006. **6**(11): p. 1445-1449.
393. Kunz-Schughart, L.A., M. Kreutz, and R. Knuechel, *Multicellular spheroids: a three-dimensional in vitro culture system to study tumour biology.* International Journal of Experimental Pathology, 1998. **79**(1): p. 1-23.
394. Iyer, S.S. and M. Rojas, *Anti-inflammatory effects of mesenchymal stem cells: novel concept for future therapies.* Expert Opinion on Biological Therapy, 2008. **8**(5): p. 569-581.
395. Weiss, D.J., et al., *Stem Cells and Cell Therapies in Lung Biology and Lung Diseases.* Proceedings of the American Thoracic Society, 2008. **5**(5): p. 637-667.
396. Yeo, L.Y., et al., *Ultrasonic Nebulisation Platforms for Pulmonary Drug Delivery.* Expert Opinion on Drug Delivery, 2010. **7**: p. 663-679.
397. Taylor, K.M.G. and O.N.M. McCallion, *Ultrasonic nebulisers for pulmonary drug delivery.* International Journal of Pharmaceutics, 1997. **153**(1): p. 93-104.
398. Harvey, C., et al., *Comparison of jet and ultrasonic nebulizer pulmonary aerosol deposition during mechanical ventilation.* European Respiratory Journal, 1997. **10**: p. 905-909.
399. Braghirolli, D.I., et al., *Bio-electrospraying of human mesenchymal stem cells: An alternative for tissue engineering.* Biomicrofluidics, 2013. **7**(4): p. 044130.
400. Abeyewickreme, A., et al., *Bio-electrospraying embryonic stem cells: interrogating cellular viability and pluripotency.* Integrative Biology, 2009. **1**(3): p. 260-266.
401. Sahoo, S., et al., *Bio-electrospraying: A potentially safe technique for delivering progenitor cells.* Biotechnology and Bioengineering, 2010. **106**(4): p. 690-698.
402. Ye, C., et al., *Bio-electrospraying is a safe technology for delivering human adipose-derived stem cells.* Biotechnology Letters, 2015. **37**(2): p. 449-456.
403. Meirelles, L.d.S. and N.B. Nardi, *Murine marrow-derived mesenchymal stem cell: isolation, in vitro expansion, and characterization.* British Journal of Haematology, 2003. **123**(4): p. 702-711.
404. Pittenger, M.F., et al., *Multilineage Potential of Adult Human Mesenchymal Stem Cells.* Science, 1999. **284**(5411): p. 143-147.

405. Romanov, Y.A., et al., *Mesenchymal Stem Cells from Human Bone Marrow and Adipose Tissue: Isolation, Characterization, and Differentiation Potentialities.* Bulletin of Experimental Biology and Medicine, 2005. **140**(1): p. 138-143.
406. De Ugarte, D.A., et al., *Comparison of Multi-Lineage Cells from Human Adipose Tissue and Bone Marrow.* Cells Tissues Organs, 2003. **174**(3): p. 101-109.
407. Kurosawa, M., et al., *Surface acoustic wave atomizer.* Sensors and Actuators A, 1995. **50**: p. 69-74.
408. Flament, M.P., P. Leterme, and A. Gayot, *Study of the Technological Parameters of Ultrasonic Nebulization.* Drug Development and Industrial Pharmacy, 2001. **27**(7): p. 643-649.
409. Guo, F., et al., *Controlling cell–cell interactions using surface acoustic waves.* Proceedings of the National Academy of Sciences, 2015. **112**(1): p. 43-48.
410. Qi, A., et al., *Miniature inhalation therapy platform using surface acoustic wave microfluidic atomization.* Lab on a Chip, 2009. **9**(15): p. 2184-2193.
411. Cortez-Jugo, C., et al., *Pulmonary monoclonal antibody delivery via a portable microfluidic nebulization platform.* Biomicrofluidics, 2015. **9**(5): p. 052603.
412. Rajapaksa, A., et al., *Effective Pulmonary Delivery of an Aerosolized Plasmid DNA Vaccine via Surface Acoustic Wave Nebulization.* Respiratory Research, 2014. **15**: p. 60.
413. Ho, J., et al., *Paper-Based Microfluidic Surface Acoustic Wave Sample Delivery and Ionization Source for Rapid and Sensitive Ambient Mass Spectrometry.* Analytical Chemistry, 2011. **83**: p. 3260-3266.
414. Heron, S.R., et al., *Surface Acoustic Wave Nebulization of Peptides As a Microfluidic Interface for Mass Spectrometry.* Analytical Chemistry, 2010. **82**: p. 3985-3989.
415. Huang, Y., et al., *Surface Acoustic Wave Nebulization Produces Ions with Lower Internal Energy than Electrospray Ionization.* Journal of The American Society for Mass Spectrometry, 2012. **23**(6): p. 1062-1070.
416. Alvarez, M., J.R. Friend, and L.Y. Yeo, *Surface Vibration Induced Spatial Ordering of Periodic Polymer Patterns on a Substrate.* Langmuir, 2008. **24**: p. 10629-10632.
417. Li, H., et al., *Effect of Surface Acoustic Waves on the Viability, Proliferation and Differentiation of Primary Osteoblast-Like Cells.* Biomicrofluidics, 2009. **3**: p. 034102.
418. Sarvi, F., et al., *Cardiogenesis of Embryonic Stem Cells with Liquid Marble Micro-bioreactor.* Advanced Healthcare Materials, 2015. **4**: p. 77-86.
419. Ode, A., et al., *CD73 and CD29 concurrently mediate the mechanically induced decrease of migratory capacity of mesenchymal stromal cells.* European Cells and Materials, 2011. **22**: p. 26-42.
420. Qin, H., et al., *The differentiation of mesenchymal stem cells into inner ear hair cell-like cells in vitro.* Acta oto-laryngologica, 2011. **131**(11): p. 1136-1141.
421. Lau, H.Y. and M. Bhatia, *Effect of CP-96,345 on the expression of adhesion molecules in acute pancreatitis in mice.* American Journal of Physiology-Gastrointestinal and Liver Physiology, 2007. **292**(5): p. G1283-G1292.
422. Schäfer, S., et al., *Immunomodulatory influence of bone marrow-derived mesenchymal stem cells on neuroinflammation in astrocyte cultures.* Journal of neuroimmunology, 2012. **249**(1): p. 40-48.
423. Heyder, J., et al., *Deposition of particles in the human respiratory tract in the size range 0.005–15 μm.* Journal of Aerosol Science, 1986. **17**(5): p. 811-825.
424. Fu, X., et al., *Hypochlorous acid oxygenates the cysteine switch domain of pro-matrilysin (MMP-7). A mechanism for matrix metalloproteinase activation and atherosclerotic plaque rupture by myeloperoxidase.* J Biol Chem, 2001. **276**(44): p. 41279-87.
425. Kobayashi, S., H. Uyama, and S. Kimura, *Enzymatic polymerization.* Chemical Reviews, 2001. **101**(12): p. 3793-3818.

426. Galhaup, C., et al., *Characterization of the major laccase isoenzyme from Trametes pubescens and regulation of its synthesis by metal ions.* Microbiology, 2002. **148**(Pt 7): p. 2159-69.
427. Giardina, P., et al., *Laccases: a never-ending story.* Cellular and Molecular Life Sciences, 2010. **67**(3): p. 369-385.
428. Brzonova, I., et al., *Enzymatic synthesis of catechol and hydroxyl-carboxic acid functionalized chitosan microspheres for iron overload therapy.* Eur J Pharm Biopharm, 2011. **79**(2): p. 294-303.
429. Kato, K., et al., *Effective encapsulation of laccase in an aluminium silicate nanotube hydrogel.* New Journal of Chemistry, 2014. **38**(8): p. 3591-3599.
430. Mano, N., V. Soukharev, and A. Heller, *A laccase-wiring redox hydrogel for efficient catalysis of O2 electroreduction.* J Phys Chem B, 2006. **110**(23): p. 11180-7.
431. Blatchley, M., M.K. Park, and S. Gerecht, *Designer hydrogels for precision control of oxygen tension and mechanical properties.* The Royal Society of Chemistry, 2015.
432. Rocasalbas, G., et al., *Laccase-assisted formation of bioactive chitosan/gelatin hydrogel stabilized with plant polyphenols.* Carbohydrate Polymers, 2013. **92**(2): p. 989-996.
433. Park, K.M. and S. Gerecht, *Hypoxia-inducible hydrogels.* Nature Communications, 2014. **5**.
434. Evans, N.D., E. Gentleman, and J.M. Polak, *Scaffolds for stem cells.* Materials Today, 2006. **9**(12): p. 26-33.
435. Mitajavila-Garcia, M.T., Simon,C.,M.Peschanski, *Embryonic stem cells:meeting the need for cell therapy.* Adv.Drug.Deliv.Rev., 2005. **57**: p. 1935-1943.
436. Boucher, R.C., et al., *Evidence for reduced Cl- and increased Na+ permeability in cystic fibrosis human primary cell cultures.* J Physiol, 1988. **405**: p. 77-103.
437. Perez, A., et al., *CFTR inhibition mimics the cystic fibrosis inflammatory profile.* American Journal of Physiology-Lung Cellular and Molecular Physiology, 2007. **292**(2): p. L383-L395.
438. Wong, A.P., et al., *Directed differentiation of human pluripotent stem cells into mature airway epithelia expressing functional CFTR protein.* Nature Biotechnology, 2012. **30**(9): p. 876-U108.
439. Firth, A.L., et al., *Generation of multiciliated cells in functional airway epithelia from human induced pluripotent stem cells.* Proc Natl Acad Sci U S A, 2014. **111**(17): p. E1723-30.
440. Shojaie, S., et al., *Acellular Lung Scaffolds Direct Differentiation of Endoderm to Functional Airway Epithelial Cells: Requirement of Matrix-Bound HS Proteoglycans.* Stem Cell Reports, 2015. **4**(3): p. 419-430.
441. Wang, L.S., et al., *Injectable biodegradable hydrogels with tunable mechanical properties for the stimulation of neurogenesic differentiation of human mesenchymal stem cells in 3D culture.* Biomaterials, 2010. **31**(6): p. 1148-1157.
442. Hoo, S.P., et al., *Thermoresponsive cellulosic hydrogels with cell-releasing behavior.* ACS Appl Mater Interfaces, 2013. **5**(12): p. 5592-600.
443. Otto, W., *in Epidermal Cells , Vol. 289 (Ed: K. Turksen).* Humana Press , New Jersey 2005. **289**: p. 251.
444. Winter, H.H. and F. Chambon, *Analysis of Linear Viscoelasticity of a Cross-Linking Polymer at the Gel Point.* Journal of Rheology, 1986. **30**(2): p. 367-382.
445. Lee, F., J.E. Chunga, and M. Kurisawa, *An injectable enzymatically crosslinked hyaluronic acid–tyramine hydrogel system with independent tuning of mechanical strength and gelation rate.* Soft Matter, 2008. **4**: p. 880-887.
446. Lee, F., J.E. Chung, and M. Kurisawa, *An injectable hyaluronic acid-tyramine hydrogel system for protein delivery.* J Control Release, 2009. **134**(3): p. 186-93.
447. Kurisawa, M., et al., *Injectable enzymatically crosslinked hydrogel system with independent tuning of mechanical strength and gelation rate for drug delivery and tissue engineering.* Journal of Materials Chemistry, 2010. **20**(26): p. 5371-5375.
448. Levental, I., P.C. Georges, and P.A. Janmey, *Soft biological materials and their impact on cell function.* Soft Matter, 2007. **3**(3): p. 299-306.

449. Cardoso, W.V. and J.N. Lu, *Regulation of early lung morphogenesis: questions, facts and controversies.* Development, 2006. **133**(9): p. 1611-1624.
450. Finck, C., et al., *Differentiation of lung epithelial cells from murine embryonic stem cells with in vivo implantation.* Biochemistry & Molecular Biology, 2013. **1**(1): p. 1-8.
451. Kubo, A., et al., *Development of definitive endoderm from embryonic stem cells in culture.* Development, 2004. **131**(7): p. 1651-1662.
452. Yasunaga, M., et al., *Induction and monitoring of definitive and visceral endoderm differentiation of mouse ES cells.* Nature Biotechnology, 2005. **23**(12): p. 1542-1550.
453. Pezzulo, A.A., et al., *The air-liquid interface and use of primary cell cultures are important to recapitulate the transcriptional profile of in vivo airway epithelia.* American Journal of Physiology-Lung Cellular and Molecular Physiology, 2011. **300**(1): p. L25-L31.
454. Lopez-Souza, N., et al., *Resistance of differentiated human airway epithelium to infection by rhinovirus.* American Journal of Physiology-Lung Cellular and Molecular Physiology, 2004. **286**(2): p. L373-L381.
455. Groneberg, D.A., et al., *Localization of the peptide transporter PEPT2 in the lung - Implications for pulmonary oligopeptide uptake.* American Journal of Pathology, 2001. **158**(2): p. 707-714.
456. Granillo, O.M., et al., *Pulmonary alveolar epithelial uptake of S-nitrosothiols is regulated by L-type amino acid transporter.* American Journal of Physiology-Lung Cellular and Molecular Physiology, 2008. **295**(1): p. L38-L43.
457. Sherwood, R.I., et al., *Prospective isolation and global gene expression analysis of definitive and visceral endoderm.* Developmental Biology, 2007. **304**(2): p. 541-555.
458. Finck, C., Rozell, B., Jensen, T., Seaton, A., Zhang, F., Kaur, A. & Girard, E. D. 2013. Differentiation of lung epithelial cells from murine embryonic stem cells with in vivo implantation. Biochemistry & Molecular Biology, 1, 1-8.
459. Timmins, N.E. and L.K. Nielsen, *Generation of multicellular tumor spheroids by the hanging-drop method.* Methods Mol Med, 2007. **140**: p. 141-51.
460. Kim, C., *Droplet-based Microfluidics for Making Uniform-sized Cellular Spheroids in Alginate Beads with the Regulation of Encapsulated Cell Number.* Biochip Journal, 2015. **9**(2): p. 105-115.

APPENDICES

Appendix I: Software

Software	Manufacturer
Flowing software	Flowing Software, Turku Centre for Biotechnology, Finland
ImageJ	National Institutes of Health, Bethesda, MD
GraphPad Prism version 6.01	GraphPad Prism Software Inc.La Jolla,CA, USA
Microsoft Office 2011 Excel	Microsoft Corporation, Redmond, Washington, USA
NIS-Element imaging software	Nikon Instruments Inc,, Japan
Quantity One Analysis 4.3.0 software	Bio-Rad Laboratories

Appendix II: Chemicals and Reagents

Chemical	Manufacturer
1-thioglycerol	Sigma-Aldrich Pty Ltd, Australia
2-mercaptoethanol	Life Technologies Pty Ltd, Australia
2% gelatin	Sigma-Aldrich Pty Ltd, Australia
3,4-dihydroxyhydrocinnamic acid	Sigma-Aldrich Pty Ltd, Australia
4',6-diamidino-2-phenylindole (DAPI)	Life technologists Pty Ltd, Australia
AlamarBlue dye	Life technologists Pty Ltd, Australia
Ascorbic acid	Sigma-Aldrich Pty Ltd, Australia
Bovine serum albumin (BSA)	Sigma-Aldrich Pty Ltd, Australia
Carboxymethyl cellulose sodium salt	Sigma-Aldrich Pty Ltd, Australia
Collagenase Type I	Life Technologies Pty Ltd, Australia
Deuterium oxide (D_2O)	Sigma-Aldrich Pty Ltd, Australia
Dialysis tubing (MWCO 124000)	Sigma-Aldrich Pty Ltd, Australia

Dimethylsulfoxide (DMSO)	Sigma-Aldrich Pty Ltd, Australia
Dimethylformamide (DMF)	Sigma-Aldrich Pty Ltd, Australia
Ethanol	BDH Chemicals, Australia
Eosin	ProSciTech Pty Ltd, Australia
Ethidium bromide	Roche Applied Sciences, Germany
Ethylenediamine tetra acetic acid, EDTA	BDH Chemicals, Australia
Fluoro-Gel mounting medium	ProSciTech Pty Ltd, Australia
Fluorescently labelled miRNA (Dharmacon Miridian miRNA-Dy547)	Millennium Science Pty Ltd, Australia
Gelatin (MW = 80–140 kDa, pI = 5)	Novachem Pty Ltd, Australia
Haematoxylin	ProSciTech Pty Ltd, Australia
Heparin sulphate salt (Sigma H-4784)	Sigma-Aldrich Pty. Ltd, Australia
Horseradish peroxidase (HRP; 100 units/mg)	Novachem Pty Ltd, Australia
Hydrogen peroxide (H_2O_2)	Merck Pty Ltd, Australia
Isopropanol	Ajax Chemicals Pty Ltd, Australia
Laccase (10 U/mg)	Sigma-Aldrich Pty Ltd, Australia
Lambda DNA (ΛdNA)	Life Technologies Pty Ltd, Australia
Lambda RNA	Life Technologies Pty Ltd, Australia
Lipofectamine®RNAiMAX Transfection Reagent	Life Technologies Pty Ltd, Australia
NP40 Cell Lysis Buffer	Life Technologies Pty Ltd, Australia
N-(3-dimethylaminopropyl)-N-ethylcarbdiimide hydrochloride (EDC)	Sigma-Aldrich Pty Ltd, Australia
N-hydroxysuccinimide (NHS)	Sigma-Aldrich Pty Ltd, Australia
Orange G Dye	Cell Signalling Pty Ltd , Australia
Phosphate Buffered Saline, PBS	Sigma-Aldrich Pty Ltd, Australia
Paraformaldehyde	ProSciTech Pty Ltd , Australia

Protease Inhibitor Cocktails	Sigma-Aldrich Pty Ltd, Australia
Polyethylenimine (MW ~25,000)	Sigma-Aldrich Pty Ltd, Australia
Polytetrafluoroethlene (PTFE)	Sigma-Aldrich Pty Ltd, Australia
Sodium hydroxide (NaOH)	BDH Chemicals Pty Ltd, Australia
Triton-X100	Sigma-Aldrich Pty. Ltd, Australia
Trypan Blue (Gibco®)	Life Technologies Pty Ltd, Australia
Tyramine hydrochloride (TYR)	Sigma-Aldrich Pty. Ltd, Australia
Tween 20	Sigma-Aldrich Pty. Ltd, Australia

Appendix III: Cell lines

Cell line	Source
Breast cancer cells (Bt474)	School of Medical Sciences, RMIT University, Australia
Lung cancer cells (A549)	School of Medical Sciences, RMIT University, Australia
Mouse embryonic stem cells (mESC)	Cell Bank Australia, Australia
Rat mesenchymal stem cells (rMSC)	Life Technologies Pty Ltd, USA

Appendix IV: Tissue Culture Media and Reagents

Medium	Manufacturers
Activin A	Bio-Scientific Pty Ltd., Australia
B27 (without retinoic acid)	Bio-Scientific Pty Ltd., Australia
Dulbecco's Modified Eagle's Medium, low Glucose, GlutaMAX™ and Pyruvate (Gibco®)	Life Technologies Pty Ltd., Australia
Dulbecco's Phosphate-Buffered Saline (DPBS) (Gibco®)	Life Technologies Pty Ltd., Australia
Fetal bovine serum, FBS	Bovogen Serum Biologicals Pty Ltd., Australia
Fetal bovine serum (Gibco®)	Life Technologies Pty Ltd., Australia
Fetal Bovine Serum-Embryonic Stem Cell-Qualified (Gibco®)	Life Technologies Pty Ltd., Australia
Fibroblast growth factor (F0291)	Sigma-Aldrich Pty Ltd., Australia
Gentamicin reagent solution (Gibco®)	Life Technologies Pty Ltd., Australia
Ham's F12 Medium (Gibco®)	Life Technologies Pty Ltd., Australia
Iscove's Modified Dulbecco's Medium (Gibco®)	Life Technologies Pty Ltd., Australia
L-glutamine (Gibco®)	Life Technologies Pty Ltd., Australia
Murine leukemia inhibitory factor	Millipore, Chemicon, Australia
Non-essential amino acids (Gibco®)	Life Technologies (Gibco®) Pty Ltd., Australia
Opti-MEM® I Reduced Serum Medium (Gibco®)	Life Technologies (Gibco®) Pty Ltd., Australia
Penicillin-Streptomycin (Gibco®)	Life Technologies (Gibco®) Pty Ltd., Australia
RPMI 1640 medium (Gibco®)	Life Technologies (Gibco®) Pty Ltd., Australia
TrypLE™ express solution (Gibco®)	Life Technologies (Gibco®) Pty Ltd., Australia
Trypsin (0.05x) (Gibco®)	Life Technologies (Gibco®) Pty Ltd., Australia
Trypsin (10x) (Gibco®)	Life Technologies (Gibco®) Pty Ltd., Australia
Wtn3a	Bio-Scientific Pty Ltd., Australia

Appendix V: Commercial Kits

Commercial Kit	Manufacturer
Cytoskeleton/Focal Adhesion Staining Kit	Merck Pty Ltd., Australia
LIVE/DEAD@ Cell Viability	Life Technologies Pty Ltd., Australia
QuantiTect Reverse Transcription Kit (50 reactions)	Qiagen Pty Ltd., Australia
QuantiTect SYBR Green RT-PCR Kit	Qiagen Pty Ltd., Australia
Quant-iT™ PicoGreen® dsDNA Assay Kit	Life Technologies Pty Ltd., Australia
RNA Mini Kit	Qiagen Pty Ltd., Australia
miRNeasy Mini Kit	Qiagen Pty Ltd., Australia
TaqMan® Gene Expression Master Mix	Life Technologies Pty Ltd., Australia
TaqMan® MicroRNA Reverse Transcription Kit	Life Technologies Pty Ltd., Australia
TaqMan® Universal Master Mix II, no UNG	Life Technologies Pty Ltd., Australia
Turbo DNA-free TM (Ambion)	Life Technologies Pty Ltd., Australia

Appendix VI: Antibodies

Antibody	Manufacturer
Alexa Fluor® 488 donkey anti-goat IgG (H+L) antibody	Life Technologies Pty Ltd., Australia
Anti-CD44 antibody conjugate	Merck Millipore Pty Ltd., Australia
Anti-CD106 antibody conjugate	Biolegend, USA
E-Cadherin	Santa Cruz Biotechnology, USA
FOX2a	Santa Cruz Biotechnology, USA
Integrate beta anti-CD29 antibody conjugate	Life Technologies Pty Ltd., Australia
Goat anti-mouse secondary antibody	Millipore Merck Pty Ltd., Australia
Goat anti-rabbit secondary antibody	Sapphire Pty Ltd., Australia

Pep2 primary antibody	Santa Cruz Biotechnology, USA
Sema4f primary antibody	Santa Cruz Biotechnology, USA
Vinculin antibody	Merck Millipore Pty Ltd., Australia
VEGF Antibody	Santa Cruz Biotechnology, USA

Appendix VII: TaqMan assays

Gene	Host	Assay ID	Manufacturer
Foxa2	Mouse	Mm01976556_s1	Applied Biosystems
GAPDH	Human	Hs02758991_g1	Applied Biosystems
GAPDH	Mouse	Mm99999915_g1	Applied Biosystems
hsa-miR-126	Human	000451	Applied Biosystems
RNU44	Human	001094	Applied Biosystems
Pou5f1 (Oct4)	Mouse	Mm00504054_m1	Applied Biosystems
Sema4f	Mouse	Mm01181883_m1	Applied Biosystems
Sox17	Mouse	Mu00488363_m1	Applied Biosystems
VEGF-A	Human	Hs00900055_m1	Applied Biosystems
Ttf1	Mouse	Mm00657018_m1	Applied Biosystems
Unc5b	Mouse	Mm00504054_m1	Applied Biosystems

Appendix VIII: Equipment and Associated Consumables

Equipment and associated consumables	Manufacturer
Balance (0.1-500 g)	U-Lab, Australia
Centrifuges:	
(i) Microcentrifuge	Zentrifugen, Germany
(ii) Bench top centrifuge	Eppendorf, Australia
(iii) High-Speed centrifuge	Thermofisher, Australia
(iv) Ultra-Speed centrifuge	Beckman, USA
Biological Safety Cabinet Class II cabinet	LAF Technologies, Australia
Countess® Automated Cell Counter	Invitrogen, USA
Countess® Automated Cell slides	Life Technologies Pty Ltd, Australia
Confocal Laser Scanning Microscope	Nikon Instruments Inc, Japan
Electrophoresis Mini-gel	Bio-Rad Laboratories, USA
Electrophoresis Power Supply PAC300	Bio-Rad Laboratories, USA
Gel-Doc System	Bio-Rad Laboratories, USA
HR3 Discovery-Hybrid stress controlled rheometer	Cornell Centre for Materials Research, Ithaca, NY, USA
CO_2 incubator	SANYO Electric Co. Ltd, Japan
Light microscope	Olympus Optical
Microcentrifuge	Eppendorf, Germany
NanoDrop Lite Microlitre Spectrophotometer	Thermo Fisher Scientific, Australia
Nuclear magnetic resonance spectroscope	ACF300, Bruker Pty Ltd, Alexandria, NSW, Australia
Phase contrast microscope	Nikon Kogaku KK, Japan
pH meter	Radiometer, Denmark

POLARstar Omega Microplate Reader	BMG LABTECH, Australia
Real-time PCR	Rotor-Gene, Qiagen Pty Ltd, Australia
Disposable folded capillary cells	ATC Scientific Pty Ltd, Australia
Filter (0.2µm)	Millipore, Australia
Centrifuge tubes:	Sarstedt, Germany
(i) 1.5 mL microcentrifuge tubes	Greiner Bio-One, Germany
(ii) 2 ml microcentrifuge tubes	VWR International Pty Ltd, Australia
(iii) 10 mL centrifuge tubes	Greiner Bio-One, Germany
(iv) 50 mL centrifuge tubes	Greiner Bio-One, Germany
Micropipette plastic tips (blue and yellow)	Greiner Bio-One, Germany
Microtitre Plates:	
(i) Microtitre Plate (96-well, flat bottom)	Greiner Bio-One, Germany
(ii) Microtitre Plate (24-well)	Greiner Bio-One, Germany
(iii) Microtitre Plate (12-well)	Greiner Bio-One, Germany
(iv) Microtitre Plate (6-well)	Greiner Bio-One, Germany
Petri dishes:	
Petri dishes (100 cm^3)	VWR International Pty Ltd, Australia
Petri dishes (35 cm^3)	Thermo Fisher Scientific Pty Ltd, Australia
Strip tubes with caps	Qiagen Pty Ltd, Australia
Syringes (5 mL, 10 mL, 20 mL, 50 mL)	Thermo Fisher Scientific Pty Ltd, Australia
Tissue culture flask (25 cm^3 and 75 cm^3)	VWR International Pty Ltd, Australia

Appendix IX: Agarose gel electrophoresis assay figure

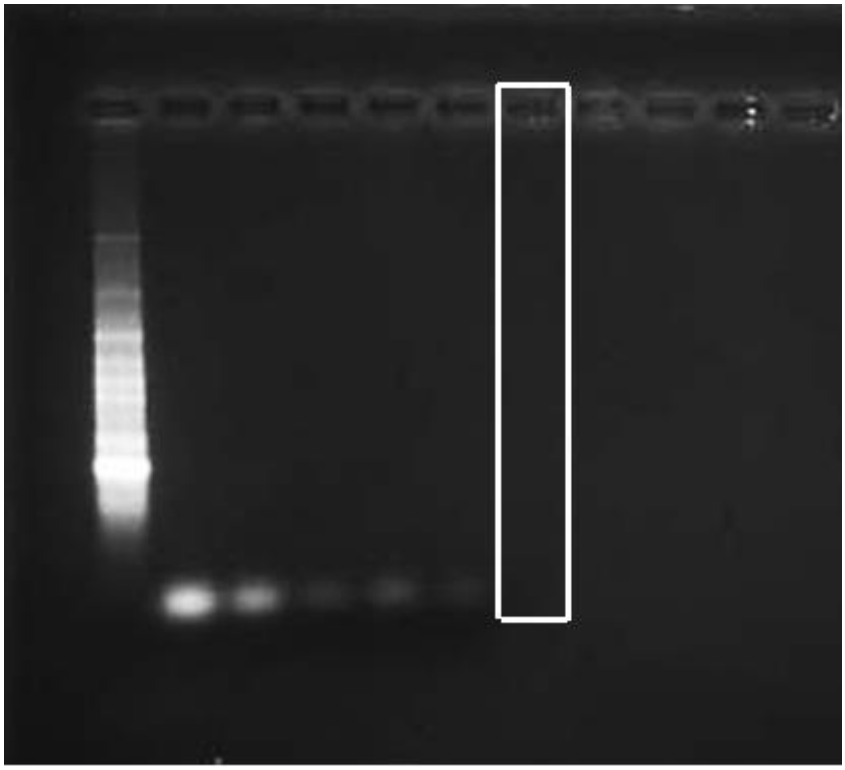

Figure shows Agarose gel electrophoresis assay of PEI/miR-126 Nano-complexes: M. RNA ladder, lane 1, miRNA alone, lanes 2 to 6 miRNA complexes N/P ratio 4 , 13 , 19 , 25 and 33.